DISSERTATION

submitted to the

Combined Faculty of Mathematics, Engineering and Natural Sciences
of Heidelberg University, Germany

for the degree of

Doctor of Natural Sciences

Put forward by

SOPHIE ELAINE KLETT

born in Pforzheim, Germany
Oral examination: 20th November 2024

Fermion Mass Hierarchy with a Radiative Origin and Experimental Insights into Neutrino Interactions

Referees: Prof. Dr. Dr. h.c. Manfred Lindner
Prof. Dr. Tilman Plehn

Abstract

The hierarchies and regular patterns that occur in the mass spectrum of fermions remain a puzzling phenomenon that the Standard Model has yet to address. In this thesis, we investigate a mechanism that could explain the mass hierarchy between fermion generations from quantum loop corrections. We propose concrete implementations of this mechanism in models that feature new generations of massive vector-like fermions, leading to a generalized seesaw mechanism for quarks and leptons. In these models, the masses of heavier families emerge from a tree level seesaw, while in contrast, lighter generations obtain masses only through higher order loop corrections. Opposed to previous studies that consider multiple scalar extensions, we realize such scenarios with a minimal scalar content and loop corrections primarily arise from new gauge interactions. For this purpose, we examine Abelian and non-Abelian Standard Model gauge extensions. The first involves an additional local $U(1)$ symmetry, while the second belongs to the class of left-right symmetric models. Our study demonstrates that realistic fermion mass patterns can naturally arise from loop factors and neither strongly hierarchical Yukawa couplings nor new global or discrete symmetries are needed. Moreover, small neutrino masses can be incorporated into the mechanism. Since models that include massive neutrinos often predict neutrino non-standard interactions, probing them is a promising approach to learn more about the mechanism behind neutrino masses. We explore the potential of a future muon collider to test neutrino non-standard interactions and the complementary insights it could provide.

Zusammenfassung

Die hierarchischen Strukturen und wiederkehrenden Muster, die im Massenspektrum von Fermionen beobachtet werden, sind bis heute eine rätselhafte Erscheinung. Um diesem Verhalten auf den Grund zu gehen, erforschen wir Mechanismen, in denen radiative Korrekturen eine Massenhierarchie zwischen den verschiedenen Generationen von Fermionen erzeugen. Zur Umsetzung des Mechanismus schlagen wir explizite Modelle vor, die sich durch neue Generationen vektorartiger Fermionen auszeichnen. Dies führt zu einem universellen Seesaw-Mechanismus für Quarks und Leptonen. Während die Massen schwerer Generationen durch einen tree-level Seesaw-Mechanismus entstehen, werden die Massen der leichten Generationen durch Quantenkorrekturen höherer Ordnung erzeugt. Im Gegensatz zu bisherigen Studien, konzentrieren wir uns vor allem darauf, wie diese Korrekturen durch neue Eichbosonen entstehen können. Dazu untersuchen wir eine abelsche und eine nicht abelsche Erweiterung der Eichgruppe des Standardmodells. Mit unserer Studie demonstrieren wir, dass Schleifenkorrekturen die Verhaltensmuster von Fermionmassen auf natürlichem Weg erklären können und dazu weder hierarchische Yukawa Kopplungen noch neue globale oder diskrete Symmetrien notwendig sind. Darüber hinaus können auch kleine Neutrinomassen in den Mechanismus integriert werden. Da Modelle, die massive Neutrinos enthalten, in vielen Fällen zu neuen Wechselwirkungen führen, ist die Erforschung solcher Neutrinointeraktionen jenseits des Standardmodells ein vielversprechender Ansatz, um mehr über die Mechanismen hinter Neutrinomassen herauszufinden. Wir untersuchen die Rolle eines hochenergetischen Myonenbeschleunigers bei der Erkundung von Nicht-Standard-Neutrinointeraktionen und zeigen, dass dieser in Zukunft vielversprechende Erkenntnisse liefern könnte.

Contents

Chapter 1

Introduction

The first observation of the muon by Anderson and Neddermeyer in 1936 [5, 6] was a groundbreaking discovery in particle physics. Even though in the beginning little was known about the new particle with a mass lighter than the proton but heavier than the electron, the muon gave a first evidence that protons, neutrons and electrons are not the only existing particles. Today we know that the muon was the precursor of a complete second generation of fermions, but many more discoveries had to follow to built up a consistent theory to describe particles and their interactions.

In the 1960s, after a number of new hadrons had been discovered, Gell-Mann and Zweig raised the idea of three quarks (up, down, strange) as the fundamental building blocks of mesons and baryons [7–9]. Together with his student Fritzsch, Gell-Mann coined the name “flavor” for these different types of quarks. However, soon it became clear that the small branching ratio of kaons decaying into two muons would be explained with an existing fourth quark (Glashow, Iliopoulos, and Maiani [10]). Only four years after this prediction, the charm quark was discovered at BNL and SLAC almost at the same time [11, 12]. Two generations of fermions provided an elegant treatment of particles and the discovery of a third lepton, the tau, in 1976 [13] evoked the question whether there would be also a third generation of quarks. In fact, Kobayashi and Maskawa already pointed out a few years earlier [14] that three quark generations would allow to describe CP violation observed in kaon decays. Indeed, shortly after another quark, the bottom, was discovered [15] and physicists were sure that the third generation of fermions should be completed with a sixth quark. Nonetheless, it took almost 18 years, until the top quark was found at an unexpected high mass of 173 GeV [16, 17]. Together with the detection of three species of light neutrinos (the tau neutrino as latest in 2000 [18]), the flavor sector of the Standard Model (SM) seems complete. Apart from neutrinos, fermion masses can be described by the Brout-Englert-Higgs mechanism [19–21]. A SM-like fourth generation of fermions is under tension due to precision measurements in the electroweak and Higgs sector [22–26].

Today, we have a much better understanding, though some puzzling features of the flavor sector are as astonishing as on the day of their discovery. From the tiny electron mass to the top quark, which weights almost as much as a gold atom, the fermion masses span already five orders of magnitude. On top of that, neutrino oscillations have proven

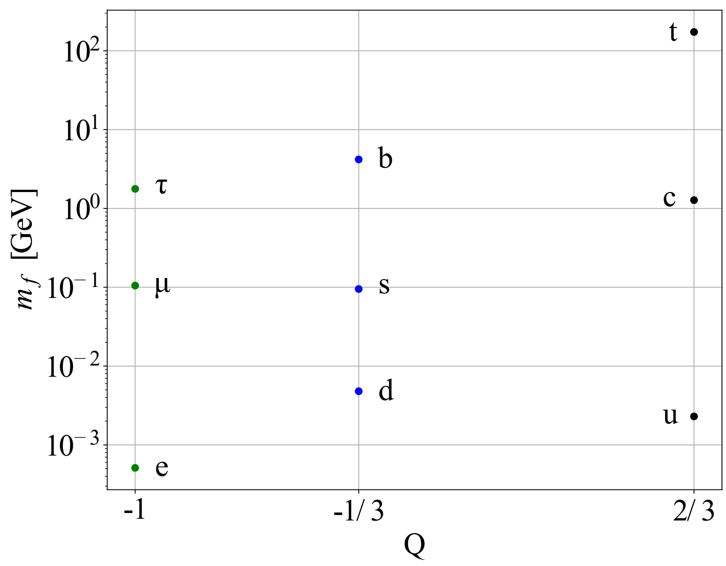

Figure 1.1 Masses of up-type quarks (up, charm and top), down-type quarks (down, strange and bottom) and charged leptons (e, μ and τ) as a function of the electric charge. Neutrino mass limits are not displayed. The data is taken from [31].

that at least two species of neutrinos are massive. Current experimental bounds limit them to the sub-eV scale [27–29] which broadens the scale of fermion masses to twelve orders of magnitude. However, fermion masses do not just randomly scatter within this range. They follow intriguing patterns as each generation is more massive than the preceding one.[1] It seems also remarkable that within one generation, colored particles are mostly heavier than uncolored ones, and up-type quarks with charge $+2/3$ in turn are heavier than down-type quarks with charge $-1/3$ (with the exception of the first generation). We illustrate these peculiar patterns in Figure 1.1. Mixing between generations occurs in the quark and lepton sector, nevertheless with completely different mixing patterns. While the quark mixing matrix is close to diagonal, mixing angles in the lepton sector seem anarchical. The SM offers no reason for the existence of exactly three generations, nor does it give a deeper reasoning for the emerging structures in masses and mixings. The fact that it can only describe these observations, but not explain, turns it into a true "flavor puzzle". Overall, it is hard to believe that the observed patterns are only governed by coincidence and non-zero neutrino masses definitely require new physics beyond the SM. Therefore, it is worth to explore models that can potentially address both issues. In this thesis we particularly concentrate on a possible mechanism that explains mass hierarchies appearing between different fermion generations. In addition, we discuss possibilities to incorporate small neutrino masses appropriately.

So far, a huge effort was put to understand the flavor structure by means of discrete or global symmetries [32–34]. Especially discrete groups with a triplet representation, as for

[1] Neutrinos are possibly an exception to this, as their mass ordering is not yet determined [30].

example A_4, S_4 or $\Delta(27)$, were popular targets to represent the three generation structure of the SM. Nevertheless, nature has realized none of these symmetries directly and the explicit breaking scheme of flavor symmetries is a key ingredient of this type of models, which usually involves a plethora of new scalars, the flavons [35]. An appealing alternative, which we will follow in this work, are models that do not need additional flavor symmetries or a multitude of new scalars. Instead, they rely on the idea of radiative loop suppression that can be understood from the following consideration:

When a fermion mass matrix, for instance in the quark sector, has the structure

$$\mathcal{M}_{u/d} = m_{t,b} \left[|\alpha\rangle\langle\alpha|\epsilon^2 + |\beta\rangle\langle\beta|\epsilon + \begin{pmatrix} 0 & 0 & 0 \\ 0 & 0 & 0 \\ 0 & 0 & 1 \end{pmatrix} \right] ,$$

where $|\alpha\rangle\langle\alpha|$, $|\beta\rangle\langle\beta|$ denote tensor products of coupling matrices which are in general different for up- and down-type quarks and $\epsilon \ll 1$ being a small parameter. Then, couplings of $\mathcal{O}(1)$ naturally lead to eigenvalues that fulfill the hierarchical relation

$$m_t : m_c : m_u \simeq 1 : \epsilon : \epsilon^2 \ , \quad m_b : m_s : m_d \simeq 1 : \epsilon : \epsilon^2 \ .$$

From this estimation we clearly see that $\epsilon \sim 10^{-2}$ leads to the observed hierarchy in fermion masses and it seems obvious to identify the expansion parameter ϵ with a loop suppression factor $\sim 1/(16\pi^2)$. In this scenario, only the third generation is massive at tree level, while second and first generation fermions obtain their masses through one-loop and two-loop quantum corrections leading to the observed hierarchies. Since the matrix rank steadily increases by including higher loop orders until all fermions have become massive, this is called the rank mechanism. Of course, partial realizations of this idea with different loop levels are possible as well. Models based on the rank mechanism were suggested in the 1980s and since then a number of related works followed [36–47]. They address the mass hierarchy by considering SM extensions with either new gauge or scalar interactions that contribute to the loop effects. Among these two possibilities, gauge extensions represent the more economical theories but are also highly restrictive and therefore received less attention in the literature. An example of the constraining character of gauge interactions is given by the proposal [44]. It describes realistic mass hierarchies but fails to reproduce experimentally observed mixing patterns.

In this work we follow the guiding principle to keep the scalar content minimal, i.e. we only consider scalars needed for symmetry breaking and explore which ingredients are necessary to realize hierarchical fermion masses by gauge loop corrections. For this we examine two different scenarios, an Abelian SM gauge extension and a non-Abelian gauge extension in the left-right symmetric model [48–50]. A natural advantage of the non-Abelian gauge extension is the existence of an additional charged gauge boson that opens the possibility for further loop corrections opposed to Abelian extensions with neutral gauge bosons alone. As a key prerequisite for a radiative origin of the fermion mass hierarchy, some generations need to stay massless at tree level. Therefore, an important ingredient for our work are seesaw-like tree level mass matrices, which we implement by introducing new vector-like fermions. The advantage of this approach is that the number of massive SM fermions at tree level is precisely controlled by the number of vector-like fermion generations. A series of papers has studied the application of the seesaw mechanism outside the neutrino sector, which was dubbed the universal seesaw mechanism [51–61]. Contrary to these works, where all three fermion generations obtain masses at tree level, we combine the tree level seesaw mechanism for the heavier fermions with radiatively induced masses for the lighter fermions. Besides charged lepton and quark masses, we also discuss possibilities to obtain sub-eV neutrino masses in the considered models.

The definite need for a mechanism that explains massive neutrinos made this topic to one of the most active research areas in particle physics and numerous theories describing small neutrino masses were proposed over the last decades (for a selection see [62–70]). Clearly, any of these theories that accomplish massive neutrinos needs to introduce new interactions beyond the SM, commonly known as neutrino non-standard interactions (NSIs). The study of NSIs is therefore an integral part of the current neutrino research program and provides a promising pathway to discover physics beyond the SM. Unfortunately, new physics that lead to neutrino NSIs can hide at vastly different energy scales. Hence, it is necessary to conduct a broad range of experiments testing different energy ranges. At low energies, neutrino oscillation experiments are sensitive to NSIs through new matter effects that modify the standard oscillation probabilities [71–73]. Alternatively, NSIs can be probed in scattering experiments at high energy colliders [74–80] or at neutrino telescopes [81–83]. The aforementioned experiments are able to constrain NSIs with first generation fermions (electron, up and down quark) and a summary of the current status is given in [84]. Though equally thrilling, NSIs with second generation fermions are mostly unexplored. It is therefore essential to investigate which type of experiment allows us to get further insights into NSIs in future and we find a muon collider to be an excellent candidate for these explorations. In the light of a persisting discrepancy between the theoretical prediction of the muon anomalous magnetic moment and its experimentally determined value [85, 86], the muon offers a particular interesting candidate to probe NSIs and in this way also a possible connection between the anomalous $(g-2)_\mu$ and neutrino mass via a muonic force.

The prospect of a high energy muon collider whose planning enters now a new stage [87–92], has brought the probe of NSIs with muons to feasible reach. We therefore devote the second last chapter of this thesis to analyze the potential of a muon collider to test four-fermion contact interactions with two neutrinos and two muons. For this, we study SM extensions that feature vector or scalar mediated NSIs with muons, such as the gauged $L_\mu - L_\tau$ model or the Zee model, and analyze the monophoton signal that results from the process $\mu^+\mu^- \to \nu\nu\gamma$ to obtain a projected sensitivities for the NSI strength. Exploring muonic NSIs in future experiments opens a new window to test beyond SM physics related to neutrinos and muons and therefore offers a chance to get further insights into the mechanisms behind neutrino mass.

The remainder of this thesis is structured as follows: In the Chapter 2 we give an introduction to the SM and point out different motivations for new physics beyond the SM. Chapter 3 elaborates the details of the flavor puzzle and summarizes theoretical attempts to solve it. In Chapter 4, we present a model which explains hierarchical fermion masses by a loop suppression mechanism in a $U(1)$ gauge extension of the SM together with phenomenological consequences. Chapter 5 extends this mechanism to a non-Abelian gauge symmetry in a left-right symmetric model. Finally, in Chapter 6 we discuss the possibility to constrain neutrino non-standard interactions with muons at a future collider, before we summarize and conclude in Chapter 7.

Chapter 2

The Standard Model and beyond

Up to now, nature has revealed the four fundamental forces gravity, strong interaction, weak interaction and electromagnetism to us. With the exception of gravity, numerous efforts in the past have led to a full description of the remaining three forces in terms of a local gauge invariant theory based on the symmetry group $\mathcal{G}_{SM} = SU(3)_C \times SU(2)_L \times U(1)_Y$. Here, the labels refer to color (C), left-chiral (L) and weak hypercharge (Y). While $SU(3)_C$ describes quantum chromodynamics (QCD), featuring eight massless mediators called the gluons, the electroweak force is unified and characterized by the Glashow-Salam-Weinberg (GSW) theory based on $SU(2)_L \times U(1)_Y$ [93–95]. Massive gauge bosons that appear in the weak interaction can be successfully described by a mechanism proposed by Brout, Englert and Higgs [19–21]. This mechanism, also known as spontaneous symmetry breaking, is not only able to explain massive gauge bosons but at the same time allows to introduce mass terms for fermions. A prediction of the SM is the existence of the Higgs boson, a neutral scalar particle, which was finally found in 2012 by ATLAS and CMS [96, 97].

With the current theory, physicists are able to test SM predictions of particle properties. For example the measured electron magnetic moment agrees with a precision of 1 part in 10^{12} with its theoretical prediction [98]. On the other hand, there are puzzling experimental and theoretical hints that the SM is not the ultimate theory. We will discuss some of these open questions at the end of this chapter. First, we discuss the SM in more detail and focus explicitly on the electroweak interaction and the Higgs mechanism, with only little reference to the strong interaction.[1]

2.1 Glashow-Salam-Weinberg theory

The Lagrangian density describing the electroweak interaction as well as the Brout-Englert-Higgs mechanism can be divided into four main parts

$$\mathcal{L} = \mathcal{L}_{gauge} + \mathcal{L}_f + \mathcal{L}_{scalar} + \mathcal{L}_{Yuk} \ , \tag{2.1}$$

[1] We refer the reader to [99] for a recent review on QCD.

which describe the gauge sector, the fermion and scalar fields and the Yukawa sector of the theory. We start by considering the gauge part.

Since $SU(2)_L$ is a rank three group, it gives rise to three gauge fields W^a_μ (a=1,2,3), while B_μ is the single gauge boson originating from the Abelian group $U(1)_Y$. The generators of the Lie algebra associated with $SU(2)_L$ are given by the operators t^a that fulfill the following relation

$$[t^a,\ t^b] = i f^{abc} t^c \ , \tag{2.2}$$

where f^{abc} are the structure constants of $SU(2)$. A convenient basis is represented by the Pauli matrices $t^a = \tau^a/2$ and one can check $f^{abc} = \epsilon^{abc}$. The generator of the Abelian group $U(1)_Y$ is simply given by an operator proportional to the identity element and hence the structure constants vanish in this case. From the gauge fields, one can define the field strength tensors

$$\begin{aligned} W^a_{\mu\nu} &= \partial_\mu W^a_\nu - \partial_\nu W^a_\mu + g f_{abc} W^b_\mu A^c_\nu \ , \\ B_{\mu\nu} &= \partial_\mu B_\nu - \partial_\nu B_\mu \ , \end{aligned} \tag{2.3}$$

such that the gauge kinetic terms are represented by

$$\mathcal{L}_{gauge} = -\frac{1}{2}\mathrm{Tr}[W_{\mu\nu}W^{\mu\nu}] - \frac{1}{4}B_{\mu\nu}B^{\mu\nu} \ , \tag{2.4}$$

with the short notation $W_{\mu\nu} \equiv W^a_{\mu\nu} t^a$. The strength of the interaction is determined by the gauge couplings g and g' and vector fields satisfy the gauge transformation

$$\begin{aligned} W_\mu \to W'_\mu &= U W_\mu U^{-1} - \frac{1}{ig}(\partial_\mu U)U^{-1},\ U = \exp(i\beta_a(x)t^a) \ , \\ B_\mu \to B'_\mu &= B_\mu - \frac{1}{g'}\partial_\mu \alpha(x) \ , \end{aligned} \tag{2.5}$$

where $W_\mu \equiv W_\mu t^a$ and the $\alpha(x)$, $\beta_a(x)$ are the local parameters of the $U(1)_Y$ and $SU(2)_L$ transformation. Using the previous transformation properties, one can show that the field strength tensor transforms like $W_{\mu\nu} \to U W_{\mu\nu} U^{-1}$ and together with Eq. (2.5), the expression $\mathcal{L}_{gauge}$ is manifestly gauge invariant. On the other hand, an explicit mass term $M_B^2 B_\mu B^\mu$ is forbidden by gauge invariance. Hence, in the unbroken theory, there are in total four massless gauge bosons. This is not what we see in nature today and further ingredients are demanded to comply with observations.

Besides the gauge bosons that mediate the forces, an other integral part of the SM are the fermion fields that make up matter. In the Glashow-Salam-Weinberg theory, left-handed fermions are assigned to doublets under the left-chiral $SU(2)_L$, whereas right-handed particles are trivial singlets. As such, $SU(2)_L$ distinguishes between left- and right-handed chirality, in contrast to quantum chromodynamics which is a vector-like theory. The fermion content of the SM is given in Table 2.1 together with the charge assignments. The strongly interacting part consists of the weak quark doublets $Q_{iL} = (u_{iL}, d_{iL})^T$ that are formed by the left-handed up- and down-type quarks and the right-handed weak singlets u_{iR} and

Field	$\mathbf{SU(3)_C}$	$\mathbf{SU(2)_L}$	$\mathbf{U(1)_Y}$
$Q_{iL} = \begin{pmatrix} u_i \\ d_i \end{pmatrix}_L$	**3**	**2**	$1/3$
$\Psi_{iL} = \begin{pmatrix} \nu_i \\ e_i \end{pmatrix}_L$	**1**	**2**	-1
u_{iR}	**3**	**1**	$4/3$
d_{iR}	**3**	**1**	$-2/3$
e_{iR}	**1**	**1**	-2

Table 2.1 Fermionic fields in the Standard Model and their charges. The index $i = 1, 2, 3$ denotes the family.

d_{iR}. On top of that, there are uncolored lepton doublets $\Psi_{iL} = (\nu_{iL}, e_{iL})^T$ composed by left-handed neutrino and charged lepton and the right-handed counterparts for the charged leptons, which are weak singlets e_{iR}. Therein, every fermion field appears as one out of a series of three copies $i = 1, 2, 3$ with exactly the same gauge charges. Even though this repetition of fermion representations does not constitute a problem in the first place, one may wonder whether there is some deeper underlying reason and we will discuss this question in more detail in the next section. It is also important to emphasize that there is no right-handed fermion field for the neutrino in the SM.

The hypercharge Y of a particle is defined by $Y/2 = Q - T_3$, where T_3 is the third component of left isospin. Under a local $SU(2)_L \times U(1)_Y$ transformation, the fermion fields transform as

$$\begin{aligned} f_L &\to \exp\left(i\beta_a(x)t^a\right)\exp\left(iq_{Y_L}\alpha(x)\right) f_L \ , \\ f_R &\to \exp\left(iq_{Y_R}\alpha(x)\right) f_R \ , \end{aligned} \tag{2.6}$$

where $q_{Y_{L/R}}$ is the hypercharge of $f_{L/R}$ and t^a are the $SU(2)$ generators of the fundamental representation. As desired, the right-handed fermion transforms trivially under the $SU(2)_L$ gauge transformation. Local gauge invariance furthermore requires to introduce the covariant derivatives

$$\begin{aligned} D_\mu f_L &= \partial_\mu - igW_\mu^a t^a - i\frac{g'}{2}q_{Y_L}B_\mu \ , \\ D_\mu f_R &= \partial_\mu - i\frac{g'}{2}q_{Y_R}B_\mu \ . \end{aligned} \tag{2.7}$$

With the help of this, it is possible to write a gauge invariant interaction between a fermionic field and the gauge fields,

$$\mathcal{L}_f = \overline{f}_L i\gamma^\mu D_\mu f_L + \overline{f}_R i\gamma^\mu D_\mu f_R \ . \tag{2.8}$$

Since left- and right-handed fermion fields transform as different representations under $SU(2)_L \times U(1)_Y$, an explicit Dirac mass term, which has the chiral structure

$$-m\overline{f}f = -m\left(\overline{f}_L f_R + \overline{f}_R f_L\right) \ , \tag{2.9}$$

is forbidden in the SM. This can be easily deduced from the tensor product decomposition in $SU(2)$. The left-handed fermion in doublet representation and the right-handed fermion in singlet representation together form a doublet according to the tensor product decomposition $\mathbf{2} \otimes \mathbf{1} = \mathbf{2}$. We will see in Section 2.2 that more ingredients are necessary to achieve fermion masses in a chiral theory. Evidently, a non-chiral theory is much simpler in this respect. If left- and right-handed components of the fermion field transform the same way, mass terms will no longer be forbidden by gauge invariance. Fermions with this property are usually called vector-like and play a mayor role in the mechanisms we present in Chapter 4 and 5 of this work.

2.2 Electroweak symmetry breaking

To coincide with experimental observations, a mechanism is needed that generates masses for the gauge bosons W and Z while keeping the photon γ a massless particle at the same time. On the other hand, a successful theory should also be capable of explaining massive fermions. In the SM, this is achieved by spontaneous symmetry breaking. The combination of left-chiral charge and hypercharge is broken to electromagnetic charge (EM):

$$SU(2)_L \times U(1)_Y \to U(1)_{\mathrm{EM}} \ .$$

The remnant symmetry in the broken theory has rank one and therefore possesses one massless force carrier, the photon. To achieve this, an uncolored complex scalar field ϕ which is in the doublet representation of $SU(2)_L$ and carries $Y = 1$ hypercharge is introduced. This particle is commonly known as the Higgs field. Under certain conditions, the Higgs boson can develop a vacuum expectation value (VEV) and thereby triggers electroweak symmetry breaking. To describe the dynamics of the additional scalar field, further terms are added to the Lagrangian

$$\mathcal{L}_{scalar} = (D_\mu \phi)^\dagger (D^\mu \phi) - V(\phi) \ , \tag{2.10}$$

where the covariant derivative for ϕ is

$$D_\mu \phi = \left(\partial_\mu - igW_\mu^a t^a - i\frac{g'}{2}B_\mu\right)\phi \ , \tag{2.11}$$

and the scalar potential includes the following gauge invariant quadratic and quartic terms:

$$V(\phi) = \mu^2 \phi^\dagger \phi + \lambda(\phi^\dagger \phi)^2 \ . \tag{2.12}$$

For $\mu^2 < 0$, the potential spontaneously develops a non-zero vacuum expectation value $\langle\phi\rangle \neq 0$ which breaks the electroweak symmetry to $U(1)_{\mathrm{EM}}$. During that process, masses are generated for those gauge bosons which correspond to the broken generators of the symmetry. In the potential, λ defines the quartic coupling parameter and for $\lambda > 0$ the vacuum is stable. To successfully break to $U(1)_{\mathrm{EM}}$, the structure of the Higgs VEV needs to be

$$\langle\phi\rangle = \frac{1}{\sqrt{2}} \begin{pmatrix} 0 \\ v \end{pmatrix} , \tag{2.13}$$

which means the VEV v resides in the neutral charge component of ϕ. Minimization of the scalar potential reveals that the minimum satisfies $v^2 = -\mu^2/\lambda$. Then, gauge boson masses are generated via the kinetic term

$$(D_\mu\phi)^\dagger(D^\mu\phi) \supset \frac{v^2}{8} g^2(W_\mu^1 + iW_\mu^2)(W^{1\mu} - iW^{2\mu}) + \frac{v^2}{8}(gW_\mu^3 - g'B_\mu)(gW^{3\mu} - g'B^\mu) \ . \tag{2.14}$$

In the current basis, it is not immediately clear which gauge bosons pick up a mass. Therefore, one has to do a basis rotation in order to identify the mass eigenstates. By redefining

$$\begin{aligned} W_\mu^\pm &= \frac{W_\mu^1 \mp iW_\mu^2}{\sqrt{2}} , \\ Z_\mu &= \frac{-g'B_\mu + gW_\mu^3}{\sqrt{g^2 + g'^2}} , \end{aligned} \tag{2.15}$$

one can show that the W and Z bosons are now massive particles and their masses are given by the expressions

$$M_Z^2 = \frac{(g^2 + g'^2)v^2}{4} , \qquad M_W^2 = \frac{g^2 v^2}{4} \ . \tag{2.16}$$

The fourth state, which is defined orthogonal to the Z, is given by the linear combination

$$A_\mu = \frac{-gB_\mu + g'W_\mu^3}{\sqrt{g^2 + g'^2}} \ . \tag{2.17}$$

It represents the massless photon with $M_A^2 = 0$, associated to the unbroken residual symmetry $U(1)_{\mathrm{EM}}$. By defining the weak mixing angles

$$\sin\theta_w = g'/(\sqrt{g^2 + g'^2}) , \qquad \cos\theta_w = g/(\sqrt{g^2 + g'^2}) ,$$

the mass of the Z boson can be rewritten as $M_Z = gv/(2\cos\theta_w)$. The Glashow-Salam-Weinberg theory therefore predicts the tree level relation

$$\frac{M_W}{M_Z} = \cos\theta_w \ . \tag{2.18}$$

As a measure of the deviation from that relation, the ρ-parameter

$$\rho \equiv \frac{M_W}{M_Z \cos\theta_w} \ , \tag{2.19}$$

is introduced. Experimental tests currently constrain $\rho_{exp} = 1.00038 \pm 0.00020$ [31], which agrees well with the predicted value. Small deviations from the tree level value $\rho_{tree} = 1$ are expected and can be explained in the SM by higher order corrections. This shows how the GSW theory successfully describes our current observations and seriously constrains other models. In more general terms, a set of scalars φ_i $(i = 1, ..., n)$, of which each has a VEV v_i, weak isospin T_i and third component of weak isospin T_{3i}, contributes to the tree level ρ parameter as

$$\rho_{tree} = \frac{\sum_i^n \left[T_i(T_i+1) - T_{3i}^2\right] |v_i|^2}{2\sum_i T_{3i}|v_i|^2} \ , \tag{2.20}$$

assuming charge conservation [100]. The relation $\rho_{tree} = 1$ is trivially fulfilled by $SU(2)$ doublets, but constrains higher dimensional scalar representations and their VEVs.

Since the Higgs boson is a complex doublet there are in total four degrees of freedom added. Expanding these degrees of freedom around the minimum of the potential yields

$$\phi = \frac{1}{\sqrt{2}} \begin{pmatrix} G_1^+ + iG_2^+ \\ v + h + iG^0 \end{pmatrix} \ . \tag{2.21}$$

Only one of these fields corresponds to a physical particle with mass $M_h^2 = 2\lambda v^2$, whereas the others are Goldstone bosons of the spontaneously broken symmetry and become the longitudinal degrees of freedom for the massive gauge bosons. As such, a complex scalar field in the doublet representation of $SU(2)$ fits exactly to describe our observation of massive W and Z bosons plus a neutral scalar particle, the Higgs boson.

The fact that the Higgs boson is in the fundamental representation of $SU(2)$ gives rise to a remarkable coincidence. As a weak doublet, it also allows to introduce a coupling between left- and right-handed fermions, because the $SU(2)$ tensor product $\mathbf{2} \otimes \mathbf{2} \otimes \mathbf{1} = \mathbf{1} \oplus \mathbf{3}$ includes a singlet now. Defining the conjugate field $\tilde{\phi} \equiv -i\tau^2\phi^*$, Yukawa couplings to quarks and charged leptons are possible and we describe them through the Lagrangian

$$\mathcal{L}_{Yuk} = -Y_{ij}^u \overline{Q}_{iL} \tilde{\phi} u_{jR} - Y_{ij}^d \overline{Q}_{iL} \phi d_{jR} - Y_{ij}^e \overline{\Psi}_{iL} \phi \ e_{jR} + h.c. \ . \tag{2.22}$$

As a reminder, we note that the indices i and j live in family space. Hence, the couplings Y^u, Y^d and Y^e are 3×3 matrices, which are in general non-diagonal. From the definition of $\tilde{\phi}$, it becomes clear that the field transforms like $\tilde{\phi} \sim (\mathbf{1}, \mathbf{2}, -1)$ under the SM gauge group and its VEV resides in the upper component of the doublet:

$$\langle \tilde{\phi} \rangle = \frac{1}{\sqrt{2}} \begin{pmatrix} v \\ 0 \end{pmatrix} \ . \tag{2.23}$$

This is an important property of $SU(2)$ and allows to write down the Yukawa couplings to up- and down-type quarks as well as charged leptons with only one scalar field. When the Higgs obtains a VEV, the fermions acquire the masses

$$\mathcal{L} \supset -m^u_{ij}\overline{u}_{iL}u_{jR} - m^d_{ij}\overline{d}_{iL}d_{jR} - m^e_{ij}\overline{e}_{iL}e_{jR} + h.c. \;, \tag{2.24}$$

with the mass matrices given by

$$m^u_{ij} = \frac{Y^u_{ij}v}{\sqrt{2}} \;, \qquad m^d_{ij} = \frac{Y^d_{ij}v}{\sqrt{2}} \;, \qquad m^e_{ij} = \frac{Y^e_{ij}v}{\sqrt{2}} \;. \tag{2.25}$$

Due to the missing ν_R, it is not possible to write down a mass term for neutrinos in a similar way as for the other fermions in the Standard Model. We discuss possible solutions to this issue in the next section.

To find the physical mass basis for the fermions, it is necessary to diagonalize the mass matrices in Eq. (2.25) by a bi-unitary transformation. In general, the matrices for up- and down-type quarks cannot be diagonalized simultaneously. This misalignment leads to physical observable effects in charged current interactions, where the Lagrangian is given by

$$\mathcal{L}_{CC} \supset \overline{u}_L\gamma^\mu W^+_\mu d_L = \overline{\hat{u}}_L V_u \gamma^\mu W^+_\mu V^\dagger_d \hat{d}_L \;. \tag{2.26}$$

In above notation, $\hat{..}$ indicates the mass eigenstates and $V_{u/d}$ are the matrices transforming between the flavor and the mass eigenbasis. Note that we suppress flavor indices for a better readability. The product of the two rotation matrices $V_{CKM} \equiv V_u V^\dagger_d$ is the Cabibbo–Kobayashi–Maskawa (CKM) matrix and parameterizes the mixing between different quark flavors that occurs in charged current weak interactions. In general, its elements are written in the form

$$V_{CKM} = \begin{pmatrix} V_{ud} & V_{us} & V_{ub} \\ V_{cd} & V_{cs} & V_{cb} \\ V_{td} & V_{ts} & V_{tb} \end{pmatrix} \;, \tag{2.27}$$

and the magnitude of each of the elements is experimentally determined with a precision of a few percent by now [31]. Contrary to the charged current interaction, the effect of flavor changing cannot be observed in neutral current interactions, as the rotation matrices transforming between the different bases simply drop out. Therefore, there are no tree level flavor changing neutral currents (FCNCs) in the Standard Model.

An equivalent to the CKM matrix in the lepton sector is given by the so-called Pontecorvo–Maki–Nakagawa–Sakata (PMNS) matrix which will be discussed in the next sections together with possible neutrino mass generation mechanisms.

2.3 Motivation for physics beyond the Standard Model

During the last sections, we already pointed at some questions that are unanswered by the SM. These can be roughly categorized into two different kind of problems. On the one hand, there is a number of experimental observations that have been made but cannot be explained by the Standard Model. This kind of problem demands for an explanation and therefore necessitates extensions to the Standard Model. Examples for this category are the origin of neutrino masses, dark matter and the baryon asymmetry of the universe. On top of that, there is a number of experimental anomalies where measured observables deviate from the Standard Model prediction. Ongoing experimental effort has to reveal whether these anomalies persist also in the future.

On the other hand, there are some puzzling features of the SM from a theoretical point of view. Prominent examples for this category are the flavor puzzle, the strong CP problem and the electroweak hierarchy problem. Even though the Standard Model can parameterize many of the observations related to these topics, it cannot give a deeper explanation for the size of the involved parameters. In the following section, we give a short overview on the different motivations mentioned so far. Details for the flavor puzzle, the basic incentive for this work, are presented in Chapter 3.

2.3.1 Experimental evidences

Neutrino masses

The first measurement of solar neutrinos in the 1960s in the Homestake experiment by Raymond Davis Jr. was a great success but its result gave rise to the puzzling question: Why was the observed electron neutrino flux well below the theoretical predictions? At the same time, the Super-Kamiokande experiment measured a deficit in the atmospheric neutrino flux [101]. Both these phenomena could be explained by neutrino oscillations and in 2001 the Sudbury Neutrino Observatory finally confirmed that neutrinos from the sun oscillate to a different flavor [102].[2] This elementary discovery solved a puzzle that persisted over thirty years and was awarded with the Nobel prize in 2015. However, it gave rise to a further question. Neutrino oscillation does not only imply that neutrinos can change their flavor while propagating, but it also implies that neutrinos are massive.

This can be easily illustrated in a simple two flavor scenario. Neutrino oscillation is a phenomenon that occurs because neutrinos are produced (detected) as flavor eigenstates $\nu_{\alpha/\beta}$ in weak interactions but propagate as mass eigenstates $\nu_{1/2}$, the stationary states of the free Hamiltonian. In general, these two bases are not aligned but can be related by a unitary matrix

$$\begin{pmatrix} \nu_\alpha \\ \nu_\beta \end{pmatrix} = \begin{pmatrix} \cos\theta & \sin\theta \\ -\sin\theta & \cos\theta \end{pmatrix} \begin{pmatrix} \nu_1 \\ \nu_2 \end{pmatrix} . \tag{2.28}$$

The oscillation probability at a distance L from the source is then given by

$$P_{\nu_\alpha \to \nu_\beta} = \sin^2(2\theta) \sin^2\left(\frac{\Delta m^2 L}{4E_\nu}\right) , \tag{2.29}$$

[2] The basic ingredient to the solution of the solar neutrino problem is the Michejew-Smirnow-Wolfenstein (MSW) effect [71, 103].

where $\Delta m^2 \equiv m_2^2 - m_1^2$ is the squared mass difference between two mass eigenstates. If both neutrinos are massless or the mixing angle θ vanishes, the probability will be zero and no oscillations will occur.

In a complete setup with three light neutrinos, which is favored by LEP data, the oscillation probability depends on two mass squared differences Δm_{21}^2 and Δm_{31}^2, three mixing angles θ_{13}, θ_{12}, θ_{23} and one CP violating phase. With Δm_{21}^2 and Δm_{31}^2 non-vanishing, at most one of the three neutrinos can be massless. Since the sign of Δm_{31}^2 is unknown, there are two possible variants of mass ordering which are called normal hierarchy (NH) and inverted hierarchy (IH):

$$m_1 < m_2 < m_3 \text{ (NH)}, \qquad m_3 < m_1 < m_2 \text{ (IH)} . \tag{2.30}$$

The actual size of the neutrino mass is currently not known, but there is a lot of experimental effort to determine their absolute values. For example, the Karlsruhe Tritium Neutrino Experiment (KATRIN) aims to measure the absolute mass scale of neutrinos emitted in tritium beta decays and puts the upper limit

$$m_\nu < 0.8\text{eV (90\% CL)} \tag{2.31}$$

on the effective electron anti-neutrino mass which is defined by $m_\nu^2 = \sum |U_{ei}^2| m_i^2$ [27]. Cosmological bounds deduced from the cosmic microwave background by the PLANCK collaboration constrain the sum of neutrino masses to [28]

$$\sum_i m_{\nu_i} < 0.12 \text{ eV} . \tag{2.32}$$

Only recently, there was an additional result by the DESI collaboration, which reported [29]

$$\sum m_\nu < 0.072 \text{ eV (95\% CL)} . \tag{2.33}$$

This has to be compared with the lower bound on the sum of neutrino masses which can be obtained from the measured squared mass difference under the assumption that the lightest neutrino is massless,

$$\sum_i m_{\nu_i} \gtrsim 0.06\text{eV (NH)} , \qquad \sum_i m_{\nu_i} \gtrsim 0.1\text{eV (IH)} . \tag{2.34}$$

Taken at face value, the outcome of the DESI study disfavors IH. However, the result needs to be treated with caution as it is not independent from assumptions and chosen priors. As explained in the previous section, it is not possible to give mass to neutrinos in the Standard Model. One of the simplest solutions to this problem would be to extend the particle content by three right-handed neutrinos with gauge charge $\nu_R \sim (\mathbf{1}, \mathbf{1}, 0)$. Then, one can add the Yukawa coupling terms

$$\mathcal{L}_{Yuk} \supset -Y^\nu \overline{\Psi}_L \tilde{\phi} \nu_R + h.c. \xrightarrow{\text{SSB}} -m_D \overline{\nu}_L \nu_R + h.c. , \tag{2.35}$$

with $m_D \equiv Y^\nu v/\sqrt{2}$ which gives mass to neutrinos after EWSB. However, this seemingly small change in the particle content has a big consequence. Since the fields ν_R do not carry $U(1)_Y$ charge, it is not forbidden by any gauge charge to write down the bare mass term

$$\mathcal{L} \supset -\frac{1}{2} M_R \overline{\nu}_R \nu_R^c + h.c. \ , \tag{2.36}$$

where ν_R^c is the charge conjugated field. This term violates lepton number by two units. It would therefore stand out from the rest of the SM which accidentally preserves lepton number. If present, the neutrino will be its own antiparticle, also called a Majorana fermion. Eqs. (2.35) and (2.36) together yield the complete neutrino mass matrix

$$\mathcal{L} \supset -\frac{1}{2} \begin{pmatrix} \overline{\nu}_L & \overline{\nu^c}_R \end{pmatrix} \begin{pmatrix} 0 & m_D \\ m_D^T & M_R \end{pmatrix} \begin{pmatrix} \nu_R \\ \nu_L^c \end{pmatrix} \ . \tag{2.37}$$

In the limit $M_R \gg m_D$,[3] diagonalization reveals three light and three heavy eigenvalues

$$m_{light} \approx \frac{1}{2} m_D^T M_R^{-1} m_D \ , \qquad m_{heavy} \approx M_R \ . \tag{2.38}$$

This mechanism is widely known as type I seesaw mechanism and can explain the small neutrino masses by suppression via a large scale M_R [62–64]. For instance, for $Y^\nu \sim \mathcal{O}(1)$, neutrino masses below the eV scale are obtained for $M_R \sim \mathcal{O}(10^{14}\mathrm{GeV})$. In the effective field theory (EFT) picture, the type I seesaw mechanism is one out of three minimal possibilities to open the dimension five lepton number violating (LNV) Weinberg operator [104]

$$\mathcal{L}_{EFT} = \frac{y_{eff}}{\Lambda} \left(\overline{\Psi_L^c} \tilde{\phi}^* \right) \left(\tilde{\phi}^\dagger \Psi_L \right) \ , \tag{2.39}$$

which generates Majorana masses for neutrinos when ϕ develops a VEV. The structure of the operator shows a suppression with respect to the scale of new physics Λ and its strength depends on the effective coupling y_{eff} of the explicit realization. The other two options to complete the Weinberg operator in a ultraviolet (UV) theory include a $SU(2)_L$ triplet scalar [65–68] or a $SU(2)_L$ triplet fermion [69].

It is experimentally challenging to reveal whether the neutrino nature is Dirac or Majorana. A consequence of the Majorana nature would be the existence of neutrinoless double beta decay ($0\nu\beta\beta$). In this process the neutrino emitted in a beta decay is directly absorbed by a second simultaneous beta decay in the same nucleus. The decay rate for $0\nu\beta\beta$ depends on the phase space factor G and the nuclear matrix element M and is given by

$$\Gamma_{0\nu\beta\beta} = G|M|^2 m_{\beta\beta}^2 \ , \tag{2.40}$$

[3]When the entries of the matrix M_R are of the order $\mathcal{O}(\mu_R)$ and those of m_D are $\mathcal{O}(\mu_D)$, then we consider the limit $\mu_R \gg \mu_D$.

where $m_{\beta\beta} \equiv \sum_i U_{ei}^2 m_i$. Evidently, this process is suppressed through the small neutrino mass. So far $0\nu\beta\beta$ was never observed. For example, the GERDA experiment currently constrains the half-life for $0\nu\beta\beta$ decay of ^{67}Ge to [105]

$$T_{1/2}^{0\nu\beta\beta}(^{67}\mathrm{Ge}) > 1.8 \times 10^{26}\mathrm{yr}\ (90\%\ \mathrm{C.L.})\ . \tag{2.41}$$

The non-observation of $0\nu\beta\beta$ does however not imply that neutrinos are not Majorana particles. If there is an unlucky cancellation of parameters, $m_{\beta\beta}$ will be zero in case of NH and $0\nu\beta\beta$ will never be observed.

Dark matter

Even though we gained a lot of knowledge about the character of baryonic matter in the last centuries, there is a huge proportion of matter with largely unknown properties. Its observation so far only relates to gravitational effects and therefore gave birth to the term Dark Matter (DM). The plethora of different observations which has established that DM indeed exists ranges from observation of small scales like galaxies to the largest observable scales in cosmology. One of the most convincing evidences is given by the velocity profile of stars circulating around the central bulge of spiral galaxies. Against expectation, the rotation velocity does not decrease with increasing distance from the center, but rather stays constant [106, 107]. This suggests a matter distribution different from the visible one. Other observations such as cosmic microwave background anisotropies or the difference of total mass to visible mass distribution in the bullet cluster permit an explanation with DM as well [108, 109]. In the current standard model of cosmology, the DM density is described by

$$\Omega_{DM} h^2 = 0.1200 \pm 0.0012\ , \tag{2.42}$$

where $\Omega_i \equiv \rho_i/\rho_c$ represents the relative density to the critical density. Todays Hubble constant is measured as $H_0 = h \cdot 100$ km s^{-1} Mpc^{-1} and $h = 0.674 \pm 0.005$ [110]. This yields $\Omega_{DM} = 0.264 \pm 0.003$ and shows that DM accounts for 26.4% of the total energy density today. In comparison, baryonic matter constitutes only 4.9% and radiation 0.0091%, leaving the largest portion to dark energy $\Omega_\Lambda \simeq 68.5\%$ [111]. Structure formation with relativistic DM particles would not have been effective and therefore suggests DM to be non-relativistic (cold). The SM does not offer such a candidate for cold DM.

Matter-antimatter asymmetry

The visible universe is formed out of atoms which are in turn composed of electrons, protons and neutrons. In contrast, structures or regions populated with a large fraction of antiparticles are not observed. The origin of the dominance of matter over antimatter supposedly formed in the early universe and the baryon (B) to antibaryon ($\overline{B}$) asymmetry can be quantified in terms of their respective number densities in relation to the photon number density

$$\frac{n_B - n_{\overline{B}}}{n_\gamma} \sim 10^{-9} \ , \tag{2.43}$$

which is known from the abundance of light isotopes produced in big bang nucleosynthesis [31]. In simpler terms, the ratio illustrates that for each 10^9 antibaryons there were $10^9 + 1$ baryons, annihilating to photons and leaving behind a single baryon. According to Sakharov, three conditions are necessary to form this asymmetry: First, there must be baryon number violation, second, C and CP needs to be violated and third, there must be a departure from thermal equilibrium [112]. Even though in principle there is CP violation in the Standard Model, the effect is too small. It cannot explain the observed asymmetry and new physics is therefore needed.

Anomalies

Over time, experiments measured a plethora of different processes and it is only natural to expect that some fraction of them deviates from the Standard Model expectation due to statistical fluctuation. When a discrepancy between theory and experiment exists over a long time and is confirmed by different experiments, this can potentially point towards new physics. An example of such a long standing anomaly is the anomalous magnetic moment of the muon, defined by $a_\mu \equiv (g_\mu - 2)/2$ [85, 86, 113–115]. Measurements of a_μ at Brookhaven National Lab (BNL) and Fermilab National Accelerator Laboratory (FNAL) are consistent with each other but show a 4.2σ discrepancy with the data driven SM prediction [31]:

$$\Delta a_\mu = a_\mu^{exp} - a_\mu^{SM} = 251(41)(43) \times 10^{-11} \ . \tag{2.44}$$

For the SM prediction, it is necessary to calculate the higher order loop corrections to a_μ^{SM}. Especially, the hadronic contribution a_μ^{Had} is subject of ongoing debate, as the data-driven dispersion relation approach and lattice calculations differ by 2.2σ [116]. Interestingly, the tension in Δa_μ would be alleviated if the lattice result for a_μ^{Had} were used. Nonetheless, it is worth to consider new physics models that can potentially lead to such signatures and we discuss some of them in Chapter 6. Of course the magnetic moment of the muon is not the only measured anomaly. Another prominent example in the neutino sector is the MiniBooNE anomaly which describes an excess of ν_e and $\overline{\nu_e}$ events in charged-current quasi-elastic scattering. Currently, it is at a significance of 4.7σ and subject of ongoing investigations [117–119].

2.3.2 Theoretical motivations

The flavor puzzle

The flavor puzzle summarizes several puzzling questions related to the flavor sector in the SM. First of all, it deals with the issue why we observe exactly three generations of fermions. The duplication of each fermion representation has no deeper origin so far, but having exactly the same number of generations in the quark and lepton sector creates the impression that a deeper mechanism might be at work. Of course, it could turn out that the three generations are merely a coincidence. In this case however, one is still confronted with the weird fact that the fermion masses cover a large range of scales. From the mass of the electron $\mathcal{O}(100 \text{ keV})$ to the top quark mass $\mathcal{O}(100 \text{ GeV})$, the SM already spans six order of magnitude. Including sub-eV neutrino mass enhances this to twelve orders. Even within one fermion species, masses are hierarchical and hence the Yukawa sector is the only part of the SM which does not treat fermions of the same representation on an equal footing. Furthermore, the mixing that occurs in the quark and lepton sector is fundamentally different. While the CKM matrix is close to diagonal, the PMNS matrix exhibits rather large mixing angles. Finally, the flavor puzzle is also closely connected to the origin of CP violation, as three generations of quarks are the minimal requirement for the appearance of a CP violating phase in the CKM matrix, which is experimentally established.

Strong CP problem

Even though there is no experimental sign of CP violation in the strong interaction, the QCD gauge symmetry allows the charge-parity violating term

$$\mathcal{L}_{QCD} \supset \frac{\theta g^2}{32\pi^2} G^a_{\mu\nu} \tilde{G}^{a\mu\nu} \ , \tag{2.45}$$

where $\tilde{G}^{a\mu\nu} \equiv \frac{1}{2}\epsilon^{\mu\nu\rho\sigma} G^a_{\rho\sigma}$ is the gluon dual field strength tensor. The size of this term is determined by the parameter θ. However, it is not a physical parameter, as a chiral rotation on the quark fields can generate a term of the same kind in the Lagrangian by the chiral anomaly. The parameter that has physical consequences involves the quark mass matrices $M_{u/d}$ and is defined as

$$\overline{\theta} = \theta + \mathrm{Arg}(\mathrm{Det}[M_u M_d]) \ . \tag{2.46}$$

If there was large CP violation in the strong interaction, this would induce a large neutron electric dipole moment. Its non-observation constrains the parameter $\overline{\theta} \leq 10^{-10}$, although there is a priori no reason why it should be so small. This phenomenon is commonly known as the strong CP problem. Several new physics models attempt to explain the smallness of $\overline{\theta}$. In one approach, called the Peccei-Quinn mechanism, $\overline{\theta}$ is promoted to a field which dynamically relaxes to zero [120–122]. Other attempts in the framework of left-right symmetric models start with a parity symmetric theory. The spontaneous breaking of parity induces a small $\overline{\theta}$ only at the two-loop level explaining its smallness [56, 123].

Naturalness

In the SM, there is only one fundamental scalar, the Higgs boson ϕ. Its mass term, described by $\mu^2\phi^\dagger\phi$, is invariant under gauge and global symmetries, i.e. the case $\mu^2 = 0$ does not enhance the symmetry of the theory. This is contrary to the case of fermion masses which are protected by chiral symmetry [124]. The Higgs mass is therefore particularly vulnerable to radiative corrections that enter quadratically in the cut-off scale Λ

$$\delta m_\phi^2 \sim \frac{\lambda^2}{16\pi^2}\Lambda^2 \; . \tag{2.47}$$

To achieve a physical mass at the electroweak scale, a tuning of the tree level mass against the radiative corrections is necessary, as $m_\phi^2(\text{phys}) = m_\phi^2(\text{tree}) + \delta m_\phi^2$. If the cut-off was chosen to be the Planck scale, one would need a tuning of 10^{-28} to achieve a Higgs mass at the electroweak scale [125]. This high amount of tuning raises suspicion and is considered as unnatural.

Chapter 3

The flavor puzzle and theoretical concepts to address it

In the previous chapter we already pointed out the main questions that are covered by the flavor puzzle, namely, the existence of three generations of fermions together with their hierarchical mass scales and the appearance of differing mixing schemes in the quark and lepton sector. To consider these issues in more detail, it is helpful to look at the flavor sector of the Standard Model from the viewpoint of symmetries. The SM Lagrangian parts $\mathcal{L}_{gauge}$, $\mathcal{L}_f$ and $\mathcal{L}_{scalar}$, as introduced in Eq. (2.1), possess a larger symmetry than the one that is gauged. Accidentally, they also preserve the global symmetry [126]

$$G_{global} = SU(3)_Q \times SU(3)_u \times SU(3)_d \times SU(3)_\Psi \times SU(3)_e \times U(1)^5 \ . \tag{3.1}$$

The $SU(3)$ groups act on fermions of the same representation and transform one fermion generation into another (Q, u, d, Ψ, e are the irreducible fermion representations as defined in Table 2.1). Once the Yukawa sector $\mathcal{L}_{Yuk}$ is included to these considerations, the global symmetry in Eq. (3.1) is no longer preserved and the residual global symmetry of the complete SM reduces to $U(1)_B \times U(1)_{L_e} \times U(1)_{L_\mu} \times U(1)_{L_\tau}$, i.e. baryon number and the three separate flavors of lepton number [127]. At the same time, the Yukawa sector gives rise to the majority of parameters that are needed to describe the SM. Out of the total 19 parameters, only three gauge couplings and two scalar couplings are unrelated to flavor. The remaining 14 parameters are needed to describe six quark masses, three lepton masses, three quark mixing angles, one CKM CP phase and a strong CP violating angle. If one incorporates neutrino masses and mixing into a more complete theory, the amount of parameters will increase even further by at least three neutrino masses, three mixing angles, a Dirac CP phase and two Majorana CP phases (depending on the nature of the neutrino). In the following chapter, we first present the current status of measuring the SM parameters in the flavor sector. After a short discussion of experimental constraints on further generations of fermions, we give an overview on theoretical concepts that address the flavor puzzle.

3.1 The flavor puzzle in numbers

3.1.1 Lepton sector

The masses of charged leptons are experimentally determined with a very high precision. Their current values are given by [31]

$$\begin{aligned} m_e &= 0.51099895000 \pm 0.00000000015 \text{ MeV} , \\ m_\mu &= 105.6583755 \pm 0.0000023 \text{ MeV} , \\ m_\tau &= 1776.86 \pm 0.12 \text{ MeV} . \end{aligned} \tag{3.2}$$

and we visualize the emerging scales in Figure 1.1 together with the masses of other SM fermions. The most precise of these values, the electron mass, is measured in Penning traps where the Larmor frequency of electrons is compared to that of trapped ions [128]. The mass of the electron is therefore known very well in atomic units, and the conversion to MeV dominates the error given above. Zeemann spectroscopy with muonium, a μ^+e^- bound state, then allows to obtain the relative size of m_μ/m_e [129]. In comparison to the first two generations, the τ mass is known with less precision. Its value is either measured by the reconstruction of invariant mass in hadronic τ decays, or by studying the $e^+e^- \to \tau^+\tau^-$ cross section near the τ mass threshold [130, 131].

Contrary to charged leptons, the absolute neutrino mass scale is not yet known. Still, oscillation experiments allow to constrain the squared mass differences and their current best fit values from global analysis are given by [30]

$$\begin{aligned} \Delta m_{21}^2 &= (7.41^{+0.21}_{-0.20}) \times 10^{-5} \text{eV}^2 , \\ \Delta m_{31}^2 &= (2.511^{+0.027}_{-0.027}) \times 10^{-3} \text{eV}^2 \text{ (NO)} , \\ \Delta m_{32}^2 &= (-2.498^{+0.032}_{-0.024}) \times 10^{-3} \text{eV}^2 \text{ (IO)} . \end{aligned} \tag{3.3}$$

Especially solar neutrino experiments, such as SNO, Super-Kamiokande and Borexino, are sensitive to the smaller mass splitting Δm_{21}^2 [132–134] and its absolute sign is determined from the resonance condition of the MSW effect [71, 103]. On the other hand, atmospheric neutrino experiments allow to determine $|\Delta m_{31}^2|$ [135]. Still, its sign is not constrained so far which leads to two possible mass orderings in the neutrino sector. The detailed study of neutrino oscillations also permits to constrain parameters of the PMNS mixing matrix. For a general setup with n generations, the PMNS matrix is described by an $n \times n$ unitary matrix which possesses n^2 free parameters. These divide into $n(n-1)/2$ Euler angles and $n(n+1)/2$ phases. However, many of these phases are not physical and can be absorbed by a redefinition of the fermion fields. If neutrinos are Dirac, further $2n-1$ phases will be absorbed which will yield $1/2(n-1)(n-2)$ physical phases in total. In the standard $n = 3$ generations picture this amounts to three mixing angles and one phase δ_{CP} which are in principle accessible in oscillation experiments. Interestingly, two further phases would be present in the PMNS matrix if neutrinos were Majorana particles. Even though many parameterizations of the PMNS matrix are possible, the commonly used one is given by

$$U_{PMNS} = \begin{pmatrix} c_{12}c_{13} & s_{12}c_{13} & s_{13}e^{-i\delta_{CP}} \\ -s_{12}c_{23} - c_{12}s_{23}s_{13}e^{i\delta_{CP}} & c_{12}c_{23} - s_{12}s_{23}s_{13}e^{i\delta_{CP}} & s_{23}c_{13} \\ s_{12}s_{23} - c_{12}c_{23}s_{13}e^{i\delta_{CP}} & -c_{12}s_{23} - s_{12}c_{23}s_{13}e^{i\delta_{CP}} & c_{23}c_{13} \end{pmatrix} P \quad (3.4)$$

where $s_{ij} \equiv \sin(\theta_{ij})$ and $c_{ij} \equiv \cos(\theta_{ij})$ are the mixing angles and the matrix P includes two Majorana phases $\eta_{1/2}$

$$P = \begin{pmatrix} e^{i\eta_1} & 0 & 0 \\ 0 & e^{i\eta_2} & 0 \\ 0 & 0 & 1 \end{pmatrix} . \quad (3.5)$$

The current best fit values for the mixing angles from global analysis are given by [30]

$$\sin^2\theta_{12} = 0.307^{+0.012}_{-0.011} , \quad \sin^2\theta_{23} = 0.572^{+0.018}_{-0.023} , \quad \sin^2\theta_{13} = 0.02203^{+0.00056}_{-0.00058} , \quad (3.6)$$

assuming normal ordering, whereas those for inverted ordering are

$$\sin^2\theta_{12} = 0.307^{+0.012}_{-0.011} , \quad \sin^2\theta_{23} = 0.578^{+0.016}_{-0.021} , \quad \sin^2\theta_{13} = 0.02219^{+0.00059}_{-0.00057} . \quad (3.7)$$

While $\sin^2\theta_{12}$ is most precisely known from solar neutrino experiments [132–134], atmospheric [135] and reactor experiments [136] provide information on $\sin^2\theta_{23}$ and $\sin^2\theta_{13}$, respectively. Knowledge about the Dirac CP phase can be retrieved from the long baseline accelerator experiments NOνA and T2K [137,138]. Within the 3σ experimental uncertainty, the current best fit value covers a wide range

$$\delta_{CP} = (108 - 404)^\circ \text{ (NO)} , \qquad \delta_{CP} = (192 - 360)^\circ \text{ (IO)} , \quad (3.8)$$

which includes the CP violating case ($\delta_{CP} = 270^\circ$) as well as the CP conserving case ($\delta_{CP} = 180^\circ$). A decisive answer whether CP violation is present in the lepton sector therefore needs further experimental input and future results of T2K and NOνA hopefully shed light on this in upcoming years. Contrary to the Dirac CP phase, Majorana phases are not observable in oscillation experiments and are therefore still unconstrained.

3.1.2 Quark sector

The experimental determination of quark masses is not straightforward as quarks do not propagate as free particles. Consequently, quark masses need to be deduced from hadron properties and different theoretical tools have to be combined with experimental results. For the three lightest quarks, chiral perturbation theory allows to derive constraints [139]. Since the masses of these quarks are small, the QCD Lagrangian has an approximate

$SU(3)_L \times SU(3)_R$ symmetry.[1] Non-perturbative effects of the strong interaction break this symmetry to the diagonal $SU(3)_V$. Thus, there are eight Goldstone modes (mesons) which obtain a mass since the approximate symmetry is explicitly violated by non-zero quark masses. Treating them as small perturbations yields a relation between the meson and quark masses. To lowest order, the chiral perturbation theory predicts

$$\begin{aligned} \frac{m_u}{m_d} &= \frac{2m_{\pi^0}^2 - m_{\pi^+}^2 + m_{K^+}^2 - m_{K^0}^2}{m_{K^0}^2 - m_{K^+}^2 + m_{\pi^+}^2} = 0.56 \\ \frac{m_s}{m_d} &= \frac{m_{K^0}^2 + m_{K^+}^2 - m_{\pi^0}^2}{m_{K^0}^2 - m_{K^+}^2 + m_{\pi^+}^2} = 20.2 \ , \end{aligned} \tag{3.9}$$

and higher order corrections improve this result [32]. Nonetheless, to determine the absolute mass scale further input from lattice calculations and QCD sum rules is needed. Altogether, the current values for the three light quarks quoted by the PDG are [31]

$$\begin{aligned} m_u &= 2.16^{+0.49}_{-0.26} \text{ MeV} \ , \\ m_d &= 4.67^{+0.48}_{-0.17} \text{ MeV} \ , \\ m_s &= 93.4^{+8.6}_{-3.4} \text{ MeV} \ . \end{aligned} \tag{3.10}$$

For the heavier charm and bottom quark, masses can be determined from quarkonium spectroscopy, i.e. by investigating the properties of charmonium ($\bar{c}c$) and bottonium ($\bar{b}b$) bound states. Together with lattice QCD results, this yields [31]

$$\begin{aligned} m_c &= 1.27 \pm 0.02 \text{ GeV} \ , \\ m_b &= 4.18^{+0.03}_{-0.02} \text{ GeV} \ . \end{aligned} \tag{3.11}$$

Since the top quark decays before hadronization, its mass can be assessed from its decay products. The most precise result stems from the decay to a lepton plus jets final state and the average value given by the PDG is [31]

$$m_t = 172.69 \pm 0.30 \text{ GeV} \ . \tag{3.12}$$

With this, the top quark is the heaviest elementary particle we have discovered so far. Comparing its mass to the electron reveals the large difference of scales $m_e/m_t \approx 10^{-6}$. When we take into account the current upper mass limit for neutrinos, the ratio even reduces to $m_\nu/m_t \lesssim 10^{-12}$.

The mixing of quarks in charged current interactions is described by the 3×3 unitary CKM matrix. In contrast to the PMNS matrix, the diagonal entries of the CKM matrix

[1] The original symmetry is $U(3)_L \times U(3)_R \simeq SU(3)_L \times SU(3)_R \times U(1)_V \times U(1)_A$. The axial $U(1)_A$ is explicitely broken by the chiral anomaly. $U(1)_V$ represents the unbroken baryon number.

are close to one and off-diagonal contributions are suppressed by different orders of $\lambda \simeq 0.2$ according to the following pattern

$$V_{CKM} \simeq \begin{pmatrix} 1 & \lambda & \lambda^3 \\ \lambda & 1 & \lambda^2 \\ \lambda^3 & \lambda^2 & 1 \end{pmatrix} . \tag{3.13}$$

This reveals that the mass bases of up- and down-type quarks are almost aligned, even though they could be in principle arbitrary. More precisely, the absolute values of the CKM matrix entries are measured to be [31]

$$\begin{pmatrix} |V_{ud}| & |V_{us}| & |V_{ub}| \\ |V_{cd}| & |V_{cs}| & |V_{cb}| \\ |V_{td}| & |V_{ts}| & |V_{tb}| \end{pmatrix} = \begin{pmatrix} 0.97373 \pm 0.00031 & 0.2243 \pm 0.0008 & 0.00382 \pm 0.00020 \\ 0.221 \pm 0.004 & 0.975 \pm 0.006. & 0.0408 \pm 0.0014 \\ 0.0086 \pm 0.0002 & 0.0415 \pm 0.0009 & 1.014 \pm 0.029 \end{pmatrix} , \tag{3.14}$$

with errors ranging at the percent level or even below. Many of the CKM elements are measured in weak decays with a semileptonic final state. For example, the element $|V_{ud}|$ can be measured in the nuclear beta decays $n \to p + e^- + \nu_e$ [140]. In a similar manner, the elements $|V_{us}|$,$|V_{cd}|$ and $|V_{cs}|$ are measured in semileptonic decays of Kaons and D-mesons [141, 142], while ones uses B-meson decays to study $|V_{ub}|$ and $|V_{cb}|$ [143]. A direct determination of $|V_{ts}|$ and $|V_{td}|$ via top decays is currently rather imprecise. Therefore, a different strategy is applied and the elements are indirectly determined from neutral meson oscillations of $\overline{B_d^0} - B_d^0$ and $\overline{B_s^0} - B_s^0$ [31]. Finally, the element $|V_{tb}|$ can be extracted from measuring the ratio of branching fractions $\mathrm{Br}(t \to Wb)/\mathrm{Br}(t \to Wq)$ where $q = b, s, d$ [144, 145]. By measuring all these parameters independently, it is possible to overconstrain the CKM matrix which depends only on three mixing angles and one phase in the three generation picture. One possibility is to test unitarity by determining the relation [31]

$$|V_{ud}|^2 + |V_{us}|^2 + |V_{ub}|^2 = 0.9985 \pm 0.0007 , \tag{3.15}$$

which would be equal to one if V_{CKM} were indeed unitary. Similar strategies apply for the second and third row of the CKM matrix. In this case, the first row result shows a mild 2.2σ deviation from the SM. If this discrepancy were confirmed, it could for example point towards additional generations of fermions which would make the three generation description incomplete. Independently from the exact parametrization of the CKM matrix, the Jarlskog invariant is a measure of CP violation in the quark sector [146]. It is defined by

$$J = \mathrm{Im}[V_{ij} V_{kl} V_{il}^* V_{kj}^*] \tag{3.16}$$

and the current experimental bound is given by [31]

$$J = \left(3.08^{+0.15}_{-0.13}\right) \times 10^{-5}. \tag{3.17}$$

Hence, the quark sector is the only part of the SM where we know for sure that CP is violated.

3.2 Constraints on further generations

While all SM parameters are measured more and more precisely, one might wonder whether there is still the possibility for further generations of fermions. After all, there is no reason why there should be exactly three generations in the SM. The presence of a fourth generation would have a number of consequences on experimental observables though. As constraints strongly depend on the gauge charges and properties of these new fermions, it is reasonable to distinguish between different scenarios and consider the two distinct cases of a chiral or a vector-like family.

In the former case, a minimal extension would be to enlarge the SM fermion content by a complete sequential fourth generation with exactly the same gauge charges as the ones of the previous three SM generations (see Table 2.1). This simple model, also sometimes called SM4 [147, 148], is in tension with experimental results though. The reason for this is that the loop induced couplings of the Higgs to gluons (Hgg) and photons ($H\gamma\gamma$) can be sensitive to a further heavy generation of fermions whose couplings to the Higgs boson are proportional to their mass. Further heavy fermions could therefore considerably change the Higgs production and decay rates. But also global fits to electroweak precision observables constrain a fourth sequential generation [22–26].

When we consider vector-like generations of fermions, these limits drastically change. Since left- and right-chiral components of vector-like fermions have the same transformation behavior under the local gauge group of the theory [149], explicit mass terms for vector-like fermions are generally allowed, as we discussed at the end of Section 2.1. Hence, the masses of those fermions are not in correlation with the coupling to the Higgs boson and constraints from Higgs observables are relaxed. Nevertheless, there are limits from direct searches at colliders. Since colored particles unavoidably interact with gluons, a new generation of vector-like quarks would have consequences on direct searches in hadron collisions. The exact bounds depend strongly on the particular gauge representation but when heavy quarks are pair produced and subsequently decay to the top or bottom quark and a W, Z or Higgs boson, constraints on their masses can arise. For example, LHC measurements limit vector-like quarks in the weak doublet or singlet representation with electric charge $+2/3$ or $-1/3$ to be heavier than ~ 1500 GeV [150–152]. On the other hand, vector-like leptons could be produced via s-channel Z or γ exchange in pp collisions. If they were coupled to standard model leptons, searches for multilepton final states would provide constraints on the vector-like mass. The current upper mass limit from LHC measurements is ~ 1000 GeV [153–155]. Future searches at high energy colliders are going to improve these bounds further and we discuss their prospects in Section 4.2.6.

3.3 Theoretical ideas to address the flavor puzzle

By now, we have illustrated in great detail what the flavor sector looks like and pointed out that there is no satisfactory answer to explain the emerging patterns of masses and mixings within the SM. Solutions to the flavor puzzle therefore involve physics beyond the SM, either through new symmetries, new particles or both. In the following we discuss a selection of well known theoretical ideas. Further detailed information can be found in [32]. A basic concept that is used to model large hierarchies starts from the heuristic approach:

$$m_u : m_c : m_t = \epsilon^8 : \epsilon^4 : 1 \ , \qquad m_d : m_s : m_b = \epsilon^4 : \epsilon^2 : 1$$
$$m_e : m_\mu : m_\tau = \epsilon^5 : \epsilon^2 : 1 \ , \qquad V_{ud} \sim 1 \ , \qquad V_{us} \sim \epsilon \ , \qquad V_{ub} \sim \epsilon^3 \ .$$

As such, masses and mixings are parameterized in terms of a suitable expansion parameter $\epsilon < 1$. We will see that ϵ can have different origins and meanings, depending on the explicit model.

Froggatt-Nielson mechanism

Symmetries have proven to be an extremely useful tool in physics and it is therefore only natural to consider them as a possible candidate to resolve the flavor puzzle. An approach in this direction was taken in the late 70s by Froggatt and Nielson [156]. Their basic idea was to introduce an extra $U(1)_{FN}$ charge that distinguishes between the different generations of fermions. The usual SM Yukawa couplings are no longer allowed due to the new symmetry. However, when a flavon field η, which typically carries one unit of the $U(1)_{FN}$ charge, obtains a VEV the symmetry is broken. This allows to generate Yukawa terms at the non-renormalizable level. With a generation dependent charge, the fermion mass is generated effectively by higher dimensional operators

$$\mathcal{L}_{eff} \supset y_{eff} \overline{Q}_{iL} \phi u_{jR} \epsilon^{n_{ij}} \ , \tag{3.18}$$

where the expansion parameter ϵ can be identified with $\epsilon \equiv \langle \eta \rangle / M$ and n_{ij} depends on the exact Froggatt-Nielson charges of the involved fermions. The new mass scale M that appears here usually corresponds to heavy fermions that are integrated out in the low energy effective field theory. For $\epsilon < 1$, the suppression of the Yukawa term can be conveniently controlled by the Froggatt-Nielson charges. Within this mechanism, both the hierarchy in masses and the mixings can be addressed. However, this comes at the cost of introducing new fermions and generation dependent Froggatt-Nielson charges that a priori have no deeper motivation. Furthermore, some aspects of this idea need to be treated with caution. First of all, if $U(1)_{FN}$ is a local gauge symmetry, this will give rise to gauge anomalies unless the fermion charges are assigned in such a way that the anomaly cancels exactly. To avoid this constraint, $U(1)_{FN}$ can be considered a global symmetry though its breaking would then result in a massless Goldstone boson (see [157–160] for a selection of papers studying the Froggatt-Nielson mechanism).

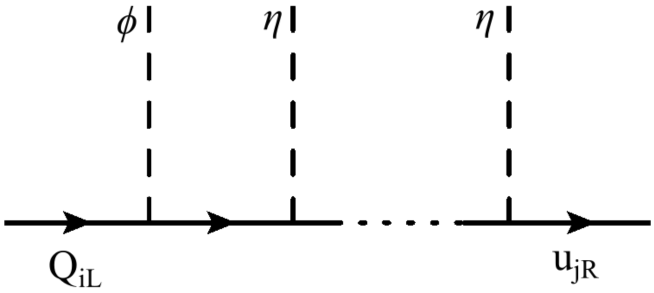

Figure 3.1 Schematic fermion mass generation in the Froggatt-Nielson mechanism.

Discrete flavor symmetries

The idea that a horizontally acting symmetry connects different generations and can therefore explain the apparent patterns in the flavor sector is at the heart of models involving discrete symmetries. Nonetheless, none of the symmetries investigated so far turned out to be explicitly realized in nature and one has to search for remnant patterns of symmetries that are nowadays broken. A key ingredient of the discussion of flavor symmetries is therefore often the precise symmetry breaking patterns. Most beneficial, the breaking of discrete symmetries does not produce Goldstone or gauge bosons and theories are hence less constrained.

Among the large number of discrete groups, A_4, S_4 or $\Delta(27)^2$ were popular targets for research due to their simple structures. The interest was especially pushed in the years before 2011, when it was not clear whether the neutrino mixing angle θ_{13} was going to be different from zero. Back then, the pattern of leptonic mixing was consistent with the matrix

$$U_{TB} = \begin{pmatrix} \sqrt{\frac{2}{3}} & \sqrt{\frac{1}{3}} & 0 \\ -\sqrt{\frac{1}{6}} & \sqrt{\frac{1}{3}} & -\sqrt{\frac{1}{2}} \\ -\sqrt{\frac{1}{6}} & \sqrt{\frac{1}{3}} & \sqrt{\frac{1}{2}} \end{pmatrix} , \tag{3.19}$$

which is also called tri-bimaximal mixing (TBM) [161]. This structure can be nicely explained by the alternating group A_4, which is the group of even permutations of four objects. Besides a three dimensional irreducible representation $\mathbf{3}$, A_4 has three distinct one dimensional representations $\mathbf{1}$, $\mathbf{1}'$ and $\mathbf{1}''$. A number of studies [162–165] investigated the mixing patterns that will appear if the lepton doublets are assigned to the $\mathbf{3}$ while the lepton singlets transform in the $\mathbf{1} + \mathbf{1}' + \mathbf{1}''$ representation. Today, we know that even though θ_{13} is small, it is non-zero and theoretical models can use the TBM as a first order approximation or investigate whether other discrete groups are suitable to explain the patterns found in leptonic mixing. A selection of these models that include non-zero θ_{13} are given in [166–170].

[2] All these discrete groups are subgroups of $SU(3)$ and have a triplet representation to unify the three generations.

Also beyond that, discrete groups have been extensively studied and reviews discussing the most important groups for model building can be found in [33, 171]. Later, studies also discuss possible connections to other problems. For example, the connection between CP transformations and flavor symmetries is discussed in [172–174], while flavor symmetries in the context of grand unifying theories are the topic of [175–177].

The studies of recent years have shown that, if existent, flavor symmetries are well hidden and large breaking effects need to be considered to construct realistic models. The specific pattern of symmetry breaking is crucial for these models which usually necessitates a large number of flavons to break the flavor symmetries in the desired way. Unfortunately, this reduces the predictive power and is a common point of criticism for this approach [35].

Clockwork mechanism

A method that has some similarity to the Froggatt-Nielson mechanism is the so-called clockwork mechanism. Originally, it was proposed in axion physics [178, 179], but was subsequently also transmitted to the scalar, gauge and fermion sectors [180]. The nice feature of the clockwork mechanism is that it is able to explain hierarchies in couplings or scales, even though there are no small parameters in the fundamental theory. To outline the basic idea, we consider a simplified setup where a fermion $\psi_{R,0}$ interacts with a chain of massive vector-like fermions $\psi_{L/R,i}$, $i = 1, .., n$ via a nearest neighbor interaction

$$\mathcal{L} = \mathcal{L}_{kin} - m \left(\sum_{j=1}^{n} \overline{\psi}_{L,j}\psi_{R,j} - q\overline{\psi}_{L,j}\psi_{R,j-1} \right) \,. \tag{3.20}$$

Then, the mass matrix has dimension $n \times (n+1)$ and is given by

$$M_\psi = m \begin{pmatrix} -q & 1 & 0 & ... & 0 \\ 0 & -q & 1 & ... & 0 \\ \vdots & & \ddots & & \vdots \\ 0 & 0 & ... & -q & 1 \end{pmatrix} \,. \tag{3.21}$$

After performing a bi-unitary transformation, the eigenvalues are given by $V_L^T M_\psi V_R = M_{diag} = \mathrm{diag}(0, M_1, M_2, ...M_n)$. Thus, there is one zero mode and n massive modes, the clockwork gears. The elements of the zeroth column of V_R are given by $(V_R)_{i0} = \mathcal{N}/q^{(n-i)}$, where $\mathcal{N}$ is a normalization factor. For the case $q > 1$, clockworking is successful, as the massless mode is exponentially distributed among the clockwork gears and in particular suppressed towards one boundary by $(V_R)_{00} \sim 1/q^n$. The chain length n thereby determines the degree of suppression. If the SM Higgs only couples to $\psi_{R,0}$, which is related to the zero mass eigenstate $\psi'_{R,0}$ by

$$\psi_{R,0} = (V_R)_{00}\psi'_{R,0} + ... \,, \tag{3.22}$$

couplings will be naturally suppressed. The dots represent further terms that are not important for our discussion. In a similar way, a suppression to the coupling of left-chiral fermions can be achieved [181, 182]. From the above, one can identify the expansion parameter $\epsilon \equiv 1/q < 1$ in this mechanism. The clockwork theory has similarities to the Froggatt-Nielson mechanism in the limit where the q's are all the same for different fermion representations, i.e. $q_{Q_{Li}} = q_{u_{Ri}} = q_{d_{Ri}}$ and the hierarchy is generated by different chain lengths $n_{Q_{L1}} > n_{Q_{L2}} > n_{Q_{L3}}$. On the other hand, a setting with universal n's and hierarchical $q_{Q_{L1}} > q_{Q_{L2}} > q_{Q_{L3}}$ is close to Randall-Sundrum models which we will not discuss here [183].

Radiative mechanism

Yet another class of models to realize hierarchical fermion masses and quark mixings is given by radiative mechanisms. The simple idea of theses theories relies on the fact that a one-loop radiative correction is typically suppressed by a factor $\epsilon \equiv 1/(16\pi^2) \sim 10^{-2}$ with respect to tree level processes. Going even to higher loop order, this effect continuously grows. If one constructs a model where only the third generation of fermions is massive at tree level and higher order one-loop and two-loop corrections induce masses for the second and first generations, one will naturally generate a hierarchy $\epsilon^2 : \epsilon : 1$. Even when dealing only with order one couplings in the fundamental theory, this can generate a considerable hierarchy in scales and masses of light fermions become calculable as there are no counter terms in the Lagrangian [184, 185].

The idea of a radiatively generated mass hierarchy has existed since the 70s, when people tried to explain the mass difference between the muon and the electron. In these early attempts, the electron mass arises from a radiative correction proportional to the muon mass [186–190]. Subsequently, this idea was also transferred to the quark sector. Especially in the late 80s, many works studied possible realizations of this idea where extended scalar sectors are responsible for the loop corrections that generate masses for the lighter fermions [36–38, 40, 41, 191]. Further papers also investigated the possibilities of radiative fermion masses in grand unified theories [192–195].

For a long period of time, interest in the topic dropped and only few works were published [42, 43, 196]. Among these, we highlight the work presented in [42]. There, the authors propose a scenario where the top quark is the only massive particle at tree level. All other fermion masses arise from radiative corrections up to 5-loop order to explain the large hierarchy between the top quark and the electron. However, this mechanism necessitates a large number of leptoquarks which are responsible for the radiative corrections.

Only a few years ago, the idea of a gauged horizontal $SO(3)_L \times SO(3)_R$ symmetry was explored by Weinberg in [44]. There, the gauge bosons of the new symmetry create radiatively suppressed fermion masses for the first two generations. This setup lacks an explanation of mixing and can therefore only be seen as a toy model. Nonetheless, the paper has caused an increasing interest in the topic again and more recent papers followed, where either enlarged scalar sectors [197–201] or new gauge interactions are considered [45–47]. It turns out that the ladder approach can be more minimal, in the sense that it does not need new scalars apart from those that are anyway required for spontaneous symmetry breaking. However, gauge extensions can be also more restrictive as the work of Weinberg [44] has shown.

In the following, we aim to investigate the necessary ingredients to realize a radiative mass hierarchy for fermions that mainly arises from gauge interactions. For this purpose, we examine two types of gauge extensions. We start by considering an Abelian $U(1)$ symmetry in Chapter 4, before we move to a non-Abelian gauge extension in Chapter 5.

Chapter 4

A radiative seesaw model for quarks and leptons

In the universal seesaw mechanism, all fermion masses result from a tree level seesaw with heavy vector-like fermion partners [51–54]. In this chapter we propose a model which realizes tree level masses only for the third and second generation fermions, while the first generation mass is attributed to one-loop gauge corrections as illustrated by the Feynman diagrams in Figure 4.1. To implement this scheme, we introduce a new $U(1)$ gauge symmetry which features a Z' responsible for the loop correction. In this way, small masses of the first generation can be explained by a loop suppression factor of $1/(16\pi^2)$. Because the rank of the fermion mass matrix is increased when one-loop corrections are taken into account, this is also sometimes called the rank mechanism. It is quite usual in many models that neutrino masses arise from different mechanisms as quark and charged lepton masses. Remarkably, our mechanism can be applied to up- and down-type quarks as well as charged leptons and neutrinos. In this way, neutrinos obtain small Dirac masses and lepton number can be a conserved quantity. The model features a number of phenomenological consequences, especially related to flavor violating observables. Further improvements in the search for lepton flavor violating decays or the measurement of neutral meson oscillation will therefore allow to test our model in future.

In the remainder of this chapter, Section 4.1 summarizes the idea of the mechanism which we apply in our proposal. After clarifying the model details in Section 4.2, we discuss the masses and mixing angles that arise in the quark and lepton sector and substantiate the mechanism by giving explicit benchmark points. Finally in Section 4.3, we discuss phenomenological consequences of the model. The scientific content of this chapter is based on work published in [1].

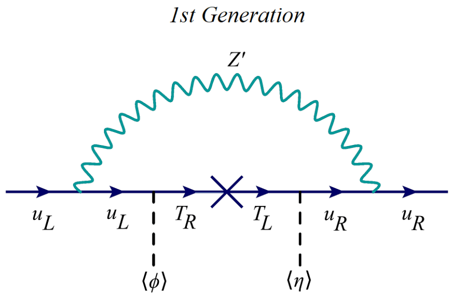

Figure 4.1 Illustration of the mass generation mechanism in the $U(1)$ gauge extension of the SM. Published in [1].

4.1 Rank mechanism

Before going into the model details, we want to highlight the main ingredients for the rank mechanism as originally proposed in [37]. First of all, we examine a mass matrix which has a tree level texture

$$M_T = \begin{pmatrix} 0 & v_{EW}|h\rangle \\ v_S\langle h| & M_P \end{pmatrix} .$$

In our notation M_P symbolizes the explicit mass of a vector-like fermion, while the n-column vector $|h\rangle$ indicates Yukawa couplings with chiral quarks. These couplings are realized by suitable scalars that obtain VEVs denoted by v_{EW} and v_S. By means of the seesaw mechanism, the vector-like fermion gives tree level mass to one other fermion. The above $(n+1)\times(n+1)$ matrix has therefore rank two and leaves $n-1$ fermions massless. In the limit $M_P \gg v_{EW}, v_S$, the non-vanishing eigenvalues are approximately given by

$$\begin{aligned} m_t &\simeq a_0\langle h \mid h\rangle \ , \\ m_P &\simeq M_P \ , \end{aligned}$$

and we define $a_0 \equiv -(v_{EW}v_S/M_P)$. At one-loop, the mass matrix receives radiative corrections and becomes

$$M_T = \left(\begin{array}{c|c} \delta M & v_{EW}|\alpha\rangle \\ \hline v_S\langle\alpha| & M_P \end{array}\right) .$$

Both, δM and $|\alpha\rangle$ indicate the quantum loop effects in the corresponding entries. Again, the rank of M_T provides information on the number of fermions that are massive. Likewise, the non-zero eigenvalues of $M_T M_T^\dagger$ (or $M_T^\dagger M_T$) can be counted. By analyzing the eigenvalue equations

$$\begin{aligned} \delta M|x\rangle + v_{EW}|\alpha\rangle x_{n+1} &= 0 \ , \\ v_S\langle\alpha \mid x\rangle + M_P x_{n+1} &= 0 \ , \end{aligned}$$

we can substitute the state x_{n+1} and arrive at

$$\left(\delta M + a_0|\alpha\rangle\langle\alpha|\right)|x\rangle \equiv M|x\rangle = 0 \ .$$

The properties of the matrix $M = \delta M + a_0|\alpha\rangle\langle\alpha|$ determine the rank of M_T. When the matrix rank of M is r, i.e. it has r non-zero eigenvalues, we find that M_T has rank $r+1$. Thus, besides the massive vector-like fermion, r generations obtain masses.

With this formalism, it is possible to investigate the rank of a mass matrix at each loop order and determine in this way the number of massive fermions. Note that for simplicity, we discuss here a scenario with a single vector-like fermion. Settings with different numbers of new fermions are considered in the next sections together with an explicit model realization of the given mechanism.

4.2 Details of the model

4.2.1 Particle content

To implement the seesaw-like matrix texture, we consider the gauge group of the SM and supplement it by an additional Abelian local symmetry such that the gauge group is given by $\mathcal{G} = \mathcal{G}_{SM} \times U(1)_X$. The fermion content of the model comprises the left-handed quark and lepton doublets

$$Q_{jL} = \begin{pmatrix} u_j \\ d_j \end{pmatrix}_L \sim (\mathbf{3}, \mathbf{2}, 1/3, 1/3) \ , \qquad \Psi_{jL} = \begin{pmatrix} \nu_j \\ e_j \end{pmatrix}_L \sim (\mathbf{1}, \mathbf{2}, -1, -1) \ , \tag{4.1}$$

and the respective weak singlets

$$\begin{aligned} u_{jR} &\sim (\mathbf{3}, \mathbf{1}, 4/3, 1/3) \ , \qquad d_{jR} \sim (\mathbf{3}, \mathbf{1}, -2/3, 1/3) \ , \\ \nu_{jR} &\sim (\mathbf{1}, \mathbf{1}, 0, -1) \ , \qquad e_{jR} \sim (\mathbf{1}, \mathbf{1}, -2, -1) \ , \end{aligned} \tag{4.2}$$

where the charges of each field are given in brackets and $j = 1, 2, 3$. In our convention, the electric charge is defined by $Q = T_3 + \frac{Y}{2}$ and T_3 is the third component of weak isospin. Note that we also include three right-handed neutrinos to be able to implement the same mass generation mechanism for all fermions. If the SM Higgs doublet carries non-zero charge under the new Abelian gauge group,

$$\phi = \begin{pmatrix} \phi^+ \\ \phi^0 \end{pmatrix} \sim (\mathbf{1}, \mathbf{2}, 1, 1/3) \ , \tag{4.3}$$

standard Yukawa couplings between left- and right-chiral fermions will be forbidden in this setup. Instead, the seesaw mechanism is realized by considering m additional generations of vector-like fermions. In detail, we regard vector-like partners for the up-type and down-type quarks

$$T_{k\,L}, T_{k\,R} \sim (\mathbf{3}, \mathbf{1}, 4/3, 2/3) \ , \qquad B_{k\,L}, B_{k\,R} \sim (\mathbf{3}, \mathbf{1}, -2/3, 0) \ , \tag{4.4}$$

as well as vector-like neutral and charged leptons

$$N_{k\,L}, N_{k\,R} \sim (\mathbf{1}, \mathbf{1}, 0, -2/3) \ , \qquad E_{k\,L}, E_{k\,R} \sim (\mathbf{1}, \mathbf{1}, -2, -4/3) \ , \tag{4.5}$$

where $k = 1, ..., m$ is a generation index for vector-like families. Ultimately, the $U(1)_X$ symmetry has to be broken. We achieve this by a new scalar singlet carrying the following gauge charges

$$\eta \sim (\mathbf{1}, \mathbf{1}, 0, 1/3) \ . \tag{4.6}$$

At the same time, the scalar η allows to have further Yukawa couplings between right-handed SM fermions and their vector-like partners giving eventually rise to a seesaw mechanism.

4.2.2 Gauge sector

As the gauge sector is enlarged by an additional symmetry, the gauge kinetic Lagrangian includes not only the field strength tensors of the strong ($G^a_{\mu\nu}$), left-chiral ($W^i_{\mu\nu}$) and weak hypercharge ($B_{\mu\nu}$) but also that of the $U(1)_X$ ($X_{\mu\nu}$)

$$\mathcal{L}_{\text{gauge}} = -\frac{1}{4} G^a_{\mu\nu} G^{\mu\nu\, a} - \frac{1}{4} W^i_{\mu\nu} W^{\mu\nu\, i} - \frac{1}{4} B_{\mu\nu} B^{\mu\nu} - \frac{1}{4} X_{\mu\nu} X^{\mu\nu} \,, \tag{4.7}$$

where $a = 1, ..., 8$, $i = 1, .., 3$ and g_s, g, g' and g_X are the corresponding gauge couplings for each symmetry. Fermions carrying non-zero $U(1)_X$ charge q_ψ interact with the neutral gauge boson X_μ according to the neutral current interaction

$$\mathcal{L}_{\text{NC}} \supset \frac{g_X}{2} \sum_{i,j} \overline{\psi}_i \gamma_\mu \left[q_\psi P_L + q_\psi P_R \right] \psi_j X^\mu \,. \tag{4.8}$$

With our choice of gauge assignments, $\psi \in \{Q, \Psi, u, d, \nu, e, T, N, E\}$ in the above equation and the vector-like down-type quark is the only fermion that does not couple to X_μ due to its vanishing gauge charge. Note that we discuss here a general scenario where the gauge boson couplings can be flavor non-diagonal [202]. This will have important consequences for the phenomenology of the model, as harsh constraints arise from flavor changing neutral currents. A detailed discussion of these limits can be found in Section 4.3.

4.2.3 Scalar sector and symmetry breaking

The scalar sector is rather minimalistic and comprises only two fields. The dynamics are described by the Lagrangian

$$\mathcal{L}_{\text{scalar}} = (D_\mu \phi)^\dagger (D^\mu \phi) + (D_\mu \eta)^\dagger (D^\mu \eta) - V(\phi, \eta) \ , \tag{4.9}$$

where the potential is given by

$$V(\phi, \eta) = -\mu_\phi^2 \phi^\dagger \phi + \frac{1}{2} \lambda_\phi (\phi^\dagger \phi)^2 - \mu_\eta^2 \eta^\dagger \eta + \frac{1}{2} \lambda_\eta (\eta^\dagger \eta)^2 + \lambda_{\phi\eta} (\phi^\dagger \phi)(\eta^\dagger \eta) \,. \tag{4.10}$$

Besides the dimensionful mass terms μ_ϕ and μ_η, the potential includes the dimensionless four-point couplings λ_ϕ and λ_η and a portal term which couples η to the SM Higgs field. Its strength is parameterized by the portal coupling $\lambda_{\phi\eta}$ which leads to a mixing between the physical scalars. According to the gauge charges, the covariant derivatives are given by

$$D_\mu \phi = \left(\partial_\mu + ig\frac{\tau^i}{2}W_\mu^i + i\frac{g^{'}}{2}B_\mu + iq_\phi \frac{g_X}{2}X_\mu\right)\phi\,, \tag{4.11}$$

and

$$D_\mu \eta = \left(\partial_\mu + iq_\eta \frac{g_X}{2}X_\mu\right)\eta\,, \tag{4.12}$$

where q_ϕ, q_η indicate the $U(1)_X$ charges of ϕ and η. We assume that the symmetry of the theory is broken in two steps. First, a non-zero VEV of η breaks the $U(1)_X$ symmetry at a high scale, followed by the spontaneous symmetry breaking of the electroweak theory by the SM Higgs field:

$$\begin{aligned} SU(3)_C \times SU(2)_L \times U(1)_Y \times U(1)_X &\xrightarrow{\langle\eta\rangle} SU(3)_C \times SU(2)_L \times U(1)_Y \\ &\xrightarrow{\langle\phi\rangle} SU(3)_C \times U(1)_{EM}\,. \end{aligned} \tag{4.13}$$

A detailed analysis of the scalar potential is beyond the scope of this work. For now, we assume that a minimum realizing the symmetry breaking exists and parameterize the VEVs of the scalar fields by

$$\langle\phi\rangle = \begin{pmatrix} 0 \\ v_{EW}/\sqrt{2} \end{pmatrix}\,, \qquad \langle\eta\rangle = \frac{v_S}{\sqrt{2}}\,, \tag{4.14}$$

where $v_S \gg v_{EW}$. The symmetry breaking induces masses for the gauge bosons of the broken generators. Similar to the SM, the charged gauge boson $W_\mu^\pm \equiv \left(W_\mu^2 \mp iW_\mu^1\right)/\sqrt{2}$ acquires a mass

$$M_{W^\pm}^2 = \frac{g^2 v_{EW}^2}{4}\,. \tag{4.15}$$

Contrary, neutral gauge boson masses are altered with respect to the SM, as ϕ is charged under $U(1)_X$. In the basis $(B,\ W^3,\ X)$, the neutral gauge boson mass matrix is given by

$$\mathcal{M}^2 = \frac{1}{4}\begin{pmatrix} g^{'2}v_{EW}^2 & -gg^{'}v_{EW}^2 & g^{'}g_X q_\phi v_{EW}^2 \\ -gg^{'}v_{EW}^2 & g^2 v_{EW}^2 & -g\,g_X q_\phi v_{EW}^2 \\ g^{'}g_X q_\phi v_{EW}^2 & -g\,g_X q_\phi v_{EW}^2 & g_X^2\left(q_\phi^2 v_{EW}^2 + q_\eta^2 v_S^2\right) \end{pmatrix}. \tag{4.16}$$

As the gauge boson corresponding to the unbroken $U(1)_{\mathrm{EM}}$ should be massless, we first perform a basis change

$$\begin{pmatrix} A \\ Y \\ X \end{pmatrix} = \begin{pmatrix} c_w & s_w & 0 \\ -s_w & c_w & 0 \\ 0 & 0 & 1 \end{pmatrix}\begin{pmatrix} B \\ W^3 \\ X \end{pmatrix}\,, \tag{4.17}$$

where $s_w \equiv \sin\theta_w = g'/\sqrt{g^2 + g'^2}$ is the weak mixing angle and the field A can be identified with the massless photon. The remaining two-by-two matrix in the subspace (Y, X) is then defined through the matrix entries

$$
\begin{aligned}
M_{YY}^2 &= \frac{v_{EW}^2 \left[g^2 c_w^2 (1 + 2 s_w^2) + g'^2 s_w^2 (1 + 2 c_w^2) \right]}{4}\,, \\
M_{XX}^2 &= \frac{g_X^2 (q_\phi^2 v_{EW}^2 + q_\eta^2 v_S^2)}{4}\,, \\
M_{YX}^2 &= -\frac{g_X q_\phi v_{EW}^2 (g c_w + g' s_w)}{4}\,.
\end{aligned}
\tag{4.18}
$$

A further diagonalization by the unitary transformation

$$
\begin{pmatrix} Z \\ Z' \end{pmatrix} = \begin{pmatrix} c_\xi & s_\xi \\ -s_\xi & c_\xi \end{pmatrix} \begin{pmatrix} Y \\ X \end{pmatrix}\,, \tag{4.19}
$$

where the mixing angles is given by

$$
\tan 2\xi = \frac{2 M_{YX}^2}{M_{YY}^2 - M_{XX}^2}\,, \tag{4.20}
$$

yields the mass eigenstates $(Z,\ Z')$ with corresponding eigenvalues

$$
M_{Z,Z'}^2 = \frac{1}{2} \left(M_{YY}^2 + M_{XX}^2 \mp (M_{YY}^2 - M_{XX}^2) \sqrt{1 + \tan^2 2\xi} \right)\,. \tag{4.21}
$$

As can be seen from the mixing angle, $Z - Z'$ mixing is proportional to $\sim v_{EW}^2/v_S^2$. Considering the limit $v_S \gg v_{EW}$, mixing effects are rather suppressed and will not be taken into account in the following. Likewise, we do not consider kinetic mixing in our work, which however can occur in general.

4.2.4 Yukawa interactions

With the assigned gauge charges, SM Yukawa couplings such as $\overline{Q}_L \phi d_R$ are forbidden due to $U(1)_X$ charge. However, new couplings with the vector-like fermions are possible. The complete gauge invariant Yukawa Lagrangian is given by

$$
\begin{aligned}
\mathcal{L}_{\text{Yuk}} = &-y_a^q \overline{Q}_{jL} \tilde{\phi} T_{kR} - y_b^q \overline{T}_{kL} \eta\, u_{jR} - y_c^q \overline{Q}_{jL} \phi B_{kR} - y_d^q \overline{B}_{kL} \eta^\dagger\, d_{jR} \\
&- y_a^\ell \overline{\Psi}_{jL} \tilde{\phi} N_{kR} - y_b^\ell \overline{N}_{kL} \eta\, \nu_{jR} - y_c^\ell \overline{\Psi}_{jL} \phi E_{kR} - y_d^\ell \overline{E}_{kL} \eta^\dagger\, e_{jR} + h.c.\,,
\end{aligned}
\tag{4.22}
$$

where the matrices $y_a,\ y_b,\ y_c$ and y_d represent Yukawa couplings for the quark (q) and lepton (ℓ) sector, respectively. On top of that, the vector-like nature of the fields $T,\ B,\ N$ and E allows the explicit mass terms

$$
\mathcal{L}_{\text{explicit}} = -\mathcal{M}_T \overline{T}_{kL} T_{kR} - \mathcal{M}_B \overline{B}_{kL} B_{kR} - \mathcal{M}_N \overline{N}_{kL} N_{kR} - \mathcal{M}_E \overline{E}_{kL} E_{kR} + h.c.\,. \tag{4.23}
$$

Note that the $m \times m$ matrices $\mathcal{M}_{T/B/N/E}$ can be taken as real and diagonal, without loss of generality. Furthermore, it is important to highlight that the $U(1)_X$ charge protects the neutrinos from getting Majorana mass at the renormalizable level. Including them would necessitate an additional scalar field. The LNV Weinberg operator $LLHH/\Lambda$ is likewise protected by the $U(1)_X$ symmetry. The first operator which would contribute to a Majorana neutrino mass is generated at dimension nine and is therefore expected to be suppressed.

4.2.5 Quark masses and mixings

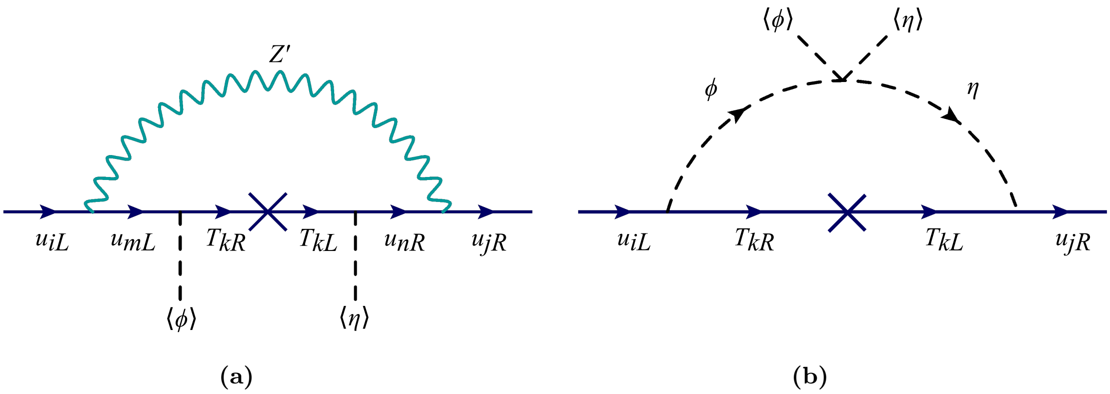

Figure 4.2 One-loop Feynman diagrams contributing to the up quark mass matrix in the $U(1)$ gauge extension of the SM. Published in [1].

Having defined the Yukawa sector in the previous section, we turn our interest first to the quark masses. When the scalars ϕ and η develop non-zero VEVs, their Yukawa couplings to quarks induces mass terms. In matrix notation, they are given by

$$\overline{\mathbf{u}}_L \mathcal{M}_u^{(0)} \mathbf{u}_R \equiv \begin{pmatrix} \overline{u}_{1L} & \overline{u}_{2L} & \overline{u}_{3L} & \overline{T}_{1L} & \dots & \overline{T}_{mL} \end{pmatrix} \left(\begin{array}{c|c} 0_{3\times 3} & y_a^q \langle\phi\rangle \\ \hline (y_b^q)^\dagger \langle\eta\rangle & \mathcal{M}_T \end{array} \right) \begin{pmatrix} u_{1R} \\ u_{2R} \\ u_{3R} \\ T_{1R} \\ \dots \\ T_{mR} \end{pmatrix},$$

for the up-type sector. The matrices y^q have dimension $3 \times m$ in this case. In a similar manner, the down-type quark mass matrix is described by

$$\overline{\mathbf{d}}_L \mathcal{M}_d^{(0)} \mathbf{d}_R \equiv \begin{pmatrix} \overline{d}_{1L} & \overline{d}_{2L} & \overline{d}_{3L} & \overline{B}_{1L} & \dots & \overline{B}_{mL} \end{pmatrix} \left(\begin{array}{c|c} 0_{3\times 3} & y_c^q \langle\phi\rangle \\ \hline (y_d^q)^\dagger \langle\eta\rangle & \mathcal{M}_B \end{array} \right) \begin{pmatrix} d_{1R} \\ d_{2R} \\ d_{3R} \\ B_{1R} \\ \dots \\ B_{mR} \end{pmatrix}.$$

If the matrices y^q consist of m linearly independent column vectors, the vector-like quarks will give mass to m SM generations via the seesaw mechanism at tree level. At one-loop, both the gauge and scalar exchange diagrams given in Figure 4.2 populate the zero entry in the mass matrix. We identify now different scenarios that can lead to hierarchical fermion masses depending on the number of vector-like fermions in the model.

First, for $m = 3$ generations of vector-like quarks, all SM quarks obtain masses at the tree level. This mechanism has already been studied in the literature and is commonly known as the universal seesaw mechanism [51–56]. A mass hierarchy for the SM fermions can be induced in this setup from an interplay of hierarchical vector-like fermion masses and Yukawa couplings. Hence, to realize a radiative mass suppression we need to consider a different scenario. We first examine a case of flavor diagonal Z' couplings. In this setup, the loop contribution is proportional to the matrix product $\sim y_a^q \left(y_b^q\right)^\dagger$ for the up quark case. Furthermore, we include four generations of vector-like fermions out of which one has no explicit mass term and does not couple to the SM quarks but only to the remaining three other vector-like fermions.[1] Then, two SM generations are massive at tree level, while the first generation mass arises from the one-loop diagrams in Figure 4.2. Note that this setting realizes a double seesaw structure and we study such a scenario in more detail in Chapter 5. For the following chapter we examine the details of a different scenario, where the Z' couplings are flavor non-diagonal as described in Eq. (4.8). For $m = 2$, it is possible to realize mass terms for the third and second generation fermions at tree level from the seesaw, while the first generation fermion mass originates from the one-loop Z' induced radiative correction. The key point is that flavor non-diagonal Z' interaction can enhance the matrix rank. The one-loop contribution to the mass matrix is given by the fermion self-energy at zero external momentum $\delta M_{ij}^u \equiv \Sigma_{ij}(\not{p} = 0)$. Explicitly calculating the contribution of the Feynman diagram given in Figure 4.2a yields

$$\delta\mathcal{M}_{ij}^u = \sum_{k=1}^{2}\sum_{m,n=1}^{3} \frac{3g_X^2 q_Q q_u [y_a^q]_{mk}[y_b^q]_{kn} v_{EW} v_S}{32\pi^2} \frac{M_{Tk}}{\left(M_{Z'}^2 - M_{T_k}^2\right)} \log\frac{M_{Z'}^2}{M_{T_k}^2}\,. \tag{4.24}$$

Useful formulas applied in the calculation of the above expression are given in Appendix C. Note that a summation over indices m and n is necessary due to non-diagonal Z' couplings. With this result at hand, the one-loop corrected mass matrix for up-type quarks is

$$\overline{\mathbf{u}}_L \mathcal{M}_u^{(1)} \mathbf{u}_R \equiv \begin{pmatrix} \overline{u}_{1L} & \overline{u}_{2L} & \overline{u}_{3L} & \overline{T}_{1L} & \overline{T}_{2L} \end{pmatrix} \left(\begin{array}{c|c} \delta\mathcal{M}^u & y_a^q\langle\phi\rangle \\ \hline \left(y_b^q\right)^\dagger\langle\eta\rangle & \mathcal{M}_T \end{array}\right) \begin{pmatrix} u_{1R} \\ u_{2R} \\ u_{3R} \\ T_{1R} \\ T_{2R} \end{pmatrix}. \tag{4.25}$$

Here, the matrix $\delta\mathcal{M}^u$ has dimension 3×3 and its entries in index notation are given by $\delta\mathcal{M}_{ij}^u$ as defined above. The Feynman diagram presented in Figure 4.2b is proportional

[1] This can be realized by an additional symmetry.

to the portal coupling $\lambda_{\phi\eta}$ and its contribution is negligible for $\lambda_{\phi\eta} \ll 1$. Furthermore, it does not change the matrix rank of $\mathcal{M}_u^{(1)}$, as it is proportional to $\sim y_a^q \left(y_b^q\right)^\dagger$ and will therefore not be included in our calculation. Is is also important to stress that the number of vector-like fermion generations can not be further reduced, because this would cause one massless generation of SM fermions. Thus, the most minimal case of a complete model of fermion masses is given by two generations of vector-like fermions. The down-type sector proceeds in a similar manner and the one-loop corrected mass matrix is given by

$$\overline{\mathbf{d}}_L \mathcal{M}_d^{(1)} \mathbf{d}_R \equiv \begin{pmatrix} \overline{d}_{1L} & \overline{d}_{2L} & \overline{d}_{3L} & \overline{B}_{1L} & \overline{B}_{2L} \end{pmatrix} \left(\begin{array}{c|c} \delta\mathcal{M}^d & y_c^q \langle\phi\rangle \\ \hline \left(y_d^q\right)^\dagger \langle\eta\rangle & \mathcal{M}_B \end{array}\right) \begin{pmatrix} d_{1R} \\ d_{2R} \\ d_{3R} \\ B_{1R} \\ B_{2R} \end{pmatrix}, \tag{4.26}$$

where the one-loop result for the down quark sector is easily deduced from Eq. (4.24) by replacing the Yukawa couplings appropriately. The fermion mass eigenstates are finally obtained by bi-unitary transformations

$$\begin{aligned} V_L^u \mathcal{M}_u^{(1)} (V_R^u)^\dagger &= \mathcal{M}_u^{\text{diag}} \equiv \text{diag}(m_u, m_c, m_t, m_{T1}, m_{T2})\,, \\ V_L^d \mathcal{M}_d^{(1)} (V_R^d)^\dagger &= \mathcal{M}_d^{\text{diag}} \equiv \text{diag}(m_d, m_s, m_b, m_{B1}, m_{B2})\,. \end{aligned} \tag{4.27}$$

As a result, the relation between flavor and mass eigenstates is given by

$$\begin{aligned} \hat{\mathbf{u}}_{L/R} &= V_{L/R}^u \mathbf{u}_{L/R}\,, \\ \hat{\mathbf{d}}_{L/R} &= V_{L/R}^d \mathbf{d}_{L/R}\,, \end{aligned} \tag{4.28}$$

and we indicate fermion mass eigenstates from now on by hatted quantities. The diagonalization procedure induces mixing between the different generations and in particular mixing between SM quarks and vector-like quarks. We provide here an approximate estimate on the size of this mixing. If we simplify the tree level mass matrix to the case of one vector-like fermion and one SM generation and further assume order one Yukawa couplings, we will find

$$\mathcal{M}_u \simeq \begin{pmatrix} 0 & v_{EW} \\ v_S & M_T \end{pmatrix}. \tag{4.29}$$

The mixing angle with the vector-like partner for left- and right-handed fermions can now be obtained from the diagonalization of the matrices $\mathcal{M}_u \mathcal{M}_u^\dagger$ and $\mathcal{M}_u^\dagger \mathcal{M}_u$, respectively. In this simple approximation:

$$\begin{aligned} \mathcal{M}_u \mathcal{M}_u^\dagger &\simeq \begin{pmatrix} v_{EW}^2 & M_T v_{EW} \\ M v_{EW} & M_T^2 + v_R^2 \end{pmatrix}, \\ \mathcal{M}_u^\dagger \mathcal{M}_u &\simeq \begin{pmatrix} v_S^2 & M_T v_S \\ M v_S & M_T^2 + v_{EW}^2 \end{pmatrix}. \end{aligned} \tag{4.30}$$

Hence, the mixing angles are given by

$$\tan 2\theta_L \simeq \frac{2M_T v_{EW}}{v_{EW}^2 - M_T^2 - v_S^2} \ , \tag{4.31}$$

$$\tan 2\theta_R \simeq \frac{2M_T v_S}{v_S^2 - M_T^2 - v_{EW}^2} \ , \tag{4.32}$$

where $\theta_L(\theta_R)$ indicates the mixing between left-handed (right-handed) fermions.

4.2.6 Neutral and charged current interactions

After having defined the fermion mass eigenstates in the previous section, we examine their couplings in charged and neutral current interactions. Even though we exemplify our notation for the quark sector only, the lepton sector is treated along the same line. In the flavor basis, the quarks couple to the Z boson according to

$$\mathcal{L} \supset Z_\mu \left[\overline{\mathbf{u}}_L \gamma^\mu g_L^u(Z) \mathbf{u}_L + \overline{\mathbf{u}}_R \gamma^\mu g_R^u(Z) \mathbf{u}_R\right] \ , \tag{4.33}$$

where we define the coupling strengths

$$\begin{aligned} g_L^u(Z) &= \frac{g}{c_w}\left[\mathbb{1} g_L^{u,SM}(Z) - \mathrm{diag}(0,0,0,\frac{1}{2},\frac{1}{2})\right] \ , \\ g_R^u(Z) &= \frac{g}{c_w}\left[\mathbb{1} g_R^{u,SM}(Z)\right] \ , \end{aligned} \tag{4.34}$$

which depend on the charges of the fermions through the relations $g_L^{u,SM}(Z) = T_3 - Q s_w^2 = 1/2 - 2/3 s_w^2$ and $g_R^{u,SM}(Z) = -Q s_w^2 = -2/3 s_w^2$. Unlike in the SM, $g_L^u(Z)$ is no longer proportional to the unit matrix and therefore induce FCNCs when transforming to the quark mass eigenbasis. The Lagrangian in the new basis is given by

$$\mathcal{L} \supset Z_\mu \left[\overline{\hat{\mathbf{u}}}_L \gamma^\mu \hat{g}_L^u(Z) \hat{\mathbf{u}}_L + \overline{\hat{\mathbf{u}}}_R \gamma^\mu \hat{g}_R^u(Z) \hat{\mathbf{u}}_R\right] \ , \tag{4.35}$$

where we include now the unitary transformations from the diagonalization of the mass matrices in the definition of the coupling matrices $\hat{g}_L^u(Z) \equiv V_L^u g_L^u(Z) (V_L^u)^\dagger$ and $\hat{g}_R^u(Z) \equiv g_R^u(Z)$. We note that even though FCNCs at the tree level are generated, this effect stems from mixing with vector-like quarks and is therefore considered to be a small effect. This is in contrast to Z' interactions. When we transform the Z' neutral current interaction to the fermion mass basis we find

$$\mathcal{L} \supset Z'_\mu \left[\overline{\hat{\mathbf{u}}}_L \gamma^\mu \hat{g}_L^u(Z') \hat{\mathbf{u}}_L + \overline{\hat{\mathbf{u}}}_R \gamma^\mu \hat{g}_R^u(Z') \hat{\mathbf{u}}_R\right] \ , \tag{4.36}$$

with

$$\begin{aligned} \hat{g}_L^u(Z') &= V_L^u \, g_L^u(Z') \, (V_L^u)^\dagger \, , \\ \hat{g}_R^u(Z') &= V_R^u \, g_R^u(Z') \, (V_R^u)^\dagger \, . \end{aligned} \tag{4.37}$$

In this case, $g_L^u(Z') = g_R^u(Z')$ denote the non-diagonal Z' couplings proportional to the gauge charge under $U(1)_X$ as introduced at the beginning of this chapter (compare to Eq. (4.8)). As a consequence, tree level FCNCs are present in Z as well as in Z' neutral currents. Besides the neutral current interaction, SM quarks also couple to the charged W boson according to

$$\mathcal{L} \supset \frac{g}{\sqrt{2}} W_\mu^+ \left[\overline{\hat{\mathbf{u}}}_L \gamma^\mu \hat{g}_L^q(W) \hat{\mathbf{d}}_L \right] + h.c. \,, \tag{4.38}$$

where the coupling matrix is given by

$$\hat{g}_L^q(W) = V_L^u \, g_L^q(W) \, (V_L^d)^\dagger \,, \tag{4.39}$$

and we defined

$$g_L^q(W) = \mathrm{diag}(1,1,1,0,0) \,. \tag{4.40}$$

The misalignment between up- and down-type quarks creates mixing between the generations and the 3×3 subspace of the coupling matrix can be identified with the CKM matrix

$$V_{\text{CKM}} \equiv \hat{g}_L^q(W)\big|_{3\times 3} \,. \tag{4.41}$$

In the scalar sector, we describe the coupling of fermions to the physical neutral scalar ϕ^0 by

$$\mathcal{L} \supset -\phi^0 \overline{\mathbf{u}}_L \mathbf{Y}_u \mathbf{u}_R + h.c. \,, \tag{4.42}$$

where

$$\mathbf{Y}_u \equiv \frac{1}{\sqrt{2}} \begin{pmatrix} \mathbf{0}_{3x3} & y_a^q \\ \mathbf{0}_{2x3} & \mathbf{0}_{2x2} \end{pmatrix} \,. \tag{4.43}$$

In the fermion mass basis the Lagrangian becomes

$$\mathcal{L} \supset -\phi^0 \overline{\hat{\mathbf{u}}}_L \hat{\mathbf{Y}}_u \hat{\mathbf{u}}_R + h.c. \;, \tag{4.44}$$

and the coupling matrix is given by

$$\hat{\mathbf{Y}}_u = V_L^u \mathbf{Y}_u (V_R^u)^\dagger \,. \tag{4.45}$$

Since the fermion mass matrix receive contributions from two scalar VEVs, the couplings to the physical Higgs have non-zero off-diagonal terms which gives rise to FCNC. We discuss limits following from non-diagonal couplings in Section 4.3. Even though in principle there can be mixing between the scalars ϕ and η, we consider this to be a negligible effect as $\lambda_{\phi\eta} \ll 1$. Furthermore, the mass of η is at a high scale and FCNCs mediated by η will therefore be hugely suppressed.

4.2.7 Lepton masses and mixings

In this section we only shortly comment on the origin of charged lepton and neutrino masses, as the previously described mechanism equally applies to the lepton sector. The one-loop corrected neutrino mass matrix is given by

$$\overline{\nu}_L \mathcal{M}_\nu^{(1)} \nu_R \equiv \begin{pmatrix} \overline{\nu}_{1L} & \overline{\nu}_{2L} & \overline{\nu}_{3L} & \overline{N}_{1L} & \overline{N}_{2L} \end{pmatrix} \left(\begin{array}{c|c} \delta\mathcal{M}^\nu & y_a^\ell \langle\phi\rangle \\ \hline \left(y_b^\ell\right)^\dagger \langle\eta\rangle & \mathcal{M}_N \end{array}\right) \begin{pmatrix} \nu_{1R} \\ \nu_{2R} \\ \nu_{3R} \\ N_{1R} \\ N_{2R} \end{pmatrix} . \tag{4.46}$$

We remind the reader that Majorana mass terms are forbidden at tree level by the $U(1)_X$ charge and can only arise at the higher dimensional operator level beyond $d = 5$ (see discussion at the end of Section 4.2.4). $\delta\mathcal{M}^\nu$ indicates the one-loop contribution from Z' exchange and arises from an expression similar to Eq. (4.24). Equally, the charged lepton mass matrix is given by

$$\overline{\mathbf{e}}_L \mathcal{M}_e^{(1)} \mathbf{e}_R \equiv \begin{pmatrix} \overline{e}_{1L} & \overline{e}_{2L} & \overline{e}_{3L} & \overline{E}_{1L} & \overline{E}_{2L} \end{pmatrix} \left(\begin{array}{c|c} \delta\mathcal{M}^e & y_c^\ell \langle\phi\rangle \\ \hline \left(y_d^\ell\right)^\dagger \langle\eta\rangle & \mathcal{M}_E \end{array}\right) \begin{pmatrix} e_{1R} \\ e_{2R} \\ e_{3R} \\ E_{1R} \\ E_{2R} \end{pmatrix} . \tag{4.47}$$

By the unitary transformations

$$\begin{aligned} \hat{\nu}_{L/R} &= V^\nu_{L/R} \nu_{L/R} \,, \\ \hat{\mathbf{e}}_{L/R} &= V^e_{L/R} \mathbf{e}_{L/R} \,, \end{aligned} \tag{4.48}$$

the mass matrices are diagonalized and yield the eigenvalues

$$\begin{aligned} V_L^\nu \mathcal{M}_\nu^{(1)} (V_R^\nu)^\dagger &= \mathcal{M}_\nu^{\text{diag}} \equiv \text{diag}(m_{\nu_1}, m_{\nu_2}, m_{\nu_3}, m_{N1}, m_{N2}) \,, \\ V_L^e \mathcal{M}_e^{(1)} (V_R^e)^\dagger &= \mathcal{M}_e^{\text{diag}} \equiv \text{diag}(m_e, m_\mu, m_\tau, m_{E1}, m_{E2}) \,. \end{aligned} \tag{4.49}$$

In the fermion mass eigenbasis, the charged current interaction is described by the Lagrangian

$$\mathcal{L} \supset \frac{g}{\sqrt{2}} W_\mu^- \left[\hat{\overline{\mathbf{e}}}_L \gamma^\mu \hat{g}_L^\ell(W) \hat{\nu}_L \right] + h.c. \,, \tag{4.50}$$

and the transformation to the mass basis is reflected by the appearance of a mixing matrix

$$\hat{g}_L^\ell(W) = V_L^e \, g_L^\ell(W) \, (V_L^\nu)^\dagger \,, \tag{4.51}$$

where

$$g_L^\ell(W) = \mathrm{diag}(1,1,1,0,0)\,. \tag{4.52}$$

Thus, mixing between the generations is described by the 5×5 matrix $\hat{g}_L^\ell(W)$. The PMNS matrix lives in the 3×3 subspace and is accordingly represented by

$$U_{\mathrm{PMNS}} \equiv \hat{g}_L^\ell(W)\Big|_{3\times 3}\,. \tag{4.53}$$

Evidently, the PMNS matrix is not unitary in this model.

4.2.8 Numerical solutions

Even though the radiative mechanism in our model generates a naturally suppressed scale for the first generation fermion masses, parameters can not be chosen arbitrary but have to be mapped to SM observables. To demonstrate that a viable parameter space exists, we give two benchmark points (BPs) in the following and show that the reproduced fermion masses and mixings agree with current experimental bounds.

For the parameters related to the $U(1)_X$ gauge symmetry we chose

$$M_{Z'} = 300 \text{ TeV}\,, \qquad g_X = 1\,, \tag{4.54}$$

in the following two scenarios. The vector-like fermion masses for BP1 are given by

$$\begin{aligned}
M_{T1} = 8.00 \text{ TeV}\,,\;\; M_{T2} &= M_{T1} + 1 \text{ GeV}\,,\\
M_{B1} = 40.00 \text{ TeV}\,,\;\; M_{B2} &= M_{B1} + 1 \text{ GeV}\,,\\
M_{N1} = 7.00 \times 10^7 \text{ TeV}\,,\;\; M_{N2} &= 1.00 \times 10^8 \text{ TeV}\,,\\
M_{E1} = 50.00 \text{ TeV}\,,\;\; M_{E2} &= 80.00 \text{ TeV}\,,
\end{aligned} \tag{4.55}$$

whereas those for BP2 are

$$\begin{aligned}
M_{T1} = 8.00 \text{ TeV}\,,\;\; M_{T2} &= 17.91 \text{ TeV}\,,\\
M_{B1} = 40.00 \text{ TeV}\,,\;\; M_{B2} &= 65.69 \text{ TeV}\,,\\
M_{N1} = 1.15 \times 10^6 \text{ TeV}\,,\;\; M_{N2} &= 1.25 \times 10^6 \text{ TeV}\,,\\
M_{E1} = 50.00 \text{ TeV}\,,\;\; M_{E2} &= 80.00 \text{ TeV}\,.
\end{aligned} \tag{4.56}$$

While BP1 has almost degenerate vector-like quark masses, BP2 shows that also a larger degeneracy is viable. The Yukawa couplings for both benchmark points are displayed in Table 4.1. The predicted masses and mixing parameters in both scenarios are presented in Table 4.2, together with current experimental bounds. We demand that our model reproduces the 3σ experimental bounds for all parameters, except for charged lepton masses which we fit to the $\pm 5\%$ level, to keep the numeric effort reasonable [30, 203]. The Jarlskog invariant is calculated from the relation introduced in Eq. (3.16).

Yukawa Couplings	Benchmark Points	
	BP1	BP2
y_a^q	$\begin{pmatrix} 0.625 & 0.513 \\ 0.186\times e^{i0.05} & 0.159 \\ 0.401 & 0.327 \end{pmatrix}$	$\begin{pmatrix} 0.631 & 0.522 \\ 0.183\times e^{i0.05} & 0.158 \\ 0.412 & 0.344 \end{pmatrix}$
y_b^q	$\begin{pmatrix} 0.332 & 0.229 \\ 0.340 & 0.224 \\ 0.294 & 0.232\times e^{i0.05} \end{pmatrix}$	$\begin{pmatrix} 0.335 & 0.227 \\ 0.352 & 0.222 \\ 0.290 & 0.230\times e^{i0.05} \end{pmatrix}$
y_c^q	$\begin{pmatrix} 1.539 & 1.287 \\ 0.195 & 0.538 \\ 1.060 & 0.754 \end{pmatrix}\epsilon_1$	$\begin{pmatrix} 1.501 & 1.341 \\ 0.205 & 0.600 \\ 1.061 & 0.795 \end{pmatrix}\epsilon_1$
y_d^q	$\begin{pmatrix} 1.110 & 0.332 \\ 0.850 & 1.506 \\ 13.969 & 12.405 \end{pmatrix}\epsilon_1$	$\begin{pmatrix} 1.129 & 0.331 \\ 0.811 & 1.624 \\ 14.076 & 13.236 \end{pmatrix}\epsilon_1$
y_a^ℓ	$\begin{pmatrix} 1.306 & 1.494 \\ 0.175 & 1.257 \\ 0.538 & 0.333 \end{pmatrix}\epsilon_1^2$	$\begin{pmatrix} 1.235\times e^{i0.1} & 0.948 \\ 0.195 & 2.283 \\ 0.443 & 0.347 \end{pmatrix}\epsilon_2$
y_b^ℓ	$\begin{pmatrix} 0.319 & 1.048 \\ 0.285 & 0.668 \\ 0.967 & 0.328 \end{pmatrix}\epsilon_1^2$	$\begin{pmatrix} 0.101 & 1.210 \\ 2.871 & 0.947 \\ 0.243 & 1.589 \end{pmatrix}\epsilon_2$
y_c^ℓ	$\begin{pmatrix} 0.678 & 1.166 \\ 0.854 & 0.574 \\ 1.474 & 0.820 \end{pmatrix}\epsilon_1$	$\begin{pmatrix} 0.484 & 1.468 \\ 0.999 & 1.281 \\ 0.617 & 0.809 \end{pmatrix}\epsilon_1$
y_d^ℓ	$\begin{pmatrix} 1.398 & 0.960 \\ 0.740 & 0.780 \\ 0.747 & 1.445 \end{pmatrix}\epsilon_1$	$\begin{pmatrix} 1.555 & 0.479 \\ 1.355 & 1.381 \\ 0.858 & 0.982 \end{pmatrix}\epsilon_1$

Table 4.1 Benchmark points used for the Yukawa couplings in the analysis of the $U(1)$ gauge extension of the SM. We used the abbreviations $\epsilon_1 = 10^{-2}, \epsilon_2 = 10^{-1}\epsilon_1^2$. Data published in [1].

Our BPs demonstrate that vector-like quark masses of a few tens of TeV can nicely describe the SM quark sector with Yukawa couplings in the range $\mathcal{O}(10^{-2})$-$\mathcal{O}(1)$. Similar scales need to be considered to fulfill observations in the charged lepton sector. To accommodate for the small neutrino masses, $\mathcal{O}(10^7)$ TeV vector-like neutral lepton masses and Yukawa couplings of the order $\mathcal{O}(10^{-4})$ need to be considered. Even though this introduces some hierarchy to the couplings, the separation is not as large as the twelve orders of magnitude that appear in the SM. As there is no symmetry that protects vector-like mass terms, they can be in principle at any scale. It would be therefore also possible to find a scenario where Yukawa couplings in the neutrino sector are $\mathcal{O}(1)$. The necessary mass suppression would then arise from the seesaw with a vector-like neutral lepton with a mass of $\mathcal{O}(10^{17}$ GeV). With the two BPs, we also demonstrate that both IH and NH for neutrino masses can correctly be reproduced.

We remind the reader that this section is intended to give a proof of concept. An in-depth analysis of the possible parameter space is outside the scope of this thesis. This also implies that further solutions at lower energy scales might be possible. Furthermore, we highlight, that the number of parameters in our models exceeds the parameters in the SM. Hence, it is not possible to predict masses and mixing angles. We rather show that our set of parameters can be selected in such a way that the observed mass hierarchies and mixing angles can be reproduced with less hierarchical Yukawa couplings. We anticipate that extending the mechanism by further symmetries could reduce the number of Yukawa couplings. We explore this possibility in more detail in the model presented in Chapter 5.

Quark Sector				**Lepton Sector**					
Observable (Masses in GeV)	**Exp. Range**	**Model Prediction**		**Observable (Masses in GeV)**	**Exp. Range (NH)**	**Exp. Range (IH)**	**Model Prediction (NH)**	**Model Prediction (IH)**
		BP1	**BP2**				**BP1**	**BP2**
$m_u/10^{-3}$	$1.38 \to 3.63$	2.12	3.07	$\frac{\Delta m^2_{21}}{10^{-5}\,\mathrm{eV}^2}$	$6.82 \to 8.04$	$6.82 \to 8.04$	7.583	7.898
m_c	$1.21 \to 1.33$	1.29	1.25	$\frac{\Delta m^2_{3\ell}}{10^{-3}\,\mathrm{eV}^2}$	$2.421 \to 2.598$	$-2.583 \to -2.412$	2.567	-2.432
m_t	$171.7 \to 174.1$	172.3	174.1					
$m_d/10^{-3}$	$4.16 \to 6.11$	4.34	5.08	$m_e/10^{-3}$	$0.485 \to 0.537$		0.511	0.527
m_s	$0.078 \to 0.126$	0.122	0.109	m_μ	$0.100 \to 0.111$		0.109	0.109
m_b	$4.12 \to 4.27$	4.18	4.13	m_τ	$1.688 \to 1.866$		1.862	1.839
$\lvert V_{\mathrm{ud}}\rvert$	$0.973 \to 0.974$	0.974	0.974	$\sin^2(\theta_{12})$	$0.269 \to 0.343$	$0.269 \to 0.343$	0.315	0.320
$\lvert V_{\mathrm{us}}\rvert$	$0.222 \to 0.227$	0.227	0.226					
$\lvert V_{\mathrm{ub}}\rvert/10^{-4}$	$31.0 \to 45.4$	38.4	44.8					
$\lvert V_{\mathrm{cd}}\rvert$	$0.209 \to 0.233$	0.226	0.226	$\sin^2(\theta_{23})$	$0.407 \to 0.618$	$0.411 \to 0.621$	0.444	0.413
$\lvert V_{\mathrm{cs}}\rvert$	$0.954 \to 1.020$	0.973	0.973					
$\lvert V_{\mathrm{cb}}\rvert/10^{-3}$	$36.8 \to 45.2$	42.3	41.9					
$\lvert V_{\mathrm{td}}\rvert/10^{-4}$	$71.0 \to 89.0$	84.0	78.7	$\sin^2(\theta_{13})$	$0.02034 \to 0.02430$	$0.02053 \to 0.02436$	0.02053	0.02300
$\lvert V_{\mathrm{ts}}\rvert/10^{-3}$	$35.5 \to 42.1$	41.6	41.4					
$\lvert V_{\mathrm{tb}}\rvert$	$0.923 \to 1.103$	0.999	0.999					
$\mathcal{J}/10^{-5}$	$2.73 \to 3.45$	3.12	3.40	$\delta_{\mathrm{cp}}/\circ$	$107 \to 403$	$192 \to 360$	0	250

Table 4.2 Fermion masses and mixing parameters reproduced by the two benchmark points in the $U(1)$ gauge extension of the SM. For NH $\Delta m^2_{3\ell} \equiv \Delta m^2_{31}$, while for IH $\Delta m^2_{3\ell} \equiv \Delta m^2_{32}$. The BPs align with the experimental 3σ ranges except for charged lepton masses which fulfill the best fit value within $\pm 5\%$. Data published in [1].

4.3 Phenomenological implications

4.3.1 FCNC processes in quark sector

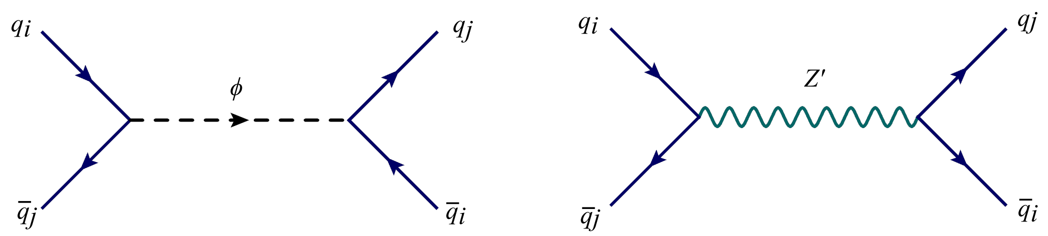

(a) **(b)**

Figure 4.3 Tree level Feynman diagrams which contribute to neutral meson mixing through **(a)** Higgs boson and **(b)** Z' mediated flavor changing currents. Figure published in [1]

The presented model has impact on a number of observables in the flavor sector, which we investigate in the following sections. The appearance of tree level flavor changing neutral currents is one of the new physics effects which becomes important in the context of neutral meson oscillations in the systems $D^0 - \overline{D^0}$, $K^0 - \overline{K^0}$, $B^0_d - \overline{B^0_d}$ and $B^0_s - \overline{B^0_s}$. Figure 4.3

shows how additional contributions from ϕ and Z' can contribute to these processes, which are usually only generated at the one-loop level in the SM.[2] To estimate the new physics contribution we follow an effective field theory approach. Integrating out heavy particles leaves us with the effective Hamiltonian [204, 205]

$$\begin{aligned}\mathcal{H}_{\text{eff}} = &-\frac{1}{2m_\phi^2}\left(\bar{\hat{q}}_i\left[(\hat{\mathbf{Y}}_q)_{ij}\frac{1+\gamma_5}{2} + (\hat{\mathbf{Y}}_q^*)_{ij}\frac{1-\gamma_5}{2}\right]\hat{q}_j\right)^2 \\ &-\frac{1}{2M_{Z'}^2}\left(\bar{\hat{q}}_i\gamma_\mu\left[\left[\hat{g}_L^q(Z')\right]_{ij}\frac{1-\gamma_5}{2} + \left[\hat{g}_R^q(Z')\right]_{ij}\frac{1+\gamma_5}{2}\right]\hat{q}_j\right)^2\,,\end{aligned} \tag{4.57}$$

which is responsible for neutral meson mixing. Note that in this general notation, $\hat{q}_i$ and $\hat{q}_j$ indicate the involved quark fields, i.e. charm and up quarks (D^0), strange and down quarks (K^0), down and bottom quarks (B_d^0) and strange and bottom quarks (B_s^0). With the effective Hamiltonian it is possible to calculate the transition matrix element $M_{12}^P = \langle P|\mathcal{H}_{\text{eff}}|\overline{P}\rangle$ for a meson $P \in \{D,\ K,\ B_d,\ B_s\}$. This allows us to obtain the mass splitting between the neutral mesons P and $\overline{P}$ that is physically observable and given by

$$\Delta m_P = 2\text{Re}(M_{12}^P)\,.$$

For Kaons, a further CP violating parameter $|\epsilon_K| \simeq \text{Im}(M_{12}^K)/(\sqrt{2}\Delta m_K)$ can be measured. The evaluation of the hadronic matrix elements involves the four-fermion operators [206]

$$\begin{aligned}\langle P|\overline{q}_i\frac{(1\pm\gamma_5)}{2}q_j\overline{q}_i\frac{(1\mp\gamma_5)}{2}q_j|\overline{P}\rangle &= f_P^2 m_P\left(\frac{1}{24}+\frac{1}{4}\frac{m_P^2}{(m_{q_i}+m_{q_j})^2}\right)B_4\,, \\ \langle P|\overline{q}_i\frac{(1\pm\gamma_5)}{2}q_j\overline{q}_i\frac{(1\pm\gamma_5)}{2}q_j|\overline{P}\rangle &= -\frac{5}{24}f_P^2 m_P\frac{m_P^2}{(m_{q_i}+m_{q_j})^2}B_2\,, \\ \langle P|\overline{q}_i\gamma_\mu\frac{(1\pm\gamma_5)}{2}q_j\overline{q}_i\gamma^\mu\frac{(1\pm\gamma_5)}{2}q_j|\overline{P}\rangle &= \frac{1}{3}m_P f_P^2 B_1\,.\end{aligned} \tag{4.58}$$

They depend not only on the so-called B parameters, but also on the meson mass m_P and the meson decay constant f_P. After using a Fierz rearrangement for the Z' current that involves fermions of mixed chirality [207], we find a transition matrix element

$$\begin{aligned}M_{12}^P = &-\frac{f_P^2 m_P}{2m_\phi^2}\Bigg[-\frac{5}{24}\frac{m_P^2}{(m_{q_i}+m_{q_j})^2}\left((\hat{\mathbf{Y}}_q)_{ij}^2 + (\hat{\mathbf{Y}}_q^*)_{ij}^2\right)\cdot B_2\cdot\eta_2(\mu) \\ &+ (\hat{\mathbf{Y}}_q)_{ij}(\hat{\mathbf{Y}}_q^*)_{ij}\left(\frac{1}{12}+\frac{1}{2}\frac{m_P^2}{(m_{q_i}+m_{q_j})^2}\right)\cdot B_4\cdot\eta_4(\mu)\Bigg] \\ &-\frac{f_P^2 m_P}{2M_{Z'}^2}\frac{1}{3}\left(\left[\hat{g}_L^q(Z')\right]_{ij}^2 + \left[\hat{g}_R^q(Z')\right]_{ij}^2\right)\cdot B_1\cdot\eta_1(\mu) \\ &-\frac{f_P^2 m_P}{M_{Z'}^2}\left[\hat{g}_L^q(Z')\right]_{ij}\left[\hat{g}_R^q(Z')\right]_{ij}\left(\frac{1}{12}+\frac{1}{2}\frac{m_P^2}{(m_{q_i}+m_{q_j})^2}\right)\cdot B_4\cdot\eta_4(\mu)\,.\end{aligned} \tag{4.59}$$

[2] Tree level FCNCs induced by Z exchange also exist, but constitute rather small effects as non-diagonal Z couplings arise only from the mixing with the vector-like quarks.

The parameters η_1, η_2 and η_4 are correction factors which take into account the running of the Wilson Coefficients (WC) when the operators are evaluated at the hadronic energy scale μ instead of the scale where heavy particles are integrated out. To find them we use the magic number technique, which is explained in detail in Appendix A and we quote here only the results. For the calculation of the mass difference for the B_d and B_s meson, we take the B parameters $(B_1, B_2, B_4) = (0.87, 0.82, 1.16)$ from [208] together with the decay constants $f_{B_d} = 0.240$ GeV and $f_{B_s} = 0.295$ GeV and the masses $m_{B_d} = 5.281$ GeV and $m_{B_s} = 5.370$ GeV. At the relevant hadronic scale $\mu = m_b$, we find for the Higgs contribution

$$\eta_2(\mu) = 1.650 \ , \quad \eta_4(\mu) = 2.259 \ , \tag{4.60}$$

while for the Z' contribution

$$\eta_1(\mu) = 0.713 \ , \quad \eta_4(\mu) = 5.446 \ . \tag{4.61}$$

In the case of $K^0 - \overline{K}^0$ mixing, the input parameters are $(B_1, B_2, B_4) = (0.60, 0.66, 1.03)$, $f_K = 0.160$ GeV and $m_K = 0.498$ GeV [206]. Calculating the η factors at a scale $\mu = 2$ GeV yields

$$\eta_2(\mu) = 2.210 \ , \quad \eta_4(\mu) = 3.523 \ , \tag{4.62}$$

for the Higgs boson induced operators and

$$\eta_1(\mu) = 0.674 \ , \quad \eta_4(\mu) = 8.181 \ , \tag{4.63}$$

for the operators related to Z'. Lastly, for neutral D-meson oscillations we consider the parameters $(B_1, B_2, B_4) = (0.865, 0.82, 1.08)$, $f_D = 0.200$ GeV and $m_D = 1.864$ GeV from [209]. At $\mu = 2.8$ GeV, we obtain the results

$$\eta_2(\mu) = 1.906 \ , \quad \eta_4(\mu) = 2.903 \ , \tag{4.64}$$

and

$$\eta_1(\mu) = 0.690 \ , \quad \eta_4(\mu) = 6.939 \ , \tag{4.65}$$

for the Higgs and Z' contributions, respectively. For the further calculation, we assume that changes in the contributions from box diagrams, which are also present in the SM, are negligible. As our model reproduces the same CKM mixing angles and fermion masses as in the SM, only tiny deviations due to the presence of vector-like quarks are expected. They are weak singlets though and a coupling to the W boson solely originates from fermion mass mixing. The additional loop suppression makes these effects insignificant compared to the tree level FCNCs.

In general, interference effects between the new physics contributions and SM processes can appear. However, in our case the additional Higgs contribution involves fermions of mixed left- and right-handed chirality and can not interfere with the left-handed currents in the SM process. Likewise, we find the dominant contribution from Z' exchange in diagrams

Observable (in GeV)	**Model Prediction**	
	BP1	**BP2**
$\Delta m_{B_d}^{\text{NP}}$	-1.402×10^{-13}	-1.495×10^{-14}
$\Delta m_{B_s}^{\text{NP}}$	2.663×10^{-14}	3.003×10^{-14}
Δm_{D}^{NP}	2.405×10^{-15}	2.036×10^{-15}
Δm_{K}^{NP}	0.504×10^{-15}	0.109×10^{-15}

Table 4.3 Neutral meson mass splittings that arise from new physics contributions in the $U(1)$ gauge extension of the SM. Both BPs are in agreement with current experimental limits. Published in [1].

where particles of left- and right-handed chirality participate. Therefore, we do not consider any interference terms. The total mass difference can now be divided in two parts

$$\Delta m_P^{\text{tot}} = \Delta m_P^{\text{SM}} + \Delta m_P^{\text{NP}} \,, \tag{4.66}$$

where Δm_P^{SM} is the theoretical SM prediction and Δm_P^{NP} labels the new new physics contribution. We evaluate whether our benchmark scenarios agree with the experimental results by demanding

$$\Delta m_P^{\text{NP}} < \Delta m_P^{\text{exp}} - \Delta m_P^{\text{SM}} \tag{4.67}$$

within a 3σ range. The theoretical predictions for neutral B-mesons in the SM are given by $\Delta m_{B_d}^{\text{SM}} = (3.475 \pm 0.513) \times 10^{-13}$ GeV and $\Delta m_{B_s}^{\text{SM}} = (1.205 \pm 0.178) \times 10^{-11}$ GeV [210]. The experimentally determined values are given by $\Delta m_{B_d}^{\text{exp}} = (3.334 \pm 0.013) \times 10^{-13}$ GeV and $\Delta m_{B_s}^{\text{exp}} = (1.169 \pm 0.001) \times 10^{-11}$ GeV [203]. Thus, we obtain the limits

$$\begin{aligned} \Delta m_{B_d}^{\text{exp}} - \Delta m_{B_d}^{\text{SM}} &= (-0.141 \pm 0.513) \times 10^{-13}\,\text{GeV}\,, \\ \Delta m_{B_s}^{\text{exp}} - \Delta m_{B_s}^{\text{SM}} &= (-0.036 \pm 0.178) \times 10^{-11}\,\text{GeV}\,. \end{aligned} \tag{4.68}$$

In the neutral K-meson system, the theoretical prediction is $\Delta m_K^{\text{SM}} = 3.074 \times 10^{-15}$ GeV [211]. However, this value only includes short distance contributions, whereas large distance effects are not calculable so far [212]. We therefore take into account a 30% uncertainty on the theoretical value. Taking into account the experimental result $\Delta m_K^{\text{exp}} = (3.484 \pm 0.006) \times 10^{-15}$ GeV [203], we find

$$\Delta m_K^{\text{exp}} - \Delta m_K^{\text{SM}} = (0.410 \pm 0.922) \times 10^{-15}\,\text{GeV}\,. \tag{4.69}$$

Note also that $|\epsilon_K|$ receives no contribution in our model, since the Yukawa couplings in the down-type sector are real. Similarly, the SM theory prediction for the mass splitting between D^0 and $\overline{D^0}$ has large theoretical uncertainties [213]. Thus, we require the new physics contribution to be less than the experimental uncertainty on the measured value $\Delta m_D^{\text{exp}} = (6.253^{+2.699}_{-2.896}) \times 10^{-15}$ GeV [203].

The results of the evaluation of Eq. (4.59) are given in Table 4.3 for the two considered benchmark points. Evidently, both scenarios are in agreement with current experimental limits. In particular, the new physics contribution to Δm_{B_d} is not far from current experimental bounds and a more precise measurement in future will be an interesting probe of our model.

4.3.2 Charged lepton flavor violation

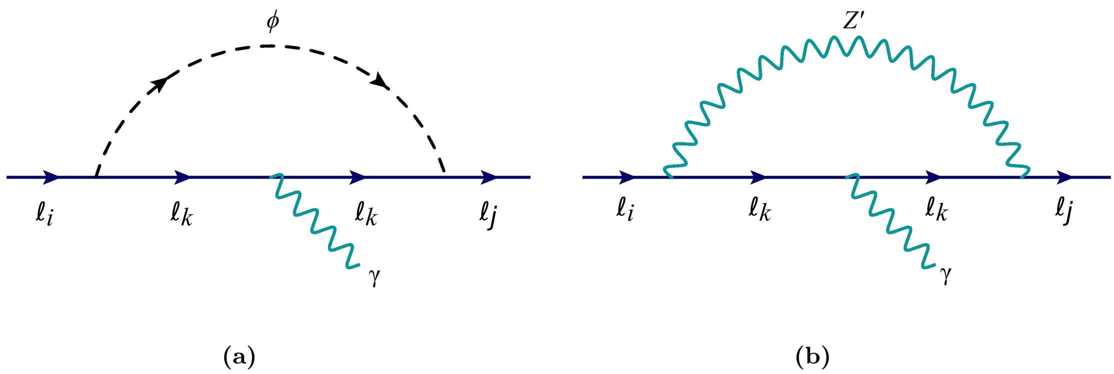

Figure 4.4 Feynman diagrams which generate the lepton flavor violating decays $\ell_i \to \ell_j \gamma$ at one-loop by exchange of the **(a)** Higgs boson or the **(b)** Z'. Published in [1]

Also in the lepton sector, there can be observable consequences from FCNCs. Especially in the decays $\ell_i \to \ell_j \gamma$, experiments put stringent constraints on new physics models that violate flavor. In our case, contributions to these processes arise at one-loop from the diagrams in Figure 4.4. The decay width of these diagrams is described by [214]

$$\Gamma(\ell_i \to \ell_j \gamma) = \sum_k \frac{(m_i^2 - m_j^2)^3 \left(|\sigma_L|^2 + |\sigma_R|^2\right)}{16\pi m_i^3} \tag{4.70}$$

where m_i and m_j indicate the masses of the ingoing and outgoing lepton, respectively. For the Higgs mediated diagram σ_L and σ_R can be identified with

$$\sigma_L = \frac{iQ_k}{16\pi^2 m_\phi^2} \left[(\rho m_i + \lambda m_j)\mathcal{F}_1(t) + \nu m_k \mathcal{F}_2(t)\right] , \tag{4.71}$$

$$\sigma_R = \frac{iQ_k}{16\pi^2 m_\phi^2} \left[(\lambda m_i + \rho m_j)\mathcal{F}_1(t) + \zeta m_k \mathcal{F}_2(t)\right] . \tag{4.72}$$

Note that a sum over the internal fermion ℓ_k with mass m_k and electric charge Q_k will be necessary if there are contributions from several different fermions inside the loop. The expressions $\mathcal{F}_1(t)$ and $\mathcal{F}_2(t)$ depend on the parameter $t = m_k^2/m_\phi^2$ and are given by

$$\begin{aligned} \mathcal{F}_1(t) &= \frac{t^2-5t-2}{12(t-1)^3} + \frac{t\ln t}{2(t-1)^4}\,, \\ \mathcal{F}_2(t) &= \frac{t-3}{2(t-1)^2} + \frac{\ln t}{(t-1)^3}\,. \end{aligned} \tag{4.73}$$

Of course, the decay amplitude depends on the involved Yukawa couplings and we identify $\rho = (\hat{\mathbf{Y}}_e)^*_{kj}(\hat{\mathbf{Y}}_e)_{ki}$, $\lambda = (\hat{\mathbf{Y}}_e)_{jk}(\hat{\mathbf{Y}}_e)^*_{ik}$, $\nu = (\hat{\mathbf{Y}}_e)^*_{kj}(\hat{\mathbf{Y}}_e)^*_{ik}$ and $\zeta = (\hat{\mathbf{Y}}_e)_{jk}(\hat{\mathbf{Y}}_e)_{ki}$.

For Z' mediated decays, the expressions slightly change. While Eq. (4.70) is still valid, the terms for σ_L and σ_R become

$$\sigma_L = \frac{iQ_k}{16\pi^2 M_{Z'}^2}\left[(\rho' m_i + \lambda' m_j)\mathcal{F}_3(t) + \nu' m_k \mathcal{F}_4(t) - \zeta' \frac{m_i m_j m_k}{M_{Z'}^2}\mathcal{F}_5(t)\right]\,, \tag{4.74}$$

$$\sigma_R = \frac{iQ_k}{16\pi^2 M_{Z'}^2}\left[(\lambda' m_i + \rho' m_j)\mathcal{F}_3(t) + \zeta' m_k \mathcal{F}_4(t) - \nu' \frac{m_i m_j m_k}{M_{Z'}^2}\mathcal{F}_5(t)\right]\,. \tag{4.75}$$

The functions appearing in these expressions depend on the parameter $t = m_k^2/M_{Z'}^2$ and are given by

$$\begin{aligned} \mathcal{F}_3(t) &= \frac{-5t^3+9t^2-30t+8}{12(t-1)^3} + \frac{3t^2\ln t}{2(t-1)^4}\,, \\ \mathcal{F}_4(t) &= \frac{t^2+t+4}{2(t-1)^2} - \frac{3t\ln t}{(t-1)^3}\,, \\ \mathcal{F}_5(t) &= \frac{-2t^2+7t-11}{6(t-1)^3} + \frac{\ln t}{(t-1)^4}\,, \end{aligned} \tag{4.76}$$

where $\lambda' = \left[\hat{g}_L^\ell(Z')\right]^*_{kj}\left[\hat{g}_L^\ell(Z')\right]_{ki}$, $\rho' = \left[\hat{g}_R^\ell(Z')\right]^*_{kj}\left[\hat{g}_R^\ell(Z')\right]_{ki}$, $\zeta' = \left[\hat{g}_L^\ell(Z')\right]^*_{kj}\left[\hat{g}_R^\ell(Z')\right]_{ki}$ and $\nu' = \left[\hat{g}_R^\ell(Z')\right]^*_{kj}\left[\hat{g}_L^\ell(Z')\right]_{ki}$. We remind the reader that the notation used for the couplings is defined in Section 4.2.6.

Further interesting flavor violating decays that arise in our model have the signature $\ell_i \to \overline{\ell}_j \ell_k \ell_l$. We determine the branching ratios of these decays to compare them to current experimental bounds and follow the calculation presented in [215]. If the decay is mediated by the scalar ϕ, the partial decay width will be

$$\Gamma(\ell_i \to \overline{\ell}_j \ell_k \ell_l) = \frac{1}{1536\pi^3}\frac{m_i^5}{m_\phi^4} S|(\hat{\mathbf{Y}}_e)^*_{ij}(\hat{\mathbf{Y}}_e)_{kl}|^2\,. \tag{4.77}$$

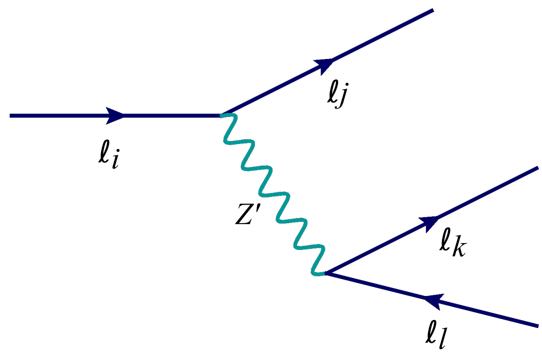

Figure 4.5 Feynman diagram responsible for the flavor violating decay $\ell_i \to \bar{\ell}_j \ell_k \ell_l$. Published in [1]

The factor S accounts for the symmetries in the final states and is chosen to be $S = 1$ when $k = l$ or $S = 2$ when one has $k \neq l$. The tree level contribution mediated by Z' is illustrated in Figure 4.5 and can be described by the partial decay width

$$\Gamma(\ell_i \to \bar{\ell}_j \ell_k \ell_l) = \frac{1}{1536\pi^3} \frac{m_i^5}{M_{Z'}^4} S \left[\frac{2}{S} |C_{LL}|^2 + \frac{2}{S} |C_{RR}|^2 + |C_{RL}|^2 + |C_{LR}|^2 \right]_{kl}^{ij} . \tag{4.78}$$

For the involved couplings with chirality $X, Y \in \{L, R\}$, we define the shorthand notation

$$[C_{XY}]_{kl}^{ij} = [\hat{g}_X^\ell(Z')]_{ij} [\hat{g}_X^\ell(Z')]_{kl} , \tag{4.79}$$

and the matrices $\hat{g}_X^\ell(Z')$ are defined in Section 4.2.6. The factor two before the terms C_{LL} and C_{RR} emerges because of interference between diagrams that are related by exchange of two identical leptons. From the calculation of the partial decay widths for our benchmark points, we find that the contribution from the Higgs boson ϕ is negligible compared to the Z' contribution. This can be understood from the fact that even though the Higgs boson has flavor non-diagonal couplings in the fermion mass eigenbasis, the couplings to first and second generation charged leptons are suppressed due to their tiny masses.

Experimental limits for the mentioned decays are usually quoted as branching ratios. From the partial decay widths, we obtain the branching ratio through the relation

$$\mathrm{BR}(\ell_i \to \bar{\ell}_j \ell_k \ell_l) = \frac{\Gamma(\ell_i \to \bar{\ell}_j \ell_k \ell_l)}{\Gamma^{\mathrm{tot}}} , \tag{4.80}$$

where $\Gamma_\mu^{\mathrm{tot}} = 3.00 \times 10^{-19}$ GeV and $\Gamma_\tau^{\mathrm{tot}} = 2.27 \times 10^{-12}$ GeV are the total decay widths for the muon and tau, respectively [203]. For our analysis, we consider the decays $\mu^- \to e^- \gamma$, $\tau^- \to e^- \gamma$, $\tau^- \to \mu^- \gamma$, $\tau^- \to \mu^- e^+ e^-$, $\tau^- \to e^- e^+ e^-$ and $\mu^- \to e^- e^+ e^-$. The resulting branching ratios for the two BPs, together with the current experimental bounds are presented in Table 4.4 [203]. As our results show, the benchmark scenarios agree with current limits. The current sensitivity for the decay $\mu^- \to e^-\gamma$ is close to our model prediction and will be therefore allow to test the model in upcoming experiments.

Process	**Experimental Limit**	**Model Prediction**	
		BP1	**BP2**
$\mathrm{BR}(\mu^- \to e^-\gamma)$	$< 4.2 \times 10^{-13}$	1.8×10^{-14}	6.3×10^{-15}
$\mathrm{BR}(\tau^- \to e^-\gamma)$	$< 3.3 \times 10^{-8}$	2.2×10^{-14}	2.2×10^{-14}
$\mathrm{BR}(\tau^- \to \mu^-\gamma)$	$< 4.4 \times 10^{-8}$	6.8×10^{-15}	3.0×10^{-15}
$\mathrm{BR}(\mu^- \to e^-e^+e^-)$	$< 1.0 \times 10^{-12}$	1.3×10^{-18}	3.9×10^{-19}
$\mathrm{BR}(\tau^- \to e^-e^+e^-)$	$< 2.7 \times 10^{-8}$	2.2×10^{-17}	1.8×10^{-17}
$\mathrm{BR}(\tau^- \to \mu^-e^+e^-)$	$< 1.8 \times 10^{-8}$	9.5×10^{-18}	4.1×10^{-18}

Table 4.4 Experimental bounds on branching ratios for lepton flavor violating decays together with the model prediction of the benchmark scenarios in the $U(1)$ gauge extension of the SM. Published in [1].

4.3.3 Other implications

Besides the processes considered so far, there is a variety of other observables that can be influenced by the additional Z' boson and the vector-like fermions. With our benchmark points we have demonstrated that some of the vector-like fermions could exist at a mass scale of a few TeV. This will have interesting implications for forthcoming collider searches. For instance, vector-like fermions could be produced in pp collisions via s-channel Z and γ exchange. While the decay of charged vector-like leptons could lead to missing energy signatures such as $2l + \not{E}_T$ or $4l + \not{E}_T$, the decay of vector-like quarks will be testable in $jj + 4l, b\bar{b} + 4l, t\bar{t} + 4l$ final states. The authors of [216] extensively study the discovery prospects for vector-like leptons at future colliders such as HL-LHC, HE-LHC and FCC-hh. According to their study, weak singlet vector-like leptons can be tested up to a mass scale $\sim$ 3 TeV with a 100 TeV pp collider. Collider limits on vector-like quarks that decay to multi-lepton final states together with jets or bottom and top quarks are investigated in [217] and show that a 100 TeV collider can probe vector-like quark masses as large as $\sim$ 7 TeV. Additionally, the new force mediator Z' can be possibly probed at upcoming collider experiments such as a high energy muon collider. The studies in [218, 219] have investigated that mediator masses of the order $\mathcal{O}(100)$ TeV could be probed in the two body scattering processes $\mu^+\mu^- \to \mu^+\mu^-$ with a muon collider with a center-of-mass energy of $\sqrt{s} = 3$ TeV and $\mathcal{L} = 1$ ab^{-1} integrated luminosity for the gauge coupling strengths $g_X = 1$ ($\sqrt{4\pi}$) [218, 219].

On top of that, flavor violating Higgs decays, such as $h \to e\tau$ and $h \to\to \mu\tau$, can in principle occur in our model. We estimated the corresponding branching ratios and found them to be below current experimental bounds.

In recent years, there is an increasing interest in the measurement of the muon magnetic moment that does not align with SM predictions [115]. In principle the anomaly can be explained by the existence of a vector-like lepton that contributes at the one-loop level to the muon $g - 2$ [220]. However, we find that the extra contributions that arise in our benchmark scenarios are three orders of magnitude too small to explain the anomaly.

Chapter 5

Hierarchy from loops in a left-right symmetric model

We have shown in the previous chapter that the flavor mass hierarchy can be partly explained by gauge loop corrections in a $U(1)$ extension of the SM. Here, we propose a complete radiative origin of the fermion mass hierarchy in a non-Abelian gauge extension. We will see in the following that non-Abelian gauge symmetries offer much more possibilities due to the emergence of additional charged and neutral gauge bosons. Among the non-Abelian gauge extensions of the SM, left-right symmetric models (LRSM) are particularly intriguing [48–50, 221, 222]. They explain not only parity violation due to spontaneous symmetry breaking, but they also include right-handed neutrinos as part of the right-handed lepton doublets. This is tempting from a symmetry point of view and opens many possibilities to incorporate massive neutrinos [63, 67]. In this chapter, we propose a mechanism in the left-right symmetric framework, where the third generation of fermions is massive at tree level, whereas the second and first generation fermions obtain masses from one-loop and two-loop quantum corrections, respectively. By implementing a double seesaw mechanism, this scenario can be entirely realized via gauge loop corrections. The scalar sector of the model comprises only those fields required for symmetry breaking and the physical spectrum consists of three neutral scalars out of which one is the SM Higgs boson. Since the rank of the fermion mass matrix is increased stepwise by including higher loop corrections, the mass hierarchy is solely created from loop factors. Our mechanism applies to quarks and charged leptons, whereas the realization of sub-eV neutrino masses necessitates the presence of lepton number violating terms at high scales.

The remainder of this chapter is structured as follows: In Section 5.1 we discuss the basic idea of our mechanism. Subsequently, in Section 5.2 we present how it can be implemented in a left-right symmetric framework and discuss the generation of quark and charged lepton masses in detail in Sections 5.3 and 5.4. Neutrinos require a special treatment which is outlined in Section 5.5, before we finally provide numerical results for our study in Section 5.6. Note that the work presented in this chapter is published in [3].

5.1 Basic mechanism

In Section 4.1 we have discussed the idea of the rank mechanism, and showed that it can be realized in a theory with seesaw-like mass matrices. The implementation of this idea in a theory with non-Abelian gauge symmetry is remarkably simple in left-right symmetric models, where the gauge symmetry is given by[1]

$$\mathcal{G}_{\text{LRSM}} = SU(3)_C \times SU(2)_R \times SU(2)_L \times U(1)_X \ .$$

In these theories, the fermion content has a parity symmetric structure, such that left-handed fermions are part of a doublet representation of $SU(2)_L$, while right-handed fermions are arranged in doublets of $SU(2)_R$. If the theory only includes two scalar fields χ_L and χ_R in the doublet representation of $SU(2)_L$ and $SU(2)_R$, respectively, Yukawa couplings connecting left-handed and right-handed SM fermions will not be possible.[2] To achieve fermion masses in this setting, another m generations of massive vector-like quarks and leptons can be introduced, which transform as singlets under $SU(2)_L \times SU(2)_R$. When the gauge symmetry is spontaneously broken by non-zero VEVs v_L and v_R, this gives rise to a generalized seesaw [53–56, 226] and the fermion mass matrices of dimension $(3+m)\times(3+m)$ have the structure

$$\mathcal{M} = \begin{pmatrix} \mathbf{0} & v_L|\alpha\rangle \\ v_R\langle\alpha| & M_T \end{pmatrix} \ . \tag{5.1}$$

Here, the Yukawa couplings are summarized by $|\alpha\rangle$ and the $m \times m$ matrix M_T represents an explicit vector-like mass. The above mass matrix has rank $2m$. The choice of m therefore regulates how many SM fermions are massive at tree level. Our objective is to have one massive SM fermion at tree level and when we consecutively include higher loop corrections the matrix rank should increase further. Specifically, we pursue a realization with no additional scalars besides those that are needed to break the gauge symmetry. Previous studies [1, 45] have shown that flavor non-diagonal gauge couplings are necessary to increase the rank of the above matrix through one-loop gauge boson corrections. Notably, the situation will change if we include further n generations of a new species of fermions such that the matrix is extended to dimension $(3 + m + n) \times (3 + m + n)$ and has a double seesaw structure as illustrated below

$$\mathcal{M} = \begin{pmatrix} \mathbf{0} & v_L|\alpha\rangle & \mathbf{0} \\ v_R\langle\alpha| & M_T & |\beta\rangle \\ \mathbf{0} & \langle\beta| & \mathbf{0} \end{pmatrix} \ . \tag{5.2}$$

In our notation, $|\beta\rangle$ is an $m \times n$ vector that includes Yukawa couplings to the new species of fermions. Since these have no explicit mass terms, the matrix rank of $\mathcal{M}$ is still $2m$ and

[1] Note that one can also identify X with $B-L$ charge. However, as discussed in [223], this would imply a breaking of $B-L$ charge which is not always desired.

[2] Many LRSMs feature a bi-doublet scalar, which allows to introduce mass terms for SM fermions directly (see e.g. [224, 225]).

the extended matrix structure allows for an enhancement of the matrix rank at one-loop due to the diagonal gauge interactions.[3] This feature of double seesaw models was already investigated in [227], where small active neutrino masses arise from one-loop radiative corrections. To our knowledge, its application to other species of fermions has not been considered so far. A two-loop correction which introduces new linear independent sets of couplings from the $SU(2)$ isospin partners to the mass matrix is then able to raise the rank even further.

While we only outline the basic idea in this section, a UV complete model that resides in the framework of LRSMs is discussed in the following sections. As illustrated in Figure 5.1, the model is able to generate third generation masses at the tree level from a seesaw relation, while the second generation masses originate from neutral current interactions at one-loop. Lastly, small masses of first generation fermions can be explained by two-loop suppression from charged gauge boson exchange, which mix only at one-loop level in our setup.

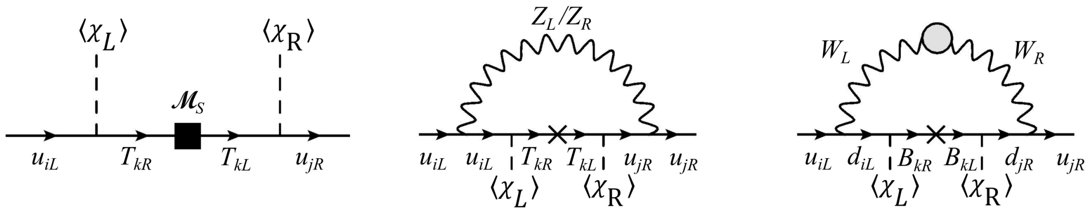

Figure 5.1 Illustration of the mass generation for quarks in the LRSM. While the third generation gets a mass at tree level (left panel), the mass of second generation fermions emerges at one-loop (middle panel) and a two-loop radiative correction is responsible for the first generation mass (right panel). The grey blob on the internal gauge boson propagator indicates mixing at one-loop level. Published in [3].

5.2 Double seesaw in a left-right symmetric model

5.2.1 Particle spectrum

To implement the double seesaw texture, which is fundamental for our mechanism, we take the universal seesaw models presented in [51–56] as a starting point. Under the gauge group $\mathcal{G}_{\rm LRSM}$, the SM fermions form doublets of either $SU(2)_L$ or $SU(2)_R$ and have the following transformation properties

$$\begin{aligned} Q_{jL} &= \begin{pmatrix} u_j \\ d_j \end{pmatrix}_L \sim (3,2,1,1/3)\ ,\ Q_{jR} = \begin{pmatrix} u_j \\ d_j \end{pmatrix}_R \sim (3,1,2,1/3)\ , \\ \Psi_{jL} &= \begin{pmatrix} \nu_j \\ e_j \end{pmatrix}_L \sim (1,2,1,-1)\quad ,\ \ \Psi_{jR} = \begin{pmatrix} \nu_j \\ e_j \end{pmatrix}_R \sim (1,1,2,-1)\ , \end{aligned} \tag{5.3}$$

[3]This is only true provided that $m < 3 + n$. If the inequality were not fulfilled, all SM fermions would be already massive at the tree level.

where the index $j = 1, 2, 3$ labels the three SM families. The scalar sector does not include the usual bi-doublet representation as it would prevent the seesaw structure. Instead, it consists of two scalar fields

$$\chi_L \sim (1, 2, 1, 1) \ , \qquad \chi_R \sim (1, 1, 2, 1) \ , \tag{5.4}$$

which will be also responsible for spontaneous symmetry breaking. In this setup, the electric charge is given by

$$Q = T_L^3 + T_R^3 + \frac{X}{2} \ , \tag{5.5}$$

with the third component of $SU(2)_L$ and $SU(2)_R$ isospin given by T_L^3 and T_R^3, respectively. Since there is no possibility to include fermion masses with the particles listed so far, a set of massive vector-like fermions is included

$$\begin{aligned} T_k \sim (3, 1, 1, 4/3) \ , \ B_k \sim (3, 1, 1, -2/3) \ , \\ N_k \sim (1, 1, 1, 0) \ , \ E_k \sim (1, 1, 1, -2) \ . \end{aligned} \tag{5.6}$$

Note that the gauge charges are assigned in such a way that each SM fermion species has $k = 1, 2$ vector-like partners of same electric charge and gauge anomalies automatically cancel due to the vector-like character of the new fermions.

To achieve a mass matrix similar to Eq. (5.2), we extend the gauge group by an additional Abelian $U(1)_{X'}$. In doing so, the complete gauge group is given by

$$\mathcal{G} \equiv SU(3)_C \times SU(2)_R \times SU(2)_L \times U(1)_X \times U(1)_{X'} \ .$$

The particles mentioned so far are not charged under $U(1)_{X'}$, but another set of fermions is added which transforms non-trivially under the new gauge group. The purpose of this is to accomplish a double seesaw texture for the tree level mass matrix. Note however that one could in principle also use a discrete symmetry, such as Z_4, to implement this idea. In more detail, we include one generation of exotic fermions, which have vector-like properties with regard to $\mathcal{G}_{\text{LRSM}}$ but are chiral concerning the new gauge symmetry $U(1)_{X'}$. Their quantum numbers are given as

$$\begin{aligned} T'_{L/R} \sim (3, 1, 1, 4/3, \mp\alpha) \ , \ B'_{L/R} \sim (3, 1, 1, -2/3, \pm\alpha) \ , \\ N'_{L/R} \sim (1, 1, 1, 0, \pm\alpha) \ , \ E'_{L/R} \sim (1, 1, 1, -2, \mp\alpha) \ , \end{aligned} \tag{5.7}$$

and are specifically chosen to cancel gauge anomalies within each generation. It is apparent that explicit masses can not be realized for this type of fermions, unless a further singlet scalar with a $U(1)_{X'}$ charge of 2α would be included. We choose not to do so, but instead add a complex scalar with gauge charges

$$\eta \sim (1, 1, 1, 0, \alpha) \ . \tag{5.8}$$

The purpose of this scalar is twofold. On the one hand, its VEV can spontaneously break the gauge symmetry $U(1)_{X'}$ and provide mass for the associated neutral gauge boson. On the other hand, its gauge charges allow a coupling of the primed fermions to the vector-like fermions. Table 5.1 summarizes the particle content of our model.

Type	Particle	$\mathbf{SU(3)_C}$	$\mathbf{SU(2)_R}$	$\mathbf{SU(2)_L}$	$\mathbf{U(1)_X}$	$\mathbf{U(1)_{X'}}$
Quarks	$Q_{jL} = \begin{pmatrix} u_j \\ d_j \end{pmatrix}_L$	**3**	**1**	**2**	1/3	0
	$Q_{jR} = \begin{pmatrix} u_j \\ d_j \end{pmatrix}_R$	**3**	**2**	**1**	1/3	0
Leptons	$\Psi_{jL} = \begin{pmatrix} \nu_j \\ e_j \end{pmatrix}_L$	**1**	**1**	**2**	-1	0
	$\Psi_{jR} = \begin{pmatrix} \nu_j \\ e_j \end{pmatrix}_R$	**1**	**2**	**1**	-1	0
BSM Fermions	$T_{1\,L/R}\ ,\ T_{2\,L/R}\ ,\ T'_{L/R}$	**3**	**1**	**1**	4/3	$\{0, 0, \mp\alpha\}$
	$B_{1\,L/R}\ ,\ B_{2\,L/R}\ ,\ B'_{L/R}$	**3**	**1**	**1**	-2/3	$\{0, 0, \pm\alpha\}$
	$N_{1\,L/R}\ ,\ N_{2\,L/R}\ ,\ N'_{L/R}$	**1**	**1**	**1**	0	$\{0, 0, \pm\alpha\}$
	$E_{1\,L/R}\ ,\ E_{2\,L/R}\ ,\ E'_{L/R}$	**1**	**1**	**1**	-2	$\{0, 0, \mp\alpha\}$
Scalars	$\chi_L = \begin{pmatrix} \chi_L^+ \\ \chi_L^0 \end{pmatrix}$	**1**	**1**	**2**	1	0
	$\chi_R = \begin{pmatrix} \chi_R^+ \\ \chi_R^0 \end{pmatrix}$	**1**	**2**	**1**	1	0
	η	**1**	**1**	**1**	0	α

Table 5.1 Particle content of the left-right symmetric model. In addition to the three SM families, we consider further two generations of vector-like fermions ($T,\ B,\ N,\ E$) and one generation of the fermions ($T',\ B',\ N',\ E'$), which are chiral under $U(1)_{X'}$. Published in [3].

5.2.2 Scalar sector

With the three scalars included in our model, the most general scalar potential is specified below

$$\begin{aligned} V(\chi_L, \chi_R, \eta) =& \mu_1^2 \chi_L^\dagger \chi_L + \mu_2^2 \chi_R^\dagger \chi_R + \lambda_{1L} (\chi_L^\dagger \chi_L)^2 + \lambda_{1R} (\chi_R^\dagger \chi_R)^2 + \lambda_2 (\chi_L^\dagger \chi_L)(\chi_R^\dagger \chi_R) \\ &+ \mu_\eta^2 \eta^\dagger \eta + \lambda_3 (\eta^\dagger \eta)^2 + \lambda_{4L} (\eta^\dagger \eta)(\chi_L^\dagger \chi_L) + \lambda_{4R} (\eta^\dagger \eta)(\chi_R^\dagger \chi_R)\ . \end{aligned} \tag{5.9}$$

LRSMs allow to define parity symmetry due to the extended gauge structure. If the couplings fulfill the relations

$$\begin{aligned} \lambda_1 &\equiv \lambda_{1L} = \lambda_{1R}\ , \\ \lambda_4 &\equiv \lambda_{4L} = \lambda_{4R}\ , \end{aligned} \tag{5.10}$$

the potential will be parity symmetric. Strictly speaking, parity symmetry also dictates $\mu_1 = \mu_2$. Nevertheless, we allow $\mu_1 \neq \mu_2$ and hence adopt a LRSM with softly broken parity symmetry.

A detailed study of the potential in Eq. (5.9) is beyond the scope of this work. For now, we assume that a non-zero VEV of η breaks the $U(1)_{X'}$ symmetry at a high scale. Subsequently, this is followed by the breaking of $SU(2)_R$ and $SU(2)_L$ according to

$$\begin{aligned} SU(3)_C \times SU(2)_R \times SU(2)_L \times U(1)_X \times U(1)_{X'} &\xrightarrow{\langle\eta\rangle} SU(3)_C \times SU(2)_R \times SU(2)_L \times U(1)_X \\ &\xrightarrow{\langle\chi_R\rangle} SU(3)_C \times SU(2)_L \times U(1)_Y \\ &\xrightarrow{\langle\chi_L\rangle} SU(3)_C \times U(1)_{EM} \ . \end{aligned} \tag{5.11}$$

By convention, we define the VEVs of the fields as

$$\langle\chi_L\rangle = \frac{1}{\sqrt{2}} \begin{pmatrix} 0 \\ v_L \end{pmatrix} , \qquad \langle\chi_R\rangle = \frac{1}{\sqrt{2}} \begin{pmatrix} 0 \\ v_R \end{pmatrix} , \qquad \langle\eta\rangle = \frac{v_\eta}{\sqrt{2}} , \tag{5.12}$$

and identify $v_L = 246$ GeV with the electroweak scale. Note that without loss of generality, all VEVs are real.

Counting degrees of freedom, we see that out of the ten real scalar components, seven become longitudinal modes for the massive gauge bosons. Therefore, the physical scalar spectrum is comparatively small and only made up of three neutral scalars. For the following calculations, we expand the neutral components of $\chi_L = (\chi_L^+, \chi_L^0)^T$, $\chi_R = (\chi_R^+, \chi_R^0)^T$ and η in terms of the fields

$$\chi_L^0 = \frac{1}{\sqrt{2}} (v_L + \sigma_L + i\rho_L) \ , \ \chi_R^0 = \frac{1}{\sqrt{2}} (v_R + \sigma_R + i\rho_R) \ , \ \eta = \frac{1}{\sqrt{2}} \left(v_\eta + \sigma_\eta + i\rho_\eta\right) \ . \tag{5.13}$$

In this notation, σ_L, σ_R and σ_η are the three physical scalars, while ρ_L, ρ_R and ρ_η become the massless Goldstone bosons that are eaten by the three neutral gauge bosons in the process of spontaneous symmetry breaking. From the potential given in Eq. (5.9) we deduce the scalar masses

$$\mathcal{L} \supset \frac{1}{2} \begin{pmatrix} \sigma_L & \sigma_R & \sigma_\eta \end{pmatrix} \mathcal{M}_\sigma^2 \begin{pmatrix} \sigma_L \\ \sigma_R \\ \sigma_\eta \end{pmatrix} , \tag{5.14}$$

where the mass matrix $\mathcal{M}_\sigma^2$ is given by

$$\mathcal{M}_\sigma^2 = \begin{pmatrix} 2\lambda_1 v_L^2 & \lambda_2 v_L v_R & \lambda_4 v_L v_\eta \\ \lambda_2 v_L v_R & 2\lambda_1 v_R^2 & \lambda_4 v_R v_\eta \\ \lambda_4 v_L v_\eta & \lambda_4 v_R v_\eta & 2\lambda_3 v_\eta^2 \end{pmatrix} . \tag{5.15}$$

To simplify our calculations, we examine the limit $\lambda_4 \ll 1$. In this case, η does not mix with the remaining scalars and its mass is determined from the $U(1)_{X'}$ symmetry breaking scale via the relation

$$M_\eta^2 = 2\lambda_3 v_\eta^2 \ . \tag{5.16}$$

We emphasize that this is a simplification which does not have to be true in general. The remaining two scalars mix due to the presence of non-zero off-diagonal mass matrix entries. A proper transformation of the basis $(\sigma_L,\ \sigma_R)$ to the new states $(h,\ H)$ via

$$\begin{pmatrix} h \\ H \end{pmatrix} = \begin{pmatrix} \cos\xi & \sin\xi \\ -\sin\xi & \cos\xi \end{pmatrix} \begin{pmatrix} \sigma_L \\ \sigma_R \end{pmatrix} \tag{5.17}$$

diagonalizes the mass matrix and yields the mass eigenstates with a mixing angle

$$\tan(2\xi) = \frac{\lambda_2 v_L v_R}{\lambda_1 (v_R^2 - v_L^2)} \ . \tag{5.18}$$

To align with experimental observations, the right-handed breaking scale needs to be larger than the left-handed one and we find the scalar mass eigenvalues

$$M_h^2 \simeq \left(2\lambda_1 - \frac{\lambda_2^2}{2\lambda_1}\right) v_L^2 \ , \tag{5.19}$$

$$M_H^2 \simeq 2\lambda_1 v_R^2 \ , \tag{5.20}$$

using $v_L \ll v_R$. Obviously, the lighter states plays the role of the SM Higgs. When we fix its mass to the experimentally observed value $M_h = 125.25$ GeV [31], we find that λ_1 is given by the expression

$$\lambda_1 = \frac{1}{8}\left(\frac{2M_h^2}{v_L^2} + \sqrt{\left(\frac{2M_h^2}{v_L^2}\right)^2 + 16\lambda_2^2}\right) \ . \tag{5.21}$$

5.2.3 Gauge boson sector

Neglecting the unbroken $SU(3)_C$ for a moment, the theory has in total eight gauge bosons stemming from the rank eight gauge symmetry $SU(2)_R \times SU(2)_L \times U(1)_X \times U(1)_{X'}$. In the following, $SU(2)_L$ $(SU(2)_R)$ gauge bosons are labeled by $W^i_{L\mu}$ $\left(W^i_{R\mu}\right)$, while we indicate the single gauge bosons from $U(1)_X$ and $U(1)_{X'}$ with B_μ and X_μ, respectively. To align with observations, seven of these gauge bosons need to become massive[4] leaving only one massless state which will be the photon. Gauge boson masses follow from the Lagrangian

$$\mathcal{L} \supset \left(D_\mu \chi_L\right)^\dagger \left(D^\mu \chi_L\right) + \left(D_\mu \chi_R\right)^\dagger \left(D^\mu \chi_R\right) + \left(D_\mu \eta\right)^\dagger \left(D^\mu \eta\right) \ , \tag{5.22}$$

after spontaneous symmetry breaking. In the literature, LRSMs often include a scalar bi-doublet and automatically induce tree level mixing of charged gauge bosons. However, in our model this scalar is not present and the states $W_L^\pm = \left(W_L^2 \mp i W_L^1\right)/\sqrt{2}$ and

[4]They absorb exactly the seven massless Goldstone modes as discussed in the previous section.

$W_R^\pm = \left(W_R^2 \mp iW_R^1\right)/\sqrt{2}$ only start to mix at one-loop level. Hence, at the tree level their masses are given by

$$M_{W_L}^2 = \frac{g_L^2 v_L^2}{4}\,, \qquad M_{W_R}^2 = \frac{g_R^2 v_R^2}{4}\,, \tag{5.23}$$

where g_L and g_R are the gauge couplings of $SU(2)_L$ and $SU(2)_R$. In the parity symmetric limit considered here, gauge couplings in the left- and right-handed sector are identical and therefore we use $g \equiv g_L = g_R$. Generally, mixing among neutral gauge bosons happens after spontaneous symmetry breaking. In the basis (W_L^3, W_R^3, B, X), the squared mass matrix is provided by the expression

$$\mathcal{M}^2 = \frac{1}{4}\begin{pmatrix} g_L^2 v_L^2 & 0 & -g_L g' v_L^2 & 0 \\ 0 & g_R^2 v_R^2 & -g_R g' v_R^2 & 0 \\ -g_L g' v_L^2 & -g_R g' v_R^2 & g'^2(v_R^2 + v_L^2) & 0 \\ 0 & 0 & 0 & g_X^2 v_\eta^2 \end{pmatrix}\,, \tag{5.24}$$

where the $U(1)_X$ and $U(1)_{X'}$ gauge couplings are given by g' and g_X. Since η is the only scalar which carries $U(1)_{X'}$ charge, the gauge boson X_μ decouples from the remaining spectrum and its mass is given by

$$M_X^2 = \frac{g_x^2 v_\eta^2}{4}\,. \tag{5.25}$$

Due to the appearance of non-diagonal matrix entries, the three leftover gauge bosons mix and the mass matrix needs to be diagonalized. As a first step, we rotate away the zero mode corresponding to the photon. In order to do so, we apply a basis transformation

$$\begin{pmatrix} A \\ Z_L \\ Z_R \end{pmatrix} = \begin{pmatrix} s_w & s_w & \sqrt{c_w^2 - s_w^2} \\ c_w & -s_w^2/c_w & -s_w\sqrt{c_w^2 - s_w^2}/c_w \\ 0 & \sqrt{c_w^2 - s_w^2}/c_w & -s_w/c_w \end{pmatrix}\begin{pmatrix} W_L^3 \\ W_R^3 \\ B \end{pmatrix}\,, \tag{5.26}$$

where $s_w \equiv \sin(\theta_w) = e/g$ is the weak mixing angle and the coupling e is defined by the relation $1/e^2 = 2/g^2 + 1/g'^2$. In the new basis (A, Z_L, Z_R), the photon A is massless. The remaining two states (Z_L, Z_R) still mix and their 2×2 mass matrix is characterized through the entries

$$\begin{aligned} M_{LL}^2 &= \frac{e^2 v_L^2}{4 s_w^2 c_w^2}\,, \\ M_{RL}^2 &= \frac{e^2 v_L^2}{4 c_w^2 \sqrt{c_w^2 - s_w^2}}\,, \\ M_{RR}^2 &= \frac{e^2}{4\left(c_w^2 - s_w^2\right)}\left(\frac{c_w^2 v_R^2}{s_w^2} + \frac{s_w^2 v_L^2}{c_w^2}\right)\,. \end{aligned} \tag{5.27}$$

Therefore, the last step to obtain the mass eigenstates is a further diagonalization. We apply a unitary transformation

$$\begin{pmatrix} Z \\ Z' \end{pmatrix} = \begin{pmatrix} \cos\zeta & \sin\zeta \\ -\sin\zeta & \cos\zeta \end{pmatrix} \begin{pmatrix} Z_L \\ Z_R \end{pmatrix} , \tag{5.28}$$

where Z and Z' are now mass eigenstates and their mixing angle is defined as

$$\tan(2\zeta) = \frac{2M_{LR}^2}{M_{LL}^2 - M_{RR}^2} . \tag{5.29}$$

The lighter of the two, defined as Z, plays the role of the SM Z boson and the final masses can be obtained from the formula

$$M_{Z,Z'}^2 = \frac{1}{2}\left(M_{LL}^2 + M_{RR}^2 \mp (M_{LL}^2 - M_{RR}^2)\sqrt{1+\tan^2(2\zeta)}\right) . \tag{5.30}$$

Of course, $Z - Z'$ mixing is subject to experimental constraints. We therefore provide a rough estimate on the mixing angle. For $g_R = g_L \simeq 0.65$, $g' = 0.428$, $\sin^2(\theta_w) = 0.231$ and a VEV of $v_R = 5$ TeV, we find $\zeta = 6.9 \times 10^{-4}$. This mixing is already quite small and will be even further suppressed for larger v_R.

5.2.4 Yukawa interactions

In this section we give the details on Yukawa interactions which are allowed with the present gauge charges and particles. As a start, we consider the quark sector. Writing down all terms that align with the gauge symmetry yields the Lagrangian

$$\begin{aligned} \mathcal{L}_{Yuk} = & - y_a^q \overline{Q}_L \tilde{\chi}_L T_R - y_b^q \overline{Q}_R \tilde{\chi}_R T_L \\ & - y_c^q \overline{Q}_L \chi_L B_R - y_d^q \overline{Q}_R \chi_R B_L \\ & - y_1^q \overline{T}_L \eta^\dagger T_R' - y_2^q \overline{T}_R \eta T_L' \\ & - y_3^q \overline{B}_L \eta B_R' - y_4^q \overline{B}_R \eta^\dagger B_L' + \ h.c. \end{aligned} \tag{5.31}$$

The Yukawa coupling matrices y_x^q, $x = a, b, c, d$ are of dimension 3×2 while those labeled by $x = 1, 2, 3, 4$ have dimension 2×1. From the Lagrangian we see that no terms appear which directly combine Q_L and Q_R at the renormalizable level. Instead, SM fermions couple to vector-like fermions $(T,\ B)$, and these in turn are connected to the primed fermions $(T',\ B')$. In addition, the gauge charges of vector-like fermions allow us to add explicit masses

$$\mathcal{L}_{VLF} = -M_T \overline{T}_L T_R - M_B \overline{B}_L B_R + \ h.c. , \tag{5.32}$$

which are described by the 2×2 matrices M_T and M_B. We emphasize that explicit mass terms for T' and B' are forbidden due to the assigned $U(1)_{X'}$ charges.

The specific characteristics of the fermions fields $N_{L/R}$ lead to a different situation in the lepton sector. As they are complete gauge singlets, lepton number violating terms are allowed in principle.[5] The presence of LNV operators will be crucial to achieve realistic neutrino masses in our model and we postpone their discussion to Section 5.5. For now, we restrict ourselves to lepton number conserving operators which are relevant for the generation of charged lepton masses. The lepton number conserving Lagrangian is defined by

$$\begin{aligned}\mathcal{L}_{Yuk} = &- y_a^\ell \overline{\Psi}_L \tilde{\chi}_L N_R - y_b^\ell \overline{\Psi}_R \tilde{\chi}_R N_L \\ &- y_c^\ell \overline{\Psi}_L \chi_L E_R - y_d^\ell \overline{\Psi}_R \chi_R E_L \\ &- y_1^\ell \overline{N}_L \eta N_R' - y_2^\ell \overline{N}_R \eta^\dagger N_L' \\ &- y_3^\ell \overline{E}_L \eta^\dagger E_R' - y_4^\ell \overline{E}_R \eta E_L' + \ h.c. \ ,\end{aligned} \tag{5.33}$$

where the superscript ℓ distinguishes the lepton Yukawa matrices from the quark ones. Similarly, we can write down the explicit vector-like masses

$$\mathcal{L}_{VLF} = -M_N \overline{N}_L N_R - M_E \overline{E}_L E_R + \ h.c. \tag{5.34}$$

The addition of right-handed lepton doublets in LRSMs allows to define parity as a symmetry. To be precise, parity can be defined by the transformation

$$\begin{aligned} Q_L \leftrightarrow Q_R \ , \quad \Psi_L \leftrightarrow \Psi_R \ , \quad T_L^{(\prime)} \leftrightarrow T_R^{(\prime)} \ , \quad B_L^{(\prime)} \leftrightarrow B_R^{(\prime)} \ , \\ N_L^{(\prime)} \leftrightarrow N_R^{(\prime)} \ , \quad E_L^{(\prime)} \leftrightarrow E_R^{(\prime)} \ , \quad \chi_L \leftrightarrow \chi_R \ , \quad \eta \leftrightarrow \eta^\dagger \ . \end{aligned} \tag{5.35}$$

Clearly, if the Lagrangian is invariant under such a transformation, this will have significant impact on the parameters of the model. In the quark sector, we can identify the Yukawa couplings

$$y_a^q = y_b^q \ , \ \ y_c^q = y_d^q \ , \ \ y_1^q = y_2^q \ , \ \ y_3^q = y_4^q \ , \tag{5.36}$$

and the same holds for lepton couplings

$$y_a^\ell = y_b^\ell \ , \ \ y_c^\ell = y_d^\ell \ , \ \ y_1^\ell = y_2^\ell \ , \ \ y_3^\ell = y_4^\ell \ . \tag{5.37}$$

Furthermore, the vector-like mass matrices need to satisfy

$$M_T = M_T^\dagger \ , \qquad M_B = M_B^\dagger \ , \qquad M_N = M_N^\dagger \ , \qquad M_E = M_E^\dagger \ . \tag{5.38}$$

Note that without loss of generality, we can choose a basis where the vector-like matrices are real and diagonal. The number of parameters is reduced significantly and we adopt a parity symmetric Lagrangian for our further analysis, i.e. we apply Eqs. (5.36 - 5.38) in the subsequent discussion. Furthermore, we point out that the strong CP angle θ is zero at tree level due to parity symmetry (compare with notation in Section 2.3).

[5] Each of the fields Ψ, N, E, N' and E' carries +1 unit of lepton number.

5.3 Quark masses

The Yukawa Lagrangian given in Eq. (5.31) is the origin of fermion masses after spontaneous symmetry breaking and we discuss the details of the up-type quark sector in this section. It is therefore convenient to drop the superscript y^q in our notation and only reintroduce it when it is not clear from the context.

In the following, we examine a setting with two vector-like up-type quarks $T_1,\ T_2$ and one additional fermion T'. Together with the three SM quarks, we arrive at a 6×6 mass matrix which is given by

$$\mathcal{M}_u^{(0)} = \begin{pmatrix} \mathbf{0} & v_L y_a/\sqrt{2} & \mathbf{0} \\ v_R y_a^\dagger/\sqrt{2} & M_T & v_\eta y_1/\sqrt{2} \\ \mathbf{0} & v_\eta y_1^\dagger/\sqrt{2} & \mathbf{0} \end{pmatrix} , \tag{5.39}$$

in the basis $(u_1, u_2, u_3, T_1, T_2, T')$. Note that with this particular setup, y_a becomes a 3×2 matrix and y_1 has dimension 2×1. All zeros appearing in the above mass matrix follow from the gauge charges of our model and no further global or discrete symmetries are needed. The tree level mass matrix has rank four demonstrating that besides the two massive states T_1 and T_2, two further states obtain a mass. These can be identified with the T' and the top quark. Hence, we get exactly what we aim for: one massive SM quark at the tree level. To illuminate this in more detail, we cast the matrix in Eq. (5.39) to the well known form of a type I seesaw. To do so, we define the matrix

$$\mathcal{M}_S \equiv \begin{pmatrix} M_T & v_\eta y_1/\sqrt{2} \\ v_\eta y_1^\dagger/\sqrt{2} & \mathbf{0} \end{pmatrix} \tag{5.40}$$

together with the Yukawa coupling $Y_a \equiv (y_a,\ \mathbf{0})$ which allows us to rewrite

$$\mathcal{M}_u^{(0)} = \begin{pmatrix} \mathbf{0} & v_L Y_a/\sqrt{2} \\ v_R Y_a^\dagger/\sqrt{2} & \mathcal{M}_S \end{pmatrix} . \tag{5.41}$$

The seesaw limit is then characterized by a hierarchy of scales $v_\eta, M_T > v_R > v_L$ and we can give the approximate expressions

$$\begin{aligned} M^{\text{light}} &\simeq -\frac{v_L v_R}{2} Y_a \mathcal{M}_S^{-1} Y_a^\dagger \ , \\ M^{\text{heavy}} &\simeq \mathcal{M}_S \ , \end{aligned} \tag{5.42}$$

for the block diagonalization of $\mathcal{M}_u^{(0)}$. Here, the rank three matrix M^{heavy} represents the three heaviest states, while M^{light} is a rank one matrix and represents the masses of SM up-type quarks. Including the form of Y_a, we can further analyze the expressions and find $Y_a \mathcal{M}_S^{-1} Y_a^\dagger = y_a (\mathcal{M}_S^{-1})_{1,1} y_a^\dagger$, where $(..)_{1,1}$ indicates the entry in the corresponding matrix.

The inverse of $\mathcal{M}_S$ is easily found by applying the general formula for block matrix inversion and we quote our result

$$\mathcal{M}_S^{-1} = \begin{pmatrix} M_T^{-1} - M_T^{-1} y_1 \left(y_1^\dagger M_T^{-1} y_1 \right)^{-1} y_1^\dagger M_T^{-1} & \sqrt{2} v_\eta^{-1} M_T^{-1} y_1 \left(y_1^\dagger M_T^{-1} y_1 \right)^{-1} \\ \sqrt{2} v_\eta^{-1} \left(y_1^\dagger M_T^{-1} y_1 \right)^{-1} y_1^\dagger M_T^{-1} & -2 v_\eta^{-2} \left(y_1^\dagger M_T^{-1} y_1 \right)^{-1} \end{pmatrix} . \tag{5.43}$$

Thus, in total we get

$$\begin{aligned} M^{\text{light}} &\simeq -\frac{v_L v_R}{2} y_a \left(M_T^{-1} - M_T^{-1} y_1 \left(y_1^\dagger M_T^{-1} y_1 \right)^{-1} y_1^\dagger M_T^{-1} \right) y_a^\dagger \\ &= -\frac{v_L v_R}{2} y_a M_T^{-1} y_a^\dagger + \frac{v_L v_R}{2} y_a \left(M_T^{-1} y_1 \left(y_1^\dagger M_T^{-1} y_1 \right)^{-1} y_1^\dagger M_T^{-1} \right) y_a^\dagger \ , \\ M^{\text{heavy}} &\simeq \mathcal{M}_S \ . \end{aligned} \tag{5.44}$$

In Appendix B.1, we give analytic expressions for the eigenvalues of M^{light}, demonstrating that indeed two quarks are massless at this level.

Now we turn our interest to the one-loop corrected mass matrix. A summary of all one-loop Feynman diagrams is given in Figure C.1 of the Appendix. Out of these, the two most important graphs are presented in Figure 5.2 and we summarize their contributions by $\delta M_u^{(1)}$. The important thing to note is that both diagrams populate the subspace $(u_1,\ u_2,\ u_3)$ and thereby enhance the matrix rank. Also other matrix entries, which vanish at tree level, are filled by loop corrections such that the mass matrix at one-loop is given by

$$\mathcal{M}_u^{(1)} = \begin{pmatrix} \delta M_u^{(1)} & v_L y_a/\sqrt{2} & \delta v_L \\ v_R y_a^\dagger/\sqrt{2} & M_T & v_\eta y_1/\sqrt{2} \\ \delta^\dagger v_R & v_\eta y_1^\dagger/\sqrt{2} & \delta \tilde{M}_u^{(1)} \end{pmatrix} . \tag{5.45}$$

Here, radiative corrections from X and η exchange contribute to $\delta \tilde{M}_u^{(1)}$. In general, mixed $\chi_L - \eta$ and $\chi_R - \eta$ diagrams can also contribute to the entries δv_L and $\delta^\dagger v_R$ (see Figure C.1 diagram c), d), g) and h)). Nonetheless, in the limit $\lambda_4 \ll 1$ they will have suppressed contributions. From the Feynman diagrams we deduce the proportionality $\delta M_u^{(1)} \sim y_a y_a^\dagger$, $\delta \tilde{M}_u^{(1)} \sim y_1^\dagger y_1$ and $\delta \sim y_a y_1$. The radiative corrections increase the matrix rank by one. Again, separating into light and heavy eigenstates we find

$$\begin{aligned} M^{\text{light}} &\simeq \delta M_u^{(1)} - \frac{v_L v_R}{2} Y_a^{(1)} \left(\mathcal{M}_S^{(1)} \right)^{-1} Y_a^{(1)\dagger} \\ M^{\text{heavy}} &\simeq \mathcal{M}_S^{(1)} \ , \end{aligned} \tag{5.46}$$

where the coupling matrix is now $Y_a^{(1)} \equiv \left(y_a,\ \delta\sqrt{2} \right)$ and the one-loop corrected $\mathcal{M}_S^{(1)}$ reads

$$\mathcal{M}_S^{(1)} = \begin{pmatrix} M_T & v_\eta y_1/\sqrt{2} \\ v_\eta y_1^\dagger/\sqrt{2} & \delta \tilde{M}_u^{(1)} \end{pmatrix} . \tag{5.47}$$

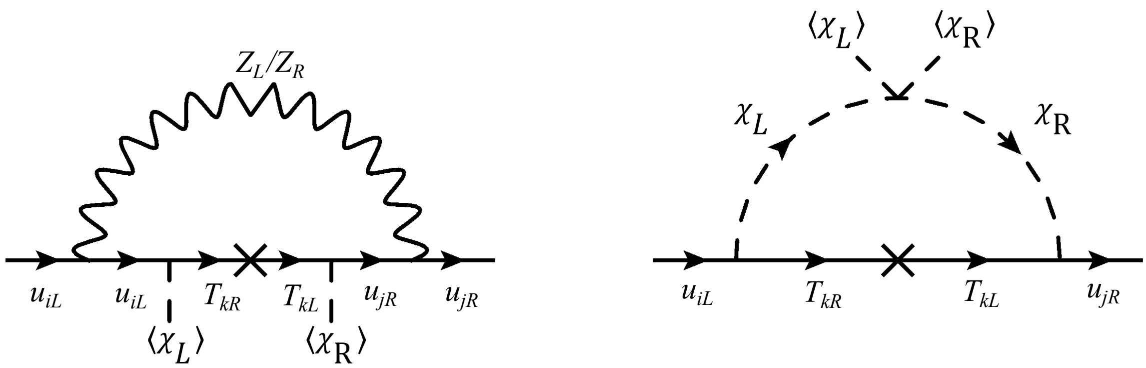

Figure 5.2 Feynman diagrams which generate the charm quark mass at one-loop order in the LRSM. Published in [3].

We emphasize that M^{light} has rank two and therefore the charm quark picks up mass.[6] The main contribution to the charm quark mass originates from the graphs in Figure 5.2. We separate the individual contributions in three different parts

$$\delta M_u^{(1)} \equiv \delta\mathcal{M}^{(1),Z} + \delta\mathcal{M}^{(1),Z'} + \delta\mathcal{M}^{(1),\chi} \ . \tag{5.48}$$

Depending on the relative size of g^2 and λ_2, either the gauge mediated or scalar diagram can be the dominant contribution. We are interested in the former case where the leading order contribution to the charm quark mass is approximately given by

$$\begin{aligned} m_c \sim \delta M_u^{(1)} &\simeq \frac{g^2}{16\pi^2} v_L v_R y_a \frac{M_T}{M_T^2 - M_Z^2} y_a^\dagger \\ &\simeq \frac{g^2}{16\pi^2} v_L v_R y_a M_T^{-1} y_a^\dagger \ , \end{aligned} \tag{5.49}$$

assuming $M_T > v_R > v_L$. In comparison to the leading term in Eq. (5.44), the $1/(16\pi^2)$ suppression naturally arises from the loop. Note that the detailed calculation of the one-loop corrections can be found in Appendix C.

Up to now, one of the quarks is still massless and we need to analyze the two-loop radiative corrections in our model. Out of the huge number of diagrams, the Feynman graph presented in Figure 5.3a is unique, as it involves Yukawa couplings from the down-type sector. As a reminder, mixing between W_L and W_R occurs only at one-loop level via an internal fermion loop as shown in Figure 5.3b. From the Feynman graph, we can easily deduce the proportionality $\delta M_u^{(2)} \sim y_c y_c^\dagger$ and we emphasize that the down-type Yukawa

[6] Because of the proportionality $\delta M_u^{(1)} \sim y_a y_a^\dagger$, the matrix rank of $\delta M_u^{(1)}$ is at maximum two, since the 3×2 matrix y_a can have at most two linear independent 3-vectors.

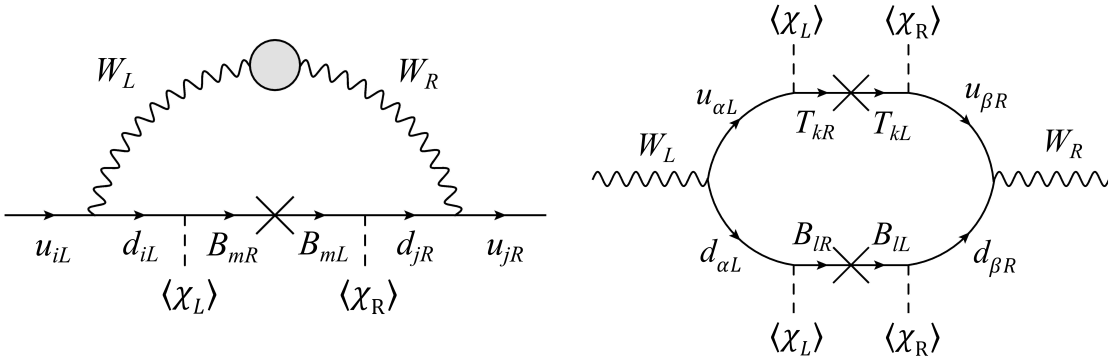

(a) **(b)**

Figure 5.3 **(a)** Two-loop Feynman diagram which generates the first generation quark mass via charged gauge boson exchange. The mixing of $W_L - W_R$ (grey circle) happens at one-loop and is illustrated in **(b)**. Published in [3].

coupling y_c is in general different from the up-type coupling y_a. This property is crucial to further raise the matrix rank. The two-loop corrected mass matrix is thus given by

$$\mathcal{M}_u^{(2)} = \begin{pmatrix} \delta M_u^{(1)} + \delta M_u^{(2)} & v_L y_a/\sqrt{2} & \delta v_L \\ v_R y_a^\dagger/\sqrt{2} & M_T & v_\eta y_1/\sqrt{2} \\ \delta v_R & v_\eta y_1^\dagger/\sqrt{2} & \delta \tilde{M}_u^{(1)} \end{pmatrix} , \tag{5.50}$$

and the linear independence of y_a and y_c guarantees that $\mathcal{M}_u^{(2)}$ is a rank six matrix, such that the up quark obtains a mass at second loop order.[7] We postpone the detailed calculation of the diagram to Appendix C and approximate the size of the two-loop contribution by

$$m_u \sim \delta M_u^{(2)} \simeq \frac{N_c}{(16\pi^2)^2} \frac{g^4 v_L^3 v_R^3 M_B}{M_T M_B M_{W_L}^2 M_{W_R}^2} , \tag{5.51}$$

where we assumed order one Yukawa couplings. Knowing that $M_{W_L}^2 \sim v_L^2$ and $M_{W_R}^2 \sim v_R^2$, this gives another suppression factor of $(16\pi^2)^{-1}$ compared to the second generation mass in Eq. (5.49). In this simplistic approximation, a ratio of $v_R/M_T \simeq 10^{-1}$ would be enough to achieve a realistic up quark mass of a few MeV.

Similar considerations are applicable to the down-type quark sector. In order to demonstrate that our model can accommodate quark masses and mixings within the experimentally allowed parameter range, we present two benchmark scenarios in Section 5.6.

[7] We have not included any other two-loop corrections to the mass matrix besides the one shown in Figure 5.3a, as it is the only diagram which enhances the matrix rank and therefore contributes to the up quark mass.

5.4 Charged lepton masses

The scheme presented in the quark sector can be transferred to the charged leptons in a straight forward way and Figure 5.4 summarizes the different mass contributions. At tree level, only the tau lepton is massive and the mass matrix is similar to Eq. (5.39) up to the replacements $M_T \leftrightarrow M_E$ and $y^q \leftrightarrow y^\ell$. The neutral gauge boson exchange diagram causes a mass for the muon and the two-loop $W_L - W_R$ exchange process is the origin of non-zero electron mass. As illustrated in the right panel of Figure 5.4, the vector-like neutrino mass M_N contributes to the electron mass and causes a correlation with the neutrino sector. This leads to a proportionality between the electron mass and the Dirac neutrino mass. Taking all vector-like fermion masses at roughly the same scale $M_N \simeq M_E \simeq M_B \simeq M_T$, the electron mass can be correctly reproduced without fine tuning. With natural order one Yukawa couplings, we expect Dirac neutrino masses at same orders as charged lepton masses. This is in conflict with experimental results and we discuss possible solutions to achieve small active neutrino masses in the following section.

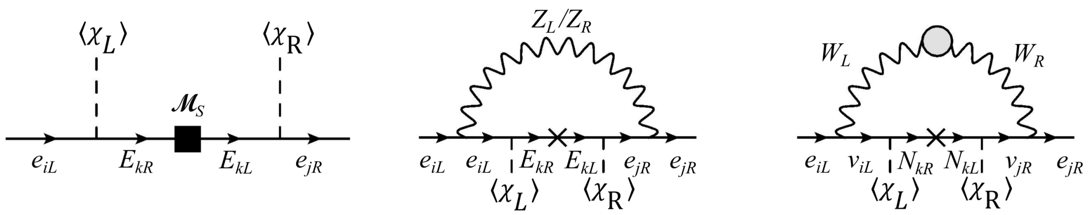

Figure 5.4 Tree level and one- and two-loop contributions to the charged lepton masses in the LRSM. Published in [3].

5.5 Neutrino masses

If there is no lepton number violation in the theory, neutrinos will be pure Dirac states and the mass matrix up to two-loop level has the following structure (we drop superscripts ℓ for a better readability):

$$\mathcal{M}^{(2)}_{\nu,\text{Dirac}} = \begin{pmatrix} \delta M^{(1)}_\nu + \delta M^{(2)}_\nu & y_a v_L/\sqrt{2} & \delta v_L \\ y_a^\dagger v_R/\sqrt{2} & M_N & y_1 v_\eta/\sqrt{2} \\ \delta^\dagger v_R & y_1^\dagger v_\eta/\sqrt{2} & \delta\tilde{M}^{(1)}_\nu \end{pmatrix} . \tag{5.52}$$

In analogy to the quark sector, we block diagonalize the above rank six matrix and find

$$\begin{aligned} M^{\text{light}}_{\nu,\text{Dirac}} &\simeq (\delta M^{(1)}_\nu + \delta M^{(2)}_\nu) - \frac{v_L v_R}{2} Y_a \left(\mathcal{M}^{(1)}_S\right)^{-1} Y_a^\dagger \\ M^{\text{heavy}}_{\nu,\text{Dirac}} &\simeq \mathcal{M}^{(1)}_S \ , \end{aligned} \tag{5.53}$$

where the matrix $\mathcal{M}_S^{(1)}$ is defined as

$$\mathcal{M}_S^{(1)} = \begin{pmatrix} M_N & y_1 v_\eta/\sqrt{2} \\ y_1^\dagger v_\eta/\sqrt{2} & \delta\tilde{M}_\nu^{(1)} \end{pmatrix} \,, \tag{5.54}$$

and $Y_a \equiv \left(y_a, \delta\sqrt{2}\right)$.[8] A realistic electron mass necessitates $M_N \simeq M_E$ and Yukawa couplings of the same order in both sectors (see discussion in Section 5.4). Therefore, the Dirac mass eigenstates of $M_{\nu,\mathrm{Dirac}}^{\mathrm{light}}$ are expected to be $\mathcal{O}(m_\tau)$, $\mathcal{O}(m_\mu)$ and $\mathcal{O}(m_e)$. Clearly, a further suppression is necessary to achieve active neutrino masses below one electron volt.

Up to now, we only considered lepton number conserving operators. However, the vector-like neutrinos $N_{1,2}$ are gauge singlets and lepton number violating operators are in general allowed. Including those, the complete Lagrangian for the neutrino sector is defined by

$$\begin{aligned}\mathcal{L}_\nu = {} & y_a \Psi^T \tilde{\chi}_L N^c + y_a' \Psi^T \tilde{\chi}_L N + M_N N N^c + y_1 N^c \eta N' + M_L' N N + y_1' N \eta N' + y_a \Psi^{cT} \tilde{\chi}_R N \\ & + y_a' \Psi^{cT} \tilde{\chi}_R N^c + M_N N^c N + y_1 N \eta^* N'^c + M_R' N^c N^c + y_1' N^c \eta N'^c + h.c. \,,\end{aligned} \tag{5.55}$$

where we change to a notation with only left-handed fields and $...^c$ is the charge conjugate of right-handed fermion fields. Note that in addition to the lepton number conserving mass M_N, the LNV masses M_R' and M_L' are present now as well. We allow a soft breaking of parity and thus $M_R' \neq M_L'$. Also in the Yukawa sector, primed parameters are LNV (y'), while unprimed ones (y) correspond to the lepton number conserving couplings (compare to definition in Eq. (5.33)). When the scalar fields obtain VEVs, the tree level neutrino mass matrix is given by

$$\mathcal{M}_\nu^{(0)} = \begin{pmatrix} 0 & 0 & y_a^{'i1}\frac{v_L}{\sqrt{2}} & y_a^{i1}\frac{v_L}{\sqrt{2}} & y_a^{'i2}\frac{v_L}{\sqrt{2}} & y_a^{i2}\frac{v_L}{\sqrt{2}} & 0 & 0 \\ 0 & 0 & y_a^{i1}\frac{v_R}{\sqrt{2}} & y_a^{'i1}\frac{v_R}{\sqrt{2}} & y_a^{i2}\frac{v_R}{\sqrt{2}} & y_a^{'i2}\frac{v_R}{\sqrt{2}} & 0 & 0 \\ y_a^{'i1}\frac{v_L}{\sqrt{2}} & y_a^{i1}\frac{v_R}{\sqrt{2}} & M_{L,11}' & M_{N1} & M_{12}' & 0 & y_1^{'1}\frac{v_\eta}{\sqrt{2}} & y_1^{1}\frac{v_\eta}{\sqrt{2}} \\ y_a^{i1}\frac{v_L}{\sqrt{2}} & y_a^{'i1}\frac{v_R}{\sqrt{2}} & M_{N1} & M_{R,11}' & 0 & M_{12}' & y_1^{1}\frac{v_\eta}{\sqrt{2}} & y_1^{'1}\frac{v_\eta}{\sqrt{2}} \\ y_a^{'i2}\frac{v_L}{\sqrt{2}} & y_a^{i2}\frac{v_R}{\sqrt{2}} & M_{12}' & 0 & M_{L,22}' & M_{N2} & y_1^{'2}\frac{v_\eta}{\sqrt{2}} & y_1^{2}\frac{v_\eta}{\sqrt{2}} \\ y_a^{i2}\frac{v_L}{\sqrt{2}} & y_a^{'i2}\frac{v_R}{\sqrt{2}} & 0 & M_{12}' & M_{N2} & M_{R,22}' & y_1^{2}\frac{v_\eta}{\sqrt{2}} & y_1^{'2}\frac{v_\eta}{\sqrt{2}} \\ 0 & 0 & y_1^{'1}\frac{v_\eta}{\sqrt{2}} & y_1^{1}\frac{v_\eta}{\sqrt{2}} & y_1^{'2}\frac{v_\eta}{\sqrt{2}} & y_1^{2}\frac{v_\eta}{\sqrt{2}} & 0 & 0 \\ 0 & 0 & y_1^{1}\frac{v_\eta}{\sqrt{2}} & y_1^{'1}\frac{v_\eta}{\sqrt{2}} & y_1^{2}\frac{v_\eta}{\sqrt{2}} & y_1^{'2}\frac{v_\eta}{\sqrt{2}} & 0 & 0 \end{pmatrix} \,, \tag{5.56}$$

where we use the basis $(\nu, \nu^c, N_1, N_1^c, N_2, N_2^c, N', N'^c)$. In the above matrix, superscripts indicate matrix entries of the coupling matrices y_a, y_a' and y_1, y_1' and the index $i = 1, 2, 3$ labels the three SM generations. To check whether light active neutrinos are viable, we will need to find the eigenvalues of the given 12×12 matrix. Though finding an analytic solution, which expresses the parameter dependencies in a meaningful way, is challenging

[8] As $\mathcal{M}_S^{(1)}$ has full rank, we do not include subdominant two-loop corrections to this matrix.

for such a big matrix. Hints for the general behavior can be found by checking the matrix rank of the LNV violating mass matrices. Since both M'_L and M'_R are rank two matrices, we conjecture four light neutrino states in our model. An extensive study of the neutrino sector entails not only a complete parameter scan but also the inclusion of further loop corrections and is outside the scope of this work. As a first approximation, we investigate the tree level matrix with only the third generation neutrino included ($i = 3$). The outcome of this study is described in the next section, together with numerical results for the quark and charged lepton sector.

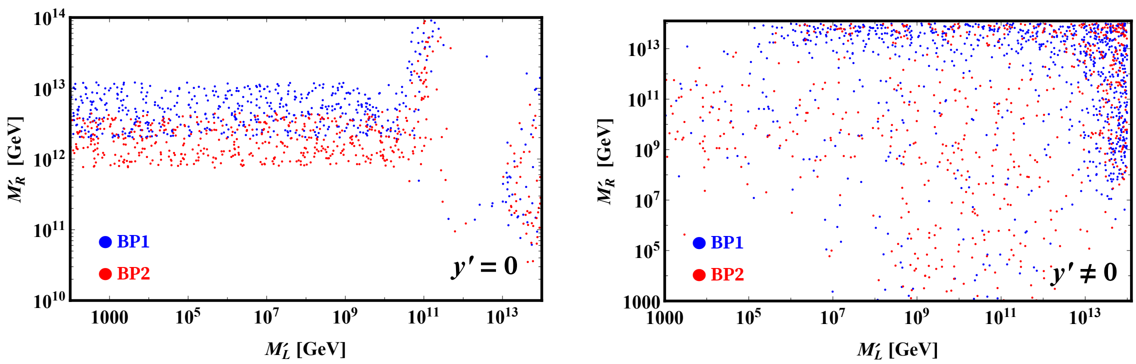

Figure 5.5 Scatter plot showing viable lepton number violating masses M'_L, M'_R that lead to a light active neutrino with $m_\nu < 0.3$ eV in the tree level approximation. Table 5.2 summarizes lepton number conserving couplings used for the BPs. Left panel: lepton number violating couplings are zero ($y' = 0$). Right panel: y'couplings are randomly selected within the interval $\{0.1,\ 1.0\}$. Published in [3].

5.6 Numerical results

As a proof of concept, we show two benchmark scenarios which align with the current measurements of fermion masses and mixings. We follow the methods presented in Sections 5.3 to 5.5 and use the results of the explicit loop calculation quoted in Appendix C. The couplings $\alpha = 1/2$ and $g_X = 1$ are fixed throughout the analysis. The symmetry breaking scales of our first benchmark point (BP1) are given by

$$v_R = 20 \text{ TeV} , \qquad v_\eta = 30 \text{ TeV} , \tag{5.57}$$

which yields the massive eigenstates $M_{W_R} = 6.53$ TeV and $M_{Z'} = 7.82$ TeV. Note that the right-handed breaking scale is in agreement with current direct searches for W' gauge bosons [228]. For the vector-like quark masses we assume

$$\begin{aligned} M_{T1} &= 9 \text{ TeV} , \quad M_{T2} = 14 \text{ TeV} , \\ M_{B1} &= 38 \text{ TeV} , \quad M_{B2} = 42 \text{ TeV}, \end{aligned} \tag{5.58}$$

while the vector-like lepton masses are

$$\begin{aligned} M_{N1} &= 60 \text{ TeV} \ , \quad M_{N2} = 65 \text{ TeV} \ , \\ M_{E1} &= 44 \text{ TeV} \ , \quad M_{E2} = 51 \text{ TeV} \ . \end{aligned} \tag{5.59}$$

In the second benchmark scenario (BP2), we choose higher scales for the symmetry breaking

$$v_R = 80 \text{ TeV} \ , \qquad v_\eta = 120 \text{ TeV} \ . \tag{5.60}$$

Therefore, the gauge bosons from the right-handed sector have larger masses $M_{W_R} = 26.13$ TeV and $M_{Z'} = 31.26$ TeV. This implies also slightly larger vector-like mass scales

$$\begin{aligned} M_{T1} &= 19 \text{ TeV} \ , \quad M_{T2} = 21 \text{ TeV} \ , \\ M_{B1} &= 47 \text{ TeV} \ , \quad M_{B2} = 49 \text{ TeV}, \end{aligned} \tag{5.61}$$

$$\begin{aligned} M_{N1} &= 82 \text{ TeV} \ , \quad M_{N2} = 85 \text{ TeV} \ , \\ M_{E1} &= 61 \text{ TeV} \ , \quad M_{E2} = 64 \text{ TeV} \ . \end{aligned} \tag{5.62}$$

Table 5.2 shows the Yukawa couplings used in BP1 and BP2. We emphasize that these parameters are enough to describe the Dirac masses in our model. The reproduced observables are presented in Table 5.3. For comparison we show the 3σ experimental bounds for observables in the quark sector, while for the tau, muon and electron mass we indicate the $\pm 5\%$ range of the best fit value [30,203]. Both our benchmark points agree with the quoted limits. We emphasize that all Yukawa couplings are manifestly order one and loop suppression factors of $1/(16\pi^2)$ explain the full hierarchy between generations. At the same time, the parameters of our model are sufficient to reproduce the mixing angles and CP violation in the quark sector. Still, it is important to note that the size of these mixing parameters is not explained in our mechanism. The vector-like fermion masses exhibit a mild hierarchy $M_T < M_B < M_E$ that accounts for the difference in third generation mass scales $m_t > m_b > m_\tau$ through the seesaw relation.

Since we chose $M_E \simeq M_N$, neutrinos receive Dirac masses in the same range as charged lepton masses. In addition, the gauge singlet fermions $N_{1,2}$ allow to introduce LNV contributions as considered in Section 5.5. Analyzing the full 12×12 matrix shown in Eq. (5.56) together with all loop corrections is challenging. For now, we check whether a light neutrino mass eigenstate arises in the tree level approximation where we only take into account $i = 3$. For our analysis, we keep the Yukawa couplings and masses provided in Table 5.2 as representatives of lepton number conserving parameters and check which LNV masses are necessary to achieve a light neutrino $m_\nu < 0.3$ eV. Starting from the assumptions $M'_L \equiv M'_{L,11} = M'_{L,22}$, $M'_R \equiv M'_{R,11} = M'_{R,22}$ and $M'_{L,12} = 0 = M'_{R,12}$, we randomly generate $M'_L,\ M'_R \in \{10^3, 10^{14}\}$ GeV and display parameter choices that lead to a light neutrino state in Figure 5.5. While the left plot shows the case $y' = 0$, i.e. all LNV Yukawa couplings vanish, the right plot considers random values $y' \in \{0.1,\ 1\}$. Clearly, allowing non-zero y' enlarges the possible parameter space in the $M'_L - M'_R$ plane. From the counting of LNV operators, we anticipate that three light active neutrinos can be achieved in the full framework. A preliminary study however suggests that a subtle tuning of parameters is necessary to agree with oscillation data. Therefore, we postpone a detailed parameter scan to future work.

Yukawa Couplings	**Benchmark Points**	
	BP1	**BP2**
y_a^q	$\begin{pmatrix} 0.616 & 0.345 \\ 0.543 & 0.742 \\ 2.291 & 0.905 \end{pmatrix}$	$\begin{pmatrix} -1.374 & 1.594 \\ -1.114 & 1.536 \\ 0.797 & 0.246 \end{pmatrix}$
y_c^q	$\begin{pmatrix} 0.233 & 0.251 \\ 0.279 & 0.376 \\ 1.569 & 1.849 \end{pmatrix}$	$\begin{pmatrix} 0.913 & 0.452 \\ 0.555 & 0.265 \\ 0.534 & 0.229 \end{pmatrix}$
y_1^q	$\begin{pmatrix} 1.21 \times e^{0.060i} \\ 1.55 \end{pmatrix}$	$\begin{pmatrix} 0.300 \times e^{0.060i} \\ -0.200 \end{pmatrix}$
y_3^q	$\begin{pmatrix} 0.740 \\ 1.320 \end{pmatrix}$	$\begin{pmatrix} 1.200 \\ 0.800 \end{pmatrix}$
y_a^ℓ	$\begin{pmatrix} 0.267 & 0.272 \\ 0.752 & 0.730 \\ 0.583 & 0.580 \end{pmatrix}$	$\begin{pmatrix} 1.217 & 1.143 \\ 0.555 & 0.519 \\ 0.552 & 0.512 \end{pmatrix}$
y_c^ℓ	$\begin{pmatrix} 0.580 & 0.371 \\ 0.860 & 0.638 \\ 0.587 & 0.430 \end{pmatrix}$	$\begin{pmatrix} 0.758 & 0.288 \\ 0.754 & 0.246 \\ 0.277 & 0.123 \end{pmatrix}$
y_1^ℓ	$\begin{pmatrix} 0.650 \\ 0.920 \end{pmatrix}$	$\begin{pmatrix} 0.600 \\ 0.700 \end{pmatrix}$
y_3^ℓ	$\begin{pmatrix} 1.680 \\ 0.740 \end{pmatrix}$	$\begin{pmatrix} 0.500 \\ 0.100 \end{pmatrix}$

Table 5.2 Yukawa couplings used for the benchmark scenarios in the LRSM. Published in [3].

Observable (Masses in GeV)	**Exp. Range**	**Model Prediction**	
		BP1	**BP2**
Quark Sector			
$m_u/10^{-3}$	$1.38 \to 3.63$	2.17	2.05
m_c	$1.21 \to 1.33$	1.27	1.23
m_t	$171.7 \to 174.1$	172.9	172.9
$m_d/10^{-3}$	$4.16 \to 6.11$	4.65	4.73
m_s	$0.078 \to 0.126$	0.094	0.120
m_b	$4.12 \to 4.27$	4.18	4.18
$\lvert V_{\text{ud}}\rvert$	$0.973 \to 0.974$	0.974	0.974
$\lvert V_{\text{us}}\rvert$	$0.222 \to 0.227$	0.227	0.226
$\lvert V_{\text{ub}}\rvert/10^{-4}$	$31.0 \to 45.4$	38.7	39.0
$\lvert V_{\text{cd}}\rvert$	$0.209 \to 0.233$	0.226	0.226
$\lvert V_{\text{cs}}\rvert$	$0.954 \to 1.020$	0.973	0.973
$\lvert V_{\text{cb}}\rvert/10^{-3}$	$36.8 \to 45.2$	40.0	40.3
$\lvert V_{\text{td}}\rvert/10^{-4}$	$71.0 \to 89.0$	80.6	80.4
$\lvert V_{\text{ts}}\rvert/10^{-3}$	$35.5 \to 42.1$	39.4	39.6
$\lvert V_{\text{tb}}\rvert$	$0.923 \to 1.103$	0.999	0.999
$\mathcal{J}/10^{-5}$	$2.73 \to 3.45$	3.06	3.05
Charged Lepton Sector			
$m_e/10^{-3}$	$0.485 \to 0.537$	0.511	0.512
m_μ	$0.100 \to 0.111$	0.106	0.106
m_τ	$1.688 \to 1.866$	1.777	1.788

Table 5.3 Predicted fermion masses and mixings for the considered benchmark points in the LRSM. For comparison we show 3σ experimental limits on the observables, apart from charged lepton masses where we displayed a $\pm 5\%$ uncertainty. Published in [3].

Chapter 6

Testing neutrino non-standard interactions at future colliders

The observation of neutrino oscillations provides a sound proof that new physics beyond the SM should exist. Our work in Chapter 4 and 5 has discussed possible realizations of small neutrino masses and adds to the extensive list of models that have been suggested during the last decades. However, the large variety of new physics proposals that underlie neutrino mass mechanisms is challenging for experimental searches. Neutrino non-standard interactions represent a way to parameterize novel physics in the neutrino sector in a general effective field theory framework. Present experiments thoroughly probe NSIs but so far the focus is mainly on interactions with up and down quarks and electrons. In this chapter, we want to focus on NSIs with muons, the second generation charged lepton. The latest measurement of the anomalous magnetic moment of the muon reinforced the suspicion that some kind of new muonic force could exist.[1] Testing the four-fermion contact interactions involving two neutrinos and two muons can therefore possibly provide further insights into neutrino mass generation and potential muon related new physics.

Combining the precision of ee colliders with the energy of pp collision, the muon collider is one of the most promising projects for the post-LHC era. In recent years, the interest in a high energy muon collider has therefore grown a lot and a plethora of studies investigated its discovery potential [218, 233–262] (a review can be found in [91]). In the following chapter, we analyze how a muon collider can be used to test NSIs with muons through the process $\mu^+\mu^- \to \nu\nu\gamma$. We start by defining the relevant NSI operators in Section 6.1. By considering a simplified toy model, Section 6.2 elaborates how NSIs can be constrained with the monophoton signal. Finally, Section 6.3 discusses three UV complete models that lead to muonic NSIs and shows the complementarity with other experiments. The content of this chapter is based on the publication [2].

[1] Note that hints on new physics from rare B meson decays vanished [229–232].

6.1 Connecting effective field theories to simplified models

In general, the effective interaction of two muons and two neutrinos $\mu\mu\nu\nu$ can be characterized by a collection of four-fermion operators that include different combinations of fermion bilinear forms. Specifically, we consider vector, axial-vector, scalar, axial-scalar and tensor interactions. At dimension six, the corresponding four-fermion interaction Lagrangian is given by

$$\mathcal{L}_{\mu\mu\nu\nu} = -2\sqrt{2}G_F \sum_{\alpha,\beta} \sum_{i=1}^{10} \epsilon_{\alpha\beta}^{\mu\mu(i)} \left(\overline{\nu}_\alpha \mathcal{O}_i \nu_\beta\right) \left(\overline{\mu} \mathcal{O}'_i \mu\right) \ , \tag{6.1}$$

where we indicate the neutrino flavor by $\alpha, \beta \in \{e,\ \mu,\ \tau\}$ and all operators are normalized to G_F, the Fermi constant. Using the definitions $P_{L/R} \equiv \left(1 \mp \gamma^5\right)/2$ and $\sigma^{\mu\nu} \equiv \frac{i}{2}\left[\gamma^\mu, \gamma^\nu\right]$, the effective couplings $\epsilon_{\alpha\beta}^{\mu\mu(i)}$ and operators $\mathcal{O}$, $\mathcal{O}'$ can be found in Table 6.1. In the SM, interactions of charged leptons and neutrinos are mediated by $W^\pm$ and Z bosons. Integrating these heavy fields out produces flavor diagonal four-fermion operators whose strength depends on the Weinberg angle θ_w and is given by

$$\begin{aligned} \epsilon_{\alpha\beta}^{\mu\mu(V,LL)} &= \delta_{\alpha\mu}\delta_{\beta\mu} + \left(-\frac{1}{2} + \sin^2\theta_w\right)\delta_{\alpha\beta} && \text{(SM)} \\ \epsilon_{\alpha\beta}^{\mu\mu(V,LR)} &= \sin^2\theta_w \delta_{\alpha\beta} && \text{(SM)} \end{aligned} \tag{6.2}$$

The coefficients reflect the fact that neutral current processes contribute to the interaction of all neutrino flavors, whereas the charged current interaction is limited to ν_μ. Figure 6.2 shows the two Feynman diagrams that contribute in the SM to the process $\mu^+\mu^- \to \nu\overline{\nu}\gamma$. In what follows we refer to these SM processes as background events, whereas signal events originate from new interactions beyond the SM.

i	$\epsilon_{\alpha\beta}^{\mu\mu(i)}$	$\mathcal{O}$	$\mathcal{O}'$
1	$\epsilon_{\alpha\beta}^{\mu\mu(V,LL)}$	$\gamma_\mu P_L$	$\gamma^\mu P_L$
2	$\epsilon_{\alpha\beta}^{\mu\mu(V,RL)}$	$\gamma_\mu P_R$	$\gamma^\mu P_L$
3	$\epsilon_{\alpha\beta}^{\mu\mu(V,LR)}$	$\gamma_\mu P_L$	$\gamma^\mu P_R$
4	$\epsilon_{\alpha\beta}^{\mu\mu(V,RR)}$	$\gamma_\mu P_R$	$\gamma^\mu P_R$
5	$\epsilon_{\alpha\beta}^{\mu\mu(S,LL)}$	P_L	P_L
6	$\epsilon_{\alpha\beta}^{\mu\mu(S,RL)}$	P_R	P_L
7	$\epsilon_{\alpha\beta}^{\mu\mu(S,LR)}$	P_L	P_R
8	$\epsilon_{\alpha\beta}^{\mu\mu(S,RR)}$	P_R	P_R
9	$\epsilon_{\alpha\beta}^{\mu\mu(T,LL)}$	$\sigma_{\mu\nu} P_L$	$\sigma^{\mu\nu} P_L$
10	$\epsilon_{\alpha\beta}^{\mu\mu(T,LL)}$	$\sigma_{\mu\nu} P_R$	$\sigma^{\mu\nu} P_R$

Table 6.1 Dimension six effective operators contributing to the interaction of two neutrinos and two muons. Published in [2].

In low energy oscillation experiments, the EFT approach is appropriate to describe neutrino non-standard interactions. However, the case is different for high energy collider experiments. With growing energy scales, the momentum transfer can become considerable and the EFT is not the right tool to investigate these regimes. For this reason, we carry out a more thorough study in this work and take propagating force mediators directly into account. In specific, we consider three different classes of new physics models that induce NSIs with muons. They cover the scenarios of a neutral gauge boson extension, a neutral scalar extension and a charged scalar extension and are portrayed in Figure 6.1.

As a start, we explore a toy Z' model. The Lagrangian of this simplified scenario is given by

$$\mathcal{L}_{\rm NSI}^{{\rm Simp},Z'} = \sum_{Y=L,R} \Big[(g_\nu)_{\alpha\beta} \overline{\nu}_\alpha \gamma^\mu P_L \nu_\beta + g_\mu^Y \overline{\mu} \gamma^\mu P_Y \mu \Big] Z'_\mu \ , \tag{6.3}$$

where the coupling strengths g_ν and g_μ^Y represent free parameter for now as well as the mass $M_{Z'}$. This type of interaction contributes to the operators $i = 1, 3$ and we define the associated effective coupling by

$$\epsilon_{\alpha\beta}^{\mu\mu(V,LY)} = \frac{(g_\nu)_{\alpha\beta} g_\mu^Y}{2\sqrt{2} G_F M_{Z'}^2} \ , \qquad Y \in \{L, R\} \ . \tag{6.4}$$

In the following, we analyze limits that can be set on the parameter space of the model given in Eq. (6.3) and present our results in terms of the effective coupling $\epsilon_{\alpha\beta}^{\mu\mu}$.

6.2 Testing NSI with a monophoton signal

Similar to dark matter searches at high energy colliders [233, 263, 264], mono-X events such as monophoton, mono-Z, mono-W or mono-jet events with large missing transverse energy are suitable to probe neutrino non-standard interactions in collider experiments. In our study, we examine the signal $\mu^+\mu^- \to \gamma + \not{E}_T$ with a single photon and missing transverse energy in the final state. For that, we implement the model Lagrangian with the `FeynRules` package [265] and carry out a Monte Carlo simulation of both the background and signal events in the process $\mu^+\mu^- \to \nu\overline{\nu}\gamma$ with the help of the software package

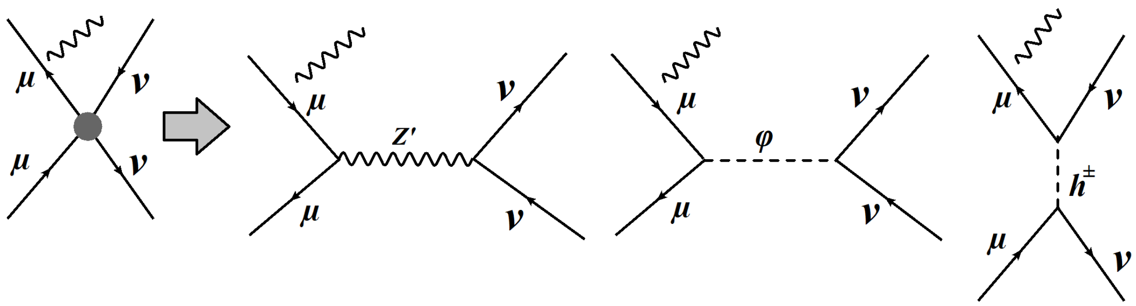

Figure 6.1 Examples of vector- and scalar-mediated four-fermion interactions that create a monophoton signal through the process $\mu^+\mu^- \to \nu\overline{\nu}\gamma$. Published in [2].

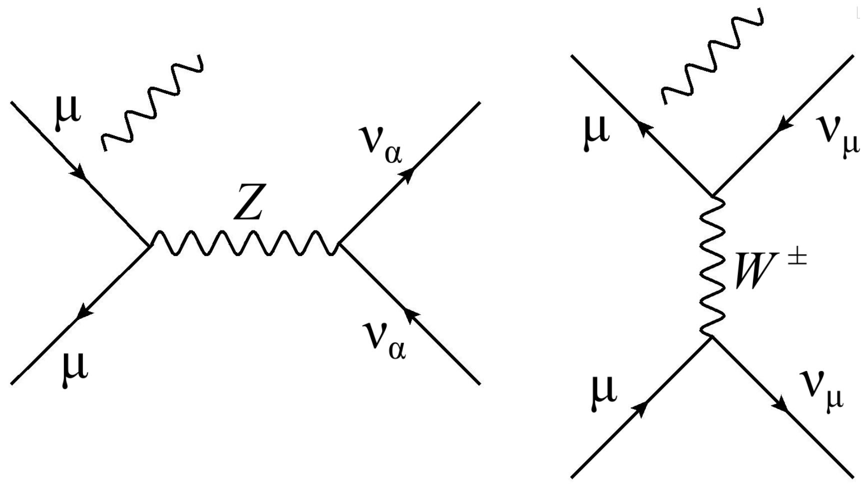

Figure 6.2 SM processes that contribute to the monophoton signal by charged and neutral current interactions.

`MadGraph5aMC@NLO` [266, 267]. The process of hadronization and parton showering is done by `Pythia8` [268], while we use the `Delphes3` package [269] for the detector simulation.[2]

In our work, we perform a cut-and-count analysis. For this we apply several steps of requirements on the signal and background events and afterwards count the number of events passing each selection step. As a basic cut we demand the events to comply with a limit on the photon pseudorapidity and transverse momentum

$$p_\gamma^T > 10 \text{ GeV} , \qquad |\eta_\gamma| < 2.44 . \tag{6.5}$$

This last criteria corresponds to an angular acceptance $10^\circ < \theta_\gamma < 170^\circ$, where θ_γ describes the angle of the photon relative to the beam axis. Next, we deploy a series of nine more selection steps which restrict the missing transverse energy $\not{E}_T$ by a threshold

$$\not{E}_T > 10,\ 20,\ 30,\ 40,\ 50,\ 60,\ 70,\ 80, 100 \text{ GeV} . \tag{6.6}$$

Out of these nine different cuts, we obtain the sensitivity to NSIs from the region that has the maximum statistical significance

$$\mathcal{S} \equiv \frac{N_S}{\sqrt{N_B + N_S + (\delta\sigma_B N_B)^2}} , \tag{6.7}$$

Here, the number of signal and background events is given by N_S and N_B, respectively. The parameter $\delta\sigma_B$ quantifies a systematic uncertainty on the background. By applying this procedure and choosing the cuts, the number of background events can be significantly reduced compared to the number of signal events. A more detailed demonstration of the efficiency of the different cuts can be found in Appendix D.

[2]We use the Delphes default card for the detector simulation.

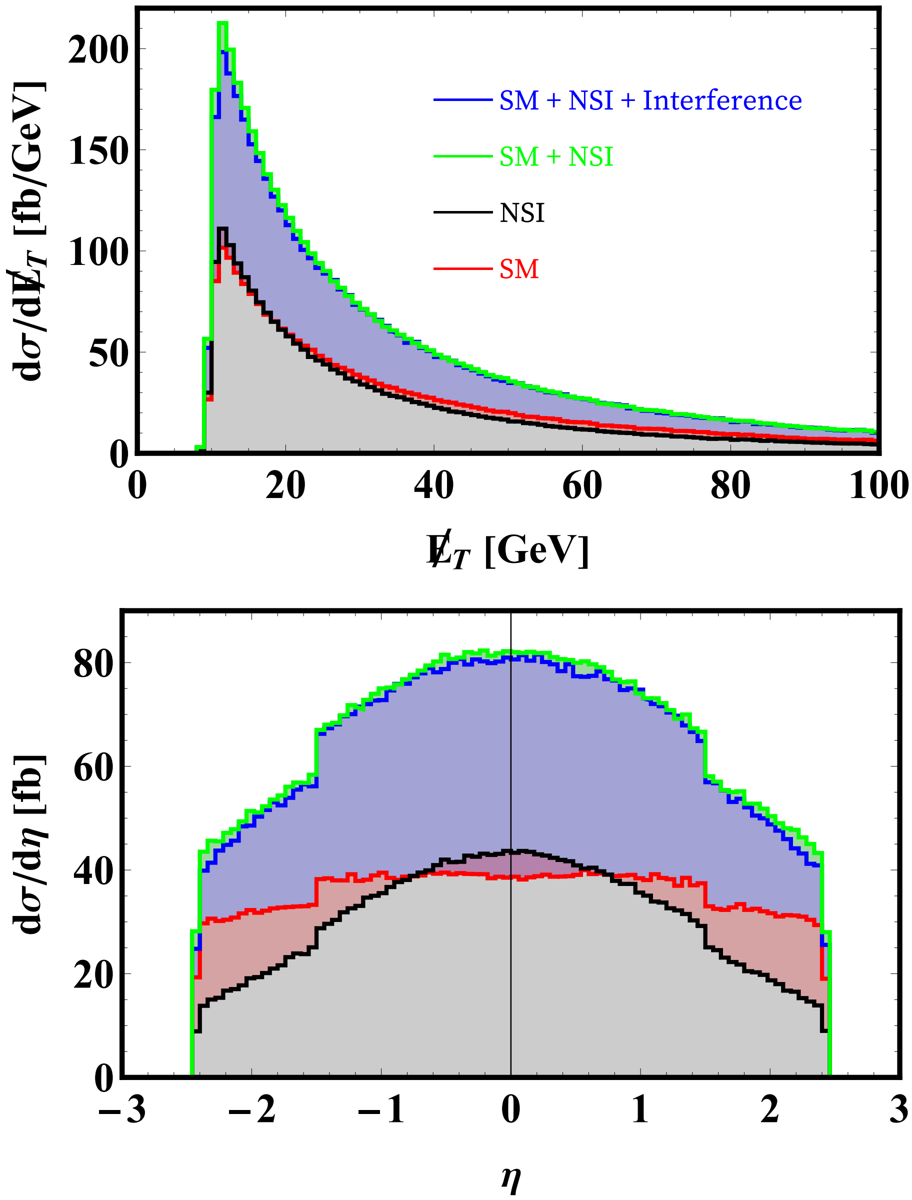

Figure 6.3 Differential cross section $d\sigma/d\not{E}_T$ and $d\sigma/d\eta$ for the process $\mu^+\mu^- \to \overline{\nu}\nu\gamma$ at a muon collider with $\sqrt{s} = 3$ TeV. Shown are the results of the Monte Carlo simulation for the SM (red), only NSI (black) and both together including interference effects (blue). For comparison we display the sum of NSI and SM contributions (green) which demonstrates that interference effects are small. For the NSI contribution, we consider the model defined in Eq. (6.3) with the parameters $M_{Z'} = 3$ TeV, $\Gamma_{Z'} = 0.3$ TeV, $g_\mu^L = g_\mu^R = 1$ and $g_\nu^{\alpha\beta} = \delta^{\alpha\tau}\delta^{\beta\tau}$. Figure published in [2].

Interference effects can in principle occur between SM and new physics contributions. To check how large these effects are, we show the differential cross sections $d\sigma/d\not{E}_T$ and $d\sigma/d\eta$ that we obtain from the Monte Carlo simulation of the process $\mu^+\mu^- \to \overline{\nu}\nu\gamma$ in Figure 6.3. While the red curve gives the SM contribution, the black line indicates the pure NSI effect following from the Lagrangian in Eq. (6.3). As the total effect including SM, NSI and interference effects (blue curve) is comparable to the sum of SM and NSI (green curve), we conclude that interference effects play a minor role and can be neglected in the following. As a consequence, the signal cross section σ_S is proportional to $\propto \epsilon^2$ [80].

The final result for the projected sensitivity to NSIs of a muon collider with a center-of-mass energy of $\sqrt{s} = 3$ TeV at 95% confidence level (CL) is shown in Figure 6.4. For the sake of simplicity, we assume that the Z' boson only couples to tau neutrinos such that $(g_\nu)_{\alpha\beta} \equiv g_\nu \delta_{\alpha\tau}\delta_{\beta\tau}$ and we consider two different scenarios which differ in the chosen decay width $\Gamma_{Z'}/M_{Z'} = 0.1$ and 0.3. Under the assumption that the coupling of the Z' to muons is vector-like, i.e. $g_\mu^L = g_\mu^R$, the upper plot displays the sensitivity to the effective coupling $|\epsilon_{\tau\tau}^{\mu\mu(V,LL)}|$ as a function of the mass $M_{Z'}$. For the ease of reading, we drop superscripts and only use the notation $|\epsilon_{\tau\tau}^{\mu\mu}|$ in the following whenever the chiral structure is clear from the context. We study two integrated luminosities $\mathcal{L} = 1,\ 10$ ab^{-1} and results are given as solid and dashed lines, respectively. For the lower luminosity, the effect of varying the systematic uncertainty within $\delta\sigma_B = 0.0\% - 0.1\%$ is shown by the width of the band. The results for $\mathcal{L} = 10$ ab^{-1} present the case $\delta\sigma_B = 0.0\%$ only [233]. For all shown benchmark scenarios one can see a clear resonance behavior. The sensitivity increases when the mediator can be produced resonantly, i.e. at $M_{Z'} \sim 3$ TeV. A larger decay width of the Z' reduces the sensitivity. For an integrated luminosity $\mathcal{L} = 1$ ab^{-1} and $\Gamma_{Z'} = 0.1 M_{Z'}$ it is possible to test the parameter space $|\epsilon_{\tau\tau}^{\mu\mu}| \gtrsim 1.5 \times 10^{-4}$ in the resonance region. Towards larger mediator masses $M_{Z'} > \sqrt{s}$, the NSI bound becomes a constant indicating that the EFT regime started.

General considerations allow to put further constraints on the viable parameter space. For example, the total decay width of the Z' ($\Gamma_{Z'}$) has to be larger than or equal to the sum of partial decay widths which leads to the constraint $\Gamma_{Z'} \geq \Gamma_{Z'\to\bar{\mu}\mu} + \Gamma_{Z'\to\bar{\nu}\nu}$. Using expressions for the partial decay widths of a Z' boson given in [74], we deduce that

$$\Gamma_{Z'} \geq \frac{M_{Z'}}{24\pi}\left[(g_\nu)^2 + \left(g_\mu^L\right)^2 + \left(g_\mu^R\right)^2\right] \geq \frac{M_{Z'}}{24\pi} 2\sqrt{2} g_\nu g_\mu^L \ . \tag{6.8}$$

This approximation is valid for the decay to one neutrino flavor and ignores phase space factors of order $\mathcal{O}(m_f^2/M_{Z'}^2)$ with $f = \nu,\ \mu$. Finally, from the definition in Eq. (6.4) we find the consistency condition

$$|\epsilon_{\tau\tau}^{\mu\mu}| \leq \frac{3\pi}{G_F M_{Z'}^2}\frac{\Gamma_{Z'}}{M_{Z'}} \ , \tag{6.9}$$

for a specific ratio $\Gamma_{Z'}/M_{Z'}$. In Figure 6.4 we illustrate this constraint by red solid and dashed lines for the two respective cases $\Gamma_{Z'} = 0.1 M_{Z'}$ and $\Gamma_{Z'} = 0.3 M_{Z'}$. For comparison, we also displayed the perturbativity bound where $g_\nu g_\mu^L = 2\pi$ by a black solid line.

In general, Z' couplings to muons do not have to be vector-like. Therefore we dismiss this assumption and take arbitrary values for g_μ^L and g_μ^R, while we fix $M_{Z'} = 1$ TeV. The projected sensitivity in the $\epsilon_{\tau\tau}^{\mu\mu(V,LL)} - \epsilon_{\tau\tau}^{\mu\mu(V,LR)}$ plane is shown in the lower part of Figure 6.4. From these results we see that constraints for a vector-like theory with $g_\mu^L = g_\mu^R$ are as stringent as for models with axial-vector couplings $g_\mu^L = -g_\mu^R$.

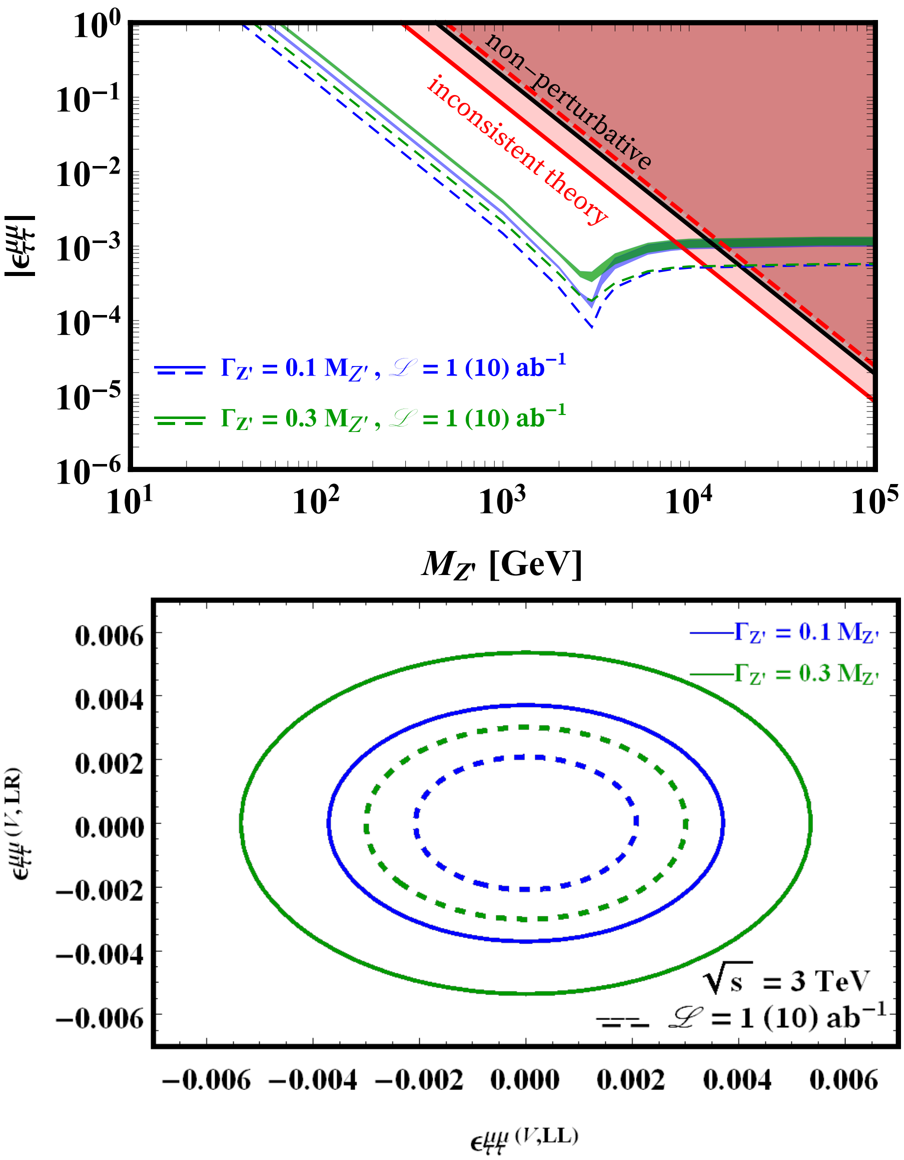

Figure 6.4 Projected sensitivity at 95% CL for NSI parameters at a muon collider with $\sqrt{s} = 3$ TeV and $\mathcal{L} = 1,\ 10\ \mathrm{ab}^{-1}$ in a toy Z' model. Upper panel: Sensitivity in the parameter plane $M_{Z'}$ vs. $|\epsilon_{\tau\tau}^{\mu\mu}|$ for a vector-like muon coupling and decay widths $\Gamma_{Z'} = 0.1(0.3)M_{Z'}$. Lower panel: Degeneracy in the $\epsilon_{\tau\tau}^{\mu\mu(V,LL)}$ vs. $\epsilon_{\tau\tau}^{\mu\mu(V,LR)}$ plane with $M_{Z'} = 1$ TeV. Published in [2].

6.3 Probing UV complete models

The previously considered toy model gave us a first impression on the sensitivity reach of a muon collider to test NSIs. However, UV complete models can lead to more complex constraints, as left-handed charged leptons and neutrinos are part of the same doublet representation of $SU(2)_L$. In the following we examine three particular UV complete models which can lead to NSIs and compare the sensitivity reach of a muon collider to other existing experiments. Figure 6.1 summarizes the three completions which we consider in the next sections.

6.3.1 Gauged $L_\mu - L_\tau$ model

As a start, we investigate the UV complete theory where the difference of individual lepton numbers $L_\mu - L_\tau$ is gauged. The lepton numbers L_μ and L_τ belong to the accidental global $U(1)$ symmetries of the SM and their difference can be gauged in an anomaly free way which makes this SM extension particularly well motivated [270, 271]. At the same time, it delivers possible solutions to the anomalous magnetic moment of the muon and to the Hubble tension [272–275]. Promoting $U(1)_{L_\mu - L_\tau}$ to a local gauge symmetry, gives rise to a Z' boson. Its interactions with fermions can be described by the Lagrangian

$$\mathcal{L} \supset g_{\mu\tau} \left[\overline{L}_\mu \gamma^\mu L_\mu + \overline{\mu}_R \gamma^\mu \mu_R - \overline{L}_\tau \gamma^\mu L_\tau - \overline{\tau}_R \gamma^\mu \tau_R\right] Z'_\mu \ , \tag{6.10}$$

where we defined the left-handed $SU(2)_L$ lepton doublets $L_\mu \equiv \left(\nu_{\mu L}, \mu_L\right)^T$, $L_\tau \equiv (\nu_{\tau L}, \tau_L)^T$ and the gauge coupling $g_{\mu\tau}$. The analysis of NSIs in this model is done in a similar way as described in Section 6.2 and we present our results in Figure 6.5. Here, the 95% CL exclusion curves in the $g_{\mu\tau} - M_{Z'}$ parameter plane are given for a benchmark scenario of a $\sqrt{s} = 3$ TeV muon collider with $\mathcal{L} = 1,\ 10\ \text{ab}^{-1}$ integrated luminosity. To simplify the comparison with NSI parameters, black dotted lines represent isocontours of the NSI coupling

$$\epsilon_{\tau\tau}^{\mu\mu} \equiv \frac{g_{\mu\tau}^2}{2\sqrt{2} G_F M_{Z'}^2} \ . \tag{6.11}$$

The regions in parameter space that explain the Hubble tension (with $\Delta N_{\text{eff}} \simeq 0.2{-}0.5$) [275] and the anomalous muon magnetic moment (at 2σ) [274, 276] are shaded in green and red color, respectively. Numerous other experimental constraints are summarized by a grey line. These bounds include four-muon searches at BaBar and CMS [277, 278] which reside in the mass range 200 MeV to 70 GeV. Limits from neutrino trident production at CCFR [279] that gives the most serious constraint for $M_{Z'} > 70$ GeV and restrictions in the low mass window from N_{eff} in cosmological observations [275] and white Dwarf cooling [280].

With an integrated luminosity of $\mathcal{L} = 1\ \text{ab}^{-1}$, the monophoton search at a muon collider is most sensitive at a mediator mass $M_{Z'} \sim 3$ TeV. There one can test the region $|\epsilon_{\tau\tau}^{\mu\mu}| \gtrsim 1.1 \times 10^{-4}$. Our result shows that the monophoton search at a muon collider could especially test yet unexplored parameter space in the high mass range of the gauged $L_\mu - L_\tau$ model, whereas for $M_{Z'} \leq 100$ GeV it cannot compete with other experimental bounds. Additionally, we note that the monophoton signal is a less sensitive probe compared to other possible signatures of this model which could also be tested at a muon collider such as $\mu^+\mu^- \to \overline{f} f \gamma$, where $f = \mu, \tau$ [219]. Still, the monophoton signal would give a direct probe of the coupling to neutrinos in a laboratory experiment.

6.3.2 Neutral scalar extension

Neutral scalar extensions do not only offer an explanation for the difference between the measured and predicted value of the muon magnetic moment. They also approach the Hubble tension by large neutrino self-interactions in a certain range of parameter space.

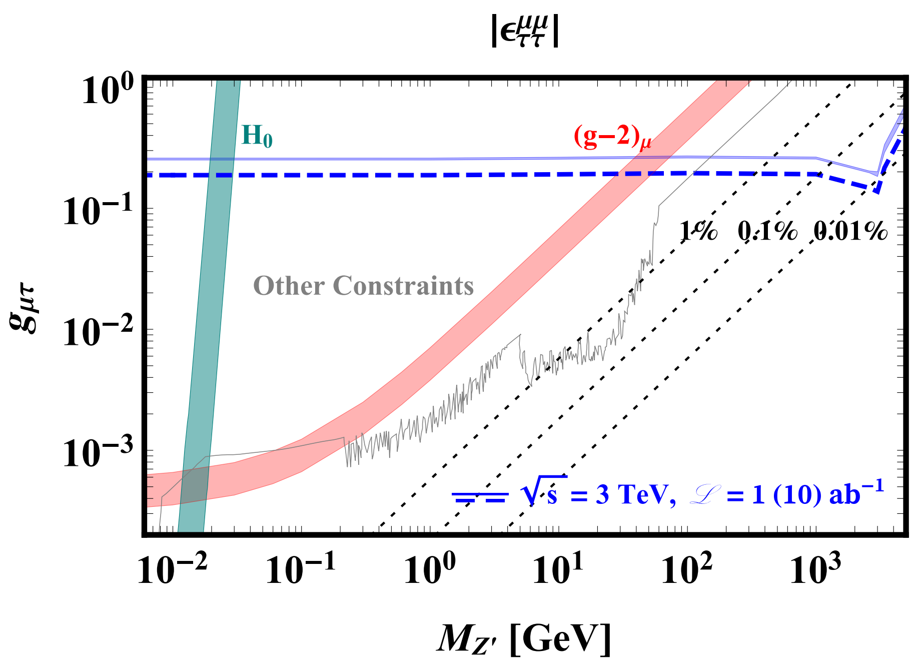

Figure 6.5 Projected sensitivity to NSIs for a $\sqrt{s} = 3$ TeV muon collider with integrated luminosity $\mathcal{L} = 1,\ 10\ \text{ab}^{-1}$ in the gauged $L_\mu - L_\tau$ model. The limits are displayed in the gauge coupling vs. gauge boson mass plane as blue solid and blue dashed line. Further experimental bounds are summarized by the grey line. Black dots indicate lines of equal NSI parameter $|\epsilon^{\mu\mu}_{\tau\tau}|$. Published in [2].

In this section, we consider a scalar field φ which couples to neutrinos and muons through the following Yukawa interaction

$$-\mathcal{L}_Y \supset \sum_{\alpha\beta} (y_\nu)_{\alpha\beta} \overline{\nu}_\alpha P_L \nu_\beta \varphi + y_\mu \overline{\mu} P_L \mu \varphi + h.c.\ , \tag{6.12}$$

where the strength of the interaction is determined by the independent couplings $(y_\nu)_{\alpha\beta}$ and y_μ. We note that such a type of coupling to muons can in general arise in two-Higgs-doublet models and for a certain range of parameters it addresses the measured discrepancy in $(g-2)_\mu$ as described in [281]. On the other hand, the Yukawa coupling to neutrinos may occur for example in type II seesaw extensions [65, 67, 68, 282]. The mixing of the charge zero component of an $SU(2)_L$ triplet scalar with the neutral part of a second Higgs doublet would then result in the Lagrangian given above. Since we deal with Yukawa couplings, their values can in principle be arbitrary and unrelated to each other. However, in this study we will proceed with the simplifying assumptions that the scalar φ solely couples to ν_τ neutrinos and we fix the relation $(y_\nu)_{\tau\tau}/10 = y_\mu$. Searches for a monophoton signal plus missing transverse energy will be especially important to test models where the coupling to charged leptons is suppressed with respect to the coupling to neutrinos, which justifies our previous parameter choice. With this selection of parameters, we present the 95 % CL exclusion plot in the parameter space M_φ vs. $(y_\nu)_{\tau\tau}$ in Figure 6.6 for a center-of-mass energy $\sqrt{s} = 3$ TeV. For a better comparison, we indicate the contour of constant NSI parameter

$$\epsilon_{\tau\tau}^{\mu\mu} \equiv \frac{(y_\nu)_{\tau\tau} y_\mu}{2\sqrt{2} G_F M_\varphi^2} \,, \tag{6.13}$$

by a black dotted line. As it was the case for the previously analyzed s-channel processes, the highest sensitivity is achieved for a mediator mass of $M_\varphi \approx 3$ TeV where one can test the NSI coupling down to $|\epsilon_{\tau\tau}^{\mu\mu}| \gtrsim 1.3 \times 10^{-4}$. Interestingly, a muon collider can test yet unconstrained regions of the parameter space where $M_\varphi \gtrsim 90$ GeV. This also includes untested areas that could explain the anomalous $(g-2)_\mu$ [281] at 2σ (red region). Other experiments set further limits to the parameter space as for example BaBar which searches for the process $e^+e^- \to \mu^+\mu^-\varphi$ with a subsequent decay $\varphi \to \mu^+\mu^-$ in the mass range $M_\varphi > 200$ MeV [278, 283] (orange domain). Regions excluded by CMS search for four-muon events [277, 283] and Z invisible decay width [284] are displayed as pink and grey area. Contrary to the previous Z' model, limits from neutrino trident production do not exists for tau neutrinos. Even though the monophoton search at a muon collider can probe parts of the parameters space that would explain the Hubble tension through large neutrino self-interactions (green area) [285], it is not competitive with Z to invisible decay searches.

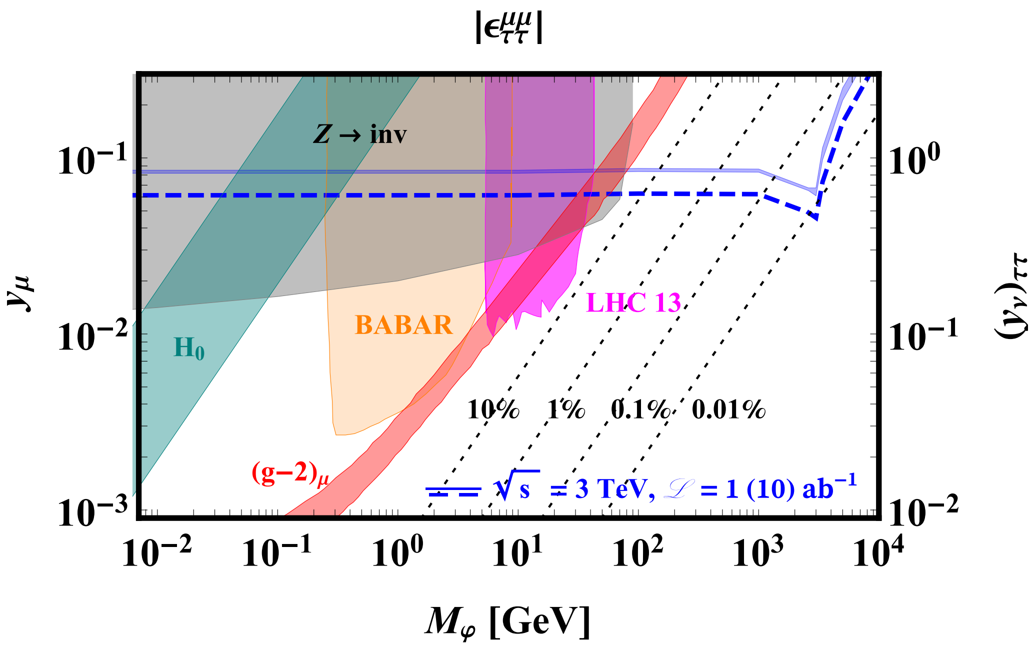

Figure 6.6 Sensitivity of a $\sqrt{s} = 3$ TeV muon collider to NSIs at the 95 % CL in the neutral scalar extension of the SM. Limits are shown in terms of the Yukawa coupling and scalar mass for the integrated luminosities $\mathcal{L} = 1,\ 10$ ab^{-1} (blue solid and blue dashed line). For comparison we display existing experimental constraints and further details can be found in the text. Red and green areas indicate the parameter space that could resolve $(g-2)_\mu$ and the Hubble tension. Dotted lines denote isocontours for the parameter $|\epsilon_{\tau\tau}^{\mu\mu}|$. Published in [2].

6.3.3 Zee model

In a final step, we focus on the Zee model [70] that is a representative of a singly charged scalar extension of the SM. The special feature of the Zee model is that is generates Majorana masses for neutrinos via a one-loop radiative process and hence can give an explanation of their small masses compared to charged leptons. In the Zee model, the scalar sector encompasses two Higgs doublets $H_{1,2} \sim (1, 2, 1/2)$ and a charged scalar $\eta^+ \sim (1, 1, 1)$ with the gauge charges under the SM symmetry group $SU(3)_C \times SU(2)_L \times U(1)_Y$ given in brackets.[3] This model is particularly interesting as it does not need an extension of the fermionic field content. We will shortly summarize the main features of the Zee model here, and refer the reader to [286] for a more detailed analysis of this model. In the following, it will be most convenient to work in the Higgs basis [287] where only one of the two Higgs doublets acquires a VEV. Let us denote denote this scalar by H_1 and its VEV in the neutral component is given by v. In this basis, the possible Yukawa couplings are

$$- \mathcal{L}_Y \supset \tilde{Y}_{\alpha\beta} L_\alpha \tilde{H}_1 \ell^c_\beta \epsilon + Y_{\alpha\beta} L_\alpha \tilde{H}_2 \ell^c_\beta \epsilon + h.c. \;, \tag{6.14}$$

where we use the notation ℓ^c_α for the left-handed antilepton field with the flavor index α and $\tilde{H}_{1,2} = i\sigma_2 H^*_{1,2}$. The Yukawa couplings are represented by 3×3 matrices $\tilde{Y}_{\alpha\beta}$, $Y_{\alpha\beta}$. On top of that, the charged singlet scalar η^+ is coupled to the lepton doublet according to

$$- \mathcal{L}_Y \supset f_{\alpha\beta} L_\alpha \epsilon L_\beta \eta^+ + h.c. \;. \tag{6.15}$$

The Levi-Civita tensor ϵ acts here on the $SU(2)_L$ indices that are suppressed in our notation and $f_{\alpha\beta}$ is an anti-symmetric Yukawa matrix whose values are forced to be small due to constarints from lepton flavor violation. Completed by a trilinear term in the scalar potential

$$- V \supset \mu H_1 \epsilon H_2 \eta^- + h.c. \;, \tag{6.16}$$

this model generates radiative neutrino masses as shown in Figure 6.7. The physical spectrum contains two neutral charged scalars h and H that are CP-even, two charged scalar h^+ and H^+, and a CP-odd scalar A.

In the charged lepton mass basis where the mass matrix is diagonal, i.e. $m_E = \mathrm{diag}\left(m_e,\ m_\mu,\ m_\tau\right)$, the neutrino mass matrix is given by

$$M_\nu = a_0 \left(f m_E Y - Y^T m_E f \right) \;, \tag{6.17}$$

where we defined

$$a_0 = \frac{\sin 2\omega}{16\pi^2} \log\left(\frac{M^2_{h^+}}{M^2_{H^+}}\right) \;, \qquad \sin 2\omega = \frac{\sqrt{2} v \mu}{M^2_{h^+} - M^2_{H^+}} \;. \tag{6.18}$$

[3] Note that we use here a convention $Q = T_{3L} + Y$ for the electric charge.

Note that ω represents the mixing angle between charged scalars. Hence, the eigenstates of the mass basis h^+ and H^+ are defined as

$$\begin{aligned} h^+ &= \cos\omega \eta^+ + \sin\omega H_2^+ \ , \\ H^+ &= -\sin\omega \eta^+ + \cos\omega H_2^+ \ . \end{aligned} \tag{6.19}$$

In this new basis, the NSI strength is determined by the Yukawa couplings

$$-\mathcal{L}_Y \supset Y_{\alpha\beta} \left(h^- \sin\omega + H^- \cos\omega \right) \nu_\alpha \ell_\beta^c + \text{ h.c.} \tag{6.20}$$

and in our case we have specifically $\beta = \mu$ such that the second column of Y provides the couplings of muons to ν_α. Eventually, integrating out the charged scalars leads to the effective NSI parameter

$$\epsilon_{\alpha\beta}^{\mu\mu} = \frac{Y_{\alpha\mu} Y_{\beta\mu}^\star}{4\sqrt{2} G_F} \left(\frac{\sin^2\omega}{M_{h^+}^2} + \frac{\cos^2\omega}{M_{H^+}^2} \right) \ . \tag{6.21}$$

In principle, the Yukawa couplings proportional to the matrix f can also lead to NSIs, however these effects have to be small since the matrix entries of f are seriously constrained by lepton flavor violating observables. We also see that for the case $M_{h^+} \ll M_{H^+}$, the NSI coupling $\epsilon_{\alpha\beta}^{\mu\mu}$ can be dominated by the contribution of the lighter scalar. To simplify the following analysis we consider that h^+ mainly couples to tau neutrinos and therefore $Y_{\tau\mu} \neq 0$, while we neglect other couplings leading to NSIs with muons for the moment, i.e. $Y_{e\mu} = Y_{\mu\mu} = 0$.

Within this setup we present the sensitivity of a high energy muon collider to probe NSIs at 95 % CL via the monophoton signal in Figure 6.8. We show the constraints as a function of the product $|Y_{\tau\mu}| \sin\omega$, which is the effective Yukawa coupling to the mass eigenstate h^+ (compare to Eq. (6.20)). Our result shows the two respective integrated luminosities $\mathcal{L} = 1, 10 \text{ ab}^{-1}$ as solid and dashed blue lines. Absolute values of the NSI parameter $|\epsilon_{\tau\tau}^{\mu\mu}|$ caused by h^+ are represented by dashed black lines. In contrast to the previously

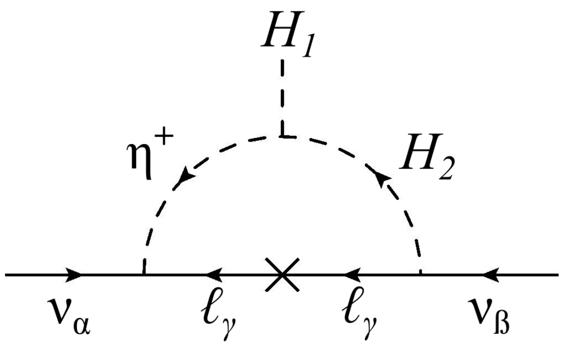

Figure 6.7 Feynman diagram that generates Majorana neutrino mass at one-loop in the Zee model.

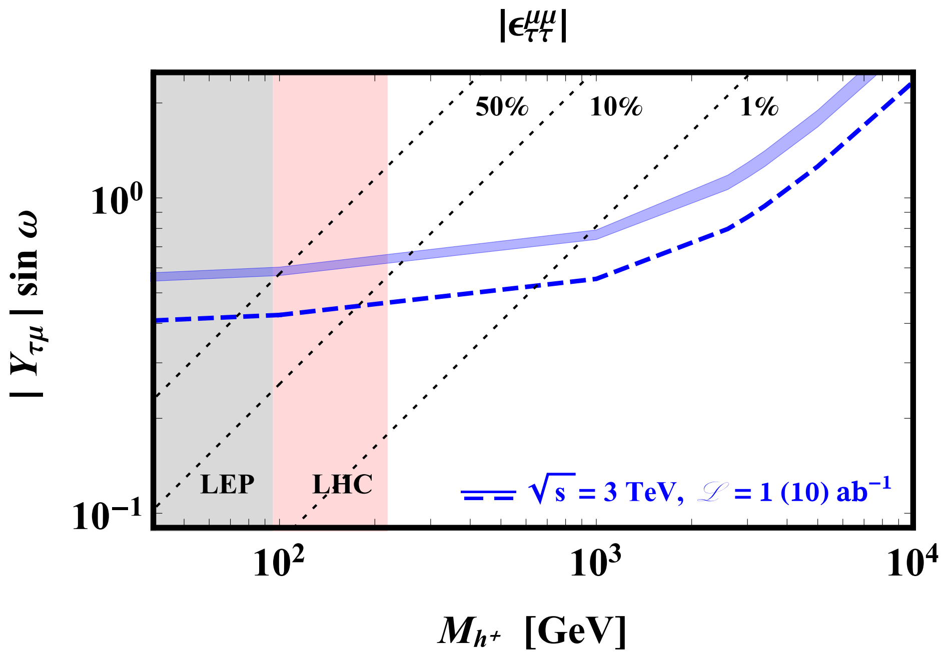

Figure 6.8 Projected sensitivity of a $\sqrt{s} = 3$ TeV muon collider to NSI parameters at 95 % CL in the Zee model. We display the results for $\mathcal{L} = 1,\ 10\ \text{ab}^{-1}$ in the coupling against mediator mass plane. For comparison, experimental bounds from LEP and LHC searches for singly charged scalars are shown as well. Black lines represent contours of constant NSI coefficient $|\epsilon^{\mu\mu}_{\tau\tau}|$. Published in [2].

considered cases, the sensitivity curve does not show a resonance behavior because the process occurs via the t-channel channel as shown in Figure 6.1. This leads to a completely different behavior and the largest sensitivity is obtained for small mediator masses. However, other experiments constrain M_{h^+} from below. For instance, LEP excludes singly charged scalars with masses below 95 GeV [286] and the ATLAS experiment at LHC even puts the more stringent bound $M_{h^+} > 219$ GeV due to smuon searches [288]. From Figure 6.8 we deduce that a muon collider can test scenarios with $|Y_{\tau\mu}|\sin\omega \geq 0.45$ at a mediator mass $M_{h^+} \approx 220$ GeV which in turn corresponds to NSI parameters $|\epsilon^{\mu\mu}_{\tau\tau}| \gtrsim 7\%$. Finally, we point out that the result shown in Figure 6.8 can be generalized to other SM extensions including singly charged scalars such as 2HDMs [289] or other radiative mass models for neutrinos [286].

Of course, realistic patterns of neutrino masses and mixing demand that more couplings besides $Y_{\tau\mu}$ are non-zero. In order to prove that the Zee model can reproduce the observed squared neutrino mass differences and mixing angles, while at the same time giving rise to large NSIs, we give a benchmark scenario here. For simplicity, we assume that all Yukawa couplings are real and a normal mass ordering. Then, we find that the couplings

$$Y_{\alpha\beta} = \begin{pmatrix} 0. & 0. & -0.00378 \\ 6.747\times 10^{-6} & 0. & -3.219\times 10^{-6} \\ 0.000115 & 2.219 & -0.143 \end{pmatrix} \tag{6.22}$$

$$a_0 f = \begin{pmatrix} 0. & -0.0000234 & -3.011 \times 10^{-12} \\ 0.0000234 & 0. & 2.843 \times 10^{-12} \\ 3.011 \times 10^{-12} & -2.843 \times 10^{-12} & 0. \end{pmatrix} \tag{6.23}$$

produce the neutrino mass splittings $\Delta m^2_{21} = 7.22 \times 10^{-5}\text{eV}^2$, $\Delta m^2_{31} = 2.449 \times 10^{-3}\text{eV}^2$ and mixing angles $\theta_{12} = 33.04^\circ$, $\theta_{23} = 51.89^\circ$ and $\theta_{13} = 8.88^\circ$ that agree within 3σ with current experimental best fit values [30]. In the case where charged scalar masses are given by $M_{H^+} \approx M_H \approx M_A \approx 2$ TeV and $M_{h^+} \approx 220$ GeV with a mixing angle $\sin\omega \approx 0.35$, NSIs can be as large as $\epsilon^{\mu\mu(h^+)}_{\tau\tau} \approx 19\%$ which is within the testable regime of a muon collider. In an explicit scenario, there are more experimental constraints to consider apart from the ones already shown in Figure 6.8. Especially lepton flavor violating decays that occur due to new scalar couplings can impose serious constraints. Nevertheless, the structure of Yukawa matrices Y and f shows us that charged lepton flavor violating decays would be suppressed if there was only a single large entry in a row. Thus, the large coupling $Y_{\tau\mu}$ constrains the other couplings of the row to be small. Note however that it is not possible to set them all to zero in order to realize the observed neutrino oscillation data. For our benchmark model, the radiative decay $\tau \to \mu\gamma$ can occur via charged scalar exchange an has an approximate branching ratio of [286]

$$\begin{aligned} \text{Br}(\tau \to \mu\gamma) &\simeq \frac{1}{\Gamma_\tau} \frac{\alpha}{4} \frac{|Y_{\tau\tau} Y^*_{\tau\mu}|^2}{(16\pi^2)^2} \frac{m_\tau^5}{144} \left(\frac{\sin^2\omega}{M_{h^+}} + \frac{\cos^2\omega}{M_{H^+}} \right)^2 \\ &\simeq 3.0 \times 10^{-9} \;, \end{aligned} \tag{6.24}$$

which is in agreement with the PDG bound $\text{BR}(\tau \to \mu\gamma) < 4.4 \times 10^{-8}$ [31]. We examined similar decays of the category $\ell_\alpha \to \ell_\beta\gamma$ and $\ell_\alpha \to \overline{\ell}_\beta \ell_\gamma \ell_\delta$ for our benchmark scenario. While all are in agreement with current limits, $\text{Br}(\tau \to \mu\gamma)$ is closest to future experimental searches. On top of that, a number of other constraints arises from new muon and tau decay channels to two neutrinos and a charged lepton. The branching ratio for the lepton flavor violating decay $\mu^- \to e^- \overline{\nu_\mu} \nu_\tau$ is for example given by

$$\begin{aligned} \text{Br}(\mu^- \to e^- \overline{\nu_\mu} \nu_\tau) &\simeq \frac{1}{\Gamma_\mu} \frac{2}{6144\pi^3} \frac{m_\mu^5}{M^4_{h^+}} \left(\sin\omega \cos\omega Y_{\tau\mu} f_{\mu e} \right)^2 \\ &\simeq 1.7 \times 10^{-7} \;. \end{aligned} \tag{6.25}$$

However, the only current constraint on LFV muon decays to two neutrinos quoted by the PDG is $\text{Br}(\mu^- \to e^- \overline{\nu_\mu} \nu_e) < 1.2\%$ [31] which constitutes a rather soft limit. For more details on the anomalous decay of muons we refer the reader to [290]. Our benchmark point contributes to the effective operator $\mathcal{L}_{\text{eff}} = 2\sqrt{2} G_F g^S_{RR} (\overline{\nu}_{\alpha L} e_R)(\overline{\mu}_R \nu_{\beta L})$ which is constrained by global fits to muon decay parameters.[4] If the lighter scalar h^+ mediates the decay, we will find $g^S_{RR} = Y_{\alpha e} Y^*_{\beta\mu} \sin^2\omega / (2\sqrt{2} G_F M^2_{h^+})$. In our case this is also below the

[4]For the notation used here see [31].

limit $|g^S_{RR}| < 0.035$ [31]. We consider similar constraints for tau decay parameters and find no conflict with existing limits. Our benchmark points also align with constraints coming from the electroweak T parameter, Higgs observables and charge-breaking minima, where more details are given in [286].

The preceding discussion shows that large NSIs can in principle occur in the Zee model. Our benchmark point demonstrates that there is some parameter space which evades all current bounds. The search for NSIs at a muon collider will therefore be able to test important parts of the parameter space of this model.

Chapter 7

Summary and conclusion

In its current form, the flavor sector of the Standard Model leaves us with many puzzling questions. The majority of parameters that describe the Standard Model are needed to characterize the emerging fermion masses and mixings, but their diverse scales and peculiar patterns remain unexplained. In addition, neutrinos are massless in this description manifesting that the Standard Model in its present state is not complete. A particularly intriguing class of solutions explains the hierarchical structure of fermion masses from radiative quantum corrections, and a number of proposals implement this idea by means of new scalar interactions. In this thesis, we have investigated the appealing and economical alternative that gauge interactions are responsible for radiative corrections, eventually leading to a hierarchy in fermion masses. Moreover, we examined how small neutrino masses can be incorporated into this scheme.

In Chapter 4, we have investigated a $U(1)_X$ Standard Model extension where fermion masses arise at the tree level or from one-loop radiative corrections. Consequently, the presence of different mass scales could be naturally explained. The basic ingredient of this model are new generations of vector-like up-type and down-type quarks ($T,\ B$) and vector-like leptons ($N,\ E$). Gauge charges are defined in such a way that a generalized seesaw mechanism occurs when two scalar fields obtain a VEV and the gauge symmetry is spontaneously broken to $SU(3)_C \times U(1)_{\text{EM}}$. The seesaw mechanism provides tree level masses for third and second generation fermions, which approximately scale with the Yukawa coupling y and vector-like fermion mass M according to $\sim y^2 v_{EW} v_S / M$. Flavor non-diagonal interactions of a Z' gauge boson are the origin of one-loop radiative corrections that provide mass for the first generation fermions. Hence, their masses are suppressed by an additional factor $1/(16\pi^2)$ and therefore naturally small (see illustration in Figure 4.1). Our idea can be employed for up- and down-type quarks as well as charged leptons and neutrinos. Interestingly, due to the particle representation and symmetries, neutrinos carry Dirac characteristic in our model.

We have given explicit benchmark scenarios to prove that fermion masses and mixing patterns can be correctly mapped with the parameters of our framework (see results in Table 4.2). Vector-like quark and charged lepton masses of several tens of TeV together with Yukawa couplings $\mathcal{O}(10^{-2})$ - $\mathcal{O}(1)$ correctly reproduce fermion masses in these sectors for $M_Z' = 300$ TeV. Realistic neutrino masses require moderately smaller Yukawa couplings of $\mathcal{O}(10^{-4})$ in connection with larger vector-like fermion masses $M_N \sim \mathcal{O}(10^7 \text{ TeV})$. Even though there is still an inherent hierarchy in the Yukawa couplings, this constitutes a significant improvement compared with the twelve orders of magnitude that separate the neutrino mass scale from the top quark. The mechanism explains the difference in fermion masses by a combination of loop suppression and slightly hierarchical heavy new physics, while the size of mixing parameters in the CKM and PMNS matrix remains unexplained. Nevertheless, the two benchmark scenarios have demonstrated that mixing in agreement with observations can be achieved for appropriately chosen parameters.

On the phenomenological side, many interesting consequences follow from our model. We have analyzed the impact of the proposed new physics on flavor violating observables. From our analysis we found that current experimental bounds on charged lepton decays $l_i \to l_j \gamma$ are close to the value predicted in our theory. Also observations of neutral meson oscillations, especially that of $B_d^0 - \overline{B_d^0}$, allows to test this model in future. If the vector-like masses were at the scale of a few TeV, signals from heavy vector-like fermions could also be found through decays to multi-lepton final states in association with jets or missing energy at future collider experiments.

The one-loop suppression nicely explains the comparatively small first generation masses. However, the model presented in Chapter 4 is not completely satisfying in the sense that it does not describe the mass difference between second and third generation fermions by a radiative process. In Chapter 5 of this work, we have demonstrated that the mass differences between all three fermion generations can be attributed to tree level, one-loop and two-loop effects within a left-right symmetric model. To realize this, we looked at a variant of the left-right symmetric model featuring two scalar doublets χ_L, χ_R and one scalar singlet η. Furthermore, we extended the fermion sector by different types of new fermions ($T,\ B,\ N,\ E$) and ($T',\ B',\ N',\ E'$). Some of them are equipped with vector-like masses, to implement a double seesaw texture after spontaneous symmetry breaking (see particle content in Table 5.1). The third generation fermions gain a tree level mass from the seesaw with heavy vector-like fermions, while the second and first generation stay massless at this level. Corrections mediated by neutral gauge bosons $Z_{L/R}$ allow that second generation fermions pick up mass at the one-loop level. The exchange of charged gauge bosons $W_{L/R}$ creates first generation masses at two-loop level (see Figure 5.1). Our setup constitutes a complete framework where the rank of the fermion mass matrix is increased by one at each loop level and the double seesaw structure is crucial for this to work. The presence of a charged gauge boson W_R, which interacts with right-handed fermion doublets, is an elementary difference to the model presented in Chapter 4. Through its mixing with the W_L boson (at one-loop), it allows to contribute radiatively to fermion masses.

Our mechanism is applicable not only for quarks but also for charged leptons, whereas small neutrino masses require an individual treatment. While loop factors account for a hierarchy between generations, the mass differences between the tau lepton and the bottom and top quark arises from a mild inverted mass hierarchy of the respective vector-like partners $M_T < M_B < M_E$ by means of the seesaw relation. It is also interesting to note that two-loop radiative corrections from charged gauge boson exchange exhibit a cross correlation between isospin partners. The mass of the first generation up quark receives therefore contributions from the masses of second and third generation down quarks. The other way around, the down quark mass is proportional to second and third generation up quark mass insertions. This could point towards a possible explanation why $m_u < m_d$ for the first generation, even though the opposite is true for quarks of the second and third generation. The charge current $W_{L/R}$ interaction also connects the electron mass to the neutrino sector and vice versa (see Figure 5.4). In this way, the Dirac masses of both sectors are related to each other and expected to exist at roughly the same scales. Sub-eV active neutrino masses therefore necessitates further lepton number violating operators. A major advantage of the presented mechanism is the minimal scalar sector. Loop corrections creating first and second generation masses arise mainly from gauge boson contributions and the model includes only those scalars essential for spontaneous symmetry breaking.

We gave explicit benchmark points demonstrating that quark masses and mixings as well as charged lepton masses comply with experimental data (see results presented in Table 5.3). For a low scale breaking of $SU(2)_R$ with $M_{W_R} \simeq 7$ TeV, vector-like fermion masses of several tens of TeV are needed and all Yukawa couplings are $\mathcal{O}(1)$. We highlight that the absolute scale of new physics is not predetermined by our mechanism though. Both, symmetry breaking scales as well as vector-like masses can be at higher values as long as their relative size is retained. The heavy vector-like neutrinos are complete gauge singlets in our framework and therefore allow to introduce lepton number violating operators. In the tree level approximation, we have shown that high scale lepton number violation leads to a light active neutrino state (see Figure 5.5). A full study of the neutrino sector which takes into account all parameter dependencies and radiative corrections up to two-loop level is left for future investigations.

Our mechanism, as it is right now, cannot explain mixing angles though it would be worth to explore in future whether new symmetries relating the up and down quark sector could shed further light on the mixing behavior. Furthermore, our model is close to left-right-symmetric models which provide an axion-free solution to the strong CP problem [56, 123]. Since parity is a symmetry of the tree level Lagrangian, contributions to the strong CP parameter $\overline{\theta}$ can only arise at higher loop order. At one-loop, first generation quarks are massless in our case and a strong CP phase is unphysical. Only at two-loop, when all quarks are massive, $\overline{\theta}$ can be non-zero and it would be an interesting subject for upcoming studies to see whether it agrees with current experimental bounds.

Eventually probing the huge variety of Standard Model extensions is critical to improve our understanding of nature. Among the many unresolved questions, the existence of massive neutrinos is one of the clearest signs for physics beyond the Standard Model. Since mechanisms that accommodate massive neutrinos usually involve new interactions, the probe of neutrino non-standard interactions can be an efficient tool to falsify theories. In Chapter 6 of this work, we have demonstrated that the monophoton signal from the scattering process $\mu^+\mu^- \to \nu\overline{\nu}\gamma$ can be used to probe neutrino non-standard interactions at a high energy muon collider. In our study we have explicitly considered muonic forces, i.e. four-fermion interactions of the type $\mu\mu\nu\nu$. This interaction is less constrained than neutrino non-standard interactions with first generation quarks and charged leptons, but equally compelling in consideration of recent measurement of the muon magnetic moment.

In our study, we have considered explicit force mediators that lead to neutrino non-standard interactions and carried out a Monte Carlo simulation to analyze the signal $\mu^+\mu^- \to \gamma + \not{E}_T$ at a muon collider with center of mass energy $\sqrt{s} = 3$ TeV. As representatives, we investigated three extensions of the Standard Model. First, the gauged $L_\mu - L_\tau$ model, second a model featuring a neutral scalar and third, Zee's radiative neutrino mass model. We presented the projected sensitivity to the NSI strength $\epsilon^{\mu\mu}_{\alpha\beta}$ at 95% confidence level for the integrated luminosities $\mathcal{L} = 1,\ 10\ \text{ab}^{-1}$ and compare them with other experimental constraints (see Figs. 6.5, 6.6 and 6.8). For the s-channel processes, highest sensitivities are achieved when the mediator is resonantly produced and our study has shown that a muon collider can probe NSI strengths as small as $|\epsilon^{\mu\mu}_{\tau\tau}| \gtrsim 1.5 \times 10^{-4}$. We highlight that the search for NSIs at a muon collider can provide complementary insights, especially when the new physics couplings to neutrinos exceed those to muons. For the neutral scalar extension, we found that parts of the parameter space can be probed which allow to explain the anomalous $(g-2)_\mu$. For the Zee model, we demonstrated that a realistic neutrino mass spectrum can lead to NSI strengths $\epsilon^{\mu\mu}_{\tau\tau} \approx 19\%$, which are testable in future. A high energy muon collider therefore shows great potential to test interesting parameter space of different models and hopefully helps us to gain further insights in new physics related to neutrinos.

This thesis demonstrates that hierarchical fermion masses can naturally arise from quantum loop corrections in both Abelian and non-Abelian gauge extensions of the Standard Model. New gauge interactions drive these corrections, and the scalar sector remains minimal, containing only fields necessary for symmetry breaking. Notably, no strongly hierarchical Yukawa couplings are required to explain quark and charged lepton masses, while neutrino masses can be incorporated straightforwardly. Our work provides a roadmap for addressing flavor mass hierarchies through radiative mechanisms, with potential extensions to explain mixing angles and promising testable signals of flavor violation in future experiments.

Appendix A

Neutral meson mixing

The Hamiltonian for $\Delta F = 2$ processes is generally given by

$$\mathcal{H}_{\text{eff}}^{\Delta F=2} = \sum_{i=1}^{5} C_i Q_i + \sum_{i=1}^{3} \tilde{C}_i \tilde{Q}_i \,. \tag{A.1}$$

The Wilson coefficients are indicated by C_i and belong to a basis of four-fermion operators

$$\begin{gathered} Q_1 = \overline{q}_{iL}^{\alpha} \gamma_\mu q_{jL}^{\alpha} \overline{q}_{iL}^{\beta} \gamma^\mu q_{jL}^{\beta} \,, \qquad Q_2 = \overline{q}_{iR}^{\alpha} q_{jL}^{\alpha} \overline{q}_{iR}^{\beta} q_{jL}^{\beta}, \qquad Q_3 = \overline{q}_{iR}^{\alpha} q_{jL}^{\beta} \overline{q}_{iR}^{\beta} q_{jL}^{\alpha} \,, \\ Q_4 = \overline{q}_{iR}^{\alpha} q_{jL}^{\alpha} \overline{q}_{iL}^{\beta} q_{jR}^{\beta} \,, \qquad\qquad Q_5 = \overline{q}_{iR}^{\alpha} q_{jL}^{\beta} \overline{q}_{iL}^{\beta} q_{jR}^{\alpha} \,, \end{gathered} \tag{A.2}$$

where $\alpha,\ \beta$ are color indices and $i, j = 1, 2, 3$ indicate the generation. The corresponding operators $\tilde{Q}_i$ are obtained from an interchange of chirality $L \leftrightarrow R$.

As we obtain the Wilson coefficients by integrating out new physics at a high scale, it is necessary to consider their renormalization group running to the energy scale that is relevant for hadron physics. The running from the high scale M_H to the low scale μ can be described by the method of magic numbers according to [208]

$$C_r(\mu) = \sum_i \sum_s (b_i^{(r,s)} + \eta c_i^{(r,s)}) \eta^{a_i} C_s(M_H) \,. \tag{A.3}$$

While $\eta = \alpha_s(M_H)/\alpha_s(m_t)$ depicts the running of the strong coupling, the numbers $b_i^{(r,s)}$, $c_i^{(r,s)}$ and a_i that enter the calculation are called magic numbers and are given for each meson in the following.

A.1 B-mesons

The magic numbers for B-meson mixing are taken from [208] and are given by

$$
\begin{aligned}
b_i^{(1,1)} &= (0.865,\ 0,\ 0,\ 0,\ 0)\ , & c_i^{(1,1)} &= (-0.017, 0, 0, 0, 0)\\
b_i^{(2,2)} &= (0,\ 1.879,\ 0.012,\ 0,\ 0)\ , & c_i^{(2,2)} &= (0,\ -0.18,\ -0.003, 0\ , 0)\\
b_i^{(3,3)} &= (0, 0.011,\ 0.54,\ 0,\ 0)\ , & c_i^{(3,3)} &= (0,\ 0,\ 0.028, 0\ , 0)\\
b_i^{(4,4)} &= (0, 0,\ 0,\ 2.87,\ 0)\ , & c_i^{(4,4)} &= (0,\ 0,\ 0,\ -0.48,\ 0.005)\\
b_i^{(5,5)} &= (0, 0,\ 0,\ 0.29,\ 0.863)\ , & c_i^{(5,5)} &= (0,\ 0,\ 0,\ -0.007,\ 0.019)\\
b_i^{(2,3)} &= (0,\ -0.493,\ 0.18,\ 0,\ 0)\ , & c_i^{(2,3)} &= (0,\ -0.014,\ 0.008,\ 0,\ 0)\\
b_i^{(3,2)} &= (0,\ -0.044,\ 0.035,\ 0,\ 0)\ , & c_i^{(3,2)} &= (0,\ 0.005,\ -0.012,\ 0,\ 0)\\
b_i^{(4,5)} &= (0,\ 0,\ 0,\ 0.961,\ -0.22)\ , & c_i^{(4,5)} &= (0,\ 0,\ 0,\ -0.25,\ -0.006)\\
b_i^{(5,4)} &= (0,\ 0,\ 0,\ 0.09,\ 0)\ , & c_i^{(5,4)} &= (0,\ 0,\ 0,\ -0.013,\ -0.016)
\end{aligned}
$$

and

$$a_i = (0.286,\ -0.692,\ 0.787,\ -1.143,\ 0.143)\ .$$

For the Higgs contributions, we have $M_H = m_\phi = 125.1$ GeV and the operators Q_2 and Q_4 are involved. With the help of Eq. (A.3) we find at $\mu = m_b$:

$$
\begin{aligned}
C_2(\mu) &= 1.650 \cdot C_2(M_H)\,, \qquad & C_3(\mu) &= -0.014 \cdot C_2(M_H)\,,\\
C_4(\mu) &= 2.259 \cdot C_4(M_H)\,, \qquad & C_5(\mu) &= 0.056 \cdot C_4(M_H)\,.
\end{aligned}
\tag{A.4}
$$

Evidently, the operators Q_3 and Q_5 originate from operator mixing, however their contribution is rather small and will therefore not be considered. The correction factors needed in the calculation of Eq. (4.59) can be read off as $\eta_2(\mu) = 1.650$ and $\eta_4(\mu) = 2.259$.

Equally, for the Z' induced operators we have $M_H = M_{Z'} = 300$ TeV and the operators Q_1 and Q_4 contribute at this scale. The evolution to μ yields

$$
\begin{gathered}
C_1(\mu) = 0.713 \cdot C_1(M_H)\,, \qquad C_4(\mu) = 5.446 \cdot C_4(M_H)\,,\\
C_5(\mu) = 0.165 \cdot C_4(M_H)\,.
\end{gathered}
\tag{A.5}
$$

We therefore deduce $\eta_1(\mu) = 0.713$, $\eta_4(\mu) = 5.446$ while the operator contribution Q_5 is negligible and will not be considered in the calculation.

A.2 K-mesons

The procedure for K-mesons is similar, but individual magic numbers have to be used. For our calculation, we take the magic numbers from [206] that are given by

$$
\begin{aligned}
b_i^{(1,1)} &= (0.82,\ 0,\ 0,\ 0,\ 0)\ , & c_i^{(1,1)} &= (-0.016, 0, 0, 0, 0) \\
b_i^{(2,2)} &= (0,\ 2.4,\ 0.011,\ 0,\ 0)\ , & c_i^{(2,2)} &= (0,\ -0.23,\ -0.002, 0\ , 0) \\
b_i^{(3,3)} &= (0, 0.0049,\ 0.43,\ 0,\ 0)\ , & c_i^{(3,3)} &= (0,\ 0.00021,\ 0.023,\ 0,\ 0) \\
b_i^{(4,4)} &= (0, 0,\ 0,\ 4.4,\ 0)\ , & c_i^{(4,4)} &= (0,\ 0,\ 0,\ -0.68,\ 0.0055) \\
b_i^{(5,5)} &= (0, 0,\ 0,\ 0.061,\ 0.82)\ , & c_i^{(5,5)} &= (0,\ 0,\ 0,\ -0.013,\ 0.018) \\
b_i^{(2,3)} &= (0,\ -0.63,\ 0.17,\ 0,\ 0)\ , & c_i^{(2,3)} &= (0,\ -0.018,\ 0.0049,\ 0,\ 0) \\
b_i^{(3,2)} &= (0,\ -0.019,\ 0.028,\ 0,\ 0)\ , & c_i^{(3,2)} &= (0,\ 0.0028,\ -0.0093,\ 0,\ 0) \\
b_i^{(4,5)} &= (0,\ 0,\ 0,\ 1.5,\ -0.17)\ , & c_i^{(4,5)} &= (0,\ 0,\ 0,\ -0.35,\ -0.0062) \\
b_i^{(5,4)} &= (0,\ 0,\ 0,\ 0.18,\ 0)\ , & c_i^{(5,4)} &= (0,\ 0,\ 0,\ -0.026,\ -0.016)
\end{aligned}
$$

and

$$a_i = (0.29, -0.69, 0.79, -1.1, 0.14).$$

For the K meson we evaluate the Wilson coefficients at $\mu = 2$ GeV and find for the Higgs induced operators

$$
\begin{aligned}
C_2(\mu) &= 2.210 \cdot C_2(M_H)\,, & C_3(\mu) &= 0.003 \cdot C_2(M_H)\,, \\
C_4(\mu) &= 3.523 \cdot C_4(M_H)\,, & C_5(\mu) &= 0.1289 \cdot C_4(M_H)\,,
\end{aligned}
\tag{A.6}
$$

from which we get the result $\eta_2(\mu) = 2.210$ and $\eta_4(\mu) = 3.523$.

For the Z' induced operators our result is

$$
\begin{gathered}
C_1(\mu) = 0.674 \cdot C_1(M_H)\,, \qquad C_4(\mu) = 8.181 \cdot C_4(M_H)\,, \\
C_5(\mu) = 0.329 \cdot C_4(M_H)\,,
\end{gathered}
\tag{A.7}
$$

and therefore $\eta_1(\mu) = 0.674$ and $\eta_4(\mu) = 8.181$.

A.3 *D*-mesons

Finally, for the D-meson we use the magic numbers [209]

$$\begin{aligned}
b_i^{(1,1)} &= (0.837,\ 0,\ 0,\ 0,\ 0)\ , & c_i^{(1,1)} &= (-0.016, 0, 0, 0, 0)\\
b_i^{(2,2)} &= (0,\ 2.163,\ 0.012,\ 0,\ 0)\ , & c_i^{(2,2)} &= (0,\ -0.2,\ -0.002, 0\ , 0)\\
b_i^{(3,3)} &= (0, 0.008,\ 0.474,\ 0,\ 0)\ , & c_i^{(3,3)} &= (0,\ 0.0,\ 0.025,\ 0,\ 0)\\
b_i^{(4,4)} &= (0, 0,\ 0,\ 3.63,\ 0)\ , & c_i^{(4,4)} &= (0,\ 0,\ 0,\ -0.56,\ 0.006)\\
b_i^{(5,5)} &= (0, 0,\ 0,\ 0.045,\ 0.839)\ , & c_i^{(5,5)} &= (0,\ 0,\ 0,\ -0.009,\ 0.018)\\
b_i^{(2,3)} &= (0,\ -0.567,\ 0.176,\ 0,\ 0)\ , & c_i^{(2,3)} &= (0,\ -0.016,\ 0.006,\ 0,\ 0)\\
b_i^{(3,2)} &= (0,\ -0.032,\ 0.031,\ 0,\ 0)\ , & c_i^{(3,2)} &= (0,\ 0.004,\ -0.01,\ 0,\ 0)\\
b_i^{(4,5)} &= (0,\ 0,\ 0,\ 1.21,\ -0.19)\ , & c_i^{(4,5)} &= (0,\ 0,\ 0,\ -0.29,\ -0.006)\\
b_i^{(5,4)} &= (0,\ 0,\ 0,\ 0.14,\ 0)\ , & c_i^{(5,4)} &= (0,\ 0,\ 0,\ -0.019,\ -0.016)
\end{aligned}$$

and

$$a_i = (0.286, -0.692, 0.787, -1.143, 0.143).$$

After evolving the Wilson coefficients induced by the Higgs to $\mu = 2.8$ GeV we get

$$\begin{aligned}
C_2(\mu) &= 1.906 \cdot C_2(M_H)\,, \qquad C_3(\mu) = -0.006 \cdot C_2(M_H)\,,\\
C_4(\mu) &= 2.903 \cdot C_4(M_H)\,, \qquad C_5(\mu) = 0.097 \cdot C_4(M_H)\,,
\end{aligned} \tag{A.8}$$

Hence, our final result is $\eta_2(\mu) = 1.906$ and $\eta_4(\mu) = 2.903$.

For the Z' we do a similar analysis and get

$$C_1(\mu) = 0.690 \cdot C_1(M_H)\,,\ C_4(\mu) = 6.939 \cdot C_4(M_H)\,,\ C_5(\mu) = 0.263 \cdot C_4(M_H)\,, \tag{A.9}$$

and as a consequence $\eta_1(\mu) = 0.690$ and $\eta_4(\mu) = 6.939$.

We note that in all considered cases, operators that are induced only by operator mixing play a secondary role are neglected in our analysis.

Appendix B

Model details for extended left-right symmetric model

B.1 Matrix eigenvalues and eigenvectors

By suitable basis rotations, it is possible to transform the Yukawa couplings to a basis where

$$y_a = \begin{pmatrix} 0 & 0 \\ 0 & a \\ b & c \end{pmatrix} \tag{B.1}$$

and

$$y_1 = \begin{pmatrix} n_1 \\ n_2 \end{pmatrix} \tag{B.2}$$

In this basis, the eigenvectors and eigenvalues of the tree level matrix M^{light} defined in Eq. (5.44) are particularly simple. While the eigenvectors are given by

$$\begin{aligned} v_1 &= \left(0\ , -\frac{-n_2 b^* + n_1 c^*}{n_1 a^*},\ 1\right)^T \ , \\ v_2 &= (1,\ 0,\ 0)^T \ , \\ v_2 &= \left(0,\ \frac{a n_1^*}{c n_1^* - b n_2^*},\ 1\right)^T \ , \end{aligned} \tag{B.3}$$

the corresponding eigenvalues are

$$\begin{aligned} e_1 &= 0\ , \\ e_2 &= 0\ , \\ e_3 &= \frac{v_L v_R(-a n_1 a^* n_1^* + c n_2 b^* n_1^* - c n_1 c^* n_1^* - b n_2 b^* n_2^* + b n_1 c^* n_2^*)}{2(M_{T_2} n_1 n_1^* + M_{T_1} n_2 n_2^*)}\ . \end{aligned} \tag{B.4}$$

We confirmed that the eigenvalue equations

$$M^{\text{light}} v_i = e_i \; v_i \; , \qquad i = 1, 2, 3 \; , \tag{B.5}$$

are fulfilled for all three eigenvalues. Since the number of non-zero eigenvalues determines the rank of a matrix, M^{light} has rank one. Thus, two fermions stay massless at tree level. By the same procedure, it is easy to show that the inclusion of one-loop corrections enhances the matrix rank of M^{light} to two, leaving one fermion massless.

B.2 Fermion interaction

For the calculation of loop diagrams it is important to define the couplings between fermions and gauge bosons or scalars appropriately. We exemplify our notation for the quark sector only, since results for leptons can be easily deduced.

When all quarks obtain masses at the two-loop level, a bi-unitary transformation

$$\begin{aligned} V_L^u \mathcal{M}_u^{(2)} (V_R^u)^\dagger &= \mathcal{M}_u^{\text{diag}} \equiv \text{diag}(m_u, m_c, m_t, m_{U_1}, m_{U_2}, m_{U_3}) \, , \\ V_L^d \mathcal{M}_d^{(2)} (V_R^d)^\dagger &= \mathcal{M}_d^{\text{diag}} \equiv \text{diag}(m_d, m_s, m_b, m_{D_1}, m_{D_2}, m_{D_3}) \, . \end{aligned} \tag{B.6}$$

diagonalizes the mass matrix and provides the mass eigenstates which are defined as

$$\begin{aligned} \hat{\mathbf{u}}_{L/R} &= V_{L/R}^u \mathbf{u}_{L/R} \, , \\ \hat{\mathbf{d}}_{L/R} &= V_{L/R}^d \mathbf{d}_{L/R} \, , \end{aligned} \tag{B.7}$$

and $\mathbf{u}$, $\mathbf{d}$ label the 6×1 vectors of flavor eigenstates. Transforming the charged current to the fermion mass basis yields

$$\mathcal{L} \supset \frac{g}{\sqrt{2}} W_{L\mu}^+ \left[\bar{\hat{\mathbf{u}}} \gamma^\mu \hat{g}_L^q(W_L) P_L \hat{\mathbf{d}} \right] + h.c. \, , \tag{B.8}$$

where the coupling matrix is defined as the matrix product

$$\hat{g}_L^q(W_L) = V_L^u \, g_L^q(W_L) \, (V_L^d)^\dagger \, , \tag{B.9}$$

and the original coupling in the flavor basis reads

$$g_L^q(W_L) = \text{diag}(1, 1, 1, 0, 0, 0) \, . \tag{B.10}$$

Note that $g_L^q(W_L)$ is not proportional to the identity matrix, owing to the fact, that T, T' and B, B' transform as singlets with respect to $SU(2)_L$ and $SU(2)_R$. A misalignment between the mass bases of the up- and down-sector leads to a non-vanishing mixing between quarks which is characterized by the CKM matrix

$$U_L \equiv \hat{g}_L^q(W_L) \, . \tag{B.11}$$

The left-right symmetric structure of our model ensures, that mixing in the right-handed sector becomes in principle observable and we therefore define the analog right-handed mixing matrix by

$$U_R \equiv \hat{g}^q_R(W_R) = V^u_R g^q_R(W_R)(V^d_R)^\dagger \,, \tag{B.12}$$

where similarly $g^q_R(W_R) = \mathrm{diag}(1,1,1,0,0,0)$.

Following the diagonalization process of the neutral gauge boson matrix in Section 5.2.3, we quote here our results for the couplings of the gauge bosons Z_L and Z_R to up-type quarks. Note that these states correspond to a basis, where the massless photon is already identified. The neutral current Lagrangian in the interaction basis is provided by

$$\begin{aligned}\mathcal{L} \supset\ & Z_{L\mu}\overline{\mathbf{u}}\gamma^\mu \left[g^u_L(Z_L)P_L + g^u_R(Z_L)P_R\right]\mathbf{u} \\ &+ Z_{R\mu}\overline{\mathbf{u}}\gamma^\mu \left[g^u_L(Z_R)P_L + g^u_R(Z_R)P_R\right]\mathbf{u}\,,\end{aligned} \tag{B.13}$$

The operators appearing in the above expression act diagonally in generation space and depend on T^3_L and T^3_R, which are the three-components of isospin under $SU(2)_L$ and $SU(2)_R$, and on the electric charge Q of the fermion. They are defined as follows:

$$\begin{aligned}g^u_L(Z_L) &= \frac{g}{c_w}\left[T^3_L - Qs^2_w\right]\,, \qquad g^u_R(Z_L) = \frac{g}{c_w}\left[-Qs^2_w\right]\,, \\ g^u_L(Z_R) &= \frac{gc_w}{\sqrt{c^2_w - s^2_w}}\left[t^2_w\left(T^3_L - Q\right)\right]\,, \qquad g^u_R(Z_R) = \frac{gc_w}{\sqrt{c^2_w - s^2_w}}\left[T^3_R - t^2_w Q\right]\,,\end{aligned} \tag{B.14}$$

and s_w is the weak mixing which stems from the mixing with the photon. A transformation to the mass eigenbasis $(Z,\ Z')$ then gives (compare definition in Eq. (5.28))

$$\begin{aligned}\mathcal{L} \supset\ & gZ_\mu\overline{\mathbf{u}}\gamma^\mu\left[c_\zeta\{g^u_L(Z_L)P_L + g^u_R(Z_L)P_R\} + s_\zeta\{g^u_L(Z_R)P_L + g^u_R(Z_R)P_R\}\right]\mathbf{u} \\ &+ gZ'_\mu\overline{\mathbf{u}}\gamma^\mu\left[-s_\zeta\{g^u_L(Z_L)P_L + g^u_R(Z_L)P_R\} + c_\zeta\{g^u_L(Z_R)P_L + g^u_R(Z_R)P_R\}\right]\mathbf{u}\ .\end{aligned} \tag{B.15}$$

If we also transform the fermions to the mass eigenbasis, the neutral current interaction will be given by

$$\begin{aligned}\mathcal{L} \supset\ & gZ_\mu\overline{\hat{\mathbf{u}}}\gamma^\mu\left[\hat{C}_L(Z)P_L + \hat{C}_R(Z)P_R\right]\hat{\mathbf{u}} \\ &+ gZ'_\mu\overline{\hat{\mathbf{u}}}\gamma^\mu\left[\hat{C}_L(Z')P_L + \hat{C}_R(Z')P_R\right]\hat{\mathbf{u}}\end{aligned} \tag{B.16}$$

where we used the abbreviations

$$\begin{aligned}\hat{C}_L(Z) &\equiv V_L C_L(Z) V_L^\dagger\,, \\ \hat{C}_R(Z) &\equiv V_R C_R(Z) V_R^\dagger\,, \\ \hat{C}_L(Z') &\equiv V_L C_L(Z') V_L^\dagger\,, \\ \hat{C}_R(Z') &\equiv V_R C_R(Z') V_R^\dagger\,,\end{aligned} \tag{B.17}$$

and we defined

$$\begin{aligned} C_L(Z) &\equiv c_\zeta g_L^u(Z_L) + s_\zeta g_L^u(Z_R) \ , \\ C_R(Z) &\equiv c_\zeta g_R^u(Z_L) + s_\zeta g_R^u(Z_R) \ , \\ C_L(Z') &\equiv -s_\zeta g_L^u(Z_L) + c_\zeta g_L^u(Z_R) \ , \\ C_R(Z') &\equiv -s_\zeta g_R^u(Z_L) + c_\zeta g_R^u(Z_R) \ . \end{aligned} \tag{B.18}$$

Clearly, the matrices defined above are not proportional to $\mathbb{1}_{6\times6}$, as SM fermions and their vector-like partners have different gauge assignments.

Next we define the couplings between fermions and scalars. Using the expansion from Eq. (5.13), the interaction Lagrangian involving σ_L and σ_R reads

$$\mathcal{L} \supset -\frac{1}{\sqrt{2}}\sigma_L \overline{\mathbf{u}}(\mathbf{Y_a} P_R + \mathbf{Y_a}^\dagger P_L)\mathbf{u} - \frac{1}{\sqrt{2}}\sigma_R \overline{\mathbf{u}}(\mathbf{Y_a}^\dagger P_R + \mathbf{Y_a} P_L)\mathbf{u} \ , \tag{B.19}$$

and the coupling matrix is defined by

$$\mathbf{Y_a} \equiv \begin{pmatrix} \mathbf{0_{3\times3}} & y_a & \mathbf{0_{3\times1}} \\ \mathbf{0_{2\times3}} & \mathbf{0_{2\times2}} & \mathbf{0_{2\times1}} \\ \mathbf{0_{1\times3}} & \mathbf{0_{1\times2}} & \mathbf{0_{1\times1}} \end{pmatrix} \ . \tag{B.20}$$

Sometimes it is more convenient to work in the scalar mass eigenbasis $(h,\ H)$. Then, using the transformation properties from Eq. (5.17), we obtain

$$\begin{aligned} \mathcal{L} \supset &-\frac{1}{\sqrt{2}} h \overline{\mathbf{u}}(\left(c_\xi \mathbf{Y_a} + s_\xi \mathbf{Y_a}^\dagger\right) P_R + \left(c_\xi \mathbf{Y_a}^\dagger + s_\xi \mathbf{Y_a}\right) P_L)\mathbf{u} \\ &-\frac{1}{\sqrt{2}} H \overline{\mathbf{u}}(\left(c_\xi \mathbf{Y_a}^\dagger - s_\xi \mathbf{Y_a}\right) P_R + \left(c_\xi \mathbf{Y_a} - s_\xi \mathbf{Y_a}^\dagger\right) P_L)\mathbf{u} \ . \end{aligned} \tag{B.21}$$

A further rotation to the fermion mass eigenstates results in

$$\begin{aligned} \mathcal{L} \supset &-\frac{1}{\sqrt{2}} h \overline{\hat{\mathbf{u}}}(V_L \left(c_\xi \mathbf{Y_a} + s_\xi \mathbf{Y_a}^\dagger\right) V_R^\dagger P_R + V_R \left(c_\xi \mathbf{Y_a}^\dagger + s_\xi \mathbf{Y_a}\right) V_L^\dagger P_L)\hat{\mathbf{u}} \\ &-\frac{1}{\sqrt{2}} H \overline{\hat{\mathbf{u}}}(V_L \left(c_\xi \mathbf{Y_a}^\dagger - s_\xi \mathbf{Y_a}\right) V_R^\dagger P_R + V_R \left(c_\xi \mathbf{Y_a} - s_\xi \mathbf{Y_a}^\dagger\right) V_L^\dagger P_L)\hat{\mathbf{u}} \ , \end{aligned} \tag{B.22}$$

which we write in short hand notation as

$$\begin{aligned} \mathcal{L} \supset &-\frac{1}{\sqrt{2}} h \overline{\hat{\mathbf{u}}}(\hat{\mathbf{C}}(\mathbf{h}) P_R + \hat{\mathbf{C}}^\dagger(\mathbf{h}) P_L)\hat{\mathbf{u}} \\ &-\frac{1}{\sqrt{2}} H \overline{\hat{\mathbf{u}}}(\hat{\mathbf{C}}(\mathbf{H}) P_R + \hat{\mathbf{C}}^\dagger(\mathbf{H}) P_L)\hat{\mathbf{u}} \ , \end{aligned} \tag{B.23}$$

with the couplings defined by

$$\begin{aligned} \mathbf{C}(\mathbf{h}) &= \left[c_\xi \mathbf{Y_a} + s_\xi \mathbf{Y_a}^\dagger\right] \ , \\ \mathbf{C}(\mathbf{H}) &= \left[-s_\xi \mathbf{Y_a} + c_\xi \mathbf{Y_a}^\dagger\right] \ , \end{aligned} \tag{B.24}$$

and

$$\begin{aligned}\hat{\mathbf{C}}(\mathbf{h}) &= V_L \mathbf{C}(\mathbf{h}) V_R^{\dagger} \,, \\ \hat{\mathbf{C}}(\mathbf{H}) &= V_L \mathbf{C}(\mathbf{H}) V_R^{\dagger} \,.\end{aligned} \tag{B.25}$$

Appendix C

Loop calculations

This section is intended to give some more details on the loop calculations that are performed in the context of Chapter 4 and 5. We start by giving some general formulas that are frequently used throughout the calculations, before we go to the details of each diagram.

The Feynman integrals that appear in our calculation are evaluated with the Mathematica `Package-X` [291]. For an easier understanding, we quote here the results for the involved integrals

$$\begin{aligned}
\int \frac{d^4k}{(2\pi)^4}\frac{1}{k^2-m^2}\frac{1}{k^2-M^2} &= \frac{i}{16\pi^2}\left(1+\tilde{\epsilon}-\frac{m^2\log\left(\frac{m^2}{M^2}\right)}{m^2-M^2}+\log\left(\mu^2/M^2\right)\right) \ , \\
\int \frac{d^4k}{(2\pi)^4}\frac{1}{k^2}\frac{1}{k^2-m^2}\frac{1}{k^2-M^2} &= \frac{-i}{16\pi^2}\frac{\log\left(\frac{m^2}{M^2}\right)}{m^2-M^2} \ , \\
\int \frac{d^4k}{(2\pi)^4}\frac{1}{k^2-m^2}\frac{1}{k^2-M_1^2}\frac{1}{k^2-M_2^2} &= \frac{i}{16\pi^2}\frac{1}{M_1^2-M_2^2}\left(-\frac{M_1^2\log\left(\frac{m^2}{M_1^2}\right)}{m^2-M_1^2}+\frac{M_2^2\log\left(\frac{m^2}{M_2^2}\right)}{m^2-M_2^2}\right) \ ,
\end{aligned} \tag{C.1}$$

and the divergence in the first integral is parameterized in terms of the quantity $\tilde{\epsilon} \equiv 1/\epsilon - \gamma_E + \log(4\pi)$. Further useful identities that we applied are given by

$$\begin{aligned}
\gamma^\mu g_{\mu\nu}\gamma^\nu &= 4\cdot\mathbb{1} \ , \\
\not{k}\not{k} &= k^2 \ , \\
\gamma^\mu (k-p)_\mu (k-p)_\nu \gamma^\nu &= (k-p)^2 \ .
\end{aligned} \tag{C.2}$$

C.1 One-loop diagrams

In Figure C.1 we give an overview over relevant one-loop Feynman diagrams that occur in the model described in Chapter 5. While these diagrams specifically illustrate contributions in the up-type quark sector, it is easy to transfer the results to the down-type quarks and leptons by appropriate replacement of the couplings and masses. As a start, we evaluate the contribution from neutral gauge boson exchange that is given in Figure C.1a. It is convenient to evaluate the diagram in the mass basis ($Z,\ Z'$), since no mixed diagrams need to be considered in this case. The exchange of the SM Z boson leads to a contribution

$$\begin{aligned}\delta\mathcal{M}^{(1),\mathrm{Z}} = i\int\frac{d^4k}{(2\pi)^4}C_L(Z)\gamma^\mu\frac{1}{\not k}\frac{y_a v_L}{\sqrt{2}}\frac{(\not k+M_T)}{k^2-M_T^2}\frac{y_a^\dagger v_R}{\sqrt{2}}\frac{1}{\not k}\\ \times\frac{1}{(k-p)^2-M_Z^2}\left[g_{\mu\nu}-(1-\xi_Z)\frac{(k-p)_\mu(k-p)_\nu}{(k-p)^2-\xi_Z M_Z^2}\right]\gamma^\nu C_R(Z)\ .\end{aligned}\tag{C.3}$$

As terms linear in $\not k$ vanish when we integrate over full momentum space, only terms proportional to M_T survive in the above expression. If we apply on top of that the relations given in Eq. (C.2), we will find

$$\delta\mathcal{M}^{(1),\mathrm{Z}} = i\frac{3C_L(Z)C_R(Z)v_Lv_R}{2}\int\frac{d^4k}{(2\pi)^4}\frac{1}{k^2}y_a\frac{M_T}{k^2-M_T^2}y_a^\dagger\frac{1}{k^2-M_Z^2}\ ,\tag{C.4}$$

for the self-energy in Landau gauge at vanishing external momentum $p=0$. With the help of Eq. (C.1), the final result

$$\delta\mathcal{M}^{(1),\mathrm{Z}} = \frac{3C_L(Z)C_R(Z)v_Lv_R}{32\pi^2}y_a\frac{M_T}{M_T^2-M_Z^2}\log\left(\frac{M_T^2}{M_Z^2}\right)y_a^\dagger\ ,\tag{C.5}$$

is obtained. In a similar way, the result for Z' exchange yields[1]

$$\delta\mathcal{M}^{(1),\mathrm{Z}'} = \frac{3C_L(Z')C_R(Z')v_Lv_R}{32\pi^2}y_a\frac{M_T}{M_T^2-M_{Z'}^2}\log\left(\frac{M_T^2}{M_{Z'}^2}\right)y_a^\dagger\ .\tag{C.6}$$

Generally, when evaluating the diagrams in Landau gauge, also the Goldstone boson contributions need to be considered in the calculation. In our model, the Goldstones ρ_L and ρ_R become the longitudinal components of the Z and Z' boson, respectively. Nevertheless, their contributions cancel exactly in Landau gauge. This can be understood in the following way. The Goldstones couple according to the Lagrangian

$$\mathcal{L}\supset-\frac{i}{\sqrt{2}}\rho_L\overline{\mathbf{u}}\left(\mathbf{Y_a}P_R+\mathbf{Y_a^\dagger}P_L\right)\mathbf{u}-\frac{i}{\sqrt{2}}\rho_R\overline{\mathbf{u}}\left(\mathbf{Y_a^\dagger}P_R+\mathbf{Y_a}P_L\right)\mathbf{u}\tag{C.7}$$

to quarks, which can be deduced from Eq. (B.19). On top of that, bilinear couplings to gauge bosons of the type $Z_\mu^{(\prime)}\partial^\mu\rho_{L(R)}$ are generated from the kinetic terms given in Eq. (5.22). To get rid of these mixed terms, a gauge fixing term is introduced to the Lagrangian that is of the form

$$\mathcal{L}_{\mathrm{GF}}\supset-\frac{1}{2\xi_Z}\left(\partial^\mu Z_\mu-i\xi_Z M_Z\hat\rho_L\right)^2-\frac{1}{2\xi_{Z'}}\left(\partial^\mu Z'_\mu-i\xi_{Z'}M_{Z'}\hat\rho_R\right)^2\ .\tag{C.8}$$

[1] Note that the one-loop contribution to the mass matrix in Chapter 4 can be easily deduced from this result and we therefore do not repeat the calculation here.

It is now easy to check that Eq. (C.8) will exactly eliminate all bilinear terms $Z_\mu^{(\prime)}\partial^\mu \rho_{L(R)}$ in Eq. (5.22) when we identify

$$\begin{pmatrix} \rho_L \\ \rho_R \end{pmatrix} = \begin{pmatrix} c_G & s_G \\ -s_G & c_G \end{pmatrix} \begin{pmatrix} \hat{\rho}_L \\ \hat{\rho}_R \end{pmatrix} , \tag{C.9}$$

where $c_G \equiv \cos(\theta_G)$, $s_G \equiv \sin(\theta_G)$ and θ_G is an appropriately chosen mixing angle. In the gauge fixing process, Golstone bosons obtain a mass that is given by

$$\mathcal{L}_{\text{mass,gold}} = -\frac{1}{2}\left(\hat{\rho}_L\ \hat{\rho}_R\right) \begin{pmatrix} \xi_Z M_Z^2 & 0 \\ 0 & \xi_{Z'} M_{Z'}^2 \end{pmatrix} \begin{pmatrix} \hat{\rho}_L \\ \hat{\rho}_R \end{pmatrix} . \tag{C.10}$$

Transferring the quark couplings to the basis $(\hat{\rho}_L,\ \hat{\rho}_R)$ then yields

$$\mathcal{L} \supset -\frac{i}{\sqrt{2}}\hat{\rho}_L \bar{\mathbf{u}}\left(\mathbf{C}(\hat{\rho}_L)P_R + \mathbf{C}(\hat{\rho}_L)^\dagger P_L\right)\mathbf{u} - \frac{i}{\sqrt{2}}\hat{\rho}_R \bar{\mathbf{u}}\left(\mathbf{C}(\hat{\rho}_R)P_R + \mathbf{C}(\hat{\rho}_R)^\dagger P_L\right)\mathbf{u} \tag{C.11}$$

where we defined

$$\begin{aligned} \mathbf{C}(\hat{\rho}_\mathbf{L}) &= \left[c_G \mathbf{Y_a} - s_G \mathbf{Y_a^\dagger}\right] , \\ \mathbf{C}(\hat{\rho}_\mathbf{R}) &= \left[s_G \mathbf{Y_a} + c_G \mathbf{Y_a^\dagger}\right] . \end{aligned} \tag{C.12}$$

Including the matrix structure of $\mathbf{Y_a}$, we find the one-loop corrections generated by the Goldstone bosons to be

$$\delta\mathcal{M}^{(1),\hat{\rho}_\mathrm{L}} = \frac{-i}{2}\int \frac{d^4k}{(2\pi)^4}\frac{1}{(k-p)^2} s_G c_G y_a \frac{\not{k}+M_T}{k^2-M_T^2} y_a^\dagger , \tag{C.13}$$

$$\delta\mathcal{M}^{(1),\hat{\rho}_\mathrm{R}} = \frac{i}{2}\int \frac{d^4k}{(2\pi)^4}\frac{1}{(k-p)^2} s_G c_G y_a \frac{\not{k}+M_T}{k^2-M_T^2} y_a^\dagger , \tag{C.14}$$

which evidently cancels.

We continue with the evaluation of the scalar contribution displayed in Figure C.1b and obtain the finite result

$$\begin{aligned} \delta\mathcal{M}^{(1),\chi} &= i\frac{\lambda_2 v_L v_R}{2} y_a \int \frac{d^4k}{(2\pi)^4} \frac{\not{k}+M_T}{\left(k^2-M_T^2\right)\left((p-k)^2-m_{\chi_L}^2\right)\left((p-k)^2-m_{\chi_R}^2\right)} y_a^\dagger \\ &= \frac{\lambda_2 v_L v_R}{32\pi^2} y_a \frac{M_T}{m_{\chi_L}^2 - m_{\chi_R}^2}\left[\frac{m_{\chi_L}^2 \log\left(\frac{M_T^2}{m_{\chi_L}^2}\right)}{M_T^2 - m_{\chi_L}^2} - \frac{m_{\chi_R}^2 \log\left(\frac{M_T^2}{m_{\chi_R}^2}\right)}{M_T^2 - m_{\chi_R}^2}\right] y_a^\dagger , \end{aligned} \tag{C.15}$$

by means of Eq. (C.1) for $p = 0$. With these results the complete contribution $\delta M_u^{(1)}$, as defined in Eq. (5.45), is given by the sum

$$\delta M_u^{(1)} \equiv \delta\mathcal{M}^{(1),Z} + \delta\mathcal{M}^{(1),Z'} + \delta\mathcal{M}^{(1),\chi} \, . \tag{C.16}$$

As a next step, the diagrams from Figure C.1i and C.1f, which contribute to the lower right zero block of the mass matrix, are evaluated. The gauge boson contribution is

$$\begin{aligned}\delta\mathcal{M}^{(1),\mathrm{X}} =& i\frac{g_X^2\alpha^2}{4}v_\eta^2\frac{y_1^\dagger}{\sqrt{2}}\int\frac{d^4k}{(2\pi)^4}\frac{1}{k^2}\frac{M_T}{k^2-M_T^2}\frac{4}{k^2-M_X^2}\frac{y_1}{\sqrt{2}} \\ &+ i\frac{g_X^2\alpha^2}{4}\frac{v_\eta^2}{M_X^2}\frac{y_1^\dagger}{\sqrt{2}}\int\frac{d^4k}{(2\pi)^4}\frac{1}{k^2}\frac{k^2M_T}{k^2-M_T^2}\left(-\frac{1}{k^2-M_X^2}+\frac{1}{k^2-\xi_XM_X^2}\right)\frac{y_1}{\sqrt{2}} \, ,\end{aligned} \tag{C.17}$$

and we already applied the simplifications given in Eq. (C.2). Substituting the mass M_X yields

$$\begin{aligned}\delta\mathcal{M}^{(1),X} =& i\frac{g_X^2\alpha^2}{4}v_\eta^2\frac{y_1^\dagger}{\sqrt{2}}\int\frac{d^4k}{(2\pi)^4}\frac{1}{k^2}\frac{M_T}{k^2-M_T^2}\frac{d}{k^2-M_X^2}\frac{y_1}{\sqrt{2}} \\ &+ \frac{i}{2}y_1^\dagger\int\frac{d^4k}{(2\pi)^4}\frac{M_T}{k^2-M_T^2}\left(-\frac{1}{k^2-M_X^2}+\frac{1}{k^2-\xi_XM_X^2}\right)y_1 \, .\end{aligned} \tag{C.18}$$

To obtain a finite and gauge independent result, the contribution from the scalar and Goldstone boson needs to be included. The diagram involving η contributes as

$$\delta\mathcal{M}^{(1),\eta} = \frac{i}{2}y_1^\dagger\int\frac{d^4k}{(2\pi)^4}\frac{M_T}{k^2-M_T^2}\frac{1}{k^2-M_\eta^2}y_1 \, . \tag{C.19}$$

From this result, the Goldstone boson contribution is obtained by simply replacing $M_\eta^2 \to \xi_X M_X^2$ and adding an extra factor i for each vertex:

$$\delta\mathcal{M}^{(1),\rho_\eta} = -\frac{i}{2}y_1^\dagger\int\frac{d^4k}{(2\pi)^4}\frac{M_T}{k^2-M_T^2}\frac{1}{k^2-\xi_XM_X^2}y_1 \, . \tag{C.20}$$

As the Goldstone contribution cancels the gauge dependent term in Eq. (C.18), the total correction to the mass matrix is expressed by

$$\begin{aligned}\delta\tilde{M}_u^{(1)} \equiv& \, \delta\mathcal{M}^{(1),X} + \delta\mathcal{M}^{(1),\eta} \\ =& \, i\frac{g_X^2\alpha^2}{4}v_\eta^2\frac{y_1^\dagger}{\sqrt{2}}\int\frac{d^4k}{(2\pi)^4}\frac{1}{k^2}\frac{M_T}{k^2-M_T^2}\frac{d}{k^2-M_X^2}\frac{y_1}{\sqrt{2}} \\ &- \frac{i}{2}y_1^\dagger\int\frac{d^4k}{(2\pi)^4}\frac{M_T}{k^2-M_T^2}\frac{1}{k^2-M_X^2}y_1 \\ &+ \frac{i}{2}y_1^\dagger\int\frac{d^4k}{(2\pi)^4}\frac{M_T}{k^2-M_T^2}\frac{1}{k^2-M_\eta^2}y_1 \, .\end{aligned} \tag{C.21}$$

We now carry out the momentum integrals and find

$$
\begin{aligned}
\delta\tilde{M}_u^{(1)} =& -i\frac{g_X^2\alpha^2}{4}v_\eta^2\frac{y_1^\dagger}{2}4M_T\frac{\log\left(\frac{M_X^2}{M_T^2}\right)}{M_X^2-M_T^2}y_1 \\
&+\frac{1}{2}y_1^\dagger\frac{1}{16\pi^2}M_T\left(1+\tilde{\epsilon}-\frac{M_X^2\log\left(\frac{M_X^2}{M_T^2}\right)}{M_X^2-M_T^2}+\log\left(\mu^2/M_T^2\right)\right)y_1 \\
&-\frac{1}{2}y_1^\dagger\frac{1}{16\pi^2}M_T\left(1+\tilde{\epsilon}-\frac{M_\eta^2\log\left(\frac{M_\eta^2}{M_T^2}\right)}{M_\eta^2-M_T^2}+\log\left(\mu^2/M_T^2\right)\right)y_1 \ .
\end{aligned}
\tag{C.22}
$$

Clearly, the integrals in the second and third row are divergent by themselves. However, together they yield a finite contribution which is

$$
\begin{aligned}
\delta\tilde{M}_u^{(1)} =& \frac{g_X^2v_\eta^2\alpha^2}{4\times 32\pi^2}y_1^\dagger 4M_T\frac{\log\left(\frac{M_X^2}{M_T^2}\right)}{M_X^2-M_T^2}y_1 \\
&-\frac{g_X^2v_\eta^2\alpha^2}{4\times 32\pi^2}y_1^\dagger M_T\frac{\log\left(\frac{M_X^2}{M_T^2}\right)}{M_X^2-M_T^2}y_1 \\
&+\frac{1}{2}y_1^\dagger\frac{1}{16\pi^2}M_T\frac{M_\eta^2\log\left(\frac{M_\eta^2}{M_T^2}\right)}{M_\eta^2-M_T^2}y_1 \ .
\end{aligned}
\tag{C.23}
$$

Further simplification provides the final result

$$
\begin{aligned}
\delta\tilde{M}_u^{(1)} =& \frac{3}{32\pi^2}\frac{g_X^2v_\eta^2\alpha^2}{4}y_1^\dagger M_T\frac{\log\left(\frac{M_T^2}{M_X^2}\right)}{M_T^2-M_X^2}y_1 \\
&+y_1^\dagger\frac{1}{32\pi^2}M_T\frac{M_\eta^2\log\left(\frac{M_T^2}{M_\eta^2}\right)}{M_T^2-M_\eta^2}y_1 \ .
\end{aligned}
\tag{C.24}
$$

The diagrams Figure C.1c and Figure C.1j contribute to the entry $\delta^\dagger v_R$ as described in Section 5.3. Likewise, the Feynman graphs Figure C.1d and Figure C.1k populate the entry δv_L. The contributions from these diagrams are similar to the results derived so far and can be obtained by an appropriate replacement of couplings. We like to emphasize, that gauge boson contributions proportional to the unit matrix in flavor space (such as electromagnetic charge Q) do not add to masses of first and second generation fermions. Hence, we do not include those terms to our numeric calculation.

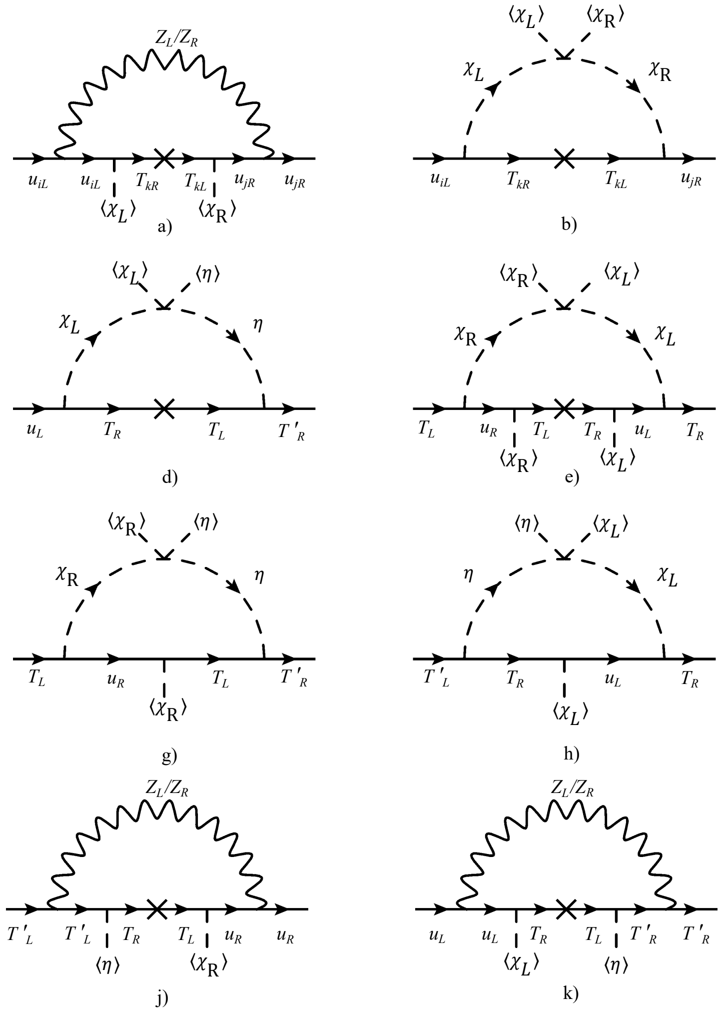

Figure C.1 Feynman diagrams contributing at one-loop level to the up-type quark mass matrix. In the limit $\lambda_4 \ll 1$, η decouples from the scalar sector and diagrams c), d) g) and h) can be neglected. Furthermore, the correction of diagram e) to the vector-like mass M_T is small and will therefore not be included in our calculation. We note that even after including all presented one-loop diagrams, one state is still massless. For the detailed calculation of the remaining diagrams see text.

C.2 Two-loop diagrams

Since there is no bi-doublet scalar in our model, the charged gauge bosons W_L and W_R only mix at the one-loop level via the Feynman diagram presented in Figure 5.3b. Their mixing can be parameterized in terms of the off-shell amplitude

$$\begin{aligned}\Pi_{\sigma\rho}(p^2) = &- iN_c\, g_{\sigma\rho} \frac{g_L g_R}{2} \frac{v_L^2 v_R^2}{4} \sum_{\alpha,\beta=1}^{3} \sum_{k,l=1}^{2} \frac{[y_a^q]_{\alpha k}}{\sqrt{2}} \frac{[y_a^{q\dagger}]_{k\beta}}{\sqrt{2}} \frac{[y_c^q]_{\alpha l}}{\sqrt{2}} \frac{[y_c^{q\dagger}]_{l\beta}}{\sqrt{2}} M_{T_k} M_{B_l} \\ &\times \int \frac{d^4k}{(2\pi)^4} \frac{1}{(p+k)^2} \frac{1}{(p+k)^2 - M_{T_k}^2} \frac{1}{k^2} \frac{1}{k^2 - M_{B_l}^2} \;.\end{aligned} \tag{C.25}$$

Note that we return to a notation where quark Yukawa couplings are labeled by an superscript q to prevent ambiguities. With the mixing being quantified through $\Pi_{\sigma\rho}(p^2)$, the full expression for the two-loop amplitude in Figure 5.3a is

$$\begin{aligned}\delta M_u^{(2)}\Big|_{ij} = \frac{g_L g_R}{2}\frac{v_L v_R}{2}\int\frac{d^4p}{(2\pi)^4}\gamma_\mu\frac{\left(g^{\mu\sigma}-p^\mu p^\sigma/M_{W_L}^2\right)}{p^2-M_{W_L}^2}\Pi_{\sigma\rho}(p^2)\\ \times\frac{\left(g^{\rho\nu}-p^\rho p^\nu/M_{W_R}^2\right)}{p^2-M_{W_R}^2}\gamma_\nu\frac{1}{p^2}\frac{[y_c^q]_{ik}}{\sqrt{2}}\frac{M_{B_k}}{p^2-M_{B_k}^2}\frac{[y_c^{q\dagger}]_{kj}}{\sqrt{2}}\ .\end{aligned} \tag{C.26}$$

For the further calculation, we introduce the notation

$$\delta M_u^{(2)}\Big|_{ij} = N_c\textstyle\sum_{\alpha,\beta=1}^{3}\sum_{k,l,m=1}^{2}\frac{g_L^2g_R^2}{4}\frac{v_L^3v_R^3}{8}\frac{M_{T_k}M_{B_l}}{M_{W_L}^2M_{W_R}^2}\frac{[y_a^q]_{\alpha k}}{\sqrt{2}}\frac{[y_a^{q\dagger}]_{k\beta}}{\sqrt{2}}\frac{[y_c^q]_{\alpha l}}{\sqrt{2}}\frac{[y_c^{q\dagger}]_{l\beta}}{\sqrt{2}}\frac{[y_c^q]_{im}}{\sqrt{2}}\frac{[y_c^{q\dagger}]_{mj}}{\sqrt{2}}M_{B_m}I_{klm}\ , \tag{C.27}$$

where all integrals are combined in the expression

$$I_{klm}\equiv\int\frac{d^4k}{(2\pi)^4}\int\frac{d^4p}{(2\pi)^4}\frac{3M_{W_L}^2M_{W_R}^2+(p^2-M_{W_L}^2)(p^2-M_{W_R}^2)}{\left((p+k)^2-M_{T_k}^2\right)\left(k^2-M_{B_l}^2\right)\left(p^2-M_{B_m}^2\right)p^2(p+k)^2k^2(p^2-M_{W_L}^2)(p^2-M_{W_R}^2)}\ . \tag{C.28}$$

The numerator of I_{klm} is composed of two terms. The authors of [223] analyzed those contributions with respect to their relative importance and found that the first part proportional to $3M_{W_L}^2M_{W_R}^2$ is suppressed with respect to the second term for the whole considered parameter space. We will therefore only proceed with the evaluation of the second term which can be rewritten as

$$I_{klm}\simeq\int\frac{d^4k}{(2\pi)^4}\int\frac{d^4p}{(2\pi)^4}\frac{1}{\left((p+k)^2-M_{T_k}^2\right)\left(k^2-M_{B_l}^2\right)\left(p^2-M_{B_m}^2\right)p^2(p+k)^2k^2}\ . \tag{C.29}$$

We follow the calculation method presented in [223, 292] and do a partial fraction decomposition to recast the expression to

$$\begin{aligned}I_{klm} = \frac{1}{M_{B_l}^2M_{T_k}^2M_{B_m}^2}\int\frac{d^4k}{(2\pi)^4}\left[\frac{1}{\left(k^2-M_{B_l}^2\right)}-\frac{1}{k^2}\right]\\ \int\frac{d^4p}{(2\pi)^4}\left[\frac{1}{\left((p+k)^2-M_{T_k}^2\right)}-\frac{1}{(p+k)^2}\right]\left[\frac{1}{\left(p^2-M_{B_m}^2\right)}-\frac{1}{p^2}\right]\ .\end{aligned} \tag{C.30}$$

Further carrying out the multiplication yields the lengthy expression

$$
\begin{aligned}
I_{klm} = &\frac{1}{M_{B_l}^2 M_{T_k}^2 M_{B_m}^2} \int \frac{d^4k}{(2\pi)^4} \int \frac{d^4p}{(2\pi)^4} \left[\frac{1}{\left(k^2 - M_{B_l}^2\right)\left((p+k)^2 - M_{T_k}^2\right)\left(p^2 - M_{B_m}^2\right)} \right. \\
&- \frac{1}{\left(k^2 - M_{B_l}^2\right)\left((p+k)^2 - M_{T_k}^2\right) p^2} - \frac{1}{\left(k^2 - M_{B_l}^2\right)(p+k)^2 \left(p^2 - M_{B_m}^2\right)} \\
&+ \frac{1}{\left(k^2 - M_{B_l}^2\right)(p+k)^2 p^2} \\
&- \frac{1}{k^2\left((p+k)^2 - M_{T_k}^2\right)\left(p^2 - M_{B_m}^2\right)} + \frac{1}{k^2\left((p+k)^2 - M_{T_k}^2\right) p^2} \\
&\left. + \frac{1}{k^2 (p+k)^2 \left(p^2 - M_{B_m}^2\right)} - \frac{1}{k^2 (p+k)^2 p^2} \right] .
\end{aligned}
\tag{C.31}
$$

To improve the readability, it is convenient to introduce the abbreviation

$$
\begin{aligned}
&\left(M_{1_1} M_{1_2} .... M_{1_{n_1}} | M_{2_1} .... M_{2_{n_2}} | M_{3_1} .... M_{3_{n_3}}\right) \\
&= \int d^n k \int d^n p \prod_{i=1}^{n_1} \prod_{j=1}^{n_2} \prod_{i=l}^{n_3} \frac{1}{\left(k^2 - M_{1_i}^2\right)} \frac{1}{\left(p^2 - M_{2_j}^2\right)} \frac{1}{\left((k+p)^2 - M_{3_l}^2\right)} ,
\end{aligned}
$$

in the following calculation and the eight terms in Eq. (C.31) are given by the much shorter term

$$
\begin{aligned}
I_{klm} = \frac{1}{M_{B_l}^2 M_{T_k}^2 M_{B_m}^2} \frac{1}{(2\pi)^8} &\left[(M_{B_l}|M_{B_m}|M_{T_k}) - (M_{B_l}|0|M_{T_k}) - (M_{B_l}|M_{B_m}|0) + (M_{B_l}|0|0) \right. \\
&\left. -(0|M_{B_m}|M_{T_k}) + (0|0|M_{T_k}) + (0|M_{B_m}|0) - (0|0|0) \right] .
\end{aligned}
$$

A useful identity, which allows a further simplification, is given by [292]

$$
(M_0|M_1|M_2) = \frac{1}{3-n} \left[M_0^2 \left(M_0 M_0|M_1|M_2\right) + M_1^2 \left(M_1 M_1|M_0|M_2\right) + M_2^2 \left(M_2 M_2|M_0|M_1\right) \right] ,
$$

where for a four dimensional integral $n = 4$. This yields in total

$$
\begin{aligned}
I_{klm} = &\frac{1}{M_{B_l}^2 M_{T_k}^2 M_{B_m}^2} \frac{1}{(2\pi)^8} \frac{1}{3-n} \left[M_{B_l}^2 (M_{B_l} M_{B_l}|M_{B_m}|M_{T_k}) \right. \\
&+ M_{B_m}^2 (M_{B_m} M_{B_m}|M_{B_l}|M_{T_k}) + M_{T_k}^2 (M_{T_k} M_{T_k}|M_{B_l}|M_{B_m}) \\
&- M_{B_l}^2 (M_{B_l} M_{B_l}|0|M_{T_k}) - M_{T_k}^2 (M_{T_k} M_{T_k}|M_{B_l}|0) - M_{B_l}^2 (M_{B_l} M_{B_l}|M_{B_m}|0) \\
&- M_{B_m}^2 (M_{B_m} M_{B_m}|M_{B_l}|0) + M_{B_l}^2 (M_{B_l} M_{B_l}|0|0) - M_{B_m}^2 (M_{B_m} M_{B_m}|0|M_{T_k}) \\
&\left. - M_{T_k}^2 (M_{T_k} M_{T_k}|0|M_{B_m}) + M_{T_k}^2 (M_{T_k} M_{T_k}|0|0) + M_{B_m}^2 (M_{B_m} M_{B_m}|0|0) \right] .
\end{aligned}
$$

The evaluation of the momentum integrals gives [292]

$$
\begin{aligned}
(MM|M_1|M_2) =& \pi^4 \left[\frac{-2}{\epsilon^2} + \frac{1}{\epsilon} \Big(1 - 2\gamma_E - 2\log\Big(\pi M^2\Big)\Big)\right] \\
&+ \pi^4 \left[-\frac{1}{2} - \frac{1}{12}\pi^2 + \gamma_E - \gamma_E^2 + (1 - 2\gamma_E)\log\Big(\pi M^2\Big) - \log\Big(\pi M^2\Big)^2 - f(a,b)\right] \\
&+ \mathcal{O}(\epsilon^2) \ .
\end{aligned}
$$

The function f depends on the variables $a = M_1^2/M^2$ and $b = M_2^2/M^2$ and is defined by

$$
\begin{aligned}
f(a,b) = & -\frac{1}{2}\log(a)\log(b) - \frac{1}{2}\left(\frac{a+b-1}{\sqrt{\Delta}}\right)\left[\mathrm{Li}_2\left(\frac{-x_2}{y_1}\right) + \mathrm{Li}_2\left(\frac{-y_2}{x_1}\right) - \mathrm{Li}_2\left(\frac{-x_1}{y_2}\right)\right. \\
& \left. -\mathrm{Li}_2\left(\frac{-y_1}{x_2}\right) + \mathrm{Li}_2\left(\frac{b-a}{x_2}\right) + \mathrm{Li}_2\left(\frac{a-b}{y_2}\right) - \mathrm{Li}_2\left(\frac{b-a}{x_1}\right) - \mathrm{Li}_2\left(\frac{a-b}{y_1}\right)\right] \ ,
\end{aligned}
$$

where $\Delta = 1 - 2(a+b) + (a-b)^2$ and $\mathrm{Li}_2(x)$ is the dilogarithm function. The further variables appearing in the above expression are given by

$$
\begin{aligned}
x_1 &= \frac{1}{2}\left(1 + b - a + \sqrt{\Delta}\right) \\
x_2 &= \frac{1}{2}\left(1 + b - a - \sqrt{\Delta}\right) \\
y_1 &= \frac{1}{2}\left(1 + a - b + \sqrt{\Delta}\right) \\
y_2 &= \frac{1}{2}\left(1 + a - b - \sqrt{\Delta}\right) \ .
\end{aligned}
$$

From its definition, it is easy to verify that f fulfills the relations $f(a,b) = f(b,a)$, $f(0,0) = \pi^2/6$ and $f(a,0) = \mathrm{Li}_2(1-a)$. The preceding results allow to recast I_{klm} to the form

$$
\begin{aligned}
I_{klm} = & \frac{1}{M_{T_k}^2 M_{B_l}^2} \frac{1}{(2\pi)^8} \frac{1}{3-n} \pi^4 \left[-f(r_1, r_2) + f(r_1, 0) + f(0, r_2) - f(0,0) \right. \\
& + r_1 \left(-f(1/r_1, r_2/r_1) + f(0, r_2/r_1) + f(1/r_1, 0) - f(0,0) \right) \\
& \left. + r_2 \left(-f(r_1/r_2, 1/r_1) + f(r_1/r_2, 0) + f(0, 1/r_2) - f(0,0) \right) \right] \ ,
\end{aligned}
$$

which depends on the variables $r_1 = M_{B_l}^2/M_{B_m}^2$ and $r_2 = M_{T_k}^2/M_{B_m}^2$. Including the basic properties of f then provides the final expression

$$
\begin{aligned}
I_{klm} = & -\frac{1}{(16\pi^2)^2} \frac{1}{M_{T_k}^2 M_{B_l}^2} \left[-\frac{\pi^2}{6}(1 + r_1 + r_2) - f(r_1, r_2) + \mathrm{Li}_2(1 - r_1) + \mathrm{Li}_2(1 - r_2) \right. \\
& + r_1 \left(-f\left(\frac{1}{r_1}, \frac{r_2}{r_1}\right) + \mathrm{Li}_2\left(1 - \frac{r_2}{r_1}\right) + \mathrm{Li}_2\left(1 - \frac{1}{r_1}\right)\right) \\
& \left. + r_2 \left(-f\left(\frac{r_1}{r_2}, \frac{1}{r_2}\right) + \mathrm{Li}_2\left(1 - \frac{r_1}{r_2}\right) + \mathrm{Li}_2\left(1 - \frac{1}{r_2}\right)\right) \right] \ .
\end{aligned}
$$

Putting altogether, Eq. (C.27) therefore becomes

$$
\begin{aligned}
\delta M_u^{(2)}\Big|_{ij} = -\frac{N_c}{(16\pi^2)^2} \sum_{\alpha,\beta=1}^{3} \sum_{k,l,m=1}^{2} \frac{g_L^2 g_R^2}{4} \frac{v_L^3 v_R^3}{8} \frac{M_{B_m}}{M_{T_k} M_{B_l} M_{W_L}^2 M_{W_R}^2} \frac{[y_a^q]_{\alpha k}}{\sqrt{2}} \frac{[y_a^{q\dagger}]_{k\beta}}{\sqrt{2}} \frac{[y_c^q]_{\alpha l}}{\sqrt{2}} \frac{[y_c^{q\dagger}]_{l\beta}}{\sqrt{2}} \\
\frac{[y_c^q]_{im}}{\sqrt{2}} \frac{[y_c^{q\dagger}]_{mj}}{\sqrt{2}} \left[-\frac{\pi^2}{6} (1 + r_1 + r_2) - f(r_1, r_2) + \mathrm{Li}_2 (1 - r_1) + \mathrm{Li}_2 (1 - r_2) \right. \\
+ r_1 \left(-f\left(\frac{1}{r_1}, \frac{r_2}{r_1}\right) + \mathrm{Li}_2 \left(1 - \frac{r_2}{r_1}\right) + \mathrm{Li}_2 \left(1 - \frac{1}{r_1}\right) \right) \\
\left. + r_2 \left(-f\left(\frac{r_1}{r_2}, \frac{1}{r_2}\right) + \mathrm{Li}_2 \left(1 - \frac{r_1}{r_2}\right) + \mathrm{Li}_2 \left(1 - \frac{1}{r_2}\right) \right) \right] \, . \qquad \text{(C.32)}
\end{aligned}
$$

Appendix D

Technical details of the collider analysis

D.1 Cut-and-count analysis

The aim of this appendix is, to provide some deeper insights on the cut-and-count analysis, which is carried out in Chapter 6. As we perform a Monte Carlo simulation for both, the SM background and the new physics signal, the cuts should be ideally optimized to include as many signal events as possible and at the same time reduce the number of background events.

In the subsequent, we consider the effect of different cuts on the signal and background cross section. For the illustration, we discuss three benchmark points for the simplified Z' model (see Section 6.1 for details) with the following parameters:

$$\begin{aligned}
\text{BP 1}: M_{Z'} &= 1\ \text{TeV}\ ,\quad \Gamma_{Z'} = 0.1\ \text{TeV}\ ,\\
g_\mu^L &= g_\mu^R = 0.0865\ ,\quad (g_\nu)_{\alpha\beta} = \delta_{\tau\alpha}\delta_{\tau\beta}\ .\\
\text{BP 2}: M_{Z'} &= 100\ \text{GeV}\ ,\quad \Gamma_{Z'} = 10\ \text{GeV}\ ,\\
g_\mu^L &= g_\mu^R = 1\ ,\quad (g_\nu)_{\alpha\beta} = \delta_{\tau\alpha}\delta_{\tau\beta}\ .\\
\text{BP 3}: M_{Z'} &= 100\ \text{GeV}\ ,\quad \Gamma_{Z'} = 30\ \text{GeV}\ ,\\
g_\mu^L &= g_\mu^R = 1\ ,\quad (g_\nu)_{\alpha\beta} = \delta_{\tau\alpha}\delta_{\tau\beta}\ .
\end{aligned} \tag{D.1}$$

The basic cut demands

$$p_\gamma^T > 10\ \text{GeV}\ ,\quad |\eta_\gamma| < 2.44\ , \tag{D.2}$$

and is implemented for all data sets. After that we apply increasing limits on the missing transverse energy $\not{E}_T$. Table D.1 shows the signal and background cross section σ_S and σ_B after each cut. Compared to the signal events, the background is efficiently reduced by the missing $\not{E}_T$ cut. For our final analysis we determine the $\not{E}_T$ cut with the maximal statistical significance for each of the data sets individually.

	$\sigma_{\mathbf{S}}$ [**fb**]			$\sigma_{\mathbf{B}}$ [**fb**]
cuts	**BP 1**	**BP 2**	**BP 3**	
before cuts	2.152	246.0	138.2	2980
basic cuts	2.107	240.5	135.4	2929
$\not{E}_T > 10$ GeV	2.105	240.5	135.3	2901
$\not{E}_T > 20$ GeV	2.058	239.7	129.7	2099
$\not{E}_T > 30$ GeV	2.020	238.5	125.4	1621
$\not{E}_T > 40$ GeV	1.991	237.3	122.0	1302
$\not{E}_T > 50$ GeV	1.965	236.0	119.2	1071
$\not{E}_T > 60$ GeV	1.943	234.7	116.8	897.2
$\not{E}_T > 70$ GeV	1.923	233.5	114.8	763.2
$\not{E}_T > 80$ GeV	1.905	232.3	113.0	656.7
$\not{E}_T > 100$ GeV	1.873	229.9	110.0	503.3

Table D.1 Signal and background cross section σ_S and σ_B for the process $\mu^+\mu^- \to \nu\nu\gamma$ after applying different cuts. For the signal we choose three benchmark scenarios in the simplified Z' model defined in Eq. (6.3). The model parameters are given in the text.

D.2 Signal-to-background ratio

In this section, we want to show how the signal-to-background ratio depends on the model parameters. We exemplify our findings again with the simplified Z' model.

Figure D.1 displays the ratio $N_S/\sqrt{N_B}$ versus the mediator mass $M_{Z'}$ for fixed couplings $g_\mu^L = g_\mu^R = 0.05$ and $(g_\nu)_{\alpha\beta} = \delta_{\tau\alpha}\delta_{\tau\beta}$. The plot shows how the largest ratio will be achieved if the resonance condition $M_{Z'} \gg \sqrt{s}$ is met. When one enters the EFT regime with $M_{Z'} \gg \sqrt{s}$, the signal-to-background ratio scales as $N_S/\sqrt{N_B} \propto \epsilon^2$. Furthermore, the two presented decay widths $\Gamma_{Z'}/M_{Z'} = 0.1$ and 0.3 show that the signal-to-background ratio decreases for broader resonances.

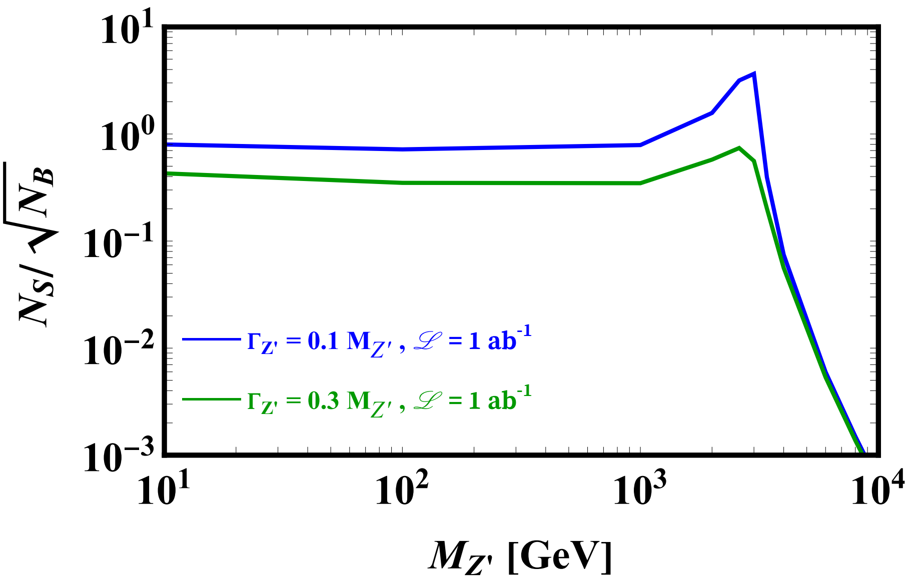

Figure D.1 Comparison of signal-to-background ratio $N_S/\sqrt{N_B}$ for the process $\mu^+\mu^- \to \overline{\nu\nu}\gamma$ in the simplified Z' model with couplings $g_\mu^L = g_\mu^R = 0.05$ and $(g_\nu)_{\alpha\beta} = \delta_{\tau\alpha}\delta_{\tau\beta}$ and $\Gamma_{Z'}/M_{Z'} = 0.1$, 0.3 at a $\sqrt{s} = 3$ TeV muon collider.

Acknowledgements

First and foremost, I would like to express my sincere gratitude to my PhD supervisor Prof. Dr. Dr. h.c. Manfred Lindner who gave me the opportunity to be part of the Max-Planck-Institut für Kernphysik in Heidelberg. Since I started my Bachelor thesis in 2017, I always appreciated the great scientific and social environment in your division and the huge spectrum of research topics that allowed me to learn from experimentalists and theorists. I am extremely thankful that you always gave me the possibility to follow my interests and that you encouraged me to develop my own ideas.

My special thanks also goes to Prof. Dr. Tilman Plehn for agreeing to become my second referee and to Prof. Dr. Björn Malte Schäfer and Prof. Dr. Loredana Gastaldo who spend their time to be part of my examination committee.

Further, I would also like to thank my collaborators: Many thanks go to Dr. Sudip Jana for guiding me throughout the last four years. It was a great pleasure to learn from you and I am glad that I could always rely on your advice and opinion. Your optimistic attitude was a constant source of motivation for me and taught me to see things more positively. Many thanks also go to Dr. Andreas Trautner. I enjoyed every discussion with you, especially because of your excitement about new ideas and your enthusiasm about physics. I am grateful that you taught me so many interesting things about group theory and I regret that I didn't had more time to work on our project. Furthermore, I would like to extend my sincere thanks to Prof. Dr. Rabindra Mohapatra. I enjoyed our collaboration a lot and I am grateful for the possibility to learn from your expertise.

Moreover, many thanks should also go to Dr. Thomas Rink, Aika Tada, Maya Hager, Manuel Salewski and Tim Herbermann for their excellent proofreading skills and many insightful comments on my writing.

I also wish to thank Marcel Neugebauer for his great companionship over the last years. I am truly blessed to have you by my side. You are always with me, no matter whether times are happy or difficult and I am glad that you never stopped reminding me of the truly important things in life.

Finally, I would like to thank my family without whom this could have never happened. My parents Dr. Regine Peschina-Klett and Dr. Alfred Klett have always been a constant source of support. Your belief in my dreams and your endless encouragement is the foundation of my journey and I am extremely thankful for the love you have shared. I would also like to thank my beloved sister Dr. Lara Klett. There is no better friend than you and your encouragement and love means everything to me.

List of Tables

List of Figures

Disclaimer

This dissertation is based on work that has been published or is in the review process. The studies were performed at the Max-Planck-Institut für Kernphysik Heidelberg from January 2021 to September 2024 and the scientific work was done by the author of this thesis in collaboration with others.

- In particular, reference [1] underlies the content of Chapter 4.
- The studies of Chapter 5 are published in reference [3].
- Chapter 6 bases on the work in reference [2].

In addition, during the doctoral studies, the author contributed to reference [4], which is not part of the scientific content of this thesis.

List of publications by Sophie Klett

[1] S. Jana, S. Klett, and M. Lindner, "Flavor seesaw mechanism," Phys. Rev. D 105 no. 11, (2022) 115015, arXiv:2112.09155 [hep-ph].

[2] S. Jana and S. Klett, "Muonic Force and Neutrino Non-Standard Interactions at Muon Colliders," arXiv:2308.07375 [hep-ph].

[3] S. Jana, S. Klett, M. Lindner, and R. N. Mohapatra, "Radiative Origin of Fermion Mass Hierarchy in Left-Right Symmetric Theory," arXiv:2409.04246 [hep-ph].

[4] S. Klett, M. Lindner, and A. Trautner, "Generating the electro-weak scale by vector-like quark condensation," SciPost Phys. 14 no. 4, (2023) 076, arXiv:2205.15323 [hep-ph]

These references can also be found as [1–4] in the following bibliography.

Bibliography

[1] S. Jana, S. Klett, and M. Lindner, "Flavor seesaw mechanism," *Phys. Rev. D* **105** no. 11, (2022) 115015, arXiv:2112.09155 [hep-ph].

[2] S. Jana and S. Klett, "Muonic Force and Neutrino Non-Standard Interactions at Muon Colliders," arXiv:2308.07375 [hep-ph].

[3] S. Jana, S. Klett, M. Lindner, and R. N. Mohapatra, "Radiative Origin of Fermion Mass Hierarchy in Left-Right Symmetric Theory," arXiv:2409.04246 [hep-ph].

[4] S. Klett, M. Lindner, and A. Trautner, "Generating the electro-weak scale by vector-like quark condensation," *SciPost Phys.* **14** no. 4, (2023) 076, arXiv:2205.15323 [hep-ph].

[5] C. D. Anderson and S. H. Neddermeyer, "Cloud Chamber Observations of Cosmic Rays at 4300 Meters Elevation and Near Sea-Level," *Phys. Rev.* **50** (1936) 263–271.

[6] S. H. Neddermeyer and C. D. Anderson, "Note on the Nature of Cosmic Ray Particles," *Phys. Rev.* **51** (1937) 884–886.

[7] M. Gell-Mann, "A Schematic Model of Baryons and Mesons," *Phys. Lett.* **8** (1964) 214–215.

[8] G. Zweig, *An SU(3) model for strong interaction symmetry and its breaking. Version 2*, pp. 22–101. 2, 1964.

[9] G. Zweig, "An SU(3) model for strong interaction symmetry and its breaking. Version 1,".

[10] S. L. Glashow, J. Iliopoulos, and L. Maiani, "Weak Interactions with Lepton-Hadron Symmetry," *Phys. Rev. D* **2** (1970) 1285–1292.

[11] **SLAC-SP-017** Collaboration, J. E. Augustin *et al.*, "Discovery of a Narrow Resonance in e^+e^- Annihilation," *Phys. Rev. Lett.* **33** (1974) 1406–1408.

[12] **E598** Collaboration, J. J. Aubert *et al.*, "Experimental Observation of a Heavy Particle J," *Phys. Rev. Lett.* **33** (1974) 1404–1406.

[13] G. Goldhaber *et al.*, "Observation in e+ e- Annihilation of a Narrow State at 1865-MeV/c**2 Decaying to K pi and K pi pi pi," *Phys. Rev. Lett.* **37** (1976) 255–259.

[14] M. Kobayashi and T. Maskawa, "CP Violation in the Renormalizable Theory of Weak Interaction," *Prog. Theor. Phys.* **49** (1973) 652–657.

[15] **E288** Collaboration, S. W. Herb *et al.*, "Observation of a Dimuon Resonance at 9.5-GeV in 400-GeV Proton-Nucleus Collisions," *Phys. Rev. Lett.* **39** (1977) 252–255.

[16] **D0** Collaboration, S. Abachi *et al.*, "Observation of the top quark," *Phys. Rev. Lett.* **74** (1995) 2632–2637, `arXiv:hep-ex/9503003`.

[17] **CDF** Collaboration, F. Abe *et al.*, "Observation of top quark production in $\bar{p}p$ collisions," *Phys. Rev. Lett.* **74** (1995) 2626–2631, `arXiv:hep-ex/9503002`.

[18] **DONUT** Collaboration, K. Kodama *et al.*, "Observation of tau neutrino interactions," *Phys. Lett. B* **504** (2001) 218–224, `arXiv:hep-ex/0012035`.

[19] F. Englert and R. Brout, "Broken Symmetry and the Mass of Gauge Vector Mesons," *Phys. Rev. Lett.* **13** (1964) 321–323.

[20] P. W. Higgs, "Broken symmetries, massless particles and gauge fields," *Phys. Lett.* **12** (1964) 132–133.

[21] P. W. Higgs, "Broken Symmetries and the Masses of Gauge Bosons," *Phys. Rev. Lett.* **13** (1964) 508–509.

[22] J. Erler and P. Langacker, "Electroweak model and constraints on new physics," `arXiv:hep-ph/0407097`.

[23] N. Chen and H.-J. He, "LHC Signatures of Two-Higgs-Doublets with Fourth Family," *JHEP* **04** (2012) 062, `arXiv:1202.3072 [hep-ph]`.

[24] A. Djouadi and A. Lenz, "Sealing the fate of a fourth generation of fermions," *Phys. Lett. B* **715** (2012) 310–314, `arXiv:1204.1252 [hep-ph]`.

[25] E. Kuflik, Y. Nir, and T. Volansky, "Implications of Higgs searches on the four generation standard model," *Phys. Rev. Lett.* **110** no. 9, (2013) 091801, `arXiv:1204.1975 [hep-ph]`.

[26] O. Eberhardt, G. Herbert, H. Lacker, A. Lenz, A. Menzel, U. Nierste, and M. Wiebusch, "Impact of a Higgs boson at a mass of 126 GeV on the standard model with three and four fermion generations," *Phys. Rev. Lett.* **109** (2012) 241802, `arXiv:1209.1101 [hep-ph]`.

[27] **KATRIN** Collaboration, M. Aker *et al.*, "Direct neutrino-mass measurement with sub-electronvolt sensitivity," *Nature Phys.* **18** no. 2, (2022) 160–166, `arXiv:2105.08533 [hep-ex]`.

[28] **Planck** Collaboration, N. Aghanim *et al.*, "Planck 2018 results. VI. Cosmological parameters," *Astron. Astrophys.* **641** (2020) A6, `arXiv:1807.06209 [astro-ph.CO]`. [Erratum: Astron.Astrophys. 652, C4 (2021)].

[29] **DESI** Collaboration, A. G. Adame *et al.*, "DESI 2024 VI: Cosmological Constraints from the Measurements of Baryon Acoustic Oscillations," arXiv:2404.03002 [astro-ph.CO].

[30] I. Esteban, M. C. Gonzalez-Garcia, M. Maltoni, T. Schwetz, and A. Zhou, "The fate of hints: updated global analysis of three-flavor neutrino oscillations," *JHEP* **09** (2020) 178, arXiv:2007.14792 [hep-ph].

[31] **Particle Data Group** Collaboration, R. L. Workman *et al.*, "Review of Particle Physics," *PTEP* **2022** (2022) 083C01.

[32] K. S. Babu, "TASI Lectures on Flavor Physics," in *Theoretical Advanced Study Institute in Elementary Particle Physics: The Dawn of the LHC Era*, pp. 49–123. 2010. arXiv:0910.2948 [hep-ph].

[33] S. F. King and C. Luhn, "Neutrino Mass and Mixing with Discrete Symmetry," *Rept. Prog. Phys.* **76** (2013) 056201, arXiv:1301.1340 [hep-ph].

[34] G. Chauhan, P. S. B. Dev, I. Dubovyk, B. Dziewit, W. Flieger, K. Grzanka, J. Gluza, B. Karmakar, and S. Zięba, "Phenomenology of lepton masses and mixing with discrete flavor symmetries," *Prog. Part. Nucl. Phys.* **138** (2024) 104126, arXiv:2310.20681 [hep-ph].

[35] F. Feruglio and A. Romanino, "Lepton flavor symmetries," *Rev. Mod. Phys.* **93** no. 1, (2021) 015007, arXiv:1912.06028 [hep-ph].

[36] B. S. Balakrishna, "Fermion Mass Hierarchy From Radiative Corrections," *Phys. Rev. Lett.* **60** (1988) 1602.

[37] B. S. Balakrishna, A. L. Kagan, and R. N. Mohapatra, "Quark Mixings and Mass Hierarchy From Radiative Corrections," *Phys. Lett. B* **205** (1988) 345–352.

[38] B. S. Balakrishna and R. N. Mohapatra, "Radiative Fermion Masses From New Physics at Tev Scale," *Phys. Lett. B* **216** (1989) 349–352.

[39] K. S. Babu, B. S. Balakrishna, and R. N. Mohapatra, "Supersymmetric Model for Fermion Mass Hierarchy," *Phys. Lett. B* **237** (1990) 221–228.

[40] K. S. Babu and X.-G. He, "Fermion Mass Hierarchy and the Strong CP Problem," *Phys. Lett. B* **219** (1989) 342–346.

[41] R. Rattazzi, "Radiative quark masses constrained by the gauge group only," *Z. Phys. C* **52** (1991) 575–582.

[42] B. A. Dobrescu and P. J. Fox, "Quark and lepton masses from top loops," *JHEP* **08** (2008) 100, arXiv:0805.0822 [hep-ph].

[43] P. W. Graham and S. Rajendran, "A Domino Theory of Flavor," *Phys. Rev. D* **81** (2010) 033002, arXiv:0906.4657 [hep-ph].

[44] S. Weinberg, "Models of Lepton and Quark Masses," *Phys. Rev. D* **101** no. 3, (2020) 035020, arXiv:2001.06582 [hep-th].

[45] G. Mohanta and K. M. Patel, "Radiatively generated fermion mass hierarchy from flavor nonuniversal gauge symmetries," *Phys. Rev. D* **106** no. 7, (2022) 075020, arXiv:2207.10407 [hep-ph].

[46] G. Mohanta and K. M. Patel, "Gauged $\mathrm{SU}(3)_F$ and loop induced quark and lepton masses," *JHEP* **10** (2023) 128, arXiv:2308.05642 [hep-ph].

[47] G. Mohanta and K. M. Patel, "Loop-induced masses for the first two generations with optimum flavour violation," arXiv:2406.19179 [hep-ph].

[48] R. N. Mohapatra and J. C. Pati, "Left-Right Gauge Symmetry and an Isoconjugate Model of CP Violation," *Phys. Rev. D* **11** (1975) 566–571.

[49] R. N. Mohapatra and J. C. Pati, "A Natural Left-Right Symmetry," *Phys. Rev. D* **11** (1975) 2558.

[50] G. Senjanovic and R. N. Mohapatra, "Exact Left-Right Symmetry and Spontaneous Violation of Parity," *Phys. Rev. D* **12** (1975) 1502.

[51] Z. G. Berezhiani, "The Weak Mixing Angles in Gauge Models with Horizontal Symmetry: A New Approach to Quark and Lepton Masses," *Phys. Lett. B* **129** (1983) 99–102.

[52] D. Chang and R. N. Mohapatra, "Small and Calculable Dirac Neutrino Mass," *Phys. Rev. Lett.* **58** (1987) 1600.

[53] A. Davidson and K. C. Wali, "Universal Seesaw Mechanism?," *Phys. Rev. Lett.* **59** (1987) 393.

[54] S. Rajpoot, "See-saw masses for quarks and leptons in an ambidextrous electroweak interaction model," *Mod. Phys. Lett. A* **2** no. 5, (1987) 307–315. [Erratum: Mod.Phys.Lett.A 2, 541 (1987)].

[55] K. S. Babu and R. N. Mohapatra, "CP Violation in Seesaw Models of Quark Masses," *Phys. Rev. Lett.* **62** (1989) 1079.

[56] K. S. Babu and R. N. Mohapatra, "A Solution to the Strong CP Problem Without an Axion," *Phys. Rev. D* **41** (1990) 1286.

[57] R. N. Mohapatra and Y. Zhang, "TeV Scale Universal Seesaw, Vacuum Stability and Heavy Higgs," *JHEP* **06** (2014) 072, arXiv:1401.6701 [hep-ph].

[58] A. Patra and S. K. Rai, "Lepton-specific universal seesaw model with left-right symmetry," *Phys. Rev. D* **98** no. 1, (2018) 015033, arXiv:1711.00627 [hep-ph].

[59] S.-P. Chen and P.-H. Gu, "U(1)Y' universal seesaw," *Nucl. Phys. B* **986** (2023) 116057, arXiv:2211.01906 [hep-ph].

[60] R. Dcruz and K. S. Babu, "Resolving W boson mass shift and CKM unitarity violation in left-right symmetric models with a universal seesaw mechanism," *Phys. Rev. D* **108** no. 9, (2023) 095011, arXiv:2212.09697 [hep-ph].

[61] T. Morozumi and A. H. Panuluh, "The third family quark mass hierarchy and FCNC in the universal seesaw model," arXiv:2407.00732 [hep-ph].

[62] P. Minkowski, "$\mu \to e\gamma$ at a Rate of One Out of 10^9 Muon Decays?," *Phys. Lett. B* **67** (1977) 421–428.

[63] R. N. Mohapatra and G. Senjanovic, "Neutrino Mass and Spontaneous Parity Nonconservation," *Phys. Rev. Lett.* **44** (1980) 912.

[64] T. Yanagida, "Horizontal gauge symmetry and masses of neutrinos," *Conf. Proc. C* **7902131** (1979) 95–99.

[65] J. Schechter and J. W. F. Valle, "Neutrino Masses in SU(2) x U(1) Theories," *Phys. Rev. D* **22** (1980) 2227.

[66] T. P. Cheng and L.-F. Li, "Neutrino Masses, Mixings and Oscillations in SU(2) x U(1) Models of Electroweak Interactions," *Phys. Rev. D* **22** (1980) 2860.

[67] R. N. Mohapatra and G. Senjanovic, "Neutrino Masses and Mixings in Gauge Models with Spontaneous Parity Violation," *Phys. Rev. D* **23** (1981) 165.

[68] G. Lazarides, Q. Shafi, and C. Wetterich, "Proton Lifetime and Fermion Masses in an SO(10) Model," *Nucl. Phys. B* **181** (1981) 287–300.

[69] R. Foot, H. Lew, X. G. He, and G. C. Joshi, "Seesaw Neutrino Masses Induced by a Triplet of Leptons," *Z. Phys. C* **44** (1989) 441.

[70] A. Zee, "A Theory of Lepton Number Violation, Neutrino Majorana Mass, and Oscillation," *Phys. Lett. B* **93** (1980) 389. [Erratum: Phys.Lett.B 95, 461 (1980)].

[71] L. Wolfenstein, "Neutrino Oscillations in Matter," *Phys. Rev. D* **17** (1978) 2369–2374.

[72] P. Coloma, M. C. Gonzalez-Garcia, M. Maltoni, J. a. P. Pinheiro, and S. Urrea, "Global constraints on non-standard neutrino interactions with quarks and electrons," arXiv:2305.07698 [hep-ph].

[73] I. Esteban, M. C. Gonzalez-Garcia, M. Maltoni, I. Martinez-Soler, and J. Salvado, "Updated constraints on non-standard interactions from global analysis of oscillation data," *JHEP* **08** (2018) 180, arXiv:1805.04530 [hep-ph]. [Addendum: JHEP 12, 152 (2020)].

[74] K. S. Babu, D. Gonçalves, S. Jana, and P. A. N. Machado, "Neutrino Non-Standard Interactions: Complementarity Between LHC and Oscillation Experiments," *Phys. Lett. B* **815** (2021) 136131, arXiv:2003.03383 [hep-ph].

[75] D. Liu, C. Sun, and J. Gao, "Constraints on neutrino non-standard interactions from LHC data with large missing transverse momentum," *JHEP* **02** (2021) 033, arXiv:2009.06668 [hep-ph].

[76] D. Choudhury, K. Ghosh, and S. Niyogi, "Probing nonstandard neutrino interactions at the LHC Run II," *Phys. Lett. B* **784** (2018) 248–254, arXiv:1801.01513 [hep-ph].

[77] A. Friedland, M. L. Graesser, I. M. Shoemaker, and L. Vecchi, "Probing Nonstandard Standard Model Backgrounds with LHC Monojets," *Phys. Lett. B* **714** (2012) 267–275, arXiv:1111.5331 [hep-ph].

[78] D. Buarque Franzosi, M. T. Frandsen, and I. M. Shoemaker, "New or ν missing energy: Discriminating dark matter from neutrino interactions at the LHC," *Phys. Rev. D* **93** no. 9, (2016) 095001, arXiv:1507.07574 [hep-ph].

[79] J. Barranco, O. G. Miranda, C. A. Moura, and J. W. F. Valle, "Constraining non-standard neutrino-electron interactions," *Phys. Rev. D* **77** (2008) 093014, arXiv:0711.0698 [hep-ph].

[80] Z. Berezhiani and A. Rossi, "Limits on the nonstandard interactions of neutrinos from e+ e- colliders," *Phys. Lett. B* **535** (2002) 207–218, arXiv:hep-ph/0111137.

[81] K. S. Babu, P. S. Dev, S. Jana, and Y. Sui, "Zee-Burst: A New Probe of Neutrino Nonstandard Interactions at IceCube," *Phys. Rev. Lett.* **124** no. 4, (2020) 041805, arXiv:1908.02779 [hep-ph].

[82] K. S. Babu, P. S. B. Dev, and S. Jana, "Probing neutrino mass models through resonances at neutrino telescopes," *Int. J. Mod. Phys. A* **37** no. 11n12, (2022) 2230003, arXiv:2202.06975 [hep-ph].

[83] G.-y. Huang, S. Jana, M. Lindner, and W. Rodejohann, "Probing new physics at future tau neutrino telescopes," *JCAP* **02** no. 02, (2022) 038, arXiv:2112.09476 [hep-ph].

[84] *Neutrino Non-Standard Interactions: A Status Report*, vol. 2. 2019. arXiv:1907.00991 [hep-ph].

[85] **Muon g-2** Collaboration, G. W. Bennett *et al.*, "Final Report of the Muon E821 Anomalous Magnetic Moment Measurement at BNL," *Phys. Rev. D* **73** (2006) 072003, arXiv:hep-ex/0602035.

[86] **Muon g-2** Collaboration, D. P. Aguillard *et al.*, "Measurement of the Positive Muon Anomalous Magnetic Moment to 0.20 ppm," arXiv:2308.06230 [hep-ex].

[87] **Muon Collider** Collaboration, D. Stratakis *et al.*, "A Muon Collider Facility for Physics Discovery," arXiv:2203.08033 [physics.acc-ph].

[88] C. Accettura *et al.*, "Towards a Muon Collider," arXiv:2303.08533 [physics.acc-ph].

[89] **Muon Collider** Collaboration, S. Jindariani *et al.*, "Promising Technologies and R&D Directions for the Future Muon Collider Detectors," arXiv:2203.07224 [physics.ins-det].

[90] C. Aime *et al.*, "Muon Collider Physics Summary," arXiv:2203.07256 [hep-ph].

[91] **Muon Collider** Collaboration, J. de Blas *et al.*, "The physics case of a 3 TeV muon collider stage," arXiv:2203.07261 [hep-ph].

[92] **P5** Collaboration, S. Asai *et al.*, "Exploring the Quantum Universe: Pathways to Innovation and Discovery in Particle Physics," arXiv:2407.19176 [hep-ex].

[93] S. L. Glashow, "Partial Symmetries of Weak Interactions," *Nucl. Phys.* **22** (1961) 579–588.

[94] S. Weinberg, "A Model of Leptons," *Phys. Rev. Lett.* **19** (1967) 1264–1266.

[95] A. Salam, "Weak and Electromagnetic Interactions," *Conf. Proc. C* **680519** (1968) 367–377.

[96] **ATLAS** Collaboration, G. Aad *et al.*, "Observation of a new particle in the search for the Standard Model Higgs boson with the ATLAS detector at the LHC," *Phys. Lett. B* **716** (2012) 1–29, arXiv:1207.7214 [hep-ex].

[97] **CMS** Collaboration, S. Chatrchyan *et al.*, "Observation of a New Boson at a Mass of 125 GeV with the CMS Experiment at the LHC," *Phys. Lett. B* **716** (2012) 30–61, arXiv:1207.7235 [hep-ex].

[98] X. Fan, T. G. Myers, B. A. D. Sukra, and G. Gabrielse, "Measurement of the Electron Magnetic Moment," *Phys. Rev. Lett.* **130** no. 7, (2023) 071801, arXiv:2209.13084 [physics.atom-ph].

[99] F. Gross *et al.*, "50 Years of Quantum Chromodynamics," *Eur. Phys. J. C* **83** (2023) 1125, arXiv:2212.11107 [hep-ph].

[100] P. Langacker, "Grand Unified Theories and Proton Decay," *Phys. Rept.* **72** (1981) 185.

[101] **Super-Kamiokande** Collaboration, Y. Fukuda *et al.*, "Evidence for oscillation of atmospheric neutrinos," *Phys. Rev. Lett.* **81** (1998) 1562–1567, arXiv:hep-ex/9807003.

[102] **SNO** Collaboration, Q. R. Ahmad *et al.*, "Measurement of the rate of $\nu_e + d \to p + p + e^-$ interactions produced by ^{8}B solar neutrinos at the Sudbury Neutrino Observatory," *Phys. Rev. Lett.* **87** (2001) 071301, arXiv:nucl-ex/0106015.

[103] S. P. Mikheev and A. Y. Smirnov, "Resonant amplification of neutrino oscillations in matter and solar neutrino spectroscopy," *Nuovo Cim. C* **9** (1986) 17–26.

[104] S. Weinberg, "Baryon and Lepton Nonconserving Processes," *Phys. Rev. Lett.* **43** (1979) 1566–1570.

[105] **GERDA** Collaboration, M. Agostini *et al.*, "Final Results of GERDA on the Search for Neutrinoless Double-β Decay," *Phys. Rev. Lett.* **125** no. 25, (2020) 252502, arXiv:2009.06079 [nucl-ex].

[106] P. Salucci, A. Lapi, C. Tonini, G. Gentile, I. Yegorova, and U. Klein, "The Universal Rotation Curve of Spiral Galaxies. 2. The Dark Matter Distribution out to the Virial Radius," *Mon. Not. Roy. Astron. Soc.* **378** (2007) 41–47, arXiv:astro-ph/0703115.

[107] X. Ou, A.-C. Eilers, L. Necib, and A. Frebel, "The dark matter profile of the milky way inferred from its circular velocity curve," 2023. https://arxiv.org/abs/2303.12838.

[108] **Planck** Collaboration, Y. Akrami *et al.*, "Planck 2018 results. IX. Constraints on primordial non-Gaussianity," *Astron. Astrophys.* **641** (2020) A9, arXiv:1905.05697 [astro-ph.CO].

[109] M. Markevitch, A. H. Gonzalez, D. Clowe, A. Vikhlinin, L. David, W. Forman, C. Jones, S. Murray, and W. Tucker, "Direct constraints on the dark matter self-interaction cross-section from the merging galaxy cluster 1E0657-56," *Astrophys. J.* **606** (2004) 819–824, arXiv:astro-ph/0309303.

[110] **Planck** Collaboration, N. Aghanim *et al.*, "Planck 2018 results. I. Overview and the cosmological legacy of Planck," *Astron. Astrophys.* **641** (2020) A1, arXiv:1807.06205 [astro-ph.CO].

[111] M. Cirelli, A. Strumia, and J. Zupan, "Dark Matter," arXiv:2406.01705 [hep-ph].

[112] A. D. Sakharov, "Violation of CP Invariance, C asymmetry, and baryon asymmetry of the universe," *Pisma Zh. Eksp. Teor. Fiz.* **5** (1967) 32–35.

[113] **Muon g-2** Collaboration, G. W. Bennett *et al.*, "Measurement of the positive muon anomalous magnetic moment to 0.7 ppm," *Phys. Rev. Lett.* **89** (2002) 101804, arXiv:hep-ex/0208001. [Erratum: Phys.Rev.Lett. 89, 129903 (2002)].

[114] **Muon g-2** Collaboration, G. W. Bennett *et al.*, "Measurement of the negative muon anomalous magnetic moment to 0.7 ppm," *Phys. Rev. Lett.* **92** (2004) 161802, arXiv:hep-ex/0401008.

[115] **Muon g-2** Collaboration, B. Abi *et al.*, "Measurement of the Positive Muon Anomalous Magnetic Moment to 0.46 ppm," *Phys. Rev. Lett.* **126** no. 14, (2021) 141801, arXiv:2104.03281 [hep-ex].

[116] S. Borsanyi *et al.*, "Leading hadronic contribution to the muon magnetic moment from lattice QCD," *Nature* **593** no. 7857, (2021) 51–55, arXiv:2002.12347 [hep-lat].

[117] **LSND** Collaboration, A. Aguilar *et al.*, "Evidence for neutrino oscillations from the observation of $\bar{\nu}_e$ appearance in a $\bar{\nu}_\mu$ beam," *Phys. Rev. D* **64** (2001) 112007, arXiv:hep-ex/0104049.

[118] **MiniBooNE** Collaboration, A. A. Aguilar-Arevalo *et al.*, "A Search for Electron Neutrino Appearance at the $\Delta m^2 \sim 1eV^2$ Scale," *Phys. Rev. Lett.* **98** (2007) 231801, arXiv:0704.1500 [hep-ex].

[119] **MiniBooNE** Collaboration, A. A. Aguilar-Arevalo *et al.*, "Significant Excess of ElectronLike Events in the MiniBooNE Short-Baseline Neutrino Experiment," *Phys. Rev. Lett.* **121** no. 22, (2018) 221801, arXiv:1805.12028 [hep-ex].

[120] R. D. Peccei and H. R. Quinn, "CP Conservation in the Presence of Instantons," *Phys. Rev. Lett.* **38** (1977) 1440–1443.

[121] S. Weinberg, "A New Light Boson?," *Phys. Rev. Lett.* **40** (1978) 223–226.

[122] F. Wilczek, "Problem of Strong P and T Invariance in the Presence of Instantons," *Phys. Rev. Lett.* **40** (1978) 279–282.

[123] K. S. Babu, R. N. Mohapatra, and N. Okada, "Parity solution to the strong CP problem and a unified framework for inflation, baryogenesis, and dark matter," *JHEP* **01** (2024) 136, arXiv:2307.14869 [hep-ph].

[124] G. 't Hooft, "Naturalness, chiral symmetry, and spontaneous chiral symmetry breaking," *NATO Sci. Ser. B* **59** (1980) 135–157.

[125] J. D. Wells, "Higgs naturalness and the scalar boson proliferation instability problem," *Synthese* **194** no. 2, (2017) 477–490, arXiv:1603.06131 [hep-ph].

[126] Y. Nir, "Flavour Physics and CP Violation," in *7th CERN–Latin-American School of High-Energy Physics*, pp. 123–156. 2015. arXiv:1605.00433 [hep-ph].

[127] S. Willenbrock, "Symmetries of the standard model," in *Theoretical Advanced Study Institute in Elementary Particle Physics: Physics in $D \geqq 4$*, pp. 3–38. 10, 2004. arXiv:hep-ph/0410370.

[128] T. Beier, H. Häffner, N. Hermanspahn, S. G. Karshenboim, H. J. Kluge, W. Quint, S. Stahl, J. Verdú, and G. Werth, "New determination of the electron's mass," *Phys. Rev. Lett.* **88** (2002) 011603.

[129] E. Tiesinga, P. J. Mohr, D. B. Newell, and B. N. Taylor, "CODATA recommended values of the fundamental physical constants: 2018*," *Rev. Mod. Phys.* **93** no. 2, (2021) 025010.

[130] **BESIII** Collaboration, M. Ablikim *et al.*, "Precision measurement of the mass of the τ lepton," *Phys. Rev. D* **90** no. 1, (2014) 012001, arXiv:1405.1076 [hep-ex].

[131] **BaBar** Collaboration, B. Aubert *et al.*, "Measurements of the tau mass and the mass difference of the tau+ and tau- at BABAR," *Phys. Rev. D* **80** (2009) 092005, arXiv:0909.3562 [hep-ex].

[132] **Super-Kamiokande** Collaboration, K. Abe *et al.*, "Solar neutrino results in Super-Kamiokande-III," *Phys. Rev. D* **83** (2011) 052010, arXiv:1010.0118 [hep-ex].

[133] **SNO** Collaboration, B. Aharmim *et al.*, "Combined Analysis of all Three Phases of Solar Neutrino Data from the Sudbury Neutrino Observatory," *Phys. Rev. C* **88** (2013) 025501, arXiv:1109.0763 [nucl-ex].

[134] **BOREXINO** Collaboration, G. Bellini *et al.*, "Neutrinos from the primary proton–proton fusion process in the Sun," *Nature* **512** no. 7515, (2014) 383–386.

[135] **IceCube** Collaboration, M. G. Aartsen *et al.*, "Determining neutrino oscillation parameters from atmospheric muon neutrino disappearance with three years of IceCube DeepCore data," *Phys. Rev. D* **91** no. 7, (2015) 072004, arXiv:1410.7227 [hep-ex].

[136] **Double Chooz** Collaboration, H. de Kerret *et al.*, "Double Chooz θ_{13} measurement via total neutron capture detection," *Nature Phys.* **16** no. 5, (2020) 558–564, arXiv:1901.09445 [hep-ex].

[137] **NOvA** Collaboration, M. A. Acero *et al.*, "First Measurement of Neutrino Oscillation Parameters using Neutrinos and Antineutrinos by NOvA," *Phys. Rev. Lett.* **123** no. 15, (2019) 151803, arXiv:1906.04907 [hep-ex].

[138] **T2K** Collaboration, K. Abe *et al.*, "Constraint on the matter–antimatter symmetry-violating phase in neutrino oscillations," *Nature* **580** no. 7803, (2020) 339–344, arXiv:1910.03887 [hep-ex]. [Erratum: Nature 583, E16 (2020)].

[139] J. Gasser and H. Leutwyler, "Quark Masses," *Phys. Rept.* **87** (1982) 77–169.

[140] J. Hardy and I. S. Towner, "$|V_{ud}|$ from nuclear β decays," *PoS* **CKM2016** (2016) 028.

[141] **FlaviaNet Working Group on Kaon Decays** Collaboration, M. Antonelli *et al.*, "An Evaluation of $|V_{us}|$ and precise tests of the Standard Model from world data on leptonic and semileptonic kaon decays," *Eur. Phys. J. C* **69** (2010) 399–424, arXiv:1005.2323 [hep-ph].

[142] **BaBar** Collaboration, J. P. Lees *et al.*, "Measurement of the $D^0 \to \pi^- e^+ \nu_e$ differential decay branching fraction as a function of q^2 and study of form factor parameterizations," *Phys. Rev. D* **91** no. 5, (2015) 052022, arXiv:1412.5502 [hep-ex].

[143] **BaBar** Collaboration, B. Aubert *et al.*, "Measurement of the inclusive electron spectrum in charmless semileptonic B decays near the kinematic endpoint and determination of |V(ub)|," *Phys. Rev. D* **73** (2006) 012006, arXiv:hep-ex/0509040.

[144] **D0** Collaboration, V. M. Abazov *et al.*, "Precision measurement of the ratio $\mathrm{B}(t \to Wb)/\mathrm{B}(t \to Wq)$ and Extraction of V_{tb}," *Phys. Rev. Lett.* **107** (2011) 121802, arXiv:1106.5436 [hep-ex].

[145] **CMS** Collaboration, V. Khachatryan *et al.*, "Measurement of the ratio $\mathcal{B}(t \to Wb)/\mathcal{B}(t \to Wq)$ in pp collisions at $\sqrt{s} = 8$ TeV," *Phys. Lett. B* **736** (2014) 33–57, arXiv:1404.2292 [hep-ex].

[146] C. Jarlskog, "Commutator of the Quark Mass Matrices in the Standard Electroweak Model and a Measure of Maximal CP Nonconservation," *Phys. Rev. Lett.* **55** (1985) 1039.

[147] P. H. Frampton, P. Q. Hung, and M. Sher, "Quarks and leptons beyond the third generation," *Phys. Rept.* **330** (2000) 263, arXiv:hep-ph/9903387.

[148] A. Lenz, "Constraints on a fourth generation of fermions from Higgs Boson searches," *Adv. High Energy Phys.* **2013** (2013) 910275.

[149] J. a. M. Alves, G. C. Branco, A. L. Cherchiglia, C. C. Nishi, J. T. Penedo, P. M. F. Pereira, M. N. Rebelo, and J. I. Silva-Marcos, "Vector-like singlet quarks: A roadmap," *Phys. Rept.* **1057** (2024) 1–69, arXiv:2304.10561 [hep-ph].

[150] **ATLAS** Collaboration, M. Aaboud *et al.*, "Search for pair production of up-type vector-like quarks and for four-top-quark events in final states with multiple b-jets with the ATLAS detector," *JHEP* **07** (2018) 089, arXiv:1803.09678 [hep-ex].

[151] **ATLAS** Collaboration, M. Aaboud *et al.*, "Combination of the searches for pair-produced vector-like partners of the third-generation quarks at $\sqrt{s} = 13$ TeV with the ATLAS detector," *Phys. Rev. Lett.* **121** no. 21, (2018) 211801, arXiv:1808.02343 [hep-ex].

[152] **CMS** Collaboration, A. M. Sirunyan *et al.*, "Search for vector-like T and B quark pairs in final states with leptons at $\sqrt{s} = 13$ TeV," *JHEP* **08** (2018) 177, arXiv:1805.04758 [hep-ex].

[153] **ATLAS** Collaboration, G. Aad *et al.*, "Search for heavy lepton resonances decaying to a Z boson and a lepton in pp collisions at $\sqrt{s} = 8$ TeV with the ATLAS detector," *JHEP* **09** (2015) 108, arXiv:1506.01291 [hep-ex].

[154] **CMS** Collaboration, A. M. Sirunyan *et al.*, "Search for vector-like leptons in multilepton final states in proton-proton collisions at $\sqrt{s} = 13$ TeV," *Phys. Rev. D* **100** no. 5, (2019) 052003, arXiv:1905.10853 [hep-ex].

[155] **ATLAS** Collaboration, G. Aad *et al.*, "Search for third-generation vector-like leptons in pp collisions at $\sqrt{s} = 13$ TeV with the ATLAS detector," *JHEP* **07** (2023) 118, arXiv:2303.05441 [hep-ex].

[156] C. D. Froggatt and H. B. Nielsen, "Hierarchy of Quark Masses, Cabibbo Angles and CP Violation," *Nucl. Phys. B* **147** (1979) 277–298.

[157] M. Leurer, Y. Nir, and N. Seiberg, "Mass matrix models," *Nucl. Phys. B* **398** (1993) 319–342, arXiv:hep-ph/9212278.

[158] K. S. Babu, T. Enkhbat, and I. Gogoladze, "Anomalous U(1) symmetry and lepton flavor violation," *Nucl. Phys. B* **678** (2004) 233–257, arXiv:hep-ph/0308093.

[159] E. Dudas and E. Palti, "Froggatt-Nielsen models from E(8) in F-theory GUTs," *JHEP* **01** (2010) 127, arXiv:0912.0853 [hep-th].

[160] M. Bauer, T. Schell, and T. Plehn, "Hunting the Flavon," *Phys. Rev. D* **94** no. 5, (2016) 056003, arXiv:1603.06950 [hep-ph].

[161] P. F. Harrison, D. H. Perkins, and W. G. Scott, "A Redetermination of the neutrino mass squared difference in tri - maximal mixing with terrestrial matter effects," *Phys. Lett. B* **458** (1999) 79–92, arXiv:hep-ph/9904297.

[162] E. Ma and G. Rajasekaran, "Softly broken A(4) symmetry for nearly degenerate neutrino masses," *Phys. Rev. D* **64** (2001) 113012, arXiv:hep-ph/0106291.

[163] E. Ma, "Quark mass matrices in the A(4) model," *Mod. Phys. Lett. A* **17** (2002) 627–630, arXiv:hep-ph/0203238.

[164] K. S. Babu, E. Ma, and J. W. F. Valle, "Underlying A(4) symmetry for the neutrino mass matrix and the quark mixing matrix," *Phys. Lett. B* **552** (2003) 207–213, arXiv:hep-ph/0206292.

[165] G. Altarelli and F. Feruglio, "Tri-bimaximal neutrino mixing, A(4) and the modular symmetry," *Nucl. Phys. B* **741** (2006) 215–235, arXiv:hep-ph/0512103.

[166] P. Chen, S. Centelles Chuliá, G.-J. Ding, R. Srivastava, and J. W. F. Valle, "Realistic tribimaximal neutrino mixing," *Phys. Rev. D* **98** no. 5, (2018) 055019, arXiv:1806.03367 [hep-ph].

[167] H. Ishimori and E. Ma, "New Simple A_4 Neutrino Model for Nonzero θ_{13} and Large δ_{CP}," *Phys. Rev. D* **86** (2012) 045030, arXiv:1205.0075 [hep-ph].

[168] R. N. Mohapatra and C. C. Nishi, "S_4 Flavored CP Symmetry for Neutrinos," *Phys. Rev. D* **86** (2012) 073007, arXiv:1208.2875 [hep-ph].

[169] M. Holthausen, M. Lindner, and M. A. Schmidt, "Lepton flavor at the electroweak scale: A complete A_4 model," *Phys. Rev. D* **87** no. 3, (2013) 033006, arXiv:1211.5143 [hep-ph].

[170] C. Hagedorn, J. Kriewald, J. Orloff, and A. M. Teixeira, "Flavour and CP symmetries in the inverse seesaw," *Eur. Phys. J. C* **82** no. 3, (2022) 194, arXiv:2107.07537 [hep-ph].

[171] H. Ishimori, T. Kobayashi, H. Ohki, Y. Shimizu, H. Okada, and M. Tanimoto, "Non-Abelian Discrete Symmetries in Particle Physics," *Prog. Theor. Phys. Suppl.* **183** (2010) 1–163, arXiv:1003.3552 [hep-th].

[172] F. Feruglio, C. Hagedorn, and R. Ziegler, "Lepton Mixing Parameters from Discrete and CP Symmetries," *JHEP* **07** (2013) 027, arXiv:1211.5560 [hep-ph].

[173] M. Holthausen, M. Lindner, and M. A. Schmidt, "CP and Discrete Flavour Symmetries," *JHEP* **04** (2013) 122, arXiv:1211.6953 [hep-ph].

[174] M.-C. Chen, M. Fallbacher, K. T. Mahanthappa, M. Ratz, and A. Trautner, "CP Violation from Finite Groups," *Nucl. Phys. B* **883** (2014) 267–305, arXiv:1402.0507 [hep-ph].

[175] C. Hagedorn, M. Lindner, and R. N. Mohapatra, "S(4) flavor symmetry and fermion masses: Towards a grand unified theory of flavor," *JHEP* **06** (2006) 042, arXiv:hep-ph/0602244.

[176] G. Altarelli, F. Feruglio, and C. Hagedorn, "A SUSY SU(5) Grand Unified Model of Tri-Bimaximal Mixing from A_4," *JHEP* **03** (2008) 052, arXiv:0802.0090 [hep-ph].

[177] C. Hagedorn, S. F. King, and C. Luhn, "A SUSY GUT of Flavour with S4 x SU(5) to NLO," *JHEP* **06** (2010) 048, arXiv:1003.4249 [hep-ph].

[178] D. E. Kaplan and R. Rattazzi, "Large field excursions and approximate discrete symmetries from a clockwork axion," *Phys. Rev. D* **93** no. 8, (2016) 085007, arXiv:1511.01827 [hep-ph].

[179] K. Choi and S. H. Im, "Realizing the relaxion from multiple axions and its UV completion with high scale supersymmetry," *JHEP* **01** (2016) 149, arXiv:1511.00132 [hep-ph].

[180] G. F. Giudice and M. McCullough, "A Clockwork Theory," *JHEP* **02** (2017) 036, arXiv:1610.07962 [hep-ph].

[181] R. Alonso, A. Carmona, B. M. Dillon, J. F. Kamenik, J. Martin Camalich, and J. Zupan, "A clockwork solution to the flavor puzzle," *JHEP* **10** (2018) 099, `arXiv:1807.09792 [hep-ph]`.

[182] K. S. Babu and S. Saad, "Flavor Hierarchies from Clockwork in SO(10) GUT," *Phys. Rev. D* **103** no. 1, (2021) 015009, `arXiv:2007.16085 [hep-ph]`.

[183] L. Randall and R. Sundrum, "A Large mass hierarchy from a small extra dimension," *Phys. Rev. Lett.* **83** (1999) 3370–3373, `arXiv:hep-ph/9905221`.

[184] G. 't Hooft, "Renormalizable Lagrangians for Massive Yang-Mills Fields," *Nucl. Phys. B* **35** (1971) 167–188.

[185] S. Weinberg, "Electromagnetic and weak masses," *Phys. Rev. Lett.* **29** (1972) 388–392.

[186] H. Georgi and S. L. Glashow, "Attempts to calculate the electron mass," *Phys. Rev. D* **7** (1973) 2457–2463.

[187] H. Georgi and S. L. Glashow, "Spontaneously broken gauge symmetry and elementary particle masses," *Phys. Rev. D* **6** (1972) 2977–2982.

[188] R. N. Mohapatra, "Gauge Model for Chiral Symmetry Breaking and Muon electron Mass Ratio," *Phys. Rev. D* **9** (1974) 3461.

[189] S. M. Barr and A. Zee, "Calculating the Electron Mass in Terms of Measured Quantities," *Phys. Rev. D* **17** (1978) 1854.

[190] S. M. Barr and A. Zee, "Calculation of the electron mass in terms of measured quantities in a left-right—symmetric model," *Phys. Rev. D* **18** (1978) 4213.

[191] H. P. Nilles, M. Olechowski, and S. Pokorski, "Does a Radiative Generation of Quark Masses Provide Us With the Correct Mass Matrices?," *Phys. Lett. B* **248** (1990) 378–386.

[192] R. Barbieri and D. V. Nanopoulos, "Hierarchical Fermion Masses From Grand Unification," *Phys. Lett. B* **95** (1980) 43–46.

[193] S. M. Barr, "Light Fermion Mass Hierarchy and Grand Unification," *Phys. Rev. D* **21** (1980) 1424.

[194] R. Barbieri, D. V. Nanopoulos, and A. Masiero, "Hierarchical Fermion Masses in E6," *Phys. Lett. B* **104** (1981) 194–198.

[195] K. S. Babu and R. N. Mohapatra, "Permutation Symmetry and the Origin of Fermion Mass Hierarchy," *Phys. Rev. Lett.* **64** (1990) 2747.

[196] A. Hernandez Galeana and J. H. Montes de Oca Yemha, "Radiative generation of light fermion masses in a SU(3)(H) horizontal symmetry model," *Rev. Mex. Fis.* **50** (2004) 522–526, arXiv:hep-ph/0406315.

[197] A. Greljo and A. E. Thomsen, "Rising through the ranks: flavor hierarchies from a gauged SU(2) symmetry," *Eur. Phys. J. C* **84** no. 2, (2024) 213, arXiv:2309.11547 [hep-ph].

[198] A. Greljo, A. E. Thomsen, and H. Tiblom, "Flavor Hierarchies From SU(2) Flavor and Quark-Lepton Unification," arXiv:2406.02687 [hep-ph].

[199] C. Arbeláez, A. E. Cárcamo Hernández, C. Dib, P. Escalona Contreras, V. K. N., and A. Zerwekh, "A common framework for fermion mass hierarchy, leptogenesis and dark matter," arXiv:2404.06577 [hep-ph].

[200] C. Bonilla, A. E. Carcamo Hernandez, S. Kovalenko, H. Lee, R. Pasechnik, and I. Schmidt, "Fermion mass hierarchy in an extended left-right symmetric model," *JHEP* **12** (2023) 075, arXiv:2305.11967 [hep-ph].

[201] P. A. C., A. E. Cárcamo Hernández, V. K. N., S. Kovalenko, R. Pasechnik, and I. Schmidt, "Left-Right model with radiative double seesaw mechanism," arXiv:2405.12283 [hep-ph].

[202] P. Langacker and M. Plumacher, "Flavor changing effects in theories with a heavy Z' boson with family nonuniversal couplings," *Phys. Rev. D* **62** (2000) 013006, arXiv:hep-ph/0001204.

[203] **Particle Data Group** Collaboration, P. A. Zyla *et al.*, "Review of Particle Physics," *PTEP* **2020** no. 8, (2020) 083C01.

[204] N. G. Deshpande and X.-G. He, "CP violation in a multi - Higgs doublet model with flavor changing neutral current," *Phys. Rev. D* **49** (1994) 4812–4819, arXiv:hep-ph/9312271.

[205] K. S. Babu and Y. Meng, "Flavor Violation in Supersymmetric Q(6) Model," *Phys. Rev. D* **80** (2009) 075003, arXiv:0907.4231 [hep-ph].

[206] M. Ciuchini *et al.*, "Delta M(K) and epsilon(K) in SUSY at the next-to-leading order," *JHEP* **10** (1998) 008, arXiv:hep-ph/9808328.

[207] P. Arnan, A. Crivellin, M. Fedele, and F. Mescia, "Generic Loop Effects of New Scalars and Fermions in $b \to s\ell^+\ell^-$, $(g-2)_\mu$ and a Vector-like 4^{th} Generation," *JHEP* **06** (2019) 118, arXiv:1904.05890 [hep-ph].

[208] D. Becirevic, M. Ciuchini, E. Franco, V. Gimenez, G. Martinelli, A. Masiero, M. Papinutto, J. Reyes, and L. Silvestrini, "$B_d - \bar{B}_d$ mixing and the $B_d \to J/\psi K_s$ asymmetry in general SUSY models," *Nucl. Phys. B* **634** (2002) 105–119, arXiv:hep-ph/0112303.

[209] **UTfit** Collaboration, M. Bona *et al.*, "Model-independent constraints on $\Delta F = 2$ operators and the scale of new physics," *JHEP* **03** (2008) 049, arXiv:0707.0636 [hep-ph].

[210] M. Artuso, G. Borissov, and A. Lenz, "CP violation in the B_s^0 system," *Rev. Mod. Phys.* **88** no. 4, (2016) 045002, arXiv:1511.09466 [hep-ph]. [Addendum: Rev.Mod.Phys. 91, 049901 (2019)].

[211] A. J. Buras and F. De Fazio, "ε'/ε in 331 Models," *JHEP* **03** (2016) 010, arXiv:1512.02869 [hep-ph].

[212] D. Nguyen Tuan, T. Inami, and H. Do Thi, "Physical constraints derived from FCNC in the 3-3-1-1 model," *Eur. Phys. J. C* **81** no. 9, (2021) 813, arXiv:2009.09698 [hep-ph].

[213] E. Golowich, J. Hewett, S. Pakvasa, and A. A. Petrov, "Implications of D^0 - $\bar{D}^0$ Mixing for New Physics," *Phys. Rev. D* **76** (2007) 095009, arXiv:0705.3650 [hep-ph].

[214] L. Lavoura, "General formulae for f(1) —> f(2) gamma," *Eur. Phys. J. C* **29** (2003) 191–195, arXiv:hep-ph/0302221.

[215] J. Aebischer, A. J. Buras, M. Cerdà-Sevilla, and F. De Fazio, "Quark-lepton connections in Z' mediated FCNC processes: gauge anomaly cancellations at work," *JHEP* **02** (2020) 183, arXiv:1912.09308 [hep-ph].

[216] P. N. Bhattiprolu and S. P. Martin, "Prospects for vectorlike leptons at future proton-proton colliders," *Phys. Rev. D* **100** no. 1, (2019) 015033, arXiv:1905.00498 [hep-ph].

[217] M. Chala, R. Gröber, and M. Spannowsky, "Searches for vector-like quarks at future colliders and implications for composite Higgs models with dark matter," *JHEP* **03** (2018) 040, arXiv:1801.06537 [hep-ph].

[218] G.-y. Huang, S. Jana, F. S. Queiroz, and W. Rodejohann, "Probing the $R_{K^{(*)}}$ Anomaly at a Muon Collider," arXiv:2103.01617 [hep-ph].

[219] G.-y. Huang, F. S. Queiroz, and W. Rodejohann, "Gauged $L_\mu - L_\tau$ at a muon collider," *Phys. Rev. D* **103** no. 9, (2021) 095005, arXiv:2101.04956 [hep-ph].

[220] R. Dermisek, K. Hermanek, N. McGinnis, and N. McGinnis, "Highly Enhanced Contributions of Heavy Higgs Bosons and New Leptons to Muon $g-2$ and Prospects at Future Colliders," *Phys. Rev. Lett.* **126** no. 19, (2021) 191801, arXiv:2011.11812 [hep-ph].

[221] J. C. Pati and A. Salam, "Lepton Number as the Fourth Color," *Phys. Rev. D* **10** (1974) 275–289. [Erratum: Phys.Rev.D 11, 703–703 (1975)].

[222] G. Senjanovic, "Spontaneous Breakdown of Parity in a Class of Gauge Theories," *Nucl. Phys. B* **153** (1979) 334–364.

[223] K. S. Babu, X.-G. He, M. Su, and A. Thapa, "Naturally Light Dirac and Pseudo-Dirac Neutrinos from Left-Right Symmetry," arXiv:2205.09127 [hep-ph].

[224] P. D. Bolton, F. F. Deppisch, C. Hati, S. Patra, and U. Sarkar, "Alternative formulation of left-right symmetry with $B - L$ conservation and purely Dirac neutrinos," *Phys. Rev. D* **100** no. 3, (2019) 035013, arXiv:1902.05802 [hep-ph].

[225] K. S. Babu and A. Thapa, "Left-Right Symmetric Model without Higgs Triplets," arXiv:2012.13420 [hep-ph].

[226] K. S. Babu, B. Dutta, and R. N. Mohapatra, "A theory of R(D*, D) anomaly with right-handed currents," *JHEP* **01** (2019) 168, arXiv:1811.04496 [hep-ph].

[227] P. S. B. Dev and A. Pilaftsis, "Minimal Radiative Neutrino Mass Mechanism for Inverse Seesaw Models," *Phys. Rev. D* **86** (2012) 113001, arXiv:1209.4051 [hep-ph].

[228] S. F. Solera, A. Pich, and L. Vale Silva, "Direct bounds on Left-Right gauge boson masses at LHC Run 2," *JHEP* **02** (2024) 027, arXiv:2309.06094 [hep-ph].

[229] **LHCb** Collaboration, R. Aaij *et al.*, "Test of lepton universality in beauty-quark decays," arXiv:2103.11769 [hep-ex].

[230] **LHCb** Collaboration, R. Aaij *et al.*, "Test of lepton universality with $B^0 \to K^{*0}\ell^+\ell^-$ decays," *JHEP* **08** (2017) 055, arXiv:1705.05802 [hep-ex].

[231] **LHCb** Collaboration, R. Aaij *et al.*, "Search for lepton-universality violation in $B^+ \to K^+\ell^+\ell^-$ decays," *Phys. Rev. Lett.* **122** no. 19, (2019) 191801, arXiv:1903.09252 [hep-ex].

[232] **LHCb** Collaboration, R. Aaij *et al.*, "Test of lepton universality in $b \to s\ell^+\ell^-$ decays," *Phys. Rev. Lett.* **131** no. 5, (2023) 051803, arXiv:2212.09152 [hep-ex].

[233] T. Han, Z. Liu, L.-T. Wang, and X. Wang, "WIMPs at High Energy Muon Colliders," *Phys. Rev. D* **103** no. 7, (2021) 075004, arXiv:2009.11287 [hep-ph].

[234] P. Bandyopadhyay and A. Costantini, "Obscure Higgs boson at Colliders," *Phys. Rev. D* **103** no. 1, (2021) 015025, arXiv:2010.02597 [hep-ph].

[235] R. Capdevilla, F. Meloni, R. Simoniello, and J. Zurita, "Hunting wino and higgsino dark matter at the muon collider with disappearing tracks," *JHEP* **06** (2021) 133, arXiv:2102.11292 [hep-ph].

[236] S. Bottaro, D. Buttazzo, M. Costa, R. Franceschini, P. Panci, D. Redigolo, and L. Vittorio, "Closing the window on WIMP Dark Matter," *Eur. Phys. J. C* **82** no. 1, (2022) 31, arXiv:2107.09688 [hep-ph].

[237] S. Bottaro, D. Buttazzo, M. Costa, R. Franceschini, P. Panci, D. Redigolo, and L. Vittorio, "The last complex WIMPs standing," *Eur. Phys. J. C* **82** no. 11, (2022) 992, arXiv:2205.04486 [hep-ph].

[238] J. Kalinowski, T. Robens, and A. F. Zarnecki, "New Physics with missing energy at future lepton colliders - Snowmass White Paper," in *Snowmass 2021*. 3, 2022. arXiv:2203.07913 [hep-ph].

[239] S. Homiller, Q. Lu, and M. Reece, "Complementary signals of lepton flavor violation at a high-energy muon collider," *JHEP* **07** (2022) 036, arXiv:2203.08825 [hep-ph].

[240] N. Chakrabarty, T. Han, Z. Liu, and B. Mukhopadhyaya, "Radiative Return for Heavy Higgs Boson at a Muon Collider," *Phys. Rev. D* **91** no. 1, (2015) 015008, arXiv:1408.5912 [hep-ph].

[241] A. Costantini, F. De Lillo, F. Maltoni, L. Mantani, O. Mattelaer, R. Ruiz, and X. Zhao, "Vector boson fusion at multi-TeV muon colliders," *JHEP* **09** (2020) 080, arXiv:2005.10289 [hep-ph].

[242] D. Buttazzo, R. Franceschini, and A. Wulzer, "Two Paths Towards Precision at a Very High Energy Lepton Collider," *JHEP* **05** (2021) 219, arXiv:2012.11555 [hep-ph].

[243] T. Han, D. Liu, I. Low, and X. Wang, "Electroweak couplings of the Higgs boson at a multi-TeV muon collider," *Phys. Rev. D* **103** no. 1, (2021) 013002, arXiv:2008.12204 [hep-ph].

[244] M. Chiesa, F. Maltoni, L. Mantani, B. Mele, F. Piccinini, and X. Zhao, "Measuring the quartic Higgs self-coupling at a multi-TeV muon collider," *JHEP* **09** (2020) 098, arXiv:2003.13628 [hep-ph].

[245] T. Han, S. Li, S. Su, W. Su, and Y. Wu, "Heavy Higgs bosons in 2HDM at a muon collider," *Phys. Rev. D* **104** no. 5, (2021) 055029, arXiv:2102.08386 [hep-ph].

[246] M. Forslund and P. Meade, "High precision higgs from high energy muon colliders," *JHEP* **08** (2022) 185, arXiv:2203.09425 [hep-ph].

[247] M. Belfkir, T. A. Chowdhury, and S. Nasri, "Doubly-charged scalars of the Minimal Left-Right Symmetric Model at Muon Colliders," arXiv:2307.16111 [hep-ph].

[248] I. Chakraborty, H. Roy, and T. Srivastava, "Searches for heavy neutrinos at multi-TeV muon collider : a resonant leptogenesis perspective," arXiv:2206.07037 [hep-ph].

[249] P. Li, Z. Liu, and K.-F. Lyu, "Heavy neutral leptons at muon colliders," *JHEP* **03** (2023) 231, arXiv:2301.07117 [hep-ph].

[250] T. H. Kwok, L. Li, T. Liu, and A. Rock, "Searching for Heavy Neutral Leptons at A Future Muon Collider," arXiv:2301.05177 [hep-ph].

[251] R. Capdevilla, D. Curtin, Y. Kahn, and G. Krnjaic, "Discovering the physics of $(g-2)_\mu$ at future muon colliders," *Phys. Rev. D* **103** no. 7, (2021) 075028, arXiv:2006.16277 [hep-ph].

[252] D. Buttazzo and P. Paradisi, "Probing the muon $g-2$ anomaly with the Higgs boson at a muon collider," *Phys. Rev. D* **104** no. 7, (2021) 075021, arXiv:2012.02769 [hep-ph].

[253] R. Capdevilla, D. Curtin, Y. Kahn, and G. Krnjaic, "Systematically testing singlet models for $(g-2)_\mu$," *JHEP* **04** (2022) 129, arXiv:2112.08377 [hep-ph].

[254] R. Dermisek, K. Hermanek, and N. McGinnis, "Di-Higgs and tri-Higgs boson signals of muon g-2 at a muon collider," *Phys. Rev. D* **104** no. 9, (2021) L091301, arXiv:2108.10950 [hep-ph].

[255] R. Capdevilla, D. Curtin, Y. Kahn, and G. Krnjaic, "No-lose theorem for discovering the new physics of (g-2)μ at muon colliders," *Phys. Rev. D* **105** no. 1, (2022) 015028, arXiv:2101.10334 [hep-ph].

[256] W. Altmannshofer, S. A. Gadam, and S. Profumo, "Snowmass White Paper: Probing New Physics with $\mu^+\mu^- \to bs$ at a Muon Collider," in *Snowmass 2021*. 3, 2022. arXiv:2203.07495 [hep-ph].

[257] P. Asadi, R. Capdevilla, C. Cesarotti, and S. Homiller, "Searching for leptoquarks at future muon colliders," *JHEP* **10** (2021) 182, arXiv:2104.05720 [hep-ph].

[258] A. Azatov, F. Garosi, A. Greljo, D. Marzocca, J. Salko, and S. Trifinopoulos, "New physics in b $\to$ s$\mu\mu$: FCC-hh or a muon collider?," *JHEP* **10** (2022) 149, arXiv:2205.13552 [hep-ph].

[259] W. Altmannshofer, S. A. Gadam, and S. Profumo, "Probing New Physics with $\mu^+\mu^- \to bs$ at a Muon Collider," arXiv:2306.15017 [hep-ph].

[260] S. Sun, Q.-S. Yan, X. Zhao, and Z. Zhao, "Constraining rare B decays by $\mu^+\mu^- \to tc$ at future lepton colliders," arXiv:2302.01143 [hep-ph].

[261] T. A. Chowdhury, A. Jueid, S. Nasri, and S. Saad, "Probing Zee-Babu states at Muon Colliders," arXiv:2306.01255 [hep-ph].

[262] S. P. Maharathy and M. Mitra, "Type-II see-saw at $\mu^+\mu^-$ collider," arXiv:2304.08732 [hep-ph].

[263] M. Low and L.-T. Wang, "Neutralino dark matter at 14 TeV and 100 TeV," *JHEP* **08** (2014) 161, arXiv:1404.0682 [hep-ph].

[264] T. Han, S. Mukhopadhyay, and X. Wang, "Electroweak Dark Matter at Future Hadron Colliders," *Phys. Rev. D* **98** no. 3, (2018) 035026, arXiv:1805.00015 [hep-ph].

[265] A. Alloul, N. D. Christensen, C. Degrande, C. Duhr, and B. Fuks, "FeynRules 2.0 - A complete toolbox for tree-level phenomenology," *Comput. Phys. Commun.* **185** (2014) 2250–2300, arXiv:1310.1921 [hep-ph].

[266] J. Alwall, R. Frederix, S. Frixione, V. Hirschi, F. Maltoni, O. Mattelaer, H. S. Shao, T. Stelzer, P. Torrielli, and M. Zaro, "The automated computation of tree-level and next-to-leading order differential cross sections, and their matching to parton shower simulations," *JHEP* **07** (2014) 079, arXiv:1405.0301 [hep-ph].

[267] J. Alwall, M. Herquet, F. Maltoni, O. Mattelaer, and T. Stelzer, "MadGraph 5 : Going Beyond," *JHEP* **06** (2011) 128, arXiv:1106.0522 [hep-ph].

[268] C. Bierlich *et al.*, "A comprehensive guide to the physics and usage of PYTHIA 8.3," arXiv:2203.11601 [hep-ph].

[269] **DELPHES 3** Collaboration, J. de Favereau, C. Delaere, P. Demin, A. Giammanco, V. Lemaître, A. Mertens, and M. Selvaggi, "DELPHES 3, A modular framework for fast simulation of a generic collider experiment," *JHEP* **02** (2014) 057, arXiv:1307.6346 [hep-ex].

[270] X. G. He, G. C. Joshi, H. Lew, and R. R. Volkas, "NEW Z-prime PHENOMENOLOGY," *Phys. Rev. D* **43** (1991) 22–24.

[271] X.-G. He, G. C. Joshi, H. Lew, and R. R. Volkas, "Simplest Z-prime model," *Phys. Rev. D* **44** (1991) 2118–2132.

[272] S. Baek, N. G. Deshpande, X. G. He, and P. Ko, "Muon anomalous g-2 and gauged L(muon) - L(tau) models," *Phys. Rev. D* **64** (2001) 055006, arXiv:hep-ph/0104141.

[273] E. Ma, D. P. Roy, and S. Roy, "Gauged L(mu) - L(tau) with large muon anomalous magnetic moment and the bimaximal mixing of neutrinos," *Phys. Lett. B* **525** (2002) 101–106, arXiv:hep-ph/0110146.

[274] D. W. P. d. Amaral, D. G. Cerdeno, P. Foldenauer, and E. Reid, "Solar neutrino probes of the muon anomalous magnetic moment in the gauged $\mathrm{U}(1)_{L_\mu - L_\tau}$," *JHEP* **12** (2020) 155, arXiv:2006.11225 [hep-ph].

[275] M. Escudero, D. Hooper, G. Krnjaic, and M. Pierre, "Cosmology with A Very Light $\mathrm{L}_\mu - \mathrm{L}_\tau$ Gauge Boson," *JHEP* **03** (2019) 071, arXiv:1901.02010 [hep-ph].

[276] J. Heeck, M. Lindner, W. Rodejohann, and S. Vogl, "Non-Standard Neutrino Interactions and Neutral Gauge Bosons," *SciPost Phys.* **6** no. 3, (2019) 038, arXiv:1812.04067 [hep-ph].

[277] **CMS** Collaboration, A. M. Sirunyan *et al.*, "Search for an $L_\mu - L_\tau$ gauge boson using Z→ 4μ events in proton-proton collisions at $\sqrt{s} = 13$ TeV," *Phys. Lett. B* **792** (2019) 345–368, arXiv:1808.03684 [hep-ex].

[278] **BaBar** Collaboration, J. P. Lees *et al.*, "Search for a muonic dark force at BABAR," *Phys. Rev. D* **94** no. 1, (2016) 011102, arXiv:1606.03501 [hep-ex].

[279] W. Altmannshofer, S. Gori, M. Pospelov, and I. Yavin, "Neutrino Trident Production: A Powerful Probe of New Physics with Neutrino Beams," *Phys. Rev. Lett.* **113** (2014) 091801, arXiv:1406.2332 [hep-ph].

[280] M. Bauer, P. Foldenauer, and J. Jaeckel, "Hunting All the Hidden Photons," *JHEP* **07** (2018) 094, arXiv:1803.05466 [hep-ph].

[281] S. Jana, V. P. K., and S. Saad, "Resolving electron and muon $g-2$ within the 2HDM," *Phys. Rev. D* **101** no. 11, (2020) 115037, arXiv:2003.03386 [hep-ph].

[282] M. Magg and C. Wetterich, "Neutrino Mass Problem and Gauge Hierarchy," *Phys. Lett. B* **94** (1980) 61–64.

[283] B. Batell, A. Freitas, A. Ismail, and D. Mckeen, "Flavor-specific scalar mediators," *Phys. Rev. D* **98** no. 5, (2018) 055026, arXiv:1712.10022 [hep-ph].

[284] V. Brdar, M. Lindner, S. Vogl, and X.-J. Xu, "Revisiting neutrino self-interaction constraints from Z and τ decays," *Phys. Rev. D* **101** no. 11, (2020) 115001, arXiv:2003.05339 [hep-ph].

[285] N. Blinov, K. J. Kelly, G. Z. Krnjaic, and S. D. McDermott, "Constraining the Self-Interacting Neutrino Interpretation of the Hubble Tension," *Phys. Rev. Lett.* **123** no. 19, (2019) 191102, arXiv:1905.02727 [astro-ph.CO].

[286] K. S. Babu, P. S. B. Dev, S. Jana, and A. Thapa, "Non-Standard Interactions in Radiative Neutrino Mass Models," *JHEP* **03** (2020) 006, arXiv:1907.09498 [hep-ph].

[287] K. S. Babu and S. Jana, "Enhanced Di-Higgs Production in the Two Higgs Doublet Model," *JHEP* **02** (2019) 193, arXiv:1812.11943 [hep-ph].

[288] **ATLAS** Collaboration, G. Aad *et al.*, "Search for direct pair production of sleptons and charginos decaying to two leptons and neutralinos with mass splittings near the W-boson mass in $\sqrt{s} = 13$ TeV pp collisions with the ATLAS detector," *JHEP* **06** (2023) 031, arXiv:2209.13935 [hep-ex].

[289] G. C. Branco, P. M. Ferreira, L. Lavoura, M. N. Rebelo, M. Sher, and J. P. Silva, "Theory and phenomenology of two-Higgs-doublet models," *Phys. Rept.* **516** (2012) 1–102, arXiv:1106.0034 [hep-ph].

[290] Y. Kuno and Y. Okada, "Muon decay and physics beyond the standard model," *Rev. Mod. Phys.* **73** (2001) 151–202, arXiv:hep-ph/9909265.

[291] H. H. Patel, “Package-X 2.0: A Mathematica package for the analytic calculation of one-loop integrals,” *Comput. Phys. Commun.* **218** (2017) 66–70, arXiv:1612.00009 [hep-ph].

[292] J. van der Bij and M. J. G. Veltman, “Two Loop Large Higgs Mass Correction to the rho Parameter,” *Nucl. Phys. B* **231** (1984) 205–234.